

**SLIT Proteins Inhibit Malignant Brain Tumour Cell Invasion via Downregulation
of Pro-Invasive Genes**

By

Mohamad Seyed Sadr

Department of Neurology and Neurosurgery

Brain Tumour Research Centre

McGill University, Montréal

May 2012

A thesis submitted to McGill University in partial fulfillment of the requirements of the
degree of Doctor of Philosophy

© Mohamad Seyed Sadr, 2012

Abstract

Most cancer deaths result from the progression of the tumour pathology whereby a localised mass evolves into an invasive and metastatic disease, spreading away from the main tumour mass. Malignant brain tumours such as glioblastoma and medulloblastoma are among the most invasive human cancers. The Slit-Robo pathway is extensively characterised as a repellent of axons and neural cells. Therefore we hypothesised that Slit proteins would repel invasive brain tumour cells.

The first chapter of this thesis provides a thorough introduction of the oncology field as it pertains to malignant brain tumour biology and to the field of Slit-Robo family of proteins. The second chapter provides evidence for Slit proteins and their inhibitory effect on malignant brain tumour cell invasion. We further characterise the signaling pathway employed by Slit proteins to impart an inhibitory effect on tumour cell invasion. We present data suggesting that Slit proteins decrease the transcriptional expression of numerous pro-invasive and pro-angiogenic genes in malignant brain tumour cells. We characterise the product of one of these genes, MMP14, as a protease of Robo proteins. A model is proposed that explains the observation that decreasing the expression of MMP14 leads to a decrease in brain tumour cell invasion.

These results suggest that malignant brain tumour cells respond to Slit by modulating a series of transcripts critical for cell invasion. Therefore, targeting malignant brain tumour cells with Slit proteins or chemical analogues that mimic Slit's effects may provide a potentially novel anti-invasive therapy.

Résumé

La transformation d'une tumeur primaire en tumeur maligne et métastatique, s'éloignant du point d'origine, est souvent la principale cause de décès chez le patient. Les tumeurs cérébrales malignes tel les glioblastomes et les médulloblastomes sont parmi les plus invasives cancers humains. La voie de signalisation de Slit-Robo a été largement caractérisée et montre l'implication de Slit-Robo dans la répulsion des axones et cellules neuronales. Dans cette étude, nous avons étudié la possibilité que Slit-Robo pourraient repousser les cellules cancéreuses invasives cérébrales.

Le premier chapitre de cette thèse présente une introduction approfondie du rôle de la famille des protéines Slit-Robo dans le contexte du cancer et de la biologie des tumeurs cérébrales. Le deuxième chapitre présente des preuves de l'implication des protéines Slit et leur rôle dans l'inhibition de l'invasion des cellules de tumeurs cérébrales. Aussi, la caractérisation de la voie de signalisation employée par les protéines Slit dans l'inhibition de l'invasion des cellules cancéreuses a été montrée. De plus, cette étude présente des résultats qui suggèrent que les protéines Slit diminuent l'expression de la transcription de gènes pro-angiogénique et pro-invasif des cellules tumorales. Nous avons aussi identifié MMP14 comme une protéase des protéines Robo et dont l'expression est influencée par les protéines Slit. Finalement, nous proposons un modèle démontrant qu'une diminution de l'expression de MMP14 induit une réduction de l'invasion des cellules tumorales du cerveau.

Acknowledgements

My undergraduate supervisor once told me that the aim of graduate studies is to transform a student into a professional. I am much indebted to all my previous supervisors, and especially my current supervisor, Rolando Del Maestro for providing me with all the tools necessary for my development. I am privileged to have a supervisor who gives me *carte blanche* so that I can develop my ideas, even the most eccentric ones. He is the model of what professional means. Pam, Rolando's wife and professional partner, provided invaluable assistance in my everyday interactions with Rolando. But more importantly, she personified the model brain tumour patient advocate, constantly reminding me the reason of "why we do what we do".

I am also delighted to have great committee members, Alyson Fournier, Ed Ruthazer, and a very helpful mentor, Josephine Nalbantoglu, who guided me and encouraged me during my graduate studies. I also thank Monique Ledermann for always making me feel welcomed and solving problems that came along. It's also important to mention Angie Giannakopoulos and Catherine Cattán, who made my life so much easier.

I am fortunate to have evolved under the supervision of Alexandre, a brilliant scientist. I also thank Tamra's guidance, Roberta's enthusiasm, Kevin's leadership, Abdulrahman's generosity, Sarah's optimism, Gabrielle's kindness, and Amir's selflessness.

I thank Debbie and Gino for their sense of humour and for making my graduate studies in *la grande région de Montréal* the most fun and enjoyable times of my life. I am particularly indebted to Vince for his kind heart, friendship, and assistance. I also would like to acknowledge Jad and Mitsuhiro for making the work environment a friendly and

delightful one. Finally, our lab would not be the same without Carmen, who micromanages everything and makes our lives so easy and delightful. I am also lucky to be surrounded by members of the Petrecca lab, and thank: Phuong for great scientific discussions, Alix for her contagious smile, Abdul for his altruism, Shahine for his kind heart, and Ahmed for his sense of humour. And especially **Gina**, well... for being *atfari*.

I am also expressing my gratitude to all the donors whose support and encouragements make our work possible. This work is supported by the Franco Di Giovanni, B-Strong, Alex Pavanel Family, Raymonde and Tony Boeckh, and Goals For Lily Funds for Brain Tumour Research. I also thank the English Montréal School Board, Brainstorm Foundation, Tony Colannino Foundation, and Brain Tumour Foundation of Canada for their financial support. My research was supported by the generous PhD studentships provided by the Christian Geada Brain Tumour Research Award, the Jeanne Timmons Costello Studentship, and the McGill F.O.M. Studentship.

Most importantly, I am forever grateful to my family. My work would not be possible if it were not for the love, kindness, and the many sacrifices of my mother Nahid and my father Bagher. They served as perfect role models and taught me great values. My brothers Ali and Emad have helped me in more ways than I can imagine and enthusiastically supported me. To my grandparents, thank you for your love! And to my extended family, I appreciate your unconditional support in everything that I do. I owe my family everything that I have achieved.

Table of Contents

Contents

Abstract	2
Résumé	3
Acknowledgements	4
Table of Contents	6
Contributions of Authors	9
Glossary of Terms	10
Chapter 1: Tumour Biology and the Hallmarks of Cancer	12
1.1 Malignant Transformation	13
I. Mitogenic Factor Independency	13
II. Tumour suppression Insensitivity	14
III. Resisting Apoptosis	15
IV. Escaping Senescence	16
V. Angiogenesis	17
VI. Escaping Immuno-surveillance	18
VII. Cancer Stem Cells	19
VIII. Invasion	21
i. Integrins	22
ii. Immunoglobulin-Like Cell Adhesion Molecules	23
iii. Cadherins	24
iv. Matrix Metalloproteinases	25
v. Invasion Assays	28
1.2 Brain Tumours	30
I. Gliomas	30
i. Pilocytic Astrocytoma	30
ii. Diffusely infiltrating astrocytomas	31
A. Diffuse astrocytoma	31
B. Anaplastic Astrocytoma	31

C. Malignant oligodendrogliomas.....	32
D. Malignant Oligoastrocytoma	33
E. Glioblastoma.....	33
II. Genes Altered in Malignant Gliomas.....	34
i. TP53 Signaling	34
ii. Receptor Tyrosine Kinases and Other Kinase Pathways	35
A. Epidermal Growth Factor Receptor	35
B. Platelet-Derived Growth Factor	36
C. Phosphatase and Tensin Homology	37
D. Neurofibromin 1 and RAS	38
iii. Retinoblastoma Pathway	38
iv. Metabolic Proteins IDH1 and IDH2	39
v. MGMT	39
III. Glioblastoma Treatment.....	40
IV. Medulloblastoma.....	43
1.3 SLIT and ROBO Proteins	47
I. Slit-Robo in the Nervous System	49
i. Commissureless and Robo3.....	50
ii. Genes and signaling pathways related to the Slit-Robo phenotypes.....	53
iii. SrGAPs identification	55
iv. SrGAPs functions.....	56
II. Slit-Robo Outside the Nervous System.....	58
i. Slit-Robo and immune cells	58
ii. Tooth development	59
iii. Trachea development	59
iv. Kidney development	59
III. Slit-Robo in Cancer	60
Chapter 2: SLIT Proteins Inhibit Brain Tumour Cell Invasion.....	63
2.1 Summary	64
2.2 Results	66
Slit2 and Sema3a inhibit medulloblastoma cell invasion.....	66
SLIT2 does not affect brain tumour cell proliferation rate.	67
Slits and Robos are expressed in all the glioma and medulloblastoma cell lines tested.....	68

U251 cell line engineered to overexpress Robo at the surface remains unresponsive to SLIT2.....	69
SLIT2 inhibits Cdc42 and Rac in medulloblastoma but not glioma cell lines.	70
SLIT2 inhibits glioma cell lines that have low-to-moderate invasive capabilities.	71
SLIT2 modulates the expression pattern of genes responsible for the invasive paradigm of UW3 cell.	72
The HPLC-based hSLIT2-myc purification yields functional SLIT2 comparable to commercial mSlit2.	75
Characterisation of <i>MMP14</i> , one of the genes modulated by SLIT2.....	76
rRobo1 is a substrate for MMP14, and it is proteolytically cleaved in the third Ig-like domain.	77
MMP14 overexpression in UW3 cells renders them insensitive to hSLIT2-myc.	81
MMP14 knockdown leads to a decrease in invasion in C6 glioma cells.	82
MMP14 knockdown leads to the sensitisation of C6 glioma cells to anti-invasive effects of hSLIT2-myc.	83
MMP14 knockdown decreases C6 glioma collagenase activity and hSLIT2-myc amplifies this decrease in MMP14 collagenase activity.	83
MMP14 knockdown enhances temozolomide toxicity in C6 cells.	84
2.3 Discussion	86
Sustained hSLIT2-myc Treatment Elicits a Transcriptional Response	89
Slit-Robo-MMP14 Model	93
MMP14's Potential Role in Axon Guidance	95
Conclusion and future prospective	97
2.4 Materials and Methods	99
2.5 Figures and Tables	110
References	178
Appendix	200

Contributions of Authors

All the figures, tables and the text presented in this thesis are derived solely from my work. Figure 4a and 5a of Chapter 2 which is the result of my experiments has been published in *Oncogene* (Werbowski-Ogilvie et al., 2006). Certain results from my work have also been published as a chapter in *Encyclopedia of Cancer, 3rd Edition* (Academic Press). The remainder of the work presented is derived from a manuscript submitted to *Oncogene*, where I am the first author. Gino Ferraro (McGill University, Canada) purified the recombinant soluble MMP14 and designed the shRNAmiR sequences and constructs used in Chapter 2, Figures 15-17. The stable cell line HEK-293 overexpressing hSLIT2-myc, which is described in (Werbowski-Ogilvie et al., 2006) was provided by Yi Rao (Northwestern University, USA). The mass spectrometry analysis was provided by the Genome Québec mass spectrometry facilities. The microarray data was obtained during a collaboration with André Nantel (BRI, National Research Council of Canada); Jean-Sébastien Deneault (BRI, National Research Council of Canada) provided technical help during the procedures and André Nantel performed the *in silico* analysis of the expression chips. I have designed and prepared all other constructs, stable cell lines, and other engineered reagents. Moreover, I have designed and performed all experiments presented in this thesis under the supervision of Rolando Del Maestro (Principal Investigator).

Glossary of Terms

Angiogenesis – Abnormal endothelial proliferation and recruitment thought to be triggered by neighboring cancer cells.

Apoptosis – A cellular process, which involves a series of intracellular events ultimately leading to programmed cell death.

Extracellular Matrix – Protein network found in the extracellular space, which serves as support for cells found in the vicinity. Such proteins may also play an important role in extracellular-to-intracellular signal transduction.

Glioma – Abnormal cellular growth thought to arise from a ‘normal’ neural precursor cell or neural stem cell. The origin of malignant glioma initiating cells is still unknown although key in vitro and in vivo experiments point towards a cancer cell of origin.

Invasion – Cellular process by which single cells or groups of cells overcome physical barriers (e.g., extracellular matrix, neighboring cells) to migrate into a target tissue. Although this process is typically present in cancer pathology, it can also occur in physiological conditions.

Medulloblastoma – Abnormal cellular growth characterised as a poorly differentiated mass of neuroepithelial origin associated with the cerebellum.

Metastasis – The propagation of malignant cells into tissues or organs other than the tissue of origin.

Mitogen – Factor that promotes cellular proliferation.

MMP14 – Membrane-bound matrix metalloprotease, responsible for cleaving matrix proteins and remodeling the extracellular matrix.

Oncogene – Gene that, once expressed abnormally (e.g., mutation, overexpression, ...) in transformed cells, may lead to malignancy.

Roundabout (Robo) – Single pass type I transmembrane proteins belong to the immunoglobulin superfamily which. These proteins bind Slits.

Senescence – Feature of most eukaryotic cells, which display finite proliferative capacities.

Slit – Soluble secreted proteins, associated with the extracellular matrix, and involved in axon guidance and patterning, as well as other facets of development. Slits bind Robo receptors.

Stem cell – Cell with pluripotent features, capable of proliferating asymmetrically to yield one stem cell (self renewal) and a differentiated cell (differentiation).

Transformation – Process by which cell acquire a series of modifications, typically at the genetic level, to bypass restrictive cellular checkpoints.

Tumour suppressor – Gene whose proper expression is necessary for the controlled and ordered growth of cells, and to prevent their transformation.

Chapter 1: Tumour Biology and the Hallmarks of Cancer

1.1 Malignant Transformation

Normal cells of all lineage and origin can transform into malignant cells and this process is poorly understood. However, it is known that a series of genetic and biochemical events accompany malignant transformation of benign cells. Acquired or inherited mutations in key genetic locations are responsible for the transition from a benign to a transformed state. Once transformed, a cascade of events still poorly understood takes place giving rise to a tumour mass. Transformed cells that successfully undergo tumorigenesis display several inter-related features that enable them to develop a malignancy; these features of cancer malignancy are discussed below.

I. Mitogenic Factor Independency

During development, pluripotent stem cells and progenitor cells are exposed to a myriad of signals to guide them to a destination point where these cells will establish the layers and subunits of individual organs. Once cells arrive at the site of differentiation, they are exposed to specific growth factors in order to enter an active proliferative state which results in organogenesis. Without these pro-mitotic cues, normal cells senesce and undergo apoptosis. However cancer cells differ from normal cells in that they are less dependent on external mitogenic factors. Malignant tumour cells have autocrine stimulation capabilities, expressing their own growth factors, secreting them into the extracellular matrix and then responding to these secreted factors (Ikushima and Miyazono, 2010). For example glioblastoma, the most common malignant brain tumour,

produces platelet derived growth factor (PDGF) and tumour growth factor α (TGF α) (de Martin et al., 1987; Pantazis et al., 1985). In addition cancers such as glioblastomas hyper-activate several pro-mitogenic pathways such as the epidermal growth factor receptor (EGFR) gene (erbB) amplification, overexpression, and constitutive activation (Gan et al., 2009a). Extracellular matrix proteins such as integrins (discussed below) can also play a role in helping the cancer cell evade its dependency on growth factors. The overexpression or alteration of integrins is known to constitutively propagate mitogenic signals from the matrix to proliferative pathways such as the MAP kinase signaling axis (Giancotti and Ruoslahti, 1999). Finally, proteins playing a central role in the signal transduction of mitogenic pathways, such as Src and Ras, may be altered to benefit cancer cells by amplifying proliferative signals in the absence of pro-mitotic signals (Angers-Loustau et al., 2004; Medema and Bos, 1993).

II. Tumour suppression Insensitivity

In addition to producing their own growth factors, cancer cells acquire inactivating mutations in genes that regulate cellular proliferation. The products of such genes, collectively called tumour suppressor proteins, are responsible for blocking uncontrolled proliferation by forcing cells to enter a dormant state (Aguirre-Ghiso, 2007).

Retinoblastoma protein (RB1) is a central inhibitor of cell cycle progression, responsible for sequestering transcription factors such as E2F that regulate the transcription of genes that promote G0-G1 to S phase transition (Weinberg, 1995a). Cyclin-dependent kinases (CDKs), of which the two best characterised are CDK4 and CDK6, orchestrate the hyper-

phosphorylation – thus inactivation – of RB1, which leads to the activation of E2F ultimately facilitating the G0-G1 to S phase transition (Vermeulen et al., 2003a; Wiedemeyer et al., 2010).

Cancer cells can also evade tumour suppression by maintaining an undifferentiated state, most notably by expressing the *c-myc* proto-oncogene. The c-Myc oncoprotein is a central regulator of gene transcription, generally responsible for synchronising the differentiation of cells during tissue genesis (Lin et al., 2009). But c-Myc's function is often perturbed in various cancers, typically leading to the suppression of pro-differentiation pathways and the transcription of pro-mitotic genes. In addition, over-expression of *c-myc* in GFAP⁺ cells (astroglial lineage) in mice leads to the development of glioma lesions, with poorly-differentiated tumour cells (Jensen et al., 2003).

III. Resisting Apoptosis

Another hallmark of cancer cells is their capability to evade apoptotic signals. The most well characterised protein in the apoptotic pathway, p53 is encoded by *tumour protein 53* (*TP53*). Many cellular stress signals, such as DNA damage, hyperactive proliferation, hypoxic events, etc. converge to p53, which forces the stressed cell into a quiescent state. If the stress signals persist, p53 activates an apoptotic cascade in order to eliminate the host cell that may potentially become transformed (Royds et al., 2006). However in over 50% of all cancers (Hollstein et al., 1991) and 35% of glioblastomas (TCGARN, 2008), *TP53* is mutated, leading to a decrease in apoptosis and resistance to senescence. P53 is also targeted for degradation by the ubiquitin ligases MDM2 (Momand et al., 1992) and

MDM4 (Riemenschneider et al., 1999). In several cancers, including a subset of glioblastomas, *mdm2* is amplified enabling cancer cells to evade the apoptotic cascade triggered by TP53 (TCGARN, 2008).

Some other methods used by cancer cells to evade programmed cell death include the overactive signal transduction of the PI3K-AKT pathway. PI3K-AKT signaling leads to the phosphorylation of the pro-apoptotic proteins Bax (Gardai et al., 2004), and Bad (Datta et al., 1997) inactivating them. In addition, they can phosphorylate MDM2 and promote its nuclear translocation which results in p53 ubiquitination and degradation (Mayo and Donner, 2001). The PI3K-AKT axis is also hyperactive in most cancers because *pten* (discussed below) which encodes a lipid phosphatase that naturally counters the kinase activity of PI3K, is often mutated or deleted in numerous cancers including glioblastomas (Li et al., 1997; Steck et al., 1997).

IV. Escaping Senescence

It is well known that cells derived from primary cultures have a finite lifespan because of an intrinsic mechanism called cellular senescence (Collado et al., 2007). This phenomenon, deregulated in most cancer cells, allows these cells to proliferate indefinitely. One of the important proteins involved in the resistance of cancer cells' senescence is telomerase reverse transcriptase (TERT), a ribonucleoprotein with reverse transcriptase enzymatic activity that maintains the length of telomeres at the end of chromosomes (Greider and Blackburn, 1985; Singer and Gottschling, 1994). Telomere length is extremely important in order to prevent DNA recombination, fusion, and

degradation, and cancer cells with activated TERT avoid senescence and apoptosis (Blasco et al., 1997). In addition cancer cells are capable of inactivating cellular senescence effectors such as p16^{INK4a} and p14^{ARF} encoded by chromosome 9p21 (Cheung et al., 2010). P16^{INK4a} inhibits telomerase activity in both malignant and normal cells (Bazarov et al., 2010). Moreover p14^{ARF} and p16^{INK4a} are activated upon exogenous expression of oncogenic Ras (Palmero et al., 1998; Serrano et al., 1997) leading to cellular senescence.

V. Angiogenesis

Once tumour cells reach a certain density, the blood and nutrient supply to the tumour core becomes insufficient, and cancer cells require the formation of new blood vessels (angiogenesis) to sustain the influx of nutrients necessary for cell growth, and the outflow of cellular waste and debris. One way cancer cells trigger angiogenesis is via expression of vascular endothelial growth factors (VEGFs). There are five VEGF genes, *VEGF-A*, *B*, *C*, *D*, and *PLGF*, which modulate multiple aspects of endothelial cell biology, including proliferation, migration, differentiation, and vessel permeability (Gerber et al., 1998; Leung et al., 1989; Plouet et al., 1989). In experimental human tumour xenografts, function blocking antibodies against VEGFs inhibited the interaction of tumour cells with endothelial cells, which led to the inhibition of tumour vascularisation and a decrease in vessel permeability (Yuan et al., 1996). Bevacizumab (Avastin) treatment, a monoclonal antibody against vascular endothelial growth factor 2, has shown efficacy in improving progression-free survival rates in patients with recurrent glioblastoma which has led this

drug to obtain conditional approval for the treatment of this disorder (Vredenburgh et al., 2007). Also the AVAglio trial, a phase III trial of concomitant treatment of bevacizumab associated with radiation therapy and temozolomide has recently been completed, and the results of the latter will dictate whether the use of bevacizumab is beneficial to patient survival (Chinot et al., 2011).

VI. Escaping Immuno-surveillance

Cancer cells express different proteins on their cell surface than normal corresponding tissue, and therefore such protein expression pattern should trigger an immune response against the tumour. However, tumour cells secrete proteins such as transforming growth factor- β (TGF- β) to dampen the host's immune-surveillance (Massague, 2008). TGF- β 's secretion significantly decreases the tumour-specific activity of cytotoxic T lymphocytes. This is achieved in part by modulating the expression of several genes directly involved in the cytotoxic T cell response, such as perforin and granzymes A and B (Thomas and Massague, 2005). Clinical trials are currently underway, aiming to neutralise TGF- β isoforms based on *in vitro* and *in vivo* experiments, which have previously demonstrated that targeting TGF- β enhances host immune response against tumour cells and decreases the tumour's proliferative and invasive capabilities (Podar et al., 2007; Thomas and Massague, 2005). Moreover, adult patients with recurrent and/or refractory anaplastic astrocytomas (World Health Organisation Grade III) are presently being recruited into an International Phase III clinical trial called the SAPPHERE' study. In this study patients are randomised to standard chemotherapy or to intratumoral trabedersen (AP 12009), an

antisense synthetic oligonucleotide directed specifically against TGF- β 2 mRNA (Bogdahn et al., 2011; Vallieres, 2009).

VII. Cancer Stem Cells

Recent advances in tumour biology suggest that most cancer cells are not identical and that within the same population of tumour cells resides a subset of cancer stem cells (CSC) capable of dividing and regenerating the CSC pool as well as to differentiate into non-CSCs that make up the remainder of the tumour (Hambardzumyan et al., 2008b; Thomas and Massague, 2005). One plausible theory as to the source of CSC in gliomagenesis may be neural stem cells or progenitor cells that have undergone genetic alterations, inactivating their proliferation and differentiation control mechanisms. The presence of neural stem cells in anatomical regions of the brain, such as the subventricular zone (SVZ), dentate gyrus of the hippocampus, and the subcortical white matter (Cameron and McKay, 2001; Eriksson et al., 1998; Nunes et al., 2003; Sanai et al., 2004) supports the idea of a stem cell precursor that would give rise to CSCs. *In vivo* evidence supporting the neural stem cell or progenitor cell theory comes from mouse models wherein nestin-positive cells (stem or progenitor cell marker) engineered to express activated forms of Akt and Ras develop gliomas with many of the features present in human pathology (Holland et al., 2000). Similarly, mice that are homozygous-deficient for *p53* and *NFI* (gene encoding the neurofibromin 1 protein) develop high grade gliomas reminiscent of the human pathology, and that neural stem cells of the SVZ

accumulate genetic insults leading to their uncontrolled expansion and gliomagenesis (Wang et al., 2009).

But what markers should be used to differentiate brain CSCs from the remainder of the tumour cell population? While there is discordance within the scientific community about *bona fide* CSC markers, there are several candidates that can label a subpopulation of cancer cells with pluripotent features and self-renewal capabilities. The first marker and perhaps the most disputed marker of CSCs is PROM1 (also known as CD133) encoded by the *PROM1* gene (Miraglia et al., 1997; Yin et al., 1997). PROM1 is a five-pass transmembrane glycoprotein with an unknown cellular function, expressed on stem cells of diverse lineage of hematological CSCs (Cox et al., 2009; Yin et al., 1997) and solid tumour CSCs (Galli et al., 2004; Ricci-Vitiani et al., 2007; Singh et al., 2004; Taylor et al., 2005). PROM1⁺ cells derived from high grade glioma tumour specimens and cell lines are resistant to ionising radiation by activating DNA damage surveillance proteins Chk1 and Chk2 (Bao et al., 2006a; Hambardzumyan et al., 2006), and to chemotherapeutic agents by overexpressing DNA damage repair protein MGMT (discussed below), drug resistant protein ABCG2 (discussed below) and anti-apoptotic proteins such as the IAP family of proteins (Liu et al., 2006). PROM1⁺ cells are also capable of recruiting endothelial cells and display increased vascularisation, blood vessel leakage, VEGF and SDF-1 expression, and necrosis when compared to PROM⁻ glioma cells (Bao et al., 2006b; Folkens et al., 2009). These are all features of aggressive gliomas with poor prognosis (Plate and Risau, 1995). This may in part explain why radiation therapy and anti-proliferative and anti-angiogenic chemotherapies fail in high grade gliomas.

Another marker of glioma CSCs is the ATP-binding cassette G2 (ABCG2). ABCG2 is part of an ATP-dependent transmembrane protein capable of pumping small molecules across the membrane (Donnenberg and Donnenberg, 2005) and is highly expressed in normal stem cells and many CSCs (Scharenberg et al., 2002). ABCG2⁺ cells are pluripotent, highly proliferative, chemotherapy-resistant partly by overexpressing MGMT, and highly malignant when tested *in vitro* and *in vivo* (Bleau et al., 2009; Hirschmann-Jax et al., 2004; Ho et al., 2007; Patrawala et al., 2005). Blocking AKT activity in ABCG2⁺ cells results in a decreased rate of drug translocation by ABCG2 and an increased cytotoxicity of chemotherapeutic agents and the reverse was observed when *pten* is ablated, suggesting that the PI3K/Akt pathway plays a vital role in the ABCG2⁺ CSC properties (Bleau et al., 2009; Hambardzumyan et al., 2008a).

VIII. Invasion

Based on figures published by the World Health Organisation (WHO), 7.6M deaths (13% of total death) in the world were due to cancer. Cancer has generally a favorable prognosis if the tumour mass is detected at an early stage. In the great majority of cancers, morbidity and mortality are associated with the spread of cancer cells at considerable distances from the tumour mass (Mareel and Leroy, 2003). Therefore the malignant manifestation of cancer is largely due to the infiltrative potential of cancer cells into surrounding tissue.

Cancer cell invasion *in vivo* strongly resembles cellular migration on artificial and matrix protein substrates (Bittner et al., 2000; Guo and Giancotti, 2004). Cellular migration can be simplified and divided into four events (Figure I-1). First, an extracellular or

intracellular cue is responsible for triggering signaling cascades inside the cytoplasm, ultimately leading to the solicitation of the cytoskeletal machinery. Next, mechanical work is produced as a result of actin polymerisation physically altering the plasma membrane giving rise to membrane ruffles or pseudopodes, in two-dimensions and three-dimensions, respectively. These membrane projections are then anchored through a complex mechanism involving a tripartite interaction between extracellular matrix components, transmembrane adhesion proteins, and intracellular cytoskeletal proteins. Finally once the cell establishes a stable anchorage, molecular signals propagate the message to the rear of the cell leading to the disassembly of adhesion complexes.

i. Integrins

One way by which tumour cells invade the ECM is by upregulating the expression or function of integrins, transmembrane proteins involved in cell-ECM adhesion (Guo and Giancotti, 2004). Integrins are expressed at the cell surface as heterodimers consisting of α and β subunits (Shapiro et al., 2007) which participate in ligand binding (e.g., extracellular matrix proteins) and cytoplasmic signal transduction (e.g., via association with receptor tyrosine kinases). Upon interaction with ECM components or neighboring cell surface proteins, integrins trigger a bi-directional signal transduction leading to intracellular recruitment of focal adhesion clusters and extracellular recruitment of pro-migratory components such as matrix proteases (Guo and Giancotti, 2004; Hood and Cheresh, 2002). Beta1 and $\alpha v \beta 3$ integrins are of particular interest in malignant glioma biology because they are expressed in malignant glial tumours but undetectable in normal brain tissue and they are thought to be in part responsible for the highly invasive and proliferative phenotypes of malignant gliomas (Gladson et al., 1995; Paulus et al., 1996;

Rooprai et al., 1999). Many integrin inhibitors are currently in preclinical and clinical trials to evaluate their safety and anti-tumour activity. Cilengitide is a cyclic peptide which inhibits $\alpha v \beta 3$ and $\alpha v \beta 5$ integrin receptors and its efficacy is currently being tested in glioblastoma patients (Reardon et al., 2008; Stupp et al., 2010). The two cilengitide clinical trials, CORE and CENTRIC trials, aim to test the effect of cilengitide in newly diagnosed glioblastoma patients with unmethylated and methylated *MGMT* promoter status, respectively. Also, Vitaxin, a humanised monoclonal antibody with inhibitory effects on integrins, is currently being evaluated in different types of cancer (Alghisi and Ruegg, 2006; Hersey et al., 2010).

ii. Immunoglobulin-Like Cell Adhesion Molecules

The immunoglobulin-like superfamily of cell adhesion molecules (IgCAM) is the largest and most diverse family of proteins whose members also play a role in tumour cell dissemination, invasion, and metastasis. For instance, neural cell adhesion molecule (NCAM), which is expressed in different tissues can associate with fibroblast growth factor receptor and adhere to the ECM and signal via $\beta 1$ integrin (Kopfstein and Christofori, 2006). However, in many cancers, a decrease in NCAM expression is associated with poor prognosis (Kopfstein and Christofori, 2006; Owens et al., 1998). CD44 is another Ig-like protein, interacting mainly with hyaluran found in the extracellular space. CD44 is overexpressed in several cancers, including malignant gliomas (Ranuncolo et al., 2002a; Ranuncolo et al., 2002b) but the level of its expression is not predictive of patient outcome. CD44 knock down in glioblastoma cell lines diminishes the invasive properties of the cancer cells *in vitro* and *in vivo* (Okada et al., 1996) perhaps by decreasing MMP-9 cell surface anchorage capabilities mediated by

CD44 (Yu and Stamenkovic, 1999). Clinical trials are under way to test different therapies targeting IgCAMs such as CD44 in different cancers (Riechelmann et al., 2008).

iii. Cadherins

Calcium-dependant cell adhesion molecules (Cadherins) participate in homodimeric cell-to-cell adhesion and play key roles during embryogenesis, development, and adulthood (Gumbiner, 1988; Gumbiner, 2000; Takeichi, 1995). Cadherins are also strongly implicated in different facets of cancer development and progression. First, the metastatic capabilities of different cancers is inversely proportional to the expression of cadherins in those tumours (Bussemakers et al., 1992; Frixen et al., 1991; Schipper et al., 1991; Tamura et al., 1996). Second, the E-cadherin (ECAD) to N-cadherin (NCAD) transition is of particular importance in carcinomas because in this model, transformed epithelial cells that were previously in contact with surrounding cells decrease their ECAD expression, lose their contact with the normal epithelium and overexpress NCAD to disseminate from the tissue (Cavallaro and Christofori, 2004; Cavallaro et al., 2002; Hirohashi, 1998; Maret et al., 2010). This E-to-N cadherin switch often accompanies epithelial malignancy, and imparts hyperinvasive and metastatic properties to carcinomas. In brain tissue, NCAD is the predominant form of cadherin and malignant brain tumour cells do not display an ECAD to NCAD switch but rather a transition from adhesive and functional NCAD to a non-adhesive (immature or non-processed) NCAD containing the 'pro-protein' domain (Maret et al., 2010). Moreover gliomas and other cancers overexpress Cadherin-11, another member of the cadherin family, and its expression too correlates with increased cell invasion and poor prognosis (Bussemakers

et al., 2000; Pishvaian et al., 1999; Tomita et al., 2000). ADH-1, a synthetic pentapeptide and a very potent antagonist of N-cadherin, is currently being studied as a potential therapy for cancers such as melanoma (Perotti et al., 2009).

iv. Matrix Metalloproteinases

The extracellular matrix (ECM) surrounding malignant tumour growth is constantly remodeled by cancer cells. ECM alterations are thought to benefit the tumour microenvironment by enhancing the proliferative and invasive aspects of cancer cells (Bellail et al., 2004). Cancer cell invasion of the surrounding tissue and ECM is one of the best indicators of tumour malignancy and is suggestive of poor prognosis. To alter the structure of the ECM, cancer cells employ several types of matrix proteases, the most important of which are matrix metalloproteinases (MMPs).

There are over 500 proteases encoded by the human genome making this family the second largest protein family (Overall and Kleifeld, 2006b). MMPs are of particular importance in brain tumour cell invasion because they are thought to be responsible for the progression of a localised tumour toward an invasive disease (Liotta et al., 1980; Stetler-Stevenson, 1994). Gene expression studies in different human cancers support the idea that the transcriptome of the localised primary tumour mass differs from that of the metastasis, and that MMPs unequivocally participate in the promotion of tumour cell dissemination, leading to tissue and matrix invasion (Minn et al., 2005a; Minn et al., 2005b; Radisky et al., 2005). MMPs help progressing tumour malignancy by enhancing ECM degradation and by activating signaling pathways that benefit tumour cell survival, growth, and invasion (McCawley and Matrisian, 2001; Overall and Kleifeld, 2006b).

There are 24 MMPs in humans and each one has been implicated in tumour biology (Yong, 2005). Two MMP family members, the gelatinase A/MMP2 and the gelatinase B/MMP9 have been well documented as promoters of glioma invasion *in vitro* and *in vivo* (Bello et al., 2001; Deryugina et al., 1998; Kachra et al., 1999). In gliomas and in astrocytes, the inactive pro-form of MMP2 is cleaved and activated by plasmin, a serine protease, and this activation leads to a pronounced increase in glioma cell invasion *in vitro* and *in vivo* (Le et al., 2003). The expression and proteolytic activity of MMP9, on the other hand, is upregulated in stressful cellular environments often found at the core of the tumour mass, such as during pro-inflammatory stimuli and hypoxia (Esteve et al., 1998; Ezhilarasan et al., 2007; Medina-Torres et al., 2011). In response to such stressful cellular events, MMP-2 and -9 activate pro-angiogenic pathways to increase blood flow to the tumour mass (Genis et al., 2006; Vu et al., 1998). Finally the expression of MMP-2 and -9 increases as a function of brain tumour grade, with the highest expression observed in highly invasive and infiltrative glioblastomas (Forsyth et al., 1999; Nakagawa et al., 1996; Nakano et al., 1995). MMP-1 and -3 are also reported to be overexpressed in different types of cancers when compared with normal tissue and their expression is associated with a poor prognosis (Murray et al., 1998; Murray et al., 1996; Nakagawa et al., 1994; Uhm et al., 1997). Moreover genetic polymorphisms in genes encoding MMP-1 and -3 are associated with a poor prognosis or increased cancer susceptibility (Bradbury et al., 2009; Woo et al., 2007).

MMP14 is another important player in ECM degradation, tumour cell invasion, and angiogenesis (Overall and Kleifeld, 2006b). Unlike most MMPs, MMP14 is membrane-bound (also referred to as membrane-type MMP1, MT1-MMP). Under normal and

pathological circumstances, MMP14 promotes the activation and function of MMP2 and MMP9 (Overall and Sodek, 1990; Seomun et al., 2008). Mouse genetic models have implicated MMP14 in cartilage and skeletal development (Holmbeck et al., 1999). In malignant glioma progression, the expression of MMP14 closely mirrors disease progression from low grade to high grade gliomas (Lampert et al., 1998; Nakada et al., 1999). The expression and activity of MMP14 is particularly important for blood vessel development and angiogenesis. Function-blocking antibodies of MMP14 interfere with endothelial cell migration in several extracellular matrix models (Galvez et al., 2001). Moreover in several models aimed at studying neo-vascularisation, MMP14 expression is required for blood vessel recruitment (Hiraoka et al., 1998; Robinet et al., 2005; Zhou et al., 2000). Interestingly, MMP14 can also directly associate with growth factors such as PDGF-B and VEGF-A to promote their pro-angiogenic, pro-invasive, and pro-mitogenic functions (Hotary et al., 2003; Lehti et al., 2005; Sounni et al., 2004). The expression of MMP14 is controlled by several signaling axes such as the insulin growth factor receptor (IGF-1R) and the PI3K-AKT-JNK pathways, channeled in part through the transcription factor sp1 (Sroka et al., 2008; Sroka et al., 2007). The stromal cells can also be induced to produce MMP14 to assist tumour invasion and angiogenesis (Markovic et al., 2009).

By the end of the 1990's several broad-spectrum anti-MMPs were developed to treat cancer patients, including glioblastoma patients, and although some trials progressed to the phase III stage, the trials failed because of severe adverse effects and failure to achieve their end point aim of increasing survival rates (Levin et al., 2006; Overall and Kleinfeld, 2006b; Tremont-Lukats and Gilbert, 2003). However, several pharmaceutical companies are working on a new generation of MMP inhibitors that are more specific and

have less ‘off-target’ effects and clinical trials in the coming years will evaluate their safety and efficacy in patients with advanced malignancies (Overall and Kleinfeld, 2006a).

v. Invasion Assays

Targeting cancer cell invasion is of particular interest and to study invasion numerous groups including ours have developed *in vitro* and *in vivo* assays to measure cancer invasion (Bos et al., 2010; Del Duca et al., 2004; Madsen et al., 2006). *In vivo* methods (reviewed extensively by (Bos et al., 2010)), especially those in large animals, mimic best the human pathology. However they are costly and time-consuming, and incompatible with high throughput screens and tests. They are best suited for preclinical studies to test potential anti-invasive compounds. On the other hand, *in vitro* models provide a simpler alternative to cancer invasion measurement and are largely compatible with high throughput studies. Two of the most widely used invasion assays are Boyden chambers and tumour spheroid matrix invasion models. In both cases, tumour cells are confronted with a protein matrix which serves as an obstacle that has to be overcome either by degrading or bypassing it. The Boyden chamber assay is short, spanning 12-48 hours and technically very simple. However, this assay fails to recapitulate the three-dimension environment witnessed by tumour cells. Spheroid preparation is more complicated to prepare and longer to assay, typically spanning seven days. However matrix invasion assays allow the measurement of cancer cell invasion in a true three dimension environment, where cells can invade in all three axes of space. In addition, most matrices used in this assay are clear and allow light to traverse it thus permitting live imaging of the invasion (Maret et al., 2010; Werbowetski-Ogilvie et al., 2006). The invasion assays in this study were performed using a collagen invasion assay, extensively characterised

by our lab and others (Angers-Loustau et al., 2004; Del Duca et al., 2004; Demuth et al., 2007; Huszthy et al., 2008; Maret et al., 2010), outlined in Figure I-2, and described in the *Material and Methods* section.

1.2 Brain Tumours

Although primary brain tumours account for a small fraction of cancer occurrences, they represent 2.4% of deaths caused by cancer. Despite invasive therapies such as surgery, chemotherapy and radiation therapy, malignant brain tumours are almost always lethal because invasive cells spread throughout the brain parenchyma and interfere with the proper functions of the organ.

I. Gliomas

Gliomas are thought to arise from a ‘normal’ neural precursor cell or neural stem cell.

The origin of malignant glioma initiating cells is still unknown although key *in vitro* and *in vivo* experiments point towards a cancer cell of origin (discussed in section 1.1).

Different types of gliomas are described below and their development and progression is summarised in Figure I-3 and discussed below.

i. Pilocytic Astrocytoma

Pilocytic astrocytomas correspond to WHO grade I and generally occur during the first two decades of life (Kleihues et al., 2000). These tumours are typically well delineated, presenting with astrocytic features, such as staining positive for GFAP, and displaying low proliferative activity. These tumours have a favorable prognosis and are typically treated by surgical resection of the mass.

ii. Diffusely infiltrating astrocytomas

Malignant astrocytomas account for over 60% of all primary brain tumours. Although the etiology of astrocytic tumours is unknown, certain factors such as ionising radiation can significantly increase the predisposition of astrocytomas. The most common grading system follows the WHO recommendations, grading histological specimens for the presence of biological features such as nuclear atypia, mitotic index, cellular density, angiogenesis, and necrotic foci. In addition to tumour grading, clinical parameters such as age, health conditions, surgery, radiotherapy, and chemotherapy are indicative of patient outcome. Different types and grades of diffusely infiltrating astrocytomas are described below.

A. Diffuse astrocytoma

Diffuse astrocytomas correspond to WHO grade II and typically affect young adults (Kleihues et al., 2000). These tumours display a disseminate nature, infiltrating the surrounding parenchyma with increased cellular density and occasional atypical nuclear staining. *TP53* mutations are observed in the majority of diffuse astrocytomas that progress to glioblastomas (Reifenberger et al., 1996; Watanabe et al., 1996). Other mutations such as gains or amplifications of chromosomes 7q and 8q, and loss or deletions of chromosomes 6, 10p, and 22q have been reported in subsets of diffuse astrocytomas (Kleihues et al., 2000).

B. Anaplastic Astrocytoma

Anaplastic astrocytomas, WHO grade III, predominantly occur during the ages of 30 to 60 years (Kleihues et al., 2000). The histopathological features include increased cellular density, presence of nuclear atypia, and an increased proliferative index and the absence of necrotic foci and neo-vascularisation. Anaplastic astrocytomas display similar features

as diffuse astrocytomas such as *TP53* mutations and are pathologically considered intermediate between diffuse astrocytomas and glioblastomas. In addition, a subset of anaplastic astrocytomas present with non-mutually exclusive genetic alterations such as *p16* deletions (30%), *PTEN* or 10q alterations (15-30%), 19q loss or deletion (35%). Anaplastic astrocytomas typically progress to glioblastomas within 2 years of diagnosis (Watanabe et al., 1997) and younger age and gross total resection of the tumour mass are favourable indicators of prognosis (Kleihues et al., 2000).

C. Malignant oligodendrogliomas

Oligodendroglioma and anaplastic oligodendroglioma, representing WHO grades II and III, respectively, are much rarer than astrocytomas, accounting for 4% of all primary brain tumours. Cells from these tumours stain positive for oligodendrocyte markers although they do not have myelination capabilities. The etiology of this disease is unknown to date but ionising radiation has been shown to increase the predisposition to oligodendrogliomas (Kleihues et al., 2000). Histologically, oligodendrogliomas and especially anaplastic oligodendrogliomas are characterised by increased cellularity, cellular atypia, and increased mitotic index. Conversely, endothelial proliferation and the presence of necrotic foci are exclusive to anaplastic oligodendrogliomas. They are also often infiltrative and contain regions of high vascularisation and necrosis. Microcalcifications are also present especially in the vicinity of vascular structures, but not exclusive to malignant oligodendrogliomas (Kleihues et al., 2000). The single most characteristic feature of malignant oligodendrogliomas is the loss of heterozygosity (LOH) of genomic regions located on chromosomes 1p and 19q. Oligodendroglioma tumours with 1p and 19q LOH tend to respond favorably to DNA alkylating agents and live longer than their counterparts lacking these genetic ablations. Chromosome 19 is the

most altered chromosome in malignant oligodendrogliomas, whereby 19q is lost in over half of all tumours (Kleihues et al., 2000). Chromosome 1 is the next most altered chromosome, with losses in over half of all malignant oligodendrogliomas. Moreover the great majority of tumours that manifest a 1p loss are also accompanied by a 19q loss. *CDKN2C* encoding p18^{INK4c} located at 1p32 is also mutated in a subset of oligodendroglioma tumours (Husemann et al., 1999; Pohl et al., 1999). Like their astrocytic counterparts, half of all oligodendrogliomas overexpress EGFR and most tumours overexpress PDGF receptors and their ligands (Kleihues et al., 2000).

D. Malignant Oligoastrocytoma

Oligoastrocytoma and anaplastic oligoastrocytoma are considered WHO grade II or grade III tumours, respectively. These tumours preferentially occur in the cerebral hemisphere and display two distinct neoplastic glial features (Kleihues et al., 2000). They present regions of moderate (grade II) to high (grade III) cellular density, accompanied by low (grade II) to high (grade III) levels of mitotic activity. While anaplastic oligoastrocytomas may display foci of angiogenesis or necrosis, oligoastrocytomas are devoid of such features. The genetic features of malignant oligoastrocytomas are reminiscent of those of astroglial and oligodendroglial counterparts with chromosomes 1p and 19q being regions most altered in these tumours (Kleihues et al., 2000).

E. Glioblastoma

Glioblastoma is the most common primary brain tumour and among the most aggressive of human malignancies. Despite radical therapies such as invasive surgery, chemotherapy, and radiotherapy, most glioblastoma patients recur within eight months of the original diagnosis and die from complications of the pathology in less than two years after diagnosis (Stupp et al., 2005).

Glioma etiology is poorly understood. Like most cancers, high grade gliomas display heterogeneous morphological and genetic features making them difficult to classify. However genome sequencing and expression studies (TCGARN, 2008) have identified key genes altered in glioblastoma and other high grade gliomas and these genes, their frequency of alterations, and their impact on cellular functions are summarised and outlined in Figure I-4 and described below.

II. Genes Altered in Malignant Gliomas

i. TP53 Signaling

The gene encoding tumour protein 53 (TP53) resides on chromosome 17p and is often altered in malignant astrocytomas (el-Azouzi et al., 1989; Fults et al., 1989; James et al., 1989). *TP53* mutations account for approximately 30% of all glioblastomas and over 65% of all secondary glioblastomas (Kleihues et al., 2000). In addition TP53 signaling is altered in almost 90% of glioblastomas (TCGARN, 2008). There is some *in vitro* evidence implicating *TP53* gene mutations in high grade astrocytoma proliferation (Mercer et al., 1990; Van Meir et al., 1995), where the overexpression of wildtype TP53 aborts the proliferative capabilities of glioblastoma cell lines. However *TP53* mutation/inactivation is not absolutely necessary for gliomagenesis (Van Meir et al., 1994). Other factors playing pivotal role in the TP53 signaling pathway are also altered in malignant gliomas. For instance *MDM2* and *MDM4* are amplified (~10%) or overexpressed in glioblastomas and p14^{ARF}, expressed by the *CDKN2A* locus, is completely abrogated in half of all glioblastomas (TCGARN, 2008) (Figures I-3 and I-4).

ii. Receptor Tyrosine Kinases and Other Kinase Pathways

Although classical chemotherapeutic agents targeted nucleic acid synthesis, DNA integrity, and cytoskeletal functions, there is now a particular interest toward understanding and targeting protein and lipid kinases and their activators/effectors, because of their pivotal role in propagating proliferative, invasive, and angiogenic signals. Below, some of these kinases and associated proteins involved in malignant glioma pathology are described.

A. Epidermal Growth Factor Receptor

Chromosome 7 often displays an abnormal karyotype in malignant gliomas. The oncogene *c-erbB1*, which encodes the epidermal growth factor receptor (EGFR) resides on this chromosome and is amplified in half of glioblastomas (Libermann et al., 1985) and ERBB2, another member of the EGFR family is mutated in 8% of glioblastomas (TCGARN, 2008). EGFR is a transmembrane glycoprotein comprised of two cysteine rich extracellular regions responsible for ligand-binding, a single pass transmembrane region, an intracellular kinase domain and several conserved intracellular tyrosine residues that are phosphorylated upon receptor activation (Gan et al., 2009a). EGFR has high affinity for epidermal growth factor (EGF), and lower affinity for other oncogenic proteins such as transforming growth factor- α (TGF- α), heparin-binding EGF-like growth factor, amphiregulin, β -cellulin, etc. (Harris et al., 2003). Upon EGF binding, EGFR dimerises (homo- or hetero-dimerisation) and activates the receptor's kinase domain, which leads to tyrosine phosphorylation of cytoplasmic substrates.

In addition to EGFR amplification, EGFR is also mutated in several cancers. The most common EGFR mutation is the variant III (EGFRvIII) mutation observed in various carcinomas such as breast (Ge et al., 2002), non-small cell lung (Okamoto et al., 2003),

colorectal (Cunningham et al., 2005) and high grade gliomas (Kleihues et al., 2000). EGFRvIII is the product of a genomic deletion of exons 2-7 of wild type EGFR, the result of which is a constitutively active EGFR, functioning independently of ligand-binding (Gan et al., 2009a; Sugawa et al., 1990).

There are currently several therapeutic agents targeting EGFR and EGFRvIII that are being evaluated for the treatment of malignant gliomas. These compounds are at different clinical trial stages, and include interfering RNA molecules targeting the expression of EGFR (Zhang et al., 2004), small molecule inhibitors such as erlotinib and gefitinib (Guillamo et al., 2009; Raizer et al., 2010), and function blocking monoclonal antibodies such cetuximab and MAb 806 (Gan et al., 2009b; Hasselbalch et al., 2010).

B. Platelet-Derived Growth Factor

The platelet-derived growth factor (PDGF) family contains five members (Reigstad et al., 2005), PDGF-A, -B, -AB, -C, and -D encoded from genes located on four different chromosomes. These proteins were first characterised in embryonic development, organogenesis, stem and progenitor cell differentiation (Adams et al., 1983; Clemmons and Van Wyk, 1981; Zetter and Antoniades, 1979), and later in tumourigenesis and cancer malignant progression (Assoian et al., 1984; Pantazis et al., 1985). PDGFs are inactive in their monomeric state, but can form homo- and hetero-dimers and bind the PDGF receptors (PDGFR- α and - β), part of the receptor tyrosine kinase super family. Upon ligand binding, PDGF receptors dimerise in homo- or hetero-fashion, which leads to the propagation of the PDGF ligands inside the cell. Some of the intracellular effectors of the PDGF-PDGFR axis include PI3K, MAPK (Such as ERK and p38), SRC, and JNK (Tallquist and Kazlauskas, 2004).

Amplification of PDGFR- α is observed in 10% of glioblastomas (TCGARN, 2008). In a series of cortical injection of newborn mice with a retrovirus expressing PDGF-B, 40% developed a brain tumour with histological features of astrocytomas, oligodendrogliomas, and primitive neuro-ectodermal tumours (Uhrbom et al., 1998). Because of the importance of PDGF/PDGFR signaling in numerous types of cancer including malignant gliomas, effort has been directed towards developing inhibitors of this pathway. Currently, there are several small molecule inhibitors of PDGFR such as imatinib mesylate (Buchdunger et al., 2000) and monoclonal function blocking antibodies against PDGFR- α (Loizos et al., 2005). Many of these inhibitors are currently in pre-clinical stages or in early stages of clinical investigation and it remains to be seen whether they will prove to be therapeutic in malignant glioma patients.

C. Phosphatase and Tensin Homology

Over 80% of all glioblastomas display a partial or complete deletion of the large arm of chromosome 10 (Li et al., 1997; Steck et al., 1997). The single most studied gene on that chromosome is phosphatase and tensin homology (*pten*) and its product PTEN is mutated or deleted in one third of all glioblastomas; PTEN is a lipid phosphatase that counters the phosphorylation of Phosphoinositide-3-kinase (PI3K) (Koul, 2008). The *pten* gene is often mutated in high grade gliomas but is rarely altered in low grade gliomas, thus suggesting that PTEN is not involved in tumour initiation but rather in the progression of the malignancy (Wechsler-Reya and Scott, 2001). In culture and *in vivo*, cells with non-functional PTEN resist apoptosis and are more tumourigenic (Chiariello et al., 1998; Furnari et al., 1997). Moreover, exogenous expression of PTEN in PTEN-deficient cells reactivates senescence and cell death pathways, and causes a regression of the malignant phenotype of numerous glioma cell lines *in vitro*, and in sub-cutaneous and orthotopic

xenograft tumour models (Cheney et al., 1998). Re-expression of PTEN also sensitises glioma cells to ionising radiation (Wick et al., 1999).

D. Neurofibromin 1 and RAS

The *NF1* gene encodes a GTPase activating protein (GAP) which binds to Ras proteins and promotes its GTPase activity resulting in its inactivation (Xu et al., 1990).

Individuals suffering from neurofibromatosis type I carry autosomal *NF1* mutations and are susceptible to develop low grade gliomas that may progress to glioblastomas (Purow and Schiff, 2009; Sorensen et al., 1986). In addition, *NF1* mutations are observed in approximately 18% of all glioblastomas (TCGARN, 2008). Although RAS is rarely mutated in glioblastomas, it serves as an effector for several kinases including EGFR and PDGFR- α and thus there are several Ras inhibitors being assessed for their safety and efficacy in glioblastoma patients (Gilbert, 2006; Sebt and Hamilton, 2000).

iii. Retinoblastoma Pathway

Retinoblastoma protein (RB) regulates cell cycle arrest, by sequestering and inhibiting transcription factors responsible for the expression of genes that promote G0-G1 exit (Weinberg, 1995b). The RB1 gene is deleted or mutated in 11% of glioblastomas (TCGARN, 2008) and proteins in its pathway are also altered in glioblastoma patients. *CDKN2A* encoding P16^{INK4A} and *CDKN2B* encoding p15^{INK4B} are each mutated in half of glioblastoma patients. These proteins inhibit the activity of cyclin-dependent kinases (CDKs) such as CDK4 and CDK6, which are responsible for phosphorylating and inactivating RB1. CDK4 and CDK6 are in turn amplified in 18% and 1% of glioblastomas, respectively (TCGARN, 2008; Vermeulen et al., 2003b; Wiedemeyer et al., 2010).

iv. Metabolic Proteins IDH1 and IDH2

Isocitrate dehydrogenase 1 and 2 (*IDH1* and *IDH2*, respectively) have recently been identified as key genes mutated in a number of astrocytomas and oligodendrogliomas (Parsons et al., 2008). *IDH1* resides on the large arm of chromosome 2, and the product of this gene, IDH1 plays a central role in cellular oxidative state by producing NADPH through the conversion of isocitrate to α -ketoglutarate, (Ohgaki and Kleihues, 2009). In the vast majority of cases where *IDH1* is mutated, the arginine at position 132 is point-mutated to a histidine residue, or less frequently to a serine residue. The incidence of this mutation is approximately 10% in glioblastoma samples analysed. Interestingly, patients carrying the *IDH1* point mutation are much younger than glioblastoma patients harboring wild type copies of *IDH1*. Moreover, most secondary glioblastoma patients carry the *IDH1* mutation while only a minority of primary glioblastoma patients present with an *IDH1* mutation. Glioblastoma patients with an *IDH1* point mutation at position 132 have a better outcome, thus *IDH1* genotyping may serve as a prognostic factor (Nobusawa et al., 2009; Sanson et al., 2009).

v. MGMT

O-6-methylguanine-DNA methyltransferase (MGMT) is a DNA repair protein encoded by *MGMT* located on chromosome 10q26. MGMT is an atypical DNA repair protein for it does not require binding partners to correct alkyl (e.g., methyl group) adducts at the O6 position of guanine (Gerson, 2004). In addition, once MGMT transfers the alkyl group from the DNA base to the sulfur atom of a conserved cysteine residue in its active site, the protein is inactivated and cannot repair any further nucleic acid (Gerson, 2004). Alkyl adducts at the O6 position lead to DNA polymerase stalling and improper incorporation of nucleotides ultimately leading to mismatch base pairing and mutational events

(Delaney and Essigmann, 2001; Loechler et al., 1984). Alkylating agents are known to induce a myriad of cancers *in vivo* (Barth and Kaur, 2009; Goth and Rajewsky, 1974) and mice expressing a copy of the human *MGMT* gene resist tumourigenesis induced by alkylating chemicals (Dumenco et al., 1993; Gerson, 2004; Nakatsuru et al., 1993).

The cytosine methylation status of the promoter region of *MGMT* has recently become an indicator of glioblastoma response to alkylating agents such as temozolomide (discussed below) (Gerson, 2004; Weller et al., 2010). Patients with hypermethylated *MGMT* promoter express less MGMT and as a result respond better to alkylating agents (Esteller et al., 2000; Hegi et al., 2004). However, certain studies show that irrespective of treatment modalities, patients with a hypermethylated *MGMT* promoter have a better progression-free survival and overall survival (van den Bent et al., 2009; Wick et al., 2009). This observation was confirmed in the RTOG0525 clinical trial in which glioblastoma patients with a methylated *MGMT* promoter had an average overall survival of 21.2 months while patients with an unmethylated promoter had an overall survival of 14.0 months (unpublished data; abstract presented at ASCO May 19, 2011). This confirmed *MGMT* promoter methylation as a critical prognostic factor for glioblastoma patients.

III. Glioblastoma Treatment

The treatment of malignant gliomas has not changed greatly during the past decades, and is comprised of surgical resection of the main tumour mass, anti-proliferative chemotherapeutic agents, and ionising radiation directed to the tumour site and its

vicinities while sparing the unaffected and vital structures of the brain. Tumour resection is the first line of treatment in malignant gliomas and the extent of resection is mainly dependent on tumour mass accessibility and location. In a double-blind clinical trial, Stupp et al. demonstrated that the gross total resection of glioblastoma is associated with a favourable overall survival (Stupp et al., 2010). However, even with aggressive resections of the main tumour mass another tumour growth may recur proximal to the resection cavity or at considerable distances from the original mass (Dandy, 1933). Nonetheless, surgery is important where indicated because it allows the confirmation of the diagnosis by histopathological means, improves the symptoms related to tumour mass or tumour-associated edema, reduces steroid use, and decreases the number of cancer cells to be targeted by other treatment modalities (Barbagallo et al., 2008; Parlato et al., 2006).

Chemotherapy has not always accompanied malignant glioma treatment for two main reasons: First most chemotherapeutics fail to permeate the blood brain barrier (BBB) and reach the tumour mass. Second the select few drugs that make it across the BBB fail to show efficacy in high grade gliomas when compared to radiotherapy alone (Stupp et al., 2005; Walker et al., 1980). This limitation was circumvented with the advent of temozolomide (TMZ), a second generation nitrosourea-derived DNA alkylating agent which replaced the melanoma chemotherapeutic agent dacarbazine (DTIC) used in the 70's (Mizuno and Decker, 1976; Newlands et al., 1997; Stevens et al., 1987).

Temozolomide is a mono-functional alkylating chemical, stable at acidic pH, thus easily absorbed by the stomach and displays a good tissue distribution for treatments of central nervous system malignancies (Brindley et al., 1986).

Temozolomide preferentially targets purines (~85% of DNA methylation), particularly guanines at the N7 (~70%) and the O6 position (~5%) (Newlands et al., 1997). The cytotoxic response of cells to TMZ is mainly due to the O6-guanine methyl adduct (Bianchi et al., 1992; Catapano et al., 1987). In 1992 TMZ safety was assessed in a Phase I clinical trial treating melanoma and high grade glioma patients and it was found to be well tolerated (Newlands et al., 1992). The results of a Phase II clinical trial was published in which TMZ efficacy was compared to procarbazine in treating glioblastoma patients concluding that the primary endpoint, six-month progression-free survival rates of TMZ-treated patients, was met and the TMZ's efficacy was confirmed (Yung et al., 2000). However, it was only in 2002 that a Phase II clinical trial studying the efficacy of concomitant TMZ and radiotherapy followed by adjuvant TMZ treatment of glioblastoma patients showed benefits for these patients (Stupp et al., 2002). This pilot study paved the way for a Phase III clinical trial resulting from the joint effort of the European Organisation for Research and Treatment of Cancer (EORTC), Brain Tumor and Radiotherapy Groups, and the National Cancer Institute of Canada (NCIC) confirming the safety and efficacy of combined TMZ and radiotherapy and adjuvant TMZ treatment versus radiotherapy treatment alone (Stupp et al., 2005). This report was accompanied by a publication by Hegi et al. (Hegi et al., 2005) demonstrating that patients with *MGMT* promoter methylation benefitted the most from the trial's regimen, and confirmed by the recently completed trial RTOG0525 (unpublished data; abstract presented at ASCO May 19 2011).

IV. Medulloblastoma

Medulloblastoma (MB) is the most common pediatric brain tumour, characterised as a poorly differentiated mass of neuroepithelial origin associated with the cerebellum (Allen and Siffert, 1997; Ellison, 2002; Packer et al., 1999). Most MBs occur during the first two decades of life, but approximately one-third present (or are detected) during adulthood (Ellison, 2002). Perioperative care, imaging modalities, surgery, and aggressive post operative treatments of MB patients have improved the prognosis of the disease. However the disease remains lethal whereby only 50-70% of MB patients are alive five years after the original diagnosis (Wechsler-Reya and Scott, 2001). Many patients recur locally or with a metastasis, because similar to diffuse gliomas, MBs have an invasive behaviour which renders current therapies unsuccessful.

Data suggests that progenitor or stem cells from the external granule layer of the cerebellum may give rise to MBs as a result of genetic and epigenetic alterations (Yang et al., 2008). Several lines of evidence support the theory of the ‘medulloblast’ cell of origin: First immunohistochemical markers such as p75NTR, TrkC, Math1, and Zic1 (Buhren et al., 2000; Pomeroy et al., 1997; Salsano et al., 2004; Yokota et al., 1996) that specifically stain granule neuron precursor cells also stain at least a subset of MB tissue samples. In addition, stem or neural precursor cell markers such as Prominin1 and CD15 label a small population of a subset of medulloblastomas and are thought to be markers of cancer stem cells (Annabi et al., 2010; Barnes et al., 2009; Enguita-German et al., 2010; Read et al., 2009; Ward et al., 2009).

The most important genetic aberration in medulloblastoma patients is the small arm of chromosome 17, affecting over one-third of tumours (Bigner et al., 1997; Cogen and McDonald, 1996). However, although *TP53* also resides on 17p7.5, the chromosome 17p anomaly in medulloblastomas has been mapped closer to 17p11-13 (Kleihues et al., 2000; Scheurlen et al., 1997). Chromosomes 1q and 10q also display fragment losses in about one-third of medulloblastomas (Kleihues et al., 2000), but once again, although *PTEN* resides on 10q23, the 10q alterations in medulloblastomas are independent of *PTEN* and are mapped in the 10q25-26 regions.

Certain autosomal dominant familial syndromes give rise to medulloblastomas such as Gorlin (also called nevoid basal cell carcinoma), Turcot, and Li-Fraumeni syndromes, and their genetic studies have revealed pathways implicated in medulloblastoma genesis (Ellison, 2002). Gorlin patients have a *PTCH* mutation and develop several types of cancers and malformations including medulloblastomas (Ellison, 2002). The *PTCH* tumour suppressor gene encodes PTCH1, a key protein which is part of the Sonic-Hedgehog (SHH) signaling, which is a central player in embryo development and organ patterning (Hatton et al., 2010; Rohatgi et al., 2007) and more specifically in controlling the proliferation rate of cells of the external granule cells of the cerebellum (Wechsler-Reya and Scott, 1999). PTCH1 inhibits the transmembrane protein Smoothened (SMO), under physiological conditions, and PTCH1 interaction with SHH relieves its inhibition of SMO, leading to SMO activation and signaling through the Gli family of transcription factors to promote cellular proliferation (Rohatgi et al., 2007). Approximately 20% of sporadic medulloblastomas have alterations in the *PTCH* or other components of SHH signaling (Pietsch et al., 1997; Thompson et al., 2006). Mice deficient for one copy of

PTCH develop medulloblastoma-like tumours within 4-6 months and this delay in development is shortened when these mice are crossed with *TP53*-null mice (Goodrich et al., 1997; Hahn et al., 1998; Wetmore et al., 2001).

Gene expression profile studies have also increased our knowledge of medulloblastoma development. For instance in a very extensive study of different CNS embryonal tumours employing an expression array system, Pomeroy et al. demonstrated that medulloblastomas are distinct from malignant gliomas, primitive neuroectodermal tumours, and teratoid/rhabdoid tumours (Pomeroy et al., 2002). They also showed strong evidence in favour of the hyperactivity of the SHH pathway in a subset of medulloblastomas which confirmed studies on patients with Gorlin syndrome. Finally, using their expression array methodology, they were able to predict a favourable outcome in patients who's tumours expressed high levels of neurotrophin-3 receptor mRNA (Pomeroy et al., 2002). GDC-0449 is a novel systemic SHH pathway inhibitor that has proven efficacy in medulloblastoma preclinical models. In a case report published in 2009, Rudin et al. demonstrated a substantial, albeit temporary, response of a refractory medulloblastoma patient with multiple metastases to GDC-0449 (Rudin et al., 2009). This study confirms that targeting the SHH pathway may influence disease progression and add to the arsenal of therapies used in medulloblastoma patients.

Patients with Turcot's syndrome present gene alterations at the adenomatous polyposis coli (*APC*) locus, which leads to a hyperactive WNT signaling ultimately increasing the expression of genes involved in cell cycle progression such as *MYC* and *Cyclin D1* (Brocardo and Henderson, 2008; Hamilton et al., 1995). However, although Turcot patients are at risk for developing medulloblastomas, *APC* is seldom mutated in sporadic

medulloblastomas (Huang et al., 2000; Raffel, 2004) suggesting that APC's function, or other components of the WNT pathway, such as β -catenin or Axin1/2 may be aberrant in medulloblastoma biology (Baeza et al., 2003; Dahmen et al., 2001; Zurawel et al., 1998).

1.3 SLIT and ROBO Proteins

Mutations in the *Sli* gene were first reported in *Drosophila melanogaster* by Nüsslein-Volhard, Weischaus and Kluding (Wu et al., 2001) in *Roux's Archives of Developmental Biology*, while screening flies for pattern formation defects. Soon after, the product of *Sli*, D-Slit was characterised as a protein secreted by glial cells of the midline, which plays a key role in the bilateral development of the fly's nervous system (Rothberg et al., 1988). In 1999, three groups have independently identified Slit proteins as soluble secreted proteins, associated with the extracellular matrix, and involved in axon guidance and patterning (Brose et al., 1999; Kidd et al., 1999; Li et al., 1999).

The mammalian genome contains 3 *Slit* genes, *Slit-1*, *Slit-2*, and *Slit-3*. The expression of Slit1 is exclusive to the nervous system, while Slit2 and Slit3 are expressed in different organs. Slit proteins are secreted glycoproteins, containing from the amino to the carboxy-terminus: four leucine rich repeats (LRR) encompassed in four domains at the amino terminus, several EGF-like domains, a laminin-G motif, and a cysteine-rich domain (Figure I-5A). In mammals, Slit proteins can undergo proteolytic cleavage to yield two fragments: The N-terminal fragment Slit-N which contains the LRRs and is responsible for the repulsive/inhibitory function of Slits (discussed below), and the C-terminal fragment Slit-C (Nguyen Ba-Charvet et al., 2001) which localises to the mitochondria but the functional significance of Slit-C remains unknown (Little et al., 2001). Moreover although Slit is a soluble secreted protein, some of it is also found

interacting with matrix- or adhesion-associated proteins such as glypicans and syndecans (Hu, 2001; Liang et al., 1999; Ronca et al., 2001; Steigemann et al., 2004).

Roundabout (Robo) was also originally identified in *Drosophila* genetic screens, as a candidate responsible for guiding axons towards and away from the midline (Seeger et al., 1993). Robo proteins belong to the immunoglobulin (Ig) superfamily which comprises several cell adhesion molecules capable of homo- and hetero-philic dimerisation (Hivert et al., 2002). Mammals express four members of the Robo family. Robos 1-3 are expressed in the nervous system among other tissues, while Robo4, the most distant family member, is exclusively expressed in endothelial cells, including those of the nervous system vasculature (Legg et al., 2008; Park et al., 2003).

All Robos are single-pass transmembrane proteins with no known enzymatic function. They share structural similarities, including five Ig-like domains, three fibronectin III domains, a transmembrane domain, and four highly conserved cytoplasmic sequences (CC1-4; Figure I-5B) (Wu et al., 2001). In addition, the Robo message can be alternatively spliced, yielding short and long isoforms. The importance of this alternative splicing was especially exemplified in a recent paper by Chen et al. whereby two isoforms of Robo3, Robo3.1 and Robo3.2 were shown to possess opposite functions and antagonise each other (Robo3 isoforms' functional significance is discussed below) (Chen et al., 2008). Robo can also undergo proteolytic cleavage (Zallen et al., 1998) but the relevance of this process remains unknown.

Robo proteins are the primary receptors for Slit ligands and bind them with lower nanomolar (~ 1 -5nM) affinities (Brose et al., 1999). Moreover in mammals, crystal

structures of ligand-receptor interactions demonstrated that the second LRR of Slits is necessary and sufficient for binding the first (primary) and second (auxiliary) Ig domains of Robos (Morlot et al., 2007).

I. Slit-Robo in the Nervous System

Most nervous systems develop along a line of symmetry and axon guidance molecules such as Slit help establish this bilateral axis (Ypsilanti et al., 2010). The role of Slit-Robo signaling has been particularly well defined in studies of the ventral midline of the *Drosophila melanogaster* model system. Commissural neurons extend axons that cross the midline once and project on the contra-lateral side and never re-cross the midline (Wong et al., 2002). Slit is responsible for preventing the re-crossing of the commissural axons by repelling them once (and only after) they have crossed the midline (Battye et al., 1999; Stein and Tessier-Lavigne, 2001). In order to prevent premature repulsion or stalling of the commissural axons on the ipsi-lateral side, the surface Robo receptor density is downregulated thus leading to the silencing of its signaling (Keleman et al., 2005; Kidd et al., 1998a; Kidd et al., 1998b; Sabatier et al., 2004). In other regions of the nervous system, Slit2 message is also expressed. For example, Slit2 is expressed by differentiated glial cells in the midline of the septum, termed the glial wedge, causing the turning of callosal axons and repelling cortical axons, *in vitro* (Shu et al., 2003). In support of the latter report, Bagri et al. also observed callosal and thalamo-cortical projection abnormalities in *Slit1*; *Slit2* double null and their single knockout counterparts (Bagri et al., 2002).

i. Commissureless and Robo3

One question remains: How do Robo-expressing axons that are repelled by a source which secretes Slit proteins become temporally insensitive to Slit so that they can cross that same source that would otherwise repel them? The answer to that question came from studies on mutations that affect the axon path finding pattern by Corey Goodman's group (Seeger et al., 1993). In a genetic screen in *drosophila* aiming to identify mutations affecting axon guidance in the midline, they identified the gene *commissureless* (*comm*) whereby most CNS commissural axons of mutant flies failed to cross the midline, projecting on the ipsi-lateral side. This was in contrast with the *robo* mutation in the same paper where growth cones that would under wild-type conditions project on their own side crossed the midline. In later reports, Kidd et al. showed that *comm* overexpression phenocopied *robo* loss, and this phenotype was due to a decrease in Robo protein expression as assessed by anti-Robo staining (Kidd et al., 1998b). Soon after Barry Dickson's lab elegantly demonstrated that Comm expression is required in commissural axons crossing the midline, that Comm physically associates with Robo (immunofluorescence and immunoprecipitation performed in Cos-7 cells), and that Comm facilitates Robo's translocation to the late endosomes and lysosomes, thus preventing its return to the cell surface (Rajagopalan et al., 2000). Myat et al. went on to dissect the molecular aspects of Comm activity by linking the Robo sequestering function of Comm to its intracellular portion and by identifying the *Drosophila* homologue of Nedd4 (DNedd4) as an important effector of Comm (Myat et al., 2002). However the *in vivo* relevance of DNedd4 in axon guidance has been challenged by Dickson's group (Keleman et al., 2005). Furthermore, Dickson's group provided *in vivo* evidence

suggesting that Comm blocks retrograde Robo trafficking along commissural axons, destined to the growth cone (Keleman et al., 2005).

Intriguingly, the *comm* gene is not conserved in mammals and therefore another mechanism must perform Comm's function to silence Robo's repulsive effects during midline crossing. Several hypotheses can be put forward to predict how axons are capable of crossing a source of repellent cues: First, because projecting axons are exposed to a myriad of cues, both attractive and repulsive, axons crossing a source of repellent cues may witness more attractive than repulsive stimuli and thus the net stimulatory effect is an attractive one. Second, Robo receptors interact with DCC genetically and physically (Stein and Tessier-Lavigne, 2001; Yu et al., 2002) and such interactions may play a role in modulating the repulsive signals of Robo. Indeed there is biochemical evidence supporting the role of Robo as a silencer of DCC, and the reverse may also be true (Stein and Tessier-Lavigne, 2001). Third, the differential expression, or spatial localisation of accessory proteins or co-receptors may also dictate the signal propagation of the Slit-Robo axis. Finally post-transcriptional and -translational modulation of Robo proteins may also dictate the Slit binding affinity and its repulsive features.

In 2004, a paper from Tessier-Lavigne's group demonstrated that commissural axons from mice lacking both copies of *Robo3*, whose product is highly expressed in axons prior to crossing the midline, failed to cross the floor plate (Sabatier et al., 2004) because they respond to Slit repellent cues prematurely. Thus Robo3/Rig-1 may partially fulfill the function of Comm in mammals for three reasons: First Robo3 protein is expressed in commissural axons preceding and reaching the midline but it is undetectable once axons cross the midline. Second *Rig-1* homozygous null commissural axons fail to cross the

floorplate and are prematurely responsive to Slit. And finally this phenotype was partially rescued with *Robo3*; *Robo1* double knockouts, *Robo3*; *Robo2* double knockouts, and *Robo3*; *Slit1*; *Slit2* triple knockouts, suggesting that Rig-1 antagonises Slit-Robo function (Sabatier et al., 2004). In a follow-up paper, Tessier-Lavigne group reported results favouring the transcriptional control of *Robo3* as a major mechanism to modulate Slit-mediated repulsion (Chen et al., 2008). In this report, the authors show that mouse *Robo3* is transcribed into two isoforms, Robo3.1 and 3.2, resulting from the alternative splicing of exon 27. The isoforms possess antagonistic effect on Slit-Robo signaling, whereby Robo3.1, expressed at a pre-crossing stage, silences Slit-Robo repulsion, while Robo3.2, expressed after crossing the floor plate assists the repellent effect of Slits (Chen et al., 2008).

The importance of Slit-Robo signaling axis in humans was also illustrated in 2006, when a genetic analysis of a rare human autosomal recessive disorder called horizontal gaze palsy with progressive scoliosis (HGPPS) revealed that chromosome 11q23-25, where *ROBO3* resides is mutated at 10 different codons (Jen et al., 2004). Nine mutations resided in the extracellular portion of ROBO3, namely in the Ig-like domains (five missense mutations) and the fibronectin III domains (three missense and one nonsense mutations). The remaining mutation was a nonsense mutation located 3' of the third conserved cytoplasmic motif. This report showed a severe phenotype resulting from mutations in a single gene involved in the Slit-Robo signaling pathway and outlined the importance of this pathway in hindbrain axon midline crossing.

ii. Genes and signaling pathways related to the Slit-Robo phenotypes

There are many genes identified in axon guidance model systems such as the fruit fly that interact with *Slit* and *Robo*. Sun et al. identified two genes expressing receptor-linked protein tyrosine phosphatases DPTP10D and DPTP69D that pheno-copied *Slit* and *Robo* mutations in *Drosophila* (Sun et al., 2000). Fritz et al. employed genetics and pharmacological means to identify *son of sevenless* (encoding Sos, a GEF involved in Ras signaling) as a potentiator of the *slit* phenotype and validated calmodulin as an effector of Slit-Robo signaling, upstream of Sos (Fritz and VanBerkum, 2000). They showed that *Slit; sos* double heterozygous have a higher proportion of severe axon guidance defects than *slit* alone. Yang et al. built on the latter report by demonstrating that Sos' GEF activity during midline axon repulsion targets Rac GTPases, independent of its Ras-GEF function (Yang and Bashaw, 2006). Bashaw et al. identified two key proteins, Enabled (Ena) and Abelson (Abl), as downstream players of Slit-Robo signaling in *drosophila*. They demonstrated direct Ena interaction with Robo's CC1 and CC2 domains, and Abl interaction with Robo's CC3 domain. Furthermore, by expressing a constitutively active form of Abl, lacking its SH3 domain, the authors observed Robo phosphorylation on multiple cytoplasmic tyrosines in the CC domains. Finally they were able to rescue *robo*'s axon mistargeting phenotype by expressing a CC1-truncated Robo in a *robo* background (Bashaw et al., 2000). Rhee et al. built on the latter findings by identifying N-Cadherin (NCAD) as a binding partner of Robo, and spatially and functionally localising it to a multi-protein complex which also includes Abl (Rhee et al., 2002). The authors used a myriad of biochemical approaches to demonstrate that upon Slit-Robo interaction, the homophilic interaction of NCAD is abolished, and Robo's effect on NCAD is dependent on its CC3 domain, confirming Abl's importance in that

complex. The disruption of the NCAD adhesion leads to β -catenin tyrosine phosphorylation, which ultimately causes the dissociation of the cadherin-catenin-cytoskeletal interactions. Finally a BCR-ABL tyrosine kinase inhibitor silences the Slit-Robo effect on NCAD adhesion. In a follow up paper, Rhee et al. identified Cables as another member in the Slit-Robo-NCAD-Abl- β -catenin complex and showed that it interacts directly with β -catenin and potentially facilitates its phosphorylation by Abl (Rhee et al., 2007). The authors noted that knocking down Cables silences the Slit-Robo effect on NCAD, and is therefore an important effector of Slit-Robo signaling. Functionally, Slit-dependent NCAD dissociation gives rise to β -catenin nuclear translocation, which leads to Tcf/Lef-association and downstream transcription of Tcf/Lef-dependent gene expression.

Somewhat analogous to axons, neural stem cells and precursor cells need to travel long distances from their site of genesis to their destination where they will differentiate and participate in the development of the tissue. To do so, they may be guided by the same cues as axons and thus they may express similar underlying mechanisms of migration as neuronal axons. For instance, during the mammalian forebrain development, neuronal precursor cells originating from the anterior subventricular zone (SVZa) migrate along the rostral migratory stream toward the olfactory bulb where they form interneurons (Kidd et al., 1998a; Nguyen-Ba-Charvet et al., 2004). The choroid plexus and the septum are regions known to secrete repellent cues and *in vitro* and *in vivo* experiments from *Slit* knockout animals confirmed that Slit proteins are in part responsible for repelling neural precursor cells originating from the SVZa (Hu, 1999; Kaneko et al., 2010; Kidd et al., 1998b; Nguyen-Ba-Charvet et al., 2004; Zou et al., 2000). Similar phenotypes were noted

in precerebellar neurons of the inferior olive and lateral reticular nuclei (Causeret et al., 2002; Causeret et al., 2004; Di Meglio et al., 2008; Gilthorpe et al., 2002), vertebral cranial ganglia sensory neurons (Shiau et al., 2008), invertebrate peripheral nervous system sensory precursor cells (Orgogozo et al., 2004), and invertebrate segment-specific sensory neurons (Kraut and Zinn, 2004).

iii. SrGAPs identification

In a two-hybrid screen for Robo1 binding partners, and potential effectors, Wong et al. uncovered a family of Rho GTPase activating proteins (GAPs) and named them Slit-Robo (sr) GAPs (Wong et al., 2001). The authors went on to demonstrate the srGAP is a family of GAPs that has three members, srGAP1-3, and all three srGAP proteins possess highly homologous RhoGAP and SH3 domains, while srGAP1 and 2 also contain a Fes/CIP4 homology (F-BAR) domain. The carboxy-terminal of srGAPs, which includes the SH3 domain, is necessary and sufficient to bind the CC2 and especially the CC3 motif of Robo1. These results were confirmed soon after when the SH3 domain of srGAP1 was crystallised at a resolution of 1.8Å and its interaction with the CC2 and CC3 domains of Robo1 confirmed by surface plasmon resonance (Li et al., 2006). Expression studies of srGAPs show that srGAP1 protein is present in the brain, lung, and spleen of rats. Moreover, srGAPs 1 and 2 have an mRNA expression pattern similar to Robo1 in the CNS, and messages of srGAP1 and 2 are detected in nervous system regions known to harbour migratory precursor cells and neural axons that are repelled by Slits, such as the anterior subventricular zone (SVZa), olfactory bulb, cortical plate of the neocortex, and retinal ganglion cells (Guerrier et al., 2009; Wu et al., 1999; Yao et al., 2008). In mice, srGAP3 message is highly expressed in many CNS structures of mice embryos and

its pattern of expression progressively diminishes during development and becomes restricted to the cortical structures and the hippocampus by adulthood (Waltereit et al., 2008). Moreover Yao et al. reported that srGAPs localise to the cytoplasm of young rat neurons but older neurons display a nuclear immunoreactivity suggesting that srGAPs may have a dual role during neurogenesis. In early stages of development srGAPs control the neural precursor migration and axon guidance via their cytoplasmic localisation, and in later stages of development srGAPs are involved in pro-differentiation events via their nuclear localisation.

The affinity of srGAPs for Rho GTPases is Slit-dependent. In coimmunoprecipitation assays, Wong et al. demonstrated that srGAP1 is a GAP for RhoA and Cdc42, but not Rac1, and its affinity for RhoA and Cdc42 diminishes and increases, respectively, when cells are treated with recombinant Slit (Wong et al., 2001). The interaction with Cdc42 and RhoA were confirmed by Rho GTPase activity assays demonstrating that srGAP1 decreases the activity of Cdc42 and RhoA in presence of Slit. Interestingly, another report showed contrasting GAP activity for srGAP3, demonstrating its activation of the GTPase activity of Cdc42 and Rac1, but not RhoA (Endris et al., 2002). The function of srGAPs in neural cell migration was also assessed whereby the transduction of a GAP-truncated form of srGAP1 (lacking GAP activity) into neural precursor cells suppressed the repellent effect of Slit in a SVZa explants assay (Wong et al., 2001).

iv. SrGAPs functions

In 2004, Madura et al. observed an increase in srGAP2 message in a facial nerve axotomy model in rats and noted that srGAP2 mRNA expression peaks at seven days after nerve ablation (Madura et al., 2004). Mattar et al. noted altered srGAP3 mRNA

levels (among other differentially expressed genes) in the ventricular zone and preplate neurons of E13.5 mice mutant for the pro-neuronal transcription factors Neogenin 1 and 2 (Mattar et al., 2004). Soon after, Yang et al. demonstrated the cellular function of SrGAP3 as a cytoskeleton remodeling protein, employing the neuroblastoma SH-SY5Y cell line (Yang et al., 2006). The expression of srGAP3 in the neuroblastoma cell line markedly diminished plasma membrane protrusions, inhibited focal adhesion complexes, and led to a loss in actin and tubulin dynamics, especially at the leading edge of the cell. In accordance with the subcellular phenotypes observed, srGAP3 expression led to a decrease in cellular migration capabilities (Yang et al., 2006). However srGAP2 expression in Cos-7 cells led to an increase in filopodia formation and this effect was dependent on the F-BAR domain of srGAP2 (Guerrier et al., 2009). Guerrier et al. also tested the expression of srGAP2 in E15 cortical progenitor cells and observed an increase in filopodia-like membrane protrusions. The authors hypothesised a role for srGAP2 in neuronal migration and went on to demonstrate that srGAP2 knock down in radial glia progenitors from E15 mice results in an increase in the number of neurons at the cortical plate (destination of the radial glia progenitors) and a corresponding decrease in the number of neurons in the intermediate zone (origin of the radial glia progenitors).

The molecular mechanism of the migratory function of srGAP2 is complex. First, srGAP2's impact on migration is dependent on the methylation status of its arginine at position 927 (in human) whereby only the methylated form of srGAP2 is capable of localising to the plasma membrane, promoting cell spreading, and inhibiting cell migration (Guo and Bao, 2010). Second, srGAP2 silences the signal transduction of Rac proteins by activating the GTPase catalytic function of Rac (thus inactivating Rac), and

by binding to formin-like 1 (FMNL1), an effector of Rac proteins, to oppose FMNL1's function (Mason et al., 2011).

The relevance of srGAPs in human pathology was demonstrated by Endris et al. in 2002. In a case report of a patient with severe mental development delay, the authors have reported a breakpoint on chromosome 3, mapping the genetic aberration to the exon 3 of srGAP3 (Endris et al., 2002) leading to its transcriptional interruption. The authors suggest that srGAP3's high expression in important cognitive structures such as cortical and hippocampal neurons may explain the cognitive impairments of the patient in question, once again reiterating the importance of Slit-Robo signaling in neurodevelopment (Endris et al., 2002).

II. Slit-Robo Outside the Nervous System

i. Slit-Robo and immune cells

Slit2 and 3 are expressed outside the CNS during development and adulthood, suggesting that Slit proteins play roles in events unrelated to the genesis of the nervous system (Kidd et al., 1999). The first instance where Slit-Robo signaling was reported outside the nervous system was in leukocyte biology. Immune cells are extremely sensitive to the signaling cues present in their environment and they respond to a chemical cue gradient via chemotaxis (Rao et al., 2002). Slit proteins were the first repellent chemotaxis cues identified in leukocyte chemotaxis and biochemical experiments confirmed that the Slit-Robo signaling occurs via G-protein coupled receptors, and may also occur via other

pathways (Rao et al., 2002; Tole et al., 2009). This challenged the model by which only G-protein coupled receptors are involved in leukocyte chemotaxis (Murphy, 1994).

ii. Tooth development

Slit-Robo signaling has also been implicated in the development of other tissues and organs. Løes et al. reported that Slit1 message is detected in the primary and secondary enamel knots of molar teeth of mice (Loes et al., 2001). A complimentary expression of Slits 2 and 3 and Robos 1 and 2 mRNAs were detected in the mesenchymal cells of teeth during the early stages of tooth development. The expression pattern of Slits and Robos seems tightly modulated during each stage of molar tooth development, suggesting a developmental role for Slit-Robo signaling in tooth development. Lu et al. reported a case of an individual with a genetic translocation disrupting the *Robo2* gene who presented with lower incisor anomalies among other phenotypes, which also included vesicoureteral reflux (Lu et al., 2007).

iii. Trachea development

During *drosophila* tracheal development, epithelial cells respond to the CNS midline cues such as Slits and Englund et al. described that tracheal epithelium expresses Robo and Robo2 proteins and mutations in Slit or Robos leads to aberrant tracheal epithelium development. It is interesting that Slit seems to act as an attractant of tracheal cells and this effect is Robo2-dependent (Englund et al., 2002).

iv. Kidney development

The expression of Slit and Robo genes has also been observed during mouse kidney development whereby different cellular component of nephrogenesis and urogenital development produce the Slit ligands and Robo receptors (Piper et al., 2000).

Grieshammer et al. built on the latter report by analysing *Slit2* and *Robo2* homozygous

knockout kidney development, and noted that the collecting ducts and ureters are dilated and contained multiple ureters (Grieshammer et al., 2004). The authors also notice that the phenotypes' severity diminishes when mice are crossed with a heterozygous *Gdnf*, suggesting that the Slit-Robo axis antagonises the attractive cue GDNF. In Lu et al's report (mentioned above) the individual with *Robo2* disruption presented with a urogenital anomaly called vesicoureteral reflux (Lu et al., 2007), and another report identified *Robo2* point mutations in 4 patients in a cohort of 78 individuals with vesicoureteral reflux (Bertoli-Avella et al., 2008). Both reports confirm the important role of Slit-Robo expression and signaling in human kidney development.

III. Slit-Robo in Cancer

The role of Robo in cancer was first suspected when Robo4 was identified and described as a Robo homologue with an expression pattern restricted to the endothelial component of vasculature (Huminiacki et al., 2002; Park et al., 2003). Several groups reported that Robo4 enhances neo-vascularisation (Bedell et al., 2005; Kaur et al., 2006; Suchting et al., 2005) and that perhaps Robo4 could serve as a pathological marker of tumour angiogenesis in tissue and serum in different cancer models (Gorn et al., 2005; Seth et al., 2005; Wang et al., 2003). However, two recent reports provided an alternative explanation for Robo4's function, suggesting that it plays a role in maintaining the homeostasis and integrity of normal vascular components and vascular genesis while it prevents pathological angiogenesis and vessel leakage in response to angiogenic factors

such as VEGFs (Jones et al., 2008; Shibata et al., 2009). The anti-angiogenic effect of Robo4 signals primarily via the inhibition of Src family kinase activation.

The promoter hypermethylation of *SLIT* genes has also been reported as an epigenetic event in numerous human cancers. In a series of reports, Farida Latif's group identified the chromosome 4p15.2 locus, encoding SLIT2 as a hotspot for CpG hypermethylation in glioma, carcinoma (breast, lung, colorectal), and leukemia cell lines and tumour specimens (Dallol et al., 2002; Dallol et al., 2003; Dunwell et al., 2009). Their study was confirmed and expanded by other groups who analysed the epigenetic status of *SLIT2*, as well as other Slit and Robo genes, in other tumour cell lines and specimens such as neuroblastomas, Wilms' tumours, renal cell, prostate, hepatic, mammary, cervical, and ovarian cancers (Astuti et al., 2004; Jin et al., 2009; Narayan et al., 2006; Sharma et al., 2007; Singh et al., 2007; Yu et al., 2010). These results confirm that the epigenetic control of Slits and Robos may be important in tumour development and progression.

Because Slit proteins repel neural precursors and axons, as well as leukocytes, we and others hypothesised that Slits can also repel cancer cells of the CNS. We reported for the first time that invading medulloblastoma cells are inhibited by Slit proteins by employing a variety of tumour cell invasion models (Werbowski-Ogilvie et al., 2006). We also showed that Slit's inhibitory effect is Robo-dependent and signals through the downregulation of Cdc42, a member of the Rho GTPase family. Soon after, several groups reported similar findings in glioma cell invasion (Mertsch et al., 2008; Yiin et al., 2009b), fibrosarcoma and squamous cell carcinoma tumour growth and metastases (Kim et al., 2008), non-transformed epithelial cell migration (Stella et al., 2009), and breast carcinoma growth (Marlow et al., 2008). Therefore several models confirm that Slit

proteins, or analogues based on the LRR motifs of Slits may serve as a powerful tool to inhibit tumour cell dissemination, invasion, and metastasis.

Chapter 2: SLIT Proteins Inhibit Brain Tumour Cell Invasion

2.1 Summary

Malignant gliomas, the most common brain tumours in adults, and medulloblastoma, the most common malignant brain tumour in children are characterised by extensive cellular proliferation and invasion. The failure of present therapies to control the invasive nature of these types of human brain cancers results in significant patient morbidity and mortality. Our studies have therefore focused on the invasive properties of cells derived from human and murine malignant gliomas and human medulloblastomas.

Recent evidence suggests that molecules known for their role in neurodevelopment are also linked to tumorigenesis. We hypothesised that brain tumour cells would respond to the same developmental cues that neural stem cells and precursor cells do during neurodevelopment. To test our hypothesis, we evaluated the effect of several developmental cues on two medulloblastoma and five glioma cell lines.

Using a collagen type I invasion assay, we demonstrate that Slit2 and Sema3a axon guidance cues are capable of inhibiting the invasion of the medulloblastoma cells.

Focusing on Slit2, we show that it decreases the overall distance of medulloblastoma cell invasion. Using an MTT proliferation assay, we confirm that Slit2 had no statistically significant effect on medulloblastoma or glioma cell proliferation. We also provide quantitative real-time PCR levels of mRNA of Slit and Robo families in multiple glioma and medulloblastoma cell lines. We have also performed Robo1 overexpression studies in

glioma cell lines that do not respond to Slit2 to assess whether we can experimentally render them responsive. We provide evidence suggesting that the medulloblastoma cell lines that respond to Slit2 decrease their Cdc42 and Rac activity while the glioma cell lines tested did not. We also show that low-to-moderately invasive glioma cell lines are inhibited by Slit2.

We have tested the transcriptional modulation of Slit2 in U251 glioma and UW3 medulloblastoma cells. We report that Slit2 treatment decreases the expression of a series of genes involved in cancer cell invasion in UW3 but has no transcriptional effect in U251. One of the Slit2 transcriptional targets, *MMP14* is further characterised. We present biochemical evidence in support of rRobo1 being a MMP14 substrate, cleaved at several sites by the membrane-bound MMP. The result of this proteolysis is an amino-terminal fragment that retains Slit2-binding capabilities, and we predict that when cleaved and soluble, this amino-terminal fragment sequesters Slit2 in physiological and pathological contexts.

Finally we demonstrate that non-responsive glioma cells can be rendered responsive to Slit2 by downregulating MMP14 expression, and that MMP14 knock down in C6 cells using a shRNA_{miR} approach decreases their invasion capabilities and renders them more susceptible to cell death when treated with cytotoxic compounds such as temozolomide, the standard chemotherapy in glioblastoma treatment.

2.2 Results

Slit2 and Sema3a inhibit medulloblastoma cell invasion.

Malignant tumour cell invasion is the most important cause of cancer recurrence and death, so our laboratory's aim has been to find novel compounds to inhibit cancer cell invasion. It is generally accepted that tumour biology mirrors many facets of development, thus we decided to test the effect of proteins relevant in neurodevelopment on malignant brain tumour cell invasion, with the hypothesis that brain tumour cells would respond to the same proteins as their neural cell counterparts. To this end, we tested the effect of NETRIN1, SLIT2, SDF1, SEMA3A, IGF1, EGF, and FGF2 on malignant brain tumour invasion. Invasion was assessed in a collagen type I invasion assay, and three different concentrations of each protein were assayed.

NETRIN1, SDF1, IGF1, EGF, and FGF2 significantly increased the invasion rate of at least one cell line and at least one concentration tested (Table 1 and Figure 1). The increase in invasion ranged between 1.15 fold to 1.6 fold, with UW3 medulloblastoma cells displaying the highest increase in invasion in response to EGF and IGF1 (Figure 1A). Because the aim of this screen was to identify compounds that decrease invasion, pro-invasive compounds were not studied further.

SLIT2 and SEMA3A had no statistically significant effect on the invasion rate of U251 and C6 glioma cell lines at any of the concentrations tested (Figure 1C and 1D). At 50 ng/ml, SLIT2 had no effect on the invasion rate of UW3 and DAOY (Figure 1A and 1B). However, SLIT2 caused a statistically significant decrease in the invasion rate of UW3

and DAOY medulloblastoma cell lines at higher concentrations, namely 100 ng/ml and 200 ng/ml (Table 1 and Figure 1). The decrease in UW3 medulloblastoma invasion was $28.4 \pm 3.1\%$ and $30.3 \pm 4.4\%$ at 100 ng/ml and 200 ng/ml, respectively (Figures 1A). In DAOY medulloblastoma invasion, SLIT2 decreased the invasion by $23.0 \pm 5.7\%$ and $32.1 \pm 4.2\%$ at 100 ng/ml and 200 ng/ml, respectively (Figure 1B). SEMA3A decreased UW3 invasion by $17.8 \pm 4.3\%$ and $18.1 \pm 4.4\%$, at 100 ng/ml and 200 ng/ml, respectively (Figures 1A). In DAOY, SEMA3A decreased the invasion by $12.3 \pm 4.6\%$ and $10.9 \pm 5.0\%$ at 100 ng/ml and 200 ng/ml, respectively (Figures 1B).

Because SLIT2 had a higher inhibitory effect on medulloblastoma cell invasion than SEMA3A, we decided to focus on SLIT2. Therefore all experiments hereafter relate to the effect of SLIT2 on brain tumour cells.

SLIT2 does not affect brain tumour cell proliferation rate.

Dallol et al. have reported *Slit2* as a tumour suppressor gene (Dallol et al., 2003) without providing an anti-proliferative function for Slit proteins. Since the collagen type I invasion assay spans several days, and because anti-proliferative compounds can indirectly decrease the invasion rate of brain tumour cells, we tested whether the anti-invasive effect of recombinant hSLIT2-myc was due to an anti-proliferative effect. To address this question, we performed an MTT proliferation assay (Figure 2). We observed no statistically significant difference in the proliferation rates of the U251 and C6 glioma cell lines (Figure 2A and 2C) nor in the UW3 and DAOY cell lines (Figure 2B and 2D) when treated with 100 ng/ml of hSLIT2-myc or with a mock treatment. The doubling-times of hSLIT2-myc and mock treated U251 cells were $23.6 \pm 0.4\text{h}$ and $23.3 \pm 0.5\text{h}$ respectively. The doubling-times of hSLIT2-myc and mock treated C6 cells were $20.3 \pm$

0.4h and 20.1 ± 0.3 h, respectively. The doubling-times of hSLIT2-myc and mock treated UW3 were $24.8\text{h} \pm 0.4\text{h}$ and $24.5 \pm 0.4\text{h}$, respectively, when treated with 100 ng/ml of hSLIT2-myc or with a mock treatment (Figure 2B and 2D). Similarly, the doubling-times of hSLIT2-myc and mock treated DAOY were $24.7 \pm 0.3\text{h}$ and $24.5 \pm 0.6\text{h}$, respectively (Figure 2B and 2D).

Therefore, we conclude that hSLIT2-myc, at a concentration of 100 ng/ml, does not have a statistically significant anti-proliferative effect on the glioma and medulloblastoma cell lines tested. We also did not observe a significant anti-proliferative effect of hSLIT2-myc at a higher concentration of 200 ng/ml (Appendix 1). Therefore we can conclude that the inhibitory effects of Slit2 on medulloblastoma cell invasion observed in our experiments are channeled through invasion mechanisms.

Slits and Robos are expressed in all the glioma and medulloblastoma cell lines tested.

Our original observations suggested that only the medulloblastoma cell lines tested responded to Slit2 and that glioma cell lines were unresponsive. As a potential explanation for these findings we hypothesised that glioma cells may not express Robo receptors or may not be sensitive to Slits. Alternatively, glioma cells may express the Robo3.1 variant which antagonises the Slit-Robo signaling pathway (Chen et al., 2008). To test the first hypothesis we evaluated the levels of Slit and Robo expression in our cell lines. At the time, there were no available commercial antibodies against the different members of Slit and Robo proteins capable of detecting endogenous proteins. Therefore we opted to evaluate Slit and Robo expressions at the mRNA level by quantitative real time RT-PCR (qRT-PCR). Our analysis (ANOVA) of Slit mRNA expressions revealed

no statistically significant difference between glioma and medulloblastoma cell lines (Figure 3A). Likewise, there were no statistically significant differences in Robo mRNA expression between glioma and medulloblastoma cell lines (Figure 3B). When we tested the levels of Robo3.1, we did not observe a significantly different expression pattern between the glioma and medulloblastoma cell lines assessed (Figure 3B).

In summary, the expression pattern of Slits and Robos tested are comparable between the hSLIT2-myc responsive medulloblastoma cell lines and the hSLIT2-myc nonresponsive glioma cell lines. Therefore the difference in response between the medulloblastoma and the glioma cell lines cannot be explained by a difference in expression pattern of Slits, Robos, or the differential expression of the Robo3.1 isoform.

U251 cell line engineered to overexpress Robo at the surface remains unresponsive to SLIT2.

In our study, medulloblastoma cell lines respond to recombinant Slit2, while gliomas cell lines do not, even though they express similar levels of Slit and Robo mRNAs. To further understand the mechanism(s) governing this difference in response, we engineered U251 stable cells overexpressing rRobo1-HA. We confirmed that U251 cells stably transduced with rRobo1-HA properly target rRobo1-HA at the cell surface by performing a cell surface biotinylation assay (Figure 4A). Then we tested whether U251-rRobo1-HA cells would respond to hSLIT2-myc in a collagen invasion assay. We observed that when U251 glioma cells overexpressed Robo1 at the cell surface, they remained resistant to the inhibitory effects of hSLIT2-myc in a wound healing migration assay (scratch assay) and a collagen type I three-dimensional invasion assay (Figure 4B and 4C, respectively). We wanted to confirm that rRobo1 overexpression can render hSLIT2-myc resistant cells

sensitive. Therefore we overexpressed rRobo1-HA in HeLa cells (Figure 4D) whose migration is not inhibited by hSLIT2-myc (Figure 4E). When treated with hSLIT2-myc, HeLa cells expressing rRobo1-HA at the cell surface (Figure 4D) migrate¹ significantly less than the same cells treated with mock conditioned media (Figure 4E). Comparing the exogenous rRobo1-HA message levels in U251-rRobo1-HA and HeLa-rRobo1-HA cells, we noted that even when HeLa cells expressed significantly less rRobo1-HA (~20% less), they responded to hSLIT2-myc and their migration was significantly inhibited by it (Figure 4F).

These experiments demonstrate that the lack of Slit2 response is not attributed to the expression of Robo proteins, or to an aberrant targeting of Robo at the cell surface.

Therefore we decided to investigate intracellular signaling pathways.

SLIT2 inhibits Cdc42 and Rac in medulloblastoma but not glioma cell lines.

Studies have shown that the Rho GTPases Cdc42 and/or Rac1 play an important role in propagating the repulsive effects of Slit proteins (Wong et al., 2001). Therefore to assess the role of Rho GTPases in brain tumour cell invasion inhibition by recombinant Slit2, we grew monolayer cultures and treated them with recombinant hSLIT2-myc (100 ng/ml) or mock treatment and carried out an active Rho GTPase pulldown assay (Figure 5A-D). These pulldown assays revealed that the activity of Cdc42 decreased by $36.4 \pm 6.0\%$ in the UW3 medulloblastoma cell line, which is responsive to hSLIT2-myc (Figure 5B). These experiments also revealed that the activity of Rac decreased by $29.8 \pm 19.0\%$ in the UW3 cell line (Figure 5C). However, the activities of Cdc42 and Rac showed no

¹ HeLa cells do not form spheroids, therefore we used a scratch assay to quantify cell migration.

significant change in the C6 glioma cell line, confirming that in this cell line Cdc42 and Rac levels are not altered in response to exogenous Slit2 (Figure 5B/C). In both cell lines, the activity of Rho showed no significant change (Figure 5D).

We have also performed G-LISA assays on U251 and C6 glioma and DAOY and UW3 medulloblastoma cell lines (Figures 5E/F), an assay that is fast, reproducible, and quantitative. We have observed a decrease of $52.4 \pm 7.4\%$ and $42.8 \pm 5.1\%$ in Cdc42 activity in UW3 and DAOY, respectively (Figure 5E). Also, we have observed a decrease of $28.6 \pm 3.9\%$ and $16.5 \pm 13.4\%$ in Rac activity in UW3 and DAOY, respectively (Figure 5F). However, the effect of hSLIT2-myc on the Rac activity of DAOY was not significant, but approached statistical significance ($p = 0.094$).

Our results confirm our observations of the Rho GTPase pulldown assays, in that Cdc42 and Rac activities are significantly decreased in response to hSLIT2-myc treatment only in the medulloblastoma cell lines tested, which are sensitive to hSLIT2-myc treatment. The Rac and Cdc42 activities of U251 and C6 glioma cell lines are not significantly altered when these cells are exposed to 100 ng/ml of hSLIT2-myc.

SLIT2 inhibits glioma cell lines that have low-to-moderate invasive capabilities.

Because our findings suggest that Cdc42 and Rac may play an important role in propagating Slit-Robo signaling, and also because our UW3 and DAOY medulloblastoma cell lines have lower invasive capabilities than the two glioma cell lines tested previously (U251 and C6), we hypothesised that exogenous hSLIT2-myc inhibits brain tumour cells that have low to moderate invasive capabilities (i.e., cell lines that have an invasive capacity of 100-300 μm after 3 days, in a collagen invasion assay).

Therefore we have tested the effect of 100 ng/ml of hSLIT2-myc on the invasion rate of other glioma cell lines that are less invasive than U251 and C6 (Figure 6). Our results demonstrate that the glioma cell lines U343 and U373 had their invasion rate inhibited by hSLIT2-myc at rates of $24.6 \pm 3.8\%$ and $21.6 \pm 3.4\%$, respectively, and this effect was statistically significant (Figure 6). However, the U87 glioma cell line, which is much more invasive, with invasive rates resembling that of U251, did not have a statistically significant response to hSLIT2-myc.

These results demonstrate that in addition to the medulloblastoma cell lines the glioma cell lines that have low to moderate invasive capabilities in a collagen 3D invasion assay are inhibited by exogenous hSLIT2-myc treatment.

SLIT2 modulates the expression pattern of genes responsible for the invasive paradigm of UW3 cell.

The anti-invasive effects of hSLIT2-myc on UW3 and DAOY, as well as on U343 and U373 cell lines, is prolonged and sustained, because we observe a significant decrease in invasion as early as the third day of recombinant hSLIT2-myc treatment, and the anti-invasive effect remains significant up to 10 days as shown previously in this model (Werbowski-Ogilvie et al., 2006). Because of this sustained effect, we hypothesised that hSLIT2-myc has an inhibitory effect that is initially channeled through cytoplasmic effectors (such as the down regulation of Cdc42 and Rac; see Figure 5), and that sustained hSLIT2-myc treatment alters the transcriptional response of invasive cells by decreasing the expression of pro-invasive genes and/or increasing the expression of anti-invasive genes. To test this concept, we have decided to study the expression pattern of

UW3 medulloblastoma cell line and U251 glioma cell line in response to a 24h treatment of hSLIT2-myc, at 100 ng/ml.

Before testing this hypothesis, we have decided to devise a novel hSLIT2-myc purification method since published methods of hSLIT2-myc purification include long procedures such as gel chromatography and dialysis steps (Kidd et al., 1998a; Nguyen-Ba-Charvet et al., 2004). We took advantage of a high pressure liquid chromatography (HPLC) method, which is fast and reliable to purify recombinant hSLIT2-myc from conditioned media (Figure 7). We used a preparative heparin column with 5ml volume capacity, since Slit-Robo interaction is heparin sulfate dependent (Fukuhara et al., 2008; Hussain et al., 2006) and it was biochemically purified from bovine brain by heparin-sepharose column liquid chromatography (Wang et al., 1999) . Using this HPLC method, we bypassed the lengthy overnight gel chromatography and the overnight dialysis steps previously reported. This shortened the procedure from 3 days to 3h (Figure 7). The elution spectrum of hSLIT2-myc was well resolved, eluting at 37 min (Figure 8A). The purity of recombinant hSLIT2-myc was also excellent as assessed by gel Coomassie stain (Figure 8B) yielding a purity greater than 88% as estimated by Coomassie signal densitometry. Typical yields would range between 2-4 mg of purified hSLIT2-myc per 1litre of conditioned media.

The activity of the purified recombinant hSLIT2-myc was tested in a collagen matrix invasion assay whereby the invasion rate of UW3 cells was assayed in the presence of commercial mSlit2, recombinant hSLIT2-myc purified by the previously published method (see above) or recombinant hSLIT2-myc purified by the HPLC-based method presented here. Based on the invasion assay, the activity of the recombinant hSLIT2-myc

purified by the HPLC-based method is comparable to commercial mSlit2 and the recombinant hSLIT2-myc purified by the previously published methods (Figure 8C).

This purified recombinant hSLIT2-myc protein was used for our expression array studies. We used the Human Exonic Evidence-Based Oligonucleotides (HEEBO) platform, which contains over 30000 constitutive exonic probes, representing all known transcripts at the time of our experiments, over 8000 alternatively spliced transcripts, and over 4000 controls (positive, negative, non-human, etc.). A schematic diagram outlining the major steps involved in the sample preparation and analysis of expression microarray is included in Figure 9.

When treated with 100 ng/ml of recombinant hSLIT2-myc, the U251 cell line did not have any significant changes in mRNA expression based on the criteria used in our studies. This was consistent with our previous results of U251 cells not responding to exogenous hSLIT2-myc in the collagen invasion assay. The UW3 cell line treated with 100 ng/ml of hSLIT2-myc displayed a transcription modulation of over 250 genes (The entire list is included in Appendix 2; the number of genes related to specific cellular mechanisms are outlined in Table 2). The description and fold change of the top 40 decreased and increased gene expressions are outlined in Tables 3 and 4, respectively.

The most interesting finding was that 15 genes out of the 40 top modulated genes were previously characterised in different cancers, including malignant brain tumours (Table 5). Moreover, the two genes with the greatest decrease in SLIT2-mediated gene expression, *hexokinase 1* and *MMP14*, yield products that are key promoters of cancer cell invasion (Belien et al., 1999; Guo et al., 2005; Marin-Hernandez et al., 2009). We

have validated by qRT-PCR eight of these genes modulated by hSLIT2-myc, and independently confirmed that they are altered in UW3 cells (Figure 10A). We have also selected for comparison ten genes previously characterised in cancer invasion and angiogenesis but not altered in our screen, such as MMP2 and MMP9 (Figure 10B). There were no statistically significant changes found when the expression of these genes was assessed.

We have also looked at MMP14 protein expression in response to hSLIT2-myc treatment. UW3 and DAOY cells treated with 100 ng/ml of recombinant hSLIT2-myc for 24h had their total MMP14 levels reduced by $38.9 \pm 6.3\%$ and $40.9 \pm 4.7\%$, respectively, as assayed by immunoblot signal densitometry (Figure 10C/D). This decrease in MMP14 also translated into a decrease in MMP14 collagenase activity, as assessed by a colorimetric assay (Figure 10E). Therefore exogenous hSLIT2-myc treatment of UW3 and DAOY leads to a decrease in MMP14 protein expression and a decrease in MMP14 collagenase activity. Moreover, our microarray results suggest that the effect of SLIT2 signaling downstream of the Slit-Robo axis targets key genes implicated in cancer cell invasion. Our data confirms our hypothesis that in addition to altering the activity of Rho GTPases, exogenous Slit2 treatment triggers a transcriptional response in cell lines that are responsive to the recombinant ligand.

The HPLC-based hSLIT2-myc purification yields functional SLIT2 comparable to commercial mSlit2.

To confirm the purity and activity of the recombinant hSLIT2-myc ligand by the method outlined in the present study, we have performed a qRT-PCR analysis on cDNA samples prepared from the mRNA of cells treated with commercial recombinant mSlit2,

previously reported method of conditioned media hSLIT2-myc concentrate, and HPLC-purified hSLIT2-myc (Figure 10F). We have analysed the expression levels of *MMP14*, *CathD*, and *Col6A1*, and we have noted that all three sources of Slit protein diminish the message levels of the aforementioned targets but that there is no significant difference in the extent of silencing of these three genes by qRT-PCR between the different sources of recombinant Slit2 (Figure 10F). These data, combined with the invasion assay (Figure 8C) confirm that recombinant hSLIT2-myc purified by the HPLC-based method presented in this work is of comparable quality to commercial mSlit2 protein.

Characterisation of *MMP14*, one of the genes modulated by SLIT2.

We decided to further characterise *MMP14*, the second most downregulated gene in our study, since metalloproteases are directly involved in glioma and medulloblastoma cell invasion and angiogenesis (Galvez et al., 2001; Lampert et al., 1998; Overall and Kleinfeld, 2006b). We first measured the levels of mRNA expression of *MMP14* by qRT-PCR and observed a trend between the levels of invasion in the collagen matrix assay and the level of *MMP14* expression (Figure 11A and 11B). U251 and C6 glioma cell lines which do not respond to hSLIT2-myc, have the highest levels of *MMP14* expression (Figure 11A). Conversely, DAOY and UW3 medulloblastoma and U343 and U373 glioma cell lines express significantly lower levels of *MMP14* and were less invasive (Figure 11A). Therefore, at the mRNA level, there appears to be a relationship between *MMP14* expression and cell line invasion in the collagen invasion assay (Figure 11B).

Next, we evaluated *MMP14* protein expression in the malignant brain tumour cell lines available by western immunoblotting. In doing so, we noted a protein expression pattern (Figure 11C/D) that mirrored the mRNA expression of the cell lines analysed in Figure

11A/B. Moreover the relationship between the MMP14 protein expression and collagen assay invasion rate was stronger than that of *MMP14* message levels and collagen assay invasion rate, with coefficients of determination (R^2) of 0.91 and 0.89, respectively (Figure 11B and 11E, respectively).

The collagenase activity of MMPs is proposed as the function responsible for cancer cell invasion (Galvez et al., 2001; Overall and Kleinfeld, 2006a), therefore we have analysed the MMP14 *in vitro* collagenase activity of the malignant brain tumour cell lines using a colorimetric, immune-immobilisation assay (Figure 11F). The MMP14 collagenase activity of the different cell lines tested is consistent with the mRNA and protein expression of MMP14, with C6 and U251 displaying the highest levels of collagenase activity, and UW3 and DAOY displaying the lowest amount of collagenase activity *in vitro* (Figure 11F). However unlike the mRNA and protein expression analyses, the trend between collagen invasion rate and MMP14 activity is weaker, with a coefficient of determination of 0.67 (Figure 11G). Taken together, these results indicate that MMP14 expression and activity play an important role in brain tumour cell invasion, *in vitro*.

rRobo1 is a substrate for MMP14, and it is proteolytically cleaved in the third Ig-like domain.

Because MMPs are known to act as ‘shedases,’ cleaving and releasing several receptors from the cell surface (Ferraro et al., 2011), we hypothesised that Robo proteins may also be targeted for shedding by MMP14. Therefore we tested the direct interaction of recombinant rRobo1-Fc and recombinant soluble MMP14-Flag (solMMP14) *in vitro*. Our results suggest that rRobo1-Fc is cleaved at many sites and potentially degraded by solMMP14 (Figure 12A/B) while the Fc fragment alone is not processed by solMMP14

(Figure 12C). The apparent molecular masses of the major proteolytic fragments of rRobo1-Fc are 140, 120, 110, and 60 kDa (Figure 12A/B, denoted by arrows). The minor proteolytic fragments of rRobo1-Fc appear below the 140, 110, and 60 kDa fragments (smears). The cleavage pattern was also observed when HEK293 cells stably overexpressing rRobo1-myc were transfected with MMP14-Flag (Figure 12D). The 60 kDa corresponding amino-terminal fragment was not detectable in HEK293 because there was no epitope tag at the amino-terminal of our rRobo1-Flag construct. These observations suggest that MMP14 mediates rRobo1 degradation, at least *in vitro*, by directly binding to rRobo1 and cleaving it at several sites and the cleavage of rRobo1 is observed in a cellular context.

Based on the molecular weight of the cleavage products of rRobo1 by MMP14 (Figure 12), and based on the biochemical co-expression experiments in HEK293 cells we were able to estimate the major cleavage site corresponding to approximately 60 kDa fragment. Other smaller fragments were also found but they may not be as critical to Robo1's function based on our knowledge of Slit-Robo binding (Figure 12A/B). Because the major cleavage occurs at the N-terminal of rRobo1, we have estimated the cleavage site to correspond to the third Ig-like domain of rRobo1. We have confirmed this hypothesis by performing LC-MS/MS (quadruple time of flight) analysis of cleaved rRobo1 products and narrowed down this cleavage site to a sequence of 8 amino acids corresponding to residues 340-355 on the rRobo1 sequence (Figure 13A). This cleavage region, indeed, corresponds to the third Ig-like domain of rRobo1. We had originally predicted the cleavage site to be around the residue 200 of rRobo1 based on the results obtained from our first round of mass spectrometry analysis (Table 6 and appendix 3).

However this proved to be suspicious since during the first round of peptide sequencing we obtained a single peptide corresponding to residues D189-I195 (and another single peptide at G287-R296), but subsequent analyses failed to identify any peptide N-terminal to K356 (Table 6). We are convinced that the peptide D189-I195 is either a contaminant or a minor product because it was not observed in other analyses of the C-terminal fragment. Moreover, when we analysed the 60 kDa (N-terminal) fragment, the most C-terminal peptide observed was K319-K338, which agrees with our prediction that the major cleavage site of rRobo1 is around or C-terminal to residue K338. A peptide analysis of the amino and carboxy termini of rRobo1-Fc is included in Table 6.

The apparent molecular mass of 60 kDa for the N-terminal fragment favours the cleavage site at a residue past K338. Assuming proteolysis at K338, the resulting N-terminal fragment would yield a predicted mass of ~35 kDa (mature rRobo1, cleaved at K338), which is smaller than the apparent mass of ~60 kDa. This may be due to the fact that rRobo1-Fc undergoes post-translational modification at residues in the N-terminal fragment. We employed NetOGlyc 3.1 (Julenius et al., 2005) to predict O-glycosylation of the predicted N-terminal fragment of rRobo1, and identified four potential residues, T86, T201, T344, and T346, with high probability of O-glycosylation (Appendix 4). We also used NetNGlyc 1.0 to predict N-glycosylation of the predicted N-terminal fragment of rRobo1, and identified two potential residues, N142 and N157 (Appendix 5). Therefore, both types of glycosylation may contribute to the increase in the apparent molecular mass of the N-terminal fragment of rRobo1. Other post-translational modifications may also contribute to the apparent mass of the rRobo1 fragment.

We were interested in identifying the amino acid residue that is proteolytically cleaved by MMP14. To this end, we analysed the carboxy-terminal fragment corresponding to the 110 kDa fragment by Edman degradation (Niall, 1973). The amino-terminal degradation of this fragment identified the sequence VQEPP, at positions 1 to 5, respectively, which corresponds to residues V347-P351 of rRobo1 (Figure 13A, Appendix 6). Therefore, we propose that the proteolysis of the 60 kDa fragment occurs at the threonine (T) 346 residue which as predicted, maps to the end of the third Ig domain of rRobo1 (Figure 13B). Based on this information, we predict that the full length rRobo1, in its mature form (i.e., having its signal peptide removed) undergoing MMP14 proteolysis would yield a 60 kDa N-terminal fragment (accounting for post-translational modifications) and would yield a predicted 200 kDa C-terminal fragment. It is important to note that the discrepancy between full-length rRobo1 and rRobo1-Fc chimera is that the latter contains only residues 19-560 of rRobo1.

There are a number of implications that result from such MMP14-induced rRobo1 cleavage site: First, once rRobo1 is cleaved by MMP14, this renders rRobo1 functionally inactive since it can no longer bind to its ligand Slit2 and propagate its inhibitory effect. Second, the 60 kDa N-terminal fragment that is cleaved and likely released into the extracellular space should still retain Slit-binding capabilities. This would, as a result, act as a Slit-sequestering agent. Indeed, when rRobo1N-Flag, corresponding to amino acid residues 1-346 of full length rRobo1, was expressed in HEK293 cells stably expressing hSLIT2-myc, anti-myc slurry co-immunoprecipitated rRobo1N-Flag (Figure 13C). Likewise, we were able to co-immunoprecipitate hSLIT2-myc when immunoprecipitating rRobo1N-Flag with anti-Flag slurry (Figure 13C). Therefore, we predict that the 60 kDa

cleaved rRobo1 amino-terminal fragment binds hSLIT2-myc and competes for its binding to intact rRobo1 at the cell surface.

MMP14 overexpression in UW3 cells renders them insensitive to hSLIT2-myc.

Next we wanted to know whether MMP14 can directly or indirectly alter the responsiveness of UW3 medulloblastoma cells to hSLIT2-myc treatment. To assess this idea we selected stable cells overexpressing MMP14 and tested the effect of hSLIT2-myc or mock treatment on the rate of invasion. As expected, UW3 cells overexpressing MMP14 had a statistically significant increase in their invasion rates when compared to mock transfected cells (Figure 14A). In addition, UW3 cells overexpressing MMP14 were no longer responsive to the anti-invasive effects of hSLIT2-myc. Furthermore, because the UW3 cells expressed MMP14 at relatively low levels, we decided to isolate UW3 clones with different levels of MMP14 expression. In doing so, we have isolated 27 clones UW3 overexpressing MMP14, of which clones 3 and 6 had the highest and second highest MMP14 protein expression, respectively (Figure 14B). Both clones expressed higher levels of MMP14 when compared to the parental UW3-MMP14-Flag stable cell line (Figure 14B). Next we measured the MMP14 collagenase activity of the stable cells and noted that their collagenase activity (Figure 14C) mirrored their MMP14 protein expression (Figure 14B), as previously observed with other cell lines (Figure 11). Moreover the UW3 clone 3 displayed significantly higher MMP14 collagenase activity when compared to the parental UW3 stable cell line overexpressing MMP14-Flag (Figure 14C). Importantly, the isolated clones and their parental UW3 cell line were not responsive to hSLIT2-myc mediated decrease in MMP14 collagenase activity (Figure

14C). This desensitisation to hSLIT2-myc was also observed at the level of invasion whereby clone 3 and the parental UW3 stable cell line had a statistically significant increase in collagen invasion assay, and that hSLIT2-myc treatment did not attenuate their invasion rate (Figure 14D).

These results are consistent with hypothesis that MMP14 attenuates the anti-invasive effect of hSLIT2-myc either directly by cleaving Robo1 at the cell surface, and/or acting indirectly through extracellular or intracellular pro-invasive effectors.

MMP14 knockdown leads to a decrease in invasion in C6 glioma cells.

We were interested to assess whether knocking down MMP14 would render C6 glioma cells responsive to hSLIT2-myc, thus decreasing their invasion. We employed a lentiviral expression system targeting MMP14 expression with different shRNAmiR sequences. We achieved knockdown of MMP14 protein expression when compared to the control shRNAmiR sequence (Figure 15A) and selected a population of C6 cells that had stably decreased MMP14 expression and we tested their invasion rates in a collagen matrix assay (Figure 15B). When compared to control shRNAmiR sequence, MMP14 knockdown significantly decreased the invasion rate of C6 cells by $10.1 \pm 2.6\%$, or 85 μm after five days of invasion (Figure 15B).

Although this decrease in invasion may seem small, it is comparable to the decreases in invasion of UW3 and DAOY when treated with exogenous SLIT2, which were 113 μm and 97 μm , respectively. Moreover C6 cells are highly invasive and it is very difficult to significantly impact their invasion rate. Therefore, we conclude that MMP14 silencing

leads to a decrease in the invasion rate of previously unresponsive C6 cells, in a collagen matrix invasion assay.

MMP14 knockdown leads to the sensitisation of C6 glioma cells to anti-invasive effects of hSLIT2-myc.

To test whether MMP14 counters the anti-invasive effects of hSLIT2-myc in C6 cells, we evaluated the effect of hSLIT2-myc on C6 cells that had lower MMP14 expression as a result of targeted shRNAmiR-mediated knockdown. As observed in Figure 15, MMP14 knockdown leads to a decrease in C6 invasion of $10.4 \pm 1.2\%$, in a collagen matrix (Figure 16A, column 3). To rule out that the anti-proliferative effect of MMP14 knockdown is the cause of the anti-invasive effect observed above, we have performed a wound healing assay (the effect of proliferation is negligible since assay spans 12h) on C6 shRNAmiR-mediated MMP14 knockdowns and noticed a significant decrease in migration (Appendix 7).

Interestingly, hSLIT2-myc treatment of C6 cells expressing lower levels of MMP14 leads to a further, statistically significant decrease in C6 invasion, causing a decrease of $20.4 \pm 0.9\%$ (Figure 16A, column 5). Therefore, in a context of MMP14 silencing, C6 glioma cells become responsive to hSLIT2-myc's anti-invasive effects.

MMP14 knockdown decreases C6 glioma collagenase activity and hSLIT2-myc amplifies this decrease in MMP14 collagenase activity.

Since we were able to decrease the invasion rate of C6 by knocking down MMP14 or by combining MMP14 silencing and hSLIT2-myc treatment, we measured the MMP14 collagenase activity in C6 cells under MMP14-targeted shRNAmiR silencing, in the presence or absence of hSLIT2-myc. MMP14-targeted knockdowns by shRNAmiR-

MMP14-1 and shRNA_{MMP14-2} led to statistically significant decreases of $38.5 \pm 6.0\%$ and $35.7 \pm 4.2\%$ in MMP14 collagenase activity (Figure 16B, columns 1-3). Recombinant hSLIT2-myc treatment of C6, alone, did not significantly alter MMP14 collagenase activity (Figure 16B, columns 4); but when hSLIT2-myc was combined with shRNA_{MMP14-1} or shRNA_{MMP14-2}, collagenase activity was decreased by $57.7 \pm 3.7\%$ and $59.8 \pm 4.3\%$, respectively (Figure 16B, bars 6-7). Taken together, these results demonstrate that the MMP14 collagenase activity of C6 cells is greatly responsible for the lack of response of C6 cells to hSLIT2-myc. These results also demonstrate that modulating the collagenase activity of hSLIT2-myc insensitive cancer cells may render such cancer cells sensitive to anti-invasive compounds such as Slit proteins.

MMP14 knockdown enhances temozolomide toxicity in C6 cells.

Cell migration and proliferation are two events that display a high level of cross talk (Corcoran and Del Maestro, 2003). Therefore our aim was to test whether MMP14 knockdown in C6 glioma cells may enhance the toxicity of anti-proliferative chemotherapies used in the treatment of malignant gliomas. The current chemotherapeutic agent of choice for the treatment of malignant brain tumours is temozolomide (TMZ). Therefore, we knocked down MMP14 in C6 cells and observed a statistically significant decrease in C6 cell proliferation (Figure 17, column 3). When MMP14 knockdown C6 cells were treated with TMZ, we observed an even greater and statistically significant decrease in cell proliferation (Figure 17, column 7). This shows that targeting the invasion and proliferation aspects of C6 glioma cells simultaneously has a compounded effect, thus leading to higher cancer cell toxicity.

2.3 Discussion

Current strategies for the treatment of malignant brain tumours fail to adequately address the invasive nature of these neoplasms. As a result, most patients with malignant brain tumours recur locally even after invasive procedures such as surgical resection, chemotherapy, and radiotherapy, and succumb to their disease.

In search for molecules that can inhibit brain cancer cell invasion, we have identified SLIT2, member of a well known family of proteins involved in axon path finding and neural migration. We have demonstrated that some brain tumour cells studied *in vitro* respond to the same axon guidance and neuronal cues that are involved in patterning the nervous system. Our results are consistent with the concept that specific signaling pathways are often conserved between different types of cells (Carmeliet and Tessier-Lavigne, 2005).

In our earlier studies, we demonstrated that SLIT2 inhibits the invasion rate of medulloblastoma cell lines, but not glioma cell lines (Werbowski-Ogilvie et al., 2006). It was unclear as to why only medulloblastoma cells respond to exogenous SLIT2. Gliomas express markers of glial lineage and could therefore lack the expression of Robo receptors generally associated with cells of neuronal lineage such as neurons, neuroblastoma, and medulloblastoma cells. Therefore, a lack of Robo expression in the glioma cell lines that were initially assessed would explain their insensitivity to recombinant SLIT2. This explanation was not consistent with our

qRT-PCR data showing that all our glioma and medulloblastoma cell lines studied express comparable levels of Slit and Robo mRNAs. They also express similar levels of Robo3.1, an isoform of Robo3 which is known to antagonise the Slit-Robo signaling pathway (Chen et al., 2008). However, because anti-Robo antibodies were not commercially available we could only analyse Robo expression at the mRNA level. Therefore we cannot rule out the possibility that Robos are differentially translated between the types of cell lines used in the present study.

Receptor trafficking and localisation is an important means of functional modulation of signaling pathways in neurodevelopment (Bouchard et al., 2008; Keleman et al., 2005) and cancer progression (Stutz et al., 2008; Ying et al., 2010). Indeed transmembrane receptors are known to be present in intracellular pools, sequestered from the cell surface (Bouchard et al., 2004; Czajkowski and Farb, 1989). To address this issue, we engineered rRobo1-HA overexpressing U251 glioma cells, targeted the receptor to the cell surface and treated these non-responsive U251 cells with exogenous SLIT2. However this did not result in any significant difference in their rates of invasion. This observation suggested that the signaling downstream of the Slit-Robo axis may be different in glioma cells that are non-responsive to SLIT2.

Ligands binding to their receptor located at the plasma membrane propagate their signal by recruiting intracellular effectors, and this is the case of Slit proteins which are known to recruit multiple cytoplasmic proteins such as Abl, Ena, srGAPs, and Rho GTPases to the cytoplasmic tail of Robo proteins. We decided to focus on the Rho family of proteins because they are key effectors of cellular migration and they play an important role in Slit-mediated neural and axon repellence (Causeret et al.,

2004; Guo and Bao, 2010). Furthermore, quantitative biochemical assays have been established to measure their endogenous activity making their study accessible. In our study we observed a significant decrease in Cdc42 activity and a moderate, but significant decrease in Rac activity in medulloblastoma cell lines treated with SLIT2. However, we did not observe any changes in Cdc42 or Rac activity in the non-responsive glioma cell lines. We had expected to see diminished activities of Cdc42 and Rac, since the activities of both Rho GTPases are modulated by Slit-Robo signaling in neuronal and cancer models (Guo and Bao, 2010; Stella et al., 2009; Yiin et al., 2009a). Moreover, the Cdc42 and Rac proteins are generally associated with a pro-migratory phenotype in medulloblastoma (Nalla et al., 2010), glioma (Dey et al., 2008), and other cancers (Heasman and Ridley, 2008). The unaltered Rho GTPase activity observed in the glioma cell lines tested suggested that upon ligand-receptor activation, there are signaling differences between the responsive and non-responsive brain tumour cell lines which channel through the Rho GTPases.

Alternatively, assuming that Rho GTPases receive activating and inactivating signals in a linear and additive (or subtractive) fashion, it is possible that the non-responsive cell lines have higher positive Rho GTPase inputs (i.e., their basal activity is higher), requiring a higher amount of negative inputs in order to observe a significant decrease in Rho GTPase activity. One piece of evidence that may support this hypothesis is that glioma cell lines which respond to SLIT2, U343 and U373, have low to moderate invasion in the collagen invasion assay. This is of course assuming that the invasion of malignant brain tumour cell lines, and especially the migration

aspect of invasion, is linearly proportional to the Rho GTPases' activity (Leve and Morgado-Diaz, 2012; Rathinam et al., 2012).

Sustained hSLIT2-myc Treatment Elicits a Transcriptional Response

Spheroid invasion assays span 5 days on average and can be maintained for 10 to 30 days depending on the experimental conditions. In our spheroid assays, we observed that recombinant SLIT2 inhibits the invasion of UW3, DAOY, U343, and U373 brain tumour cells over a prolonged period. Therefore we hypothesised that the sustained inhibitory effect of SLIT2 may be the result of an immediate and transient cytoplasmic response combined with longer lasting transcriptional changes whereby recombinant SLIT2 treatment alters the invasive paradigm by modulating the transcription of invasion-related genes. More specifically, we predicted that SLIT2 treatment would decrease the expression of pro-invasive genes and/or increase the expression of anti-invasive genes. To test this hypothesis we carried out expression array analyses on the SLIT2-responsive UW3 medulloblastoma cell line as well as the SLIT2-unresponsive U251 glioma cell line. Our findings confirmed our hypothesis whereby SLIT2 modulates the expression of a series of genes responsible for the invasive paradigm. Many of these genes are known oncogenes and play key roles in carcinogenesis, angiogenesis, and tumour invasion and metastasis. This observation was particularly promising because if Slit proteins (or chemical analogues) were to be used as therapeutics, they would have a broad inhibitory effect on pro-cancer genes.

We have validated the differential expression of eight genes identified in our screen and characterised one of SLIT2's targets, MMP14. A number of reasons led us to focus on MMP14: First the expression of several metalloproteases, including MMP14, correlates with malignant glioma invasion and tumour grade (Sato et al., 2005). Indeed, in a cohort of 41 glioma patients, MMP14 expression as assessed by immune-histochemistry inversely correlated with progression-free survival and overall survival of patients (Snuderl et al., 2008). Moreover, the expression of MMP14 was indicative of the invasiveness of the tumour. Second, MMP14 is known to proteolytically activate other proteases involved in malignant brain tumour invasion such as MMP2 (Atkinson et al., 1995). Third, MMP14 is itself activated by another family of proteases, the proprotein convertases, which are also strongly implicated in cancer (Seidah, 2011) and in malignant gliomas (Maret et al., 2010). Fourth, MMP14 interacts and cleaves proteins implicated in Slit-Robo signaling: Syndecan-1 is cleaved by MMP14, the result of which enhances tumour cell migration *in vitro* (Endo et al., 2003). Also MMP14 is functionally required in an ischemia model for the shedding activity of NCAD and ECAD (Covington et al., 2006). Finally a wide range of biological tools are commercially available to modulate the activity of metalloproteases such as MMP14.

First we screened the expression levels of MMP14 in the glioma and medulloblastoma cell lines available and observed that MMP14's expression correlates with the invasive potential of the cell lines in a collagen invasion assay. This observation supports a role for MMP14's collagenase activity in invasion and is consistent with our previous observations that collagen matrix glioma invasion is metalloprotease-dependent (Del Maestro et al., 1995; Tamaki et al., 1997; Tamaki et al., 1996). The malignant glioma cell

line C6 displayed the highest expression of MMP14 and the highest collagenase activity and it is also the cell line than has the greatest invasive potential in our collagen-based invasion model. Our observations are consistent with Beliën et al.'s data showing that C6 cells have high levels of MMP14 expression and activity and that the expression of MMP14 is responsible for the white matter tract migratory potential of glioma cells, *in vitro* (Belien et al., 1999). Furthermore, the cell lines that express higher levels of MMP14 message, protein, and collagenase activity were those that did not respond to SLIT2 treatment.

These compelling results, combined with the fact that matrix metalloproteases are known to cleave transmembrane proteins, warranted the evaluation of Robo proteins as possible substrates of MMP14. Robo proteins are known to undergo proteolytic modifications: In a *Drosophila* model of commissural axon guidance, Coleman et al. showed that the ADAM family member Kuzbanian/ADAM10 (a metalloproteases) cleaves Robo and this proteolysis is necessary for Slit-mediated Sos recruitment (Coleman et al., 2010). Also, in a screen of sera from hepatocellular carcinoma patients, Buratani's group identified a soluble fragment of ROBO1 corresponding to the ectodomain of the full length protein (Ito et al., 2006) and provided *in vitro* evidence suggesting that an unknown metalloprotease and an unknown gamma-secretase are responsible for ROBO1 proteolyses (Seki et al., 2010). Interestingly Buratani's group was able to detect a ROBO1 fragment in U251 malignant glioma conditioned and in many other cell lines they screened (Ito et al., 2006). Finally mRobo1 fragments have been detected in sera of small cell lung carcinomas (SCLC) mice, and an ELISA-based screen of SCLC patients' sera revealed an increase in ROBO1 in SCLC patients when compared with subjects

without cancer (Taguchi et al., 2011). Interestingly, the mouse Robo1 peptide identified in that screen, K98-R111², was also detected in our screen (A. Taguchi, personal communication).

Combining purified recombinant rRobo1-Fc with purified recombinant soluble MMP14, or overexpressing rRobo1-Fc in cells expressing MMP14 leads to rRobo1 proteolysis at a number of sites. The major proteolytic fragment, which corresponds to the carboxy-terminal portion of rRobo1-Fc has an apparent molecular mass of 110 kDa; and its corresponding amino-terminal cleaved rRobo1 fragment has an apparent mass of 60 kDa. Based on the results from different chromatography and mass spectrometry techniques employed, we have mapped the cleavage site of rRobo1 to the carboxy-terminus of threonine (T) 346. The proteolysis of rRobo1-Fc at T346 leads to the inactivation of rRobo1 and to the release of rRobo1 cleaved fragment in the extracellular space, where it retains its Slit-binding function and acts as a Slit-sequestering agent. Coleman et al. have also proposed that in *Drosophila* Robo is cleaved by Kuzbanian somewhere within or near the fibronectin III domain of the protein (Coleman et al., 2010) and suggested in their model that cleaved Robo receptor can retain Slit-binding capabilities. In our system, rRobo1 is cleaved immediately after the third Ig domain of Robo, yielding a shorter amino-terminal fragment than in the latter study. However, because the first and second Ig domains necessary for Slit-binding are intact, Slit-Robo interaction is not affected, as shown by our immuno-precipitation assays. Indeed, transmembrane receptor shedding is a ubiquitous mechanism observed in physiological and pathological conditions (Bazil and Strominger, 1994; Ferraro et al., 2011; Hooper et al., 1997; Ludwig et al., 2005). In

² Corresponds to K137-R150 of rRobo1

certain cases the soluble – ectodomain – fragment retains ligand-binding capabilities such as TGF- β co-receptor betaglycan which is cleaved by MMP14 and acts to sequester TGF- β from the lumen (Hawinkels et al., 2010). Therefore in our system, the fragment of Robo1 detected may also have pathological importance because the carboxy-terminal fragment of rRobo1 detected has a similar apparent molecular mass to Ito et al.'s report (Ito et al., 2006).

Slit-Robo-MMP14 Model

Functionally, MMP14-dependent Robo1 proteolysis can have a significant impact on invasion. First in invasive cells such as C6 cells, where MMP14 is expressed at high levels, Robo1 proteins would get processed by MMP14 and their amino-terminal fragment would be shed into the extracellular space. In such a scenario Robo1's proteolytic fragment can bind Slit proteins in the extracellular matrix and compete for their binding to intact Robo receptors at the cell surface. The proteolysis of Robo1, which would ultimately inactivate the receptor, would diminish the silencing effects of MMP14 through Slit-Robo mediated signals. The ultimate outcome of this model is a net increase in cell invasion through sustained – or perhaps even increased – levels of MMP14 at the cell surface favouring a pro-invasive phenotype, and diminished anti-invasive effects of Slit-Robo signaling (Figure C-1A). In the second model, low-to-moderately invasive cells such as UW3 which express low basal amounts of MMP14 would not display a significant amount of Robo1 proteolysis. Upon treatment with exogenous SLIT2, the majority of Robo1 receptors at the cell surface would bind their ligand and propagate Slit-Robo mediated inhibition of invasion. Persistent SLIT2 treatment would silence MMP14 expression, which would in turn diminish the amount of MMP14 at the cell

surface. The ultimate effect in this model is a significant decrease in cell invasion due to direct MMP14 silencing and indirect decrease in the activity of other pro-invasive proteins such as Cdc42, Rac1, and MMP2 (Figure C-1B).

Our experimental observations support this model: Moreover, several results support the validity of our model. First, overexpressing MMP14 in UW3 cells that express low levels of MMP14 increases their invasion rate and makes UW3 resistant to SLIT2-mediated inhibition of invasion in a collagen invasion model. This is perhaps caused by MMP14 cleaving Robo1 receptors at the surface of UW3 cells and inactivating them. This would generate cleaved, soluble Robo1 fragments, which would interfere with Slit-Robo binding. Another possibility would be that MMP14 activates other MMPs such as MMP2 and MMP9, which could also cleave Robo and/or other pro-invasive factors. This would ultimately lead to an increase in invasion, thus negating the anti-invasive effects of Slit proteins. Finally, MMP14 may modulate the expression pattern of pro-invasive genes, which would result in an increase in invasion via a transcriptional response.

Second, the treatment of UW3, DAOY, U343, and U373 with SLIT2 decreases invasion, possibly by silencing MMP14 expression and activity. This effect on invasion is persistent even when SLIT2 is washed off the cells, suggesting that MMP14's activity is under the control of SLIT2-responsive elements, and although there is no direct evidence, we can predict that such SLIT2-responsive elements work at transcriptional or post-transcriptional levels to modulate MMP14 expression and activity, possibly channeled through Cdc42 and Rac GTPases. Third, the overexpression of MMP14 increases UW3 cells' invasion rate in a collagen matrix, and renders them non-responsive to SLIT2-

mediated inhibition of invasion. Fourth, silencing MMP14 in C6 cells renders them sensitive to exogenous SLIT2. Indeed, MMP14 knockdown leads to a decrease in C6 cell invasion. Moreover, treatment of MMP14 knockdown C6 cells with SLIT2 leads to a further decrease in invasion rate when compared to MMP14 knockdown alone. These results may be explained by two possible, non-exclusive models. First, MMP14 knockdown may lead to an overall decrease in invasion which as a result, may render C6 cells more sensitive and permissive to the anti-invasive effects of SLIT2. Second, MMP14 knockdown may lead to a decrease in Robo1 proteolysis, which would provide a greater number of active Robo receptors at the cell surface for SLIT2 to bind to and transduce its anti-invasive signals. These results are consistent with the model presented in Figure C-1.

Finally, because the current chemotherapeutic standard of treatment is that alkylating agent temozolomide, we decided to carry out *in vitro* combinatorial treatment on C6 cells to assess invasion and proliferation rates as a result of MMP14 knockdown and TMZ treatments. Indeed, treating C6 cells with MMP14-targeted shRNAiRs renders these cells more sensitive to the cytotoxic effects of TMZ. This suggests that targeting cancer cells with anti-invasive compounds may facilitate the effect of anti-proliferative agents.

MMP14's Potential Role in Axon Guidance

It is conceivable that our findings of MMP14-mediated Robo1 proteolysis play a role in axon pathfinding. Neurite outgrowth and axon is a non-pathological tissue invasion event (Muir, 1994), and axons must degrade the extracellular matrix that acts as a physical barrier in order to reach and innervate their target. Proteases have long been known to be

expressed and secreted by developing neuronal cultures (Bai and Pfaff, 2011; Krystosek and Seeds, 1981). Receptor shedding is also functionally relevant in axon guidance: DCC is proteolytically shed by a yet unknown metalloprotease, the result of which diminishes netrin-mediated axon outgrowth (Galko and Tessier-Lavigne, 2000). And more recently ADAM10 was shown to shed Robo in *Drosophila*, an event that is required for Robo-mediated repulsion (Coleman et al., 2010). In the fruit fly system, MMPs are genetically and functionally required for axon guidance. In a model of motor axon de-fasciculation of intersegmental nerve branch b, motor neurons projecting their axons do not branch out in *Mmp1* and *Mmp2* miss-expressing and *Timp* (tissue inhibitor of MMPs) overexpressing animals (Miller et al., 2011; Miller et al., 2008).

Metalloproteases such as MMP14 may impact Slit-Robo signaling in a similar fashion to *Comm* in *Drosophila* whereby their expression would be temporally modulated to inactivate Slit-Robo repulsion when axons are crossing structures that secrete Slit proteins. This could happen in *cis*, with the expression and the spatial localisation of MMPs at the growth cone or in *trans* with the expression and perhaps secretion of MMPs by stationary cells which guide axons. Because in our model, the cleaved portion of the Robo1 receptor maintains its Slit-binding ability, we predict that the cleaved ectodomain of Robo may also serve to silence Slit-Robo signaling. Therefore Robo receptors, whether cleaved on the surface of neurons or other cells lining the path of guided axons, may provide a source of Slit-binding soluble particles which would act as competitive inhibitors of Robo proteins.

Conclusion and future prospective

Most cancer deaths can be attributed to the invasion of cancer cells at distances away from the main tumour mass. Therefore, the invasive cascade provides several potential targets for therapy. We have identified a novel protein that inhibits brain tumour cell invasion *in vitro*, SLIT2. We based our initial hypothesis on the fact that there is a strong relationship between tumourigenesis and tissue development. We screened several proteins associated with neural development to see whether we could identify potential candidates that may inhibit malignant brain tumour cell invasion. We built upon our original findings and discovered that SLIT2 inhibited malignant brain tumour cell invasion by decreasing Cdc42 and Rac activity, two important effectors of cancer cell invasion. These findings confirmed that Slit proteins may serve as models of anti-invasive therapies because of their immediate effect on Rho GTPases. In addition, we have uncovered another mechanism by which Slit proteins inhibit malignant brain tumour cell invasion. A 24 hour treatment of malignant brain tumour cells with purified SLIT2 suffices for the induction of a transcriptional expression pattern which collectively decreases the expression of important genes promoting cancer cell invasion. These findings further strengthen the potential of Slit proteins as an attractive model for the study of anti-invasive therapy. Moreover, we have characterised a transcriptional target of SLIT2, MMP14, and have demonstrated that this protein too, could serve as an anti-invasive therapeutic target. Importantly, we show that the Slit-Robo signaling pathway may be negatively regulated by MMP14. This feedback inhibitory loop is triggered by Slit-Robo binding, which leads to a decrease in MMP14 expression, ultimately leading to an increase in cell surface functional Robo concentration. Alternatively, cells expressing high levels of MMP14 would decrease the numbers of functional Robo proteins at their

cell surface, ultimately leading to a decrease in Slit-Robo signaling (Figure C-1A).

Finally, the treatment of highly invasive glioma cells with MMP14 knockdown increases the cytotoxicity of TMZ treatment.

Slit proteins are large macromolecules of approximately 200 kDa. Therefore using Slit proteins intravenously as a therapeutic agent would not be feasible since such a protein would have limited penetration through the blood-brain barrier. However a number of methods using continuous direct injection of large macromolecules into the brain using convection-enhanced delivery (Bogdahn et al., 2011) would be practical and this technology could be explored in pre-clinical trials such as animal models.

Slit proteins may serve as models for anti-invasive analogues. There is a wealth of information about the structure and function of the second LRR of Slit proteins providing biochemists a template for designing small molecule analogues that are functionally active. A Slit protein analogue with sub-micromolar affinities for Robos would be feasible for preclinical testing in cancer invasion animal models. In order for these analogues to show efficacy in brain tumours, they would also have to have a good tissue distribution and be able to cross the blood brain barrier. Finally, anti-invasive therapies would only succeed if used in conjunction with anti-proliferative and anti-angiogenic compounds. There has never been any anti-invasive compounds approved for the treatment of malignant brain tumours; our work may provide a new avenue for preclinical and clinical anti-invasive research, ultimately targeting one of the most recalcitrant aspects of cancer.

2.4 Materials and Methods

Recombinant proteins, treatment conditions, antibodies, constructs, and other

reagents. Recombinant mSlit2 was purchased from R&D Systems. Recombinant hSLIT2-myc was purified in house (described below). NETRIN1, SDF1, SEMA3A were from R&D Systems. IGF, EGF, and FGF2 were from Invitrogen. The duration of treatment of proteins varied depending on the assay: For invasion assays spheroids were treated with media containing the protein of interest for the entire duration of the invasion assay (media was changed every 48h). For wound healing assays, monolayers were treated with media containing the protein of interest for the entire duration of the migration assay. For the transcriptional response assay (microarray), HPLC-purified hSLIT2-myc was used to treat the monolayer for 24h. The antibodies used in this study were: c-Myc 9E10 and HA 16B12 (Covance), Flag M2 and β -tubulin DM1A (sigma), α -tubulin polyclonal raised in rabbit (Cell Signaling Technology), anti-MMP14 (Abcam); Cdc42, Rac1 and Rho antibodies were obtained from Santa Cruz Biotechnology, BD Transduction Laboratories and Upstate Biotechnology, respectively. The following constructs were used in this study: hSLIT2-myc cloned in pCDNA3.1 Myc, rRobo1-HA cloned in pCS2+, rRobo1-myc cloned in pCDNA3.1 Myc, rRobo1-myc cloned in pCDNA3.1 Flag. All rRobo cDNAs clones have been described (Werbowsky-Ogilvie et al., 2006) and the primer sequences are includes below. Soluble MMP14-Flag and full length MMP14-Flag were provided by Chris Overall (University of British Columbia).

The N-terminal fragment rRobo1-Flag (corresponding to residues 1-350) was cloned into pcDNA3.1 Flag. Temozolomide was obtained from Merck and used at 30ug.ml⁻¹.

Reverse transcription-polymerase chain reaction and qPCR. Total RNA was extracted using the RNeasy kit (Qiagen). First strand cDNA was synthesised using the First-Strand cDNA Synthesis Kit (GE). A Lightcycler platform and SYBR green fluorescent dyes were used for the qPCR step. Products were subjected to a melting curve analysis followed by being resolved on an agarose gel. In cases where the amplification efficiency between the target and reference message differed by more than 5%, the signal was corrected for PCR efficiency.

G-LISA active Rho GTPase assay. The commercially available GLISA kit (Cytoskeleton) was used according to the manufacturer's protocol. Briefly, treated and untreated cells were lysed with lysis buffer provided. Cell lysates were incubated in 96 well plates coated with the PAK binding domain of Cdc42 and Rac. Lysate were allowed to rock on a micro-orbital shaker for 1 hour at 4degC. Plates were washed with supplied wash buffer 3x and incubated in primary and secondary antibodies in succession. Levels of GTP bound Cdc42 and rac were assessed by luminescence using a UV spectrometer.

Active Rho GTPase pulldown assays. Rac1, Cdc42 and Rho activity assays were performed using nonradioactive Activity Assay kits (Upstate Biotechnology). Briefly, UW3 and C6 monolayer cultures were treated with concentrated Slit2 or HEK conditioned medium diluted in serum-free DMEM for 24 h, and lysed. Cell lysates were affinity precipitated with a GST fusion-protein corresponding to the p21-binding domain of human PAK1 bound to glutathione–agarose (Rac and Cdc42) or the Rho binding

domain of Rhotekin bound to agarose beads and run on 15% SDS–PAGE. Western blot analysis was used to detect activated Rho GTPase proteins. Total Cdc42, Rac1 and Rho levels were determined by western blot analysis and used as loading controls.

Cell culture. All culture reagents were obtained from Gibco BRL (Invitrogen) unless otherwise stated. Cell lines: U251 (derived from human glioblastoma) UW228-3 (UW3) (human medulloblastoma cell line derived from one of three cell aliquots taken from the same tumor resected from a 9-year-old girl), and DAOY (human medulloblastoma derived from tumor biopsy from a 4-year-old boy). HEK 293 and HEK 293 cells stably overexpressing full-length human Slit2 with a c-Myc tag were provided by Yi Rao (Northwestern University). All cell lines were purchased from the American Type Culture Collection (ATCC) (Rockville, MD, USA) except the UW3 cell line, which was provided by John R Silber (University of Washington).

Cell surface biotinylation. Monolayers were washed three times with ice-cold PBS and incubated with EZ-Link NHS-SS-Biotin (Fisher Scientific) in PBS (200ng/ml) for 30 min at 4degC. Excess biotin was quenched with ice-cold TBS (3x) followed by ice-cold PBS (3x). Cells were lysed and scraped off the plate with 0.5 ml of RIPA. Immobilised Streptavidin beads (Fisher Scientific) were added to the total proteinto bind biotinylated proteins for 2h, 4degC. The beads were washed with RIPA buffer (3x) and resuspended in 2× Laemmli buffer, boiled, and resolved on an SDS-PAGE and immunoblotted.

Spheroid preparation and invasion assay. Cells were trypsinised and hanging drops were prepared as previously described (Del Duca et al., 2004). Aggregates consisting of 40 000 cells/drop and 25 000 cells/drop (UW3 and DAOY, and U251 and C6,

respectively) were prepared. Spheroids were imaged at $t=0$, $t=3$ days, and $t=5$ days Northern Eclipse 6.0 software (Werbowetski et al., 2004). Spheroids of all cell lines were implanted into a three dimensional collagen I gels. A collagen solution was prepared consisting of 3.2 mg/ml collagen type I in 0.012M HCl (Vitrogen) and 10-fold concentrated DMEM. The pH of the solution was adjusted by the addition of 0.1M NaOH. Five hundred microliters of this solution was added to 24-well plates and spheroids were implanted into the gel using a Pasteur pipette. After gelation at 37degC in a humidified atmosphere of 5% carbon dioxide for 30–60 min, the gel was overlaid with 500 μ l DMEM and cell invasion was recorded for 5 days using an inverted phase contrast light microscope (Zeiss Axiovert 25) and digital camera (QImaging Retiga 1 300). Total invasion distance was calculated at the same time each day from the center of the spheroid to the population of invading cells most distant from the spheroid. The original radius of the spheroids was subtracted from these values.

Wound healing assay. The migration assay was done as previously described (Maret et al., 2010). Briefly, cells were seeded at 220,000 cells density and a scratch was generated using a 200 μ l micro-pipette tip. Cells were allowed to migrate into the wound and the number of cells entering the wound were counted and quantified, where the number of cells in the wound is proportional to the extent of cell migration.

Stable cell lines. Mammalian cells seeded in 6 well plates were transfected with Lipofectamine LTX at 60% density. 48h post-transfection, cells were seeded in 10 cm Petri plates and selected with the mammalian selection marker. Cells were grown until colonies were visible. For clones selected from the stable line, cells were seeded in 96 well plates at a density of 1-2 cells per well, maintained in regular culture media

supplemented with the selection marker. Clones were expanded and isolated and the expression of target cDNA was monitored by western immunoblotting.

Recombinant hSLIT2-myc preparation. Conditioned medium was collected from HEK293-hSLIT2-myc confluent monolayer cultures and concentrated using concentration tubes (Millipore). The Concentrate was injected into a Rheodyne injector equipped with a 5ml preparative loop. The condition for the sample loading was phosphate buffered saline at a rate of 0.5ml per minute. We used a 5ml preparative Heparin column (GE), and eluted the sample a gradient increase of PBS-0.5M NaCl solution. Fractions 35 to 38 were collected and concentrated. A sample was resolved via SDS-PAGE and visualised by Coomassie staining.

For the standard method of purification, as described previously (Werbowetski-Ogilvie et al., 2006), we collected conditioned media from HEK293-hSLIT2-myc confluent monolayer cultures, applied to a Heparin column (Bio-Rad) overnight, eluted with concentration of PBS-1M NaCl, dialysed overnight against 30x volume of PBS and concentrated using concentration tubes (Millipore).

Mass spectrometry analysis. In gel tryptic digest and tandem mass spectrometry (LC-MS/MS, QTOF) analysis were conducted on excised bands (McGill University and Genome Quebec Innovation Centre). Mascot scores were obtained and significance was determined as the minimum threshold required to be considered a nonrandom assignment. See Appendix 3 for the mass spectrometry parameters and raw data from a representative run.

RNA extraction and microarray analysis. RNA was extracted using Qiagen's RNA extraction kit, as recommended. Samples were Cy3-labeled or Cy5-labeled during cDNA synthesis, and pooled controls were hybridised to HEEBO spotted arrays (Invitrogen). Slides were scanned and fluorescence intensities were quantified using the QuantArray software package (Perkin-Elmer). Inversion of fluorophores in cDNA probes were done (dye swap) to account for nonspecific dye-associated effects on hybridisation and signal detection. We then applied the Lowess scatter smoothing algorithm from the GeneSpring 7.0 software package (Agilent Technologies) to normalise the raw fluorescence data. The "Filter on Confidence" and ANOVA (Welch t test) statistical tools from GeneSpring were used to identify genes with reproducible changes in transcript abundance. In both cases, we applied the Benjamini and Hochberg False Discovery Rate multiple testing correction algorithm. The same software package was used to perform hierarchical clustering and principal component analysis.

Statistical tests. All tests were performed using SPSS Pack 9.0 software (SPSS Inc., IL, USA). Descriptive statistics were applied: one-way ANOVA's, independent sample two-tailed t-tests, unpaired t-tests and Tukey's test for multiple comparisons. P values less than 0.05 were considered significant. For all correlation studies, parametric analyses were used. We have used the R^2 method to estimate correlations and trends and set relationships with $R^2 > 0.8$ as trending $R^2 > 0.9$ as correlative.

In vitro MMP14 activity assay. rRobo1-Fc (R&D Systems) which corresponds to residues 19-560 of rRobo1 fused to IgG1 Fc domain (with a linker peptide IEGRMD) was added to soluble MMP14 (solMMP14-Flag) for 8h in MMP digestion buffer, 50 mM Tris-HCl, pH 7.5, 10 mM CaCl₂, 0.15 M NaCl, 0.05% Brij35. Samples were then

denatured with boiling Lameli buffer and resolved by SDS-PAGE. Recombinant Fc-IEGRMD (Fc IgG1 with linker peptide) was used as control.

MTT cell proliferation assay. Cells were seeded at 2000 cell per well density in a 96 well plate. MTT was added 24h after treatment at 2mgml^{-1} 25ul for 4h at 37C; media was vacuumed and replaced with 100ul of DMSO for 1h at 37C, and the absorption was detected by spectrophotometer at 595nm. The exponential growth function (also known as the Malthusian growth model), whereby $Y = Y_0 e^{nX}$ where Y is the population number at time point X and Y_0 is the population at time $X = 0$, and n is the growth rate. The R2 is the coefficient of determination, which is calculated by the software as follows: For a function Y(X) the ln value (natural log) of Y and X values are first obtained, and the observed values are compared to a modelled function (ideal) using the equation $R^2 = 1 - SS_{\text{err}} / SS_{\text{tot}}$, where SS_{err} is the residual (error) sum of squares and SS_{tot} is the total sum of squares. The coefficient measures how the experimental function deviates from the predicted (ideal) function.

Collagenase activity. We analysed MMP14-specific collagenase activity using the an ELISA-based colorimetric detection kit commercially available (GE). Briefly, media from cells cultured in 24wp was removed and replaced with extraction buffer and incubated at 4degC for 15min. The supernatant was then serially diluted and assayed as per manufacturer's recommendations. The readings were done at $t=0$ and $t=2.5\text{h}$. A standard curve was prepared on the same plate. The units of collagenase activity are expressed in $\Delta\text{OD}_{405} \times 10^3 / t^2$ where ΔOD_{405} is the OD_{405} at time 2.5h - OD_{405} at time 0h, and t is the duration of the assay. The values are multiplied by 10^3 to simplify their representation.

Band Intensity Quantification. Signal intensity from western immunoblot film papers was quantified using the Image J software. Briefly, films were scanned with an HP G4 series scanner at high resolution and the image was converted to an 8-bit gray scale. Once loaded in Image J, the bands were outlined, labeled, and the intensity of the signal was plotted. The signal was computed by the software (integration). In all cases, reference proteins (e.g., tubulin) were used to account for loading discrepancies. In the case of MMP14, the signal intensity of total MMP14 (pro and mature forms) was evaluated.

Immunoprecipitation. Cells expressing the cDNA of interest (e.g., rRobo1N-Flag or hSLIT2-myc) were lysed in RIPA and the soluble fraction was incubated with anti-Flag M2 or anti-myc (Sigma) slurry for two hours, washed 3x with RIPA, boiled in Laemmli buffer, resolved by SDS-PAGE, transferred onto a nitrocellulose membrane, and immunoblotted with the appropriate antibody.

Sequences of shRNAmiR. The following sequences were used to target Rat MMP14 mRNA and have been published (Ferraro et al., 2011).

shRNAmiR-MMP14-1: GAAACCATAGAACCTTTGCATG

shRNAmiR-MMP14-2: GTCATCAGGCAACACGAAGTTC

Non-targeting shRNAmiR-Ctl: AATTCTCCGAACGTGTCACGT

Primer Sequences.

rRobo1 (Cloning)

F: ATGAAATGGAAACATCTTCCTC; R: TCTGCTCTCGCTTCTATAGAAGC

rRobo1N (Cloning)

F: ATGAAATGGAAACATCTTCCTC; R: CAAAATGTGG TGGCTCTTGAAC

ROBO1

F: GCATATGGAATTAGTGATCCAAGC; R: CCTGCTTGTGGTCCACC

ROBO2

F: GATCAGATTGTTGCTCAAGGTCG; R: GTAAATCCCTCCTTTAACCAGC

ROBO3

F: GGGAAGCTGATGATGTCACATAC; R: TCCTTCTGCCAGAAGATGGCAG

ROBO3.1

F: GCAGCAGGCAGCATGTCCTC; R: TCTCGGCGTTTCTGTCCTGG

ROBO3.2

F: GCAGCAGGCAGCATGTCCTC; R: CACAGTCTCCTGTGGCAGCA

ROBO4

F: AGCAGCCTCAGCAGTCG; R: TCTGGAAGCAGGGGCAC

SLIT1

F: TGGCCTTCCCTGACTTCAGGTGTG; R: GTTCCTTGTAGCCAGTCTTCACCC

SLIT2

F: CAGATCAAAAGCAAGAAATTCCG; R: GAACATCTTATGCTGCACATTTTC

SLIT3

F: GACCCCAGGCCAACATC; R: TCCAGTGCCAGGGGGTC

hS14 (reference)

F: GGCAGACCGAGATGAATCCTCA; R: CAGGTCCAGGGGTCTTGGTCC

MMP14

F: ATGTCTCCCGCCCCA; R: TCAGACCTTGTCCAGCAGG

Collagen VI alpha 1

F: ACTCTTTTGTGATGCACACCA; R: AAGCTGTAAGCGTTTGCGTA

PIK3R3

F: GGACACGGACAGGATTGACA; R: ACCCACGGAATCGAGAAAGA

ARHGDIA

F: CAGGAAAGGCGTCAAGATTG; R: GTCAGGAACTCGTACTCCTC
ITGA3 (integrin)

F: GAAGGAACAAAGACAGGCAAAC; R: TGGTGAGTGAGAAGTGGCATC
HK1 (hexokinase1)

F: TCCGTAGTGGGAAAAAGAGAA; R: GACAATG TGATCAAACAGCTC
APP

F: ACTGACCACTCGACCAGGT; R: TTTGAACCCACATCTTCTGCAA
cathepsin D

F: CATTGTGGACACAGGCACTTC; R: GACACCTTGAGCGTGTAGTCC
MAGED2

F: CCAGACGAAGATTCCCATCAAGC; R: TGACAGCCTCACTGGACCGA
p53

F: ATAGTGTGGTGGTGCCCTATGA; R: TGTGATGATGGTGAGGATGG
p21

F: CCTAATCCGCCACAGGAA; R: ACC TCCGGGAGAGAG GAA AA
p16INK4a

F: GGGGGCACCAGAGGCAGT; R: GGTTGTGGCGGGGGCAGTT
EGFR

F: GATCACGGCTCGTGTGTCC; R: ATGCCTATGCCATTGCAAAC
NCAD

F: CCACCTTAAAATCTGCAGGC; R: GTGCATGAAGGACAGCCTCT
ABL1

F: AAGTCAGATGCTACTGGCCG; R: GGAGCAGGGAAGAAGGAATC
MMP2

F: GGAAAGCCAGGATCCATTTT; R: ATGCCGCCTTTAACTGGAG
MMP9

F: TTGGTCCACCTGGTTCAACT; R: ACGACGTCTTCCAGTACCGA

Furin

F: CCTGCTCACTGCCTGTGG; R: CTCTGGAGCTGGATGGTGA

PC5

F: AATCCCTCTTTGTCCGCTTT; R: TTATCTCGAGCAGAGGGACC

RAT-Robo1-HA

F: TACCCATACGATGTTCCAGATTACGCT (spanning HA tag); R:
AGAGTGAGGAGAGATATCATGAC

Edman degradation. N-terminal protein sequencing was performed by Alphalyse (Palo Alto, USA). The sample preparation was as follows: Recombinant rRobo1-Fc was treated with MMP14 for 8h and the sample was resolved on a 5-20% gradient polyacrylamide gel. The gel was transferred onto a PVDF membrane and the membrane was stained with 0.4% m/v Coomassie Brilliant Blue 250 for 5min and destained for 2h. The band corresponding the 110 kDa fragment (c-terminal fragment) was cut out using a blade and sent for Edman degradation.

2.5 Figures and Tables

Figure I-1. A schematic diagram depicting key events involved in cellular migration. (A) A stationary cell is tethered at focal adhesion sites (FA) where transmembrane adhesion molecules participate in linking the FA sites to the extracellular matrix (ECM). (B) Upon a pro-migratory stimulus (of extra- or intra-cellular origin), the cell may secrete ECM-degrading enzymes leading to ECM degradation (white arrows on micrograph) at the leading edge of the cell. (C) The pro-migratory stimulus activates the disassembly of FAs at the rear-end of the migratory cell and promotes the protrusion of the membrane at the front-end of the cell filling in the newly degraded space. (D) New FA sites form and mature and the cell adopts a stationary position. Below, the scanning electron micrographs demonstrating C6 cells in a three-dimensional collagen type I matrix, as used in our studies (Del Maestro et al., 1995). Permission granted from Springer-Verlag New-York Inc.

Figure I-1

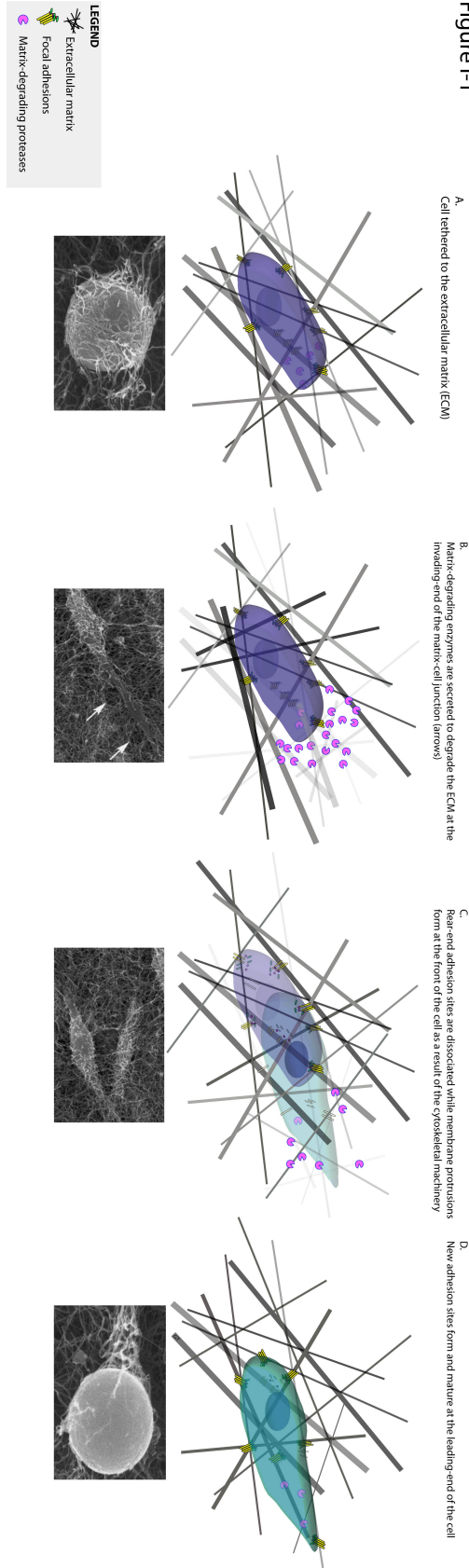
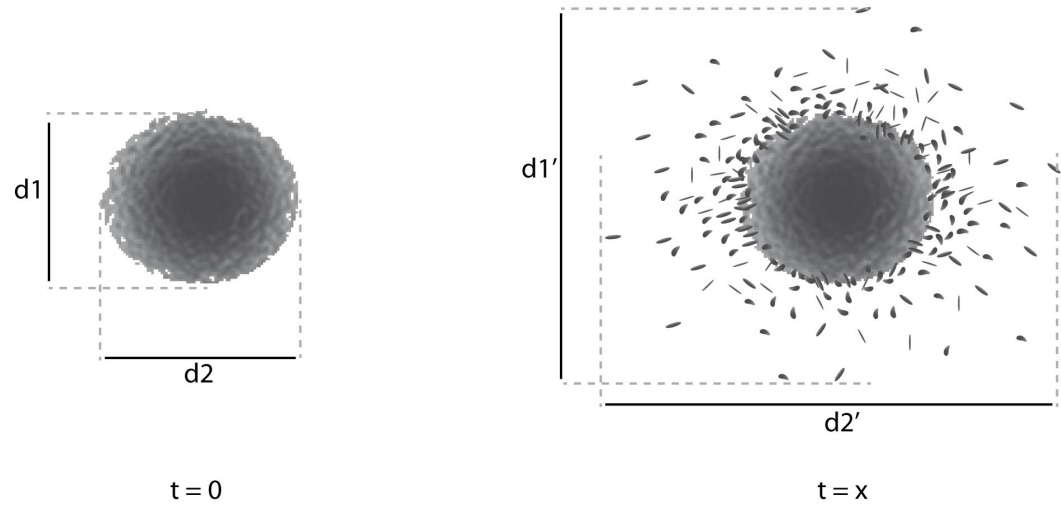


Figure I-2. The collagen type I invasion assay. A cell aggregate – spheroid – is implanted in a collagen type I matrix and allowed to invade the matrix for a determined duration ($t = x$). The invasion is quantified by measuring the difference between the average radius (measured on two orthogonal axes) of the spheroid at times 0 and x .

Figure I-2



At $t = x$, relative invasion distance = $0.5 \cdot (d1' + d2') - 0.5 \cdot (d1 + d2)$

Figure I-3. Diagram depicting the different genetic alterations that glioma cells of origin undergo during their progression, giving rise to glioblastomas.

Figure I-3

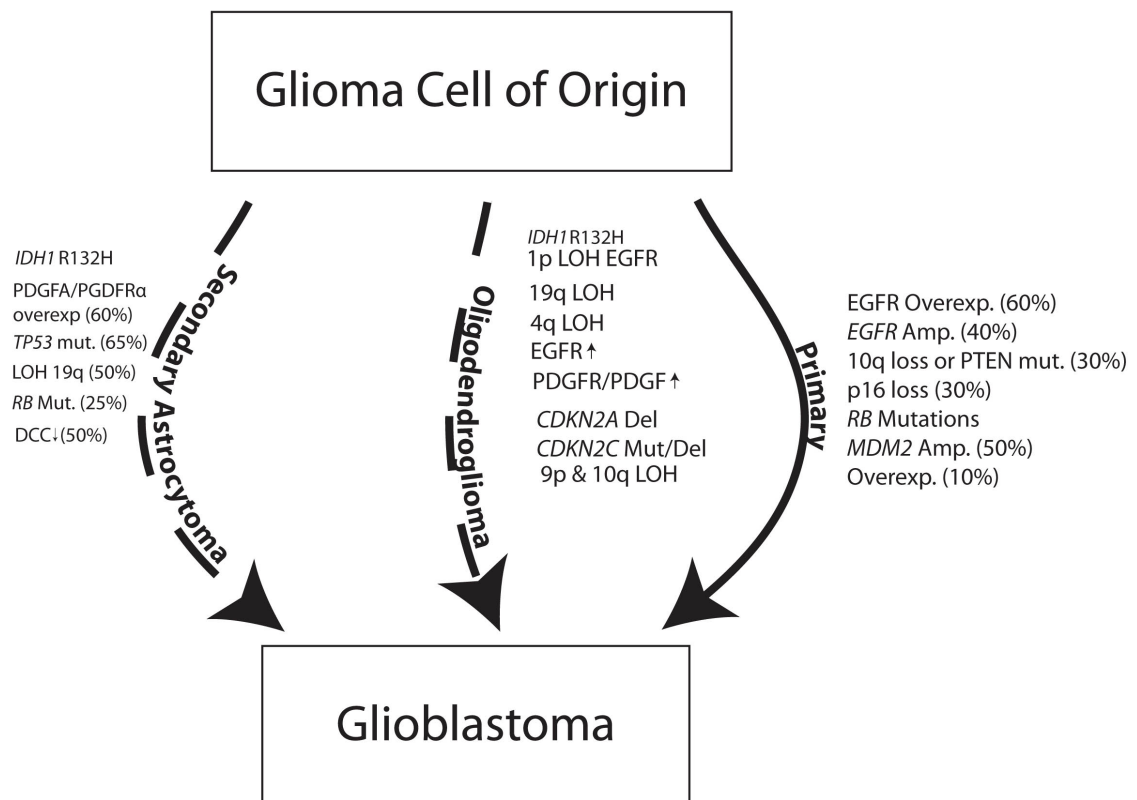


Figure I-4. Schematic diagram depicting the different cellular processes impacted by gliomagenesis, and the frequency of the different genetic and epigenetic aberrations observed in glioblastomas.

Figure I-4

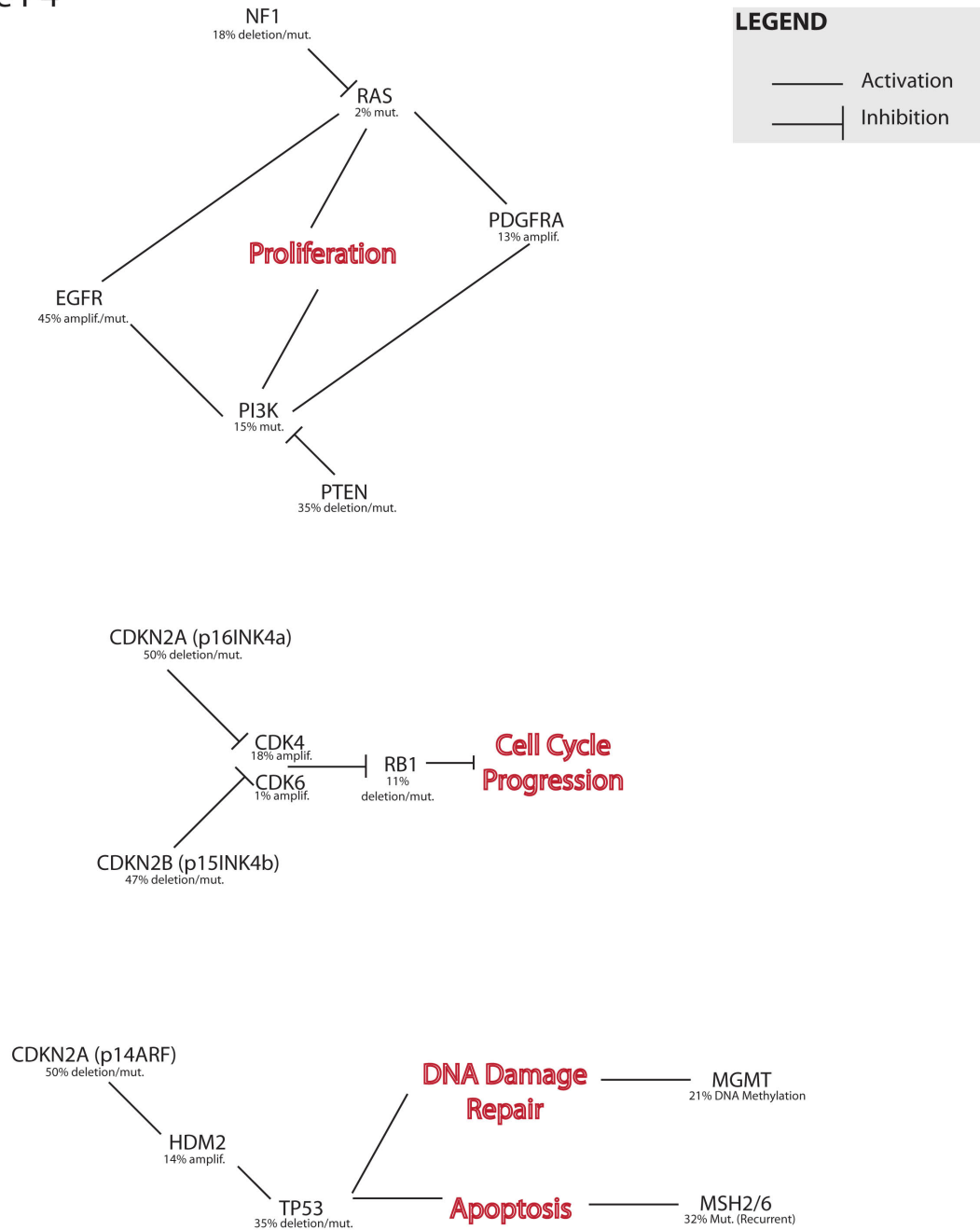
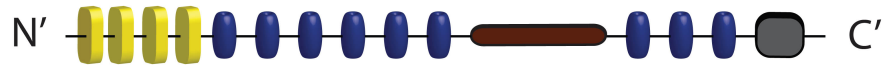






Figure I-5. Schematic diagram depicting the conserved domains of prototypical SLIT (A) and ROBO (B) proteins.

Figure I-5

A. **SLIT**



-  leucine rich repeats
-  EGF Domains
-  Laminin G Domain
-  Cysteine Knot

B. **ROBO**







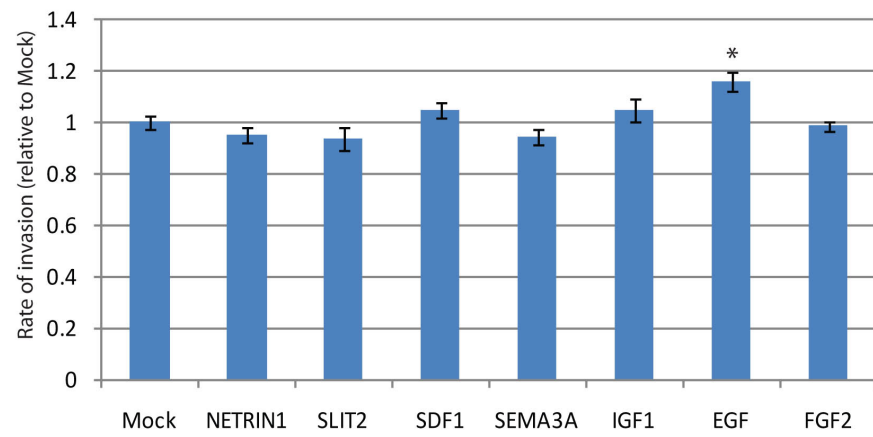
-  Immunoglobulin Domain
-  Fibronectin type 3 repeats
-  transmembrane Domain
-  Conserved Cytoplasmic Sequences

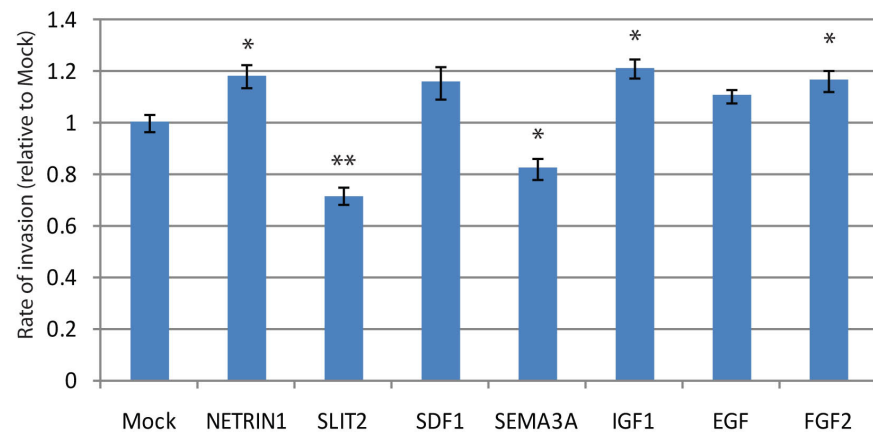
Figure 1. Spheroids were prepared and implanted in collagen type I using two medulloblastoma cell lines, UW3 (A) and DAOY (B), and two glioma cell lines, U251 (C) and C6 (D). The spheroids were treated with mock (conditioned media), or commercially obtained recombinant proteins (commercial): NETRIN1, SLIT2, SDF1, SEMA3A, IGF1, EGF, and FGF2, at 50 (low), 100 (intermediate), and 200 (high) ng/ml for 5 days (media was changed every 48h). Invasion distance was measured on days 0 and 5 and invasion (relative to day 0) is reported. All values are standardised to mock treatment (HEK293 conditioned media). Values are means from three independent experiments \pm s.e.m. Statistical analysis: one-way ANOVA followed by Dunnett's post-hoc test. Statistically significant differences are indicated by asterisks, where *, $p < 0.05$, and **, $p < 0.01$.

Figure 1. A.

UW3 - Low



UW3 - Intermediate



UW3 - High

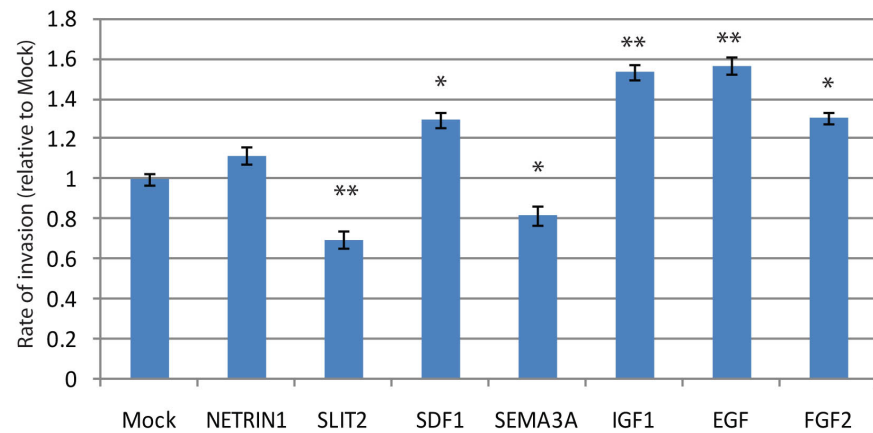


Figure 1. B.

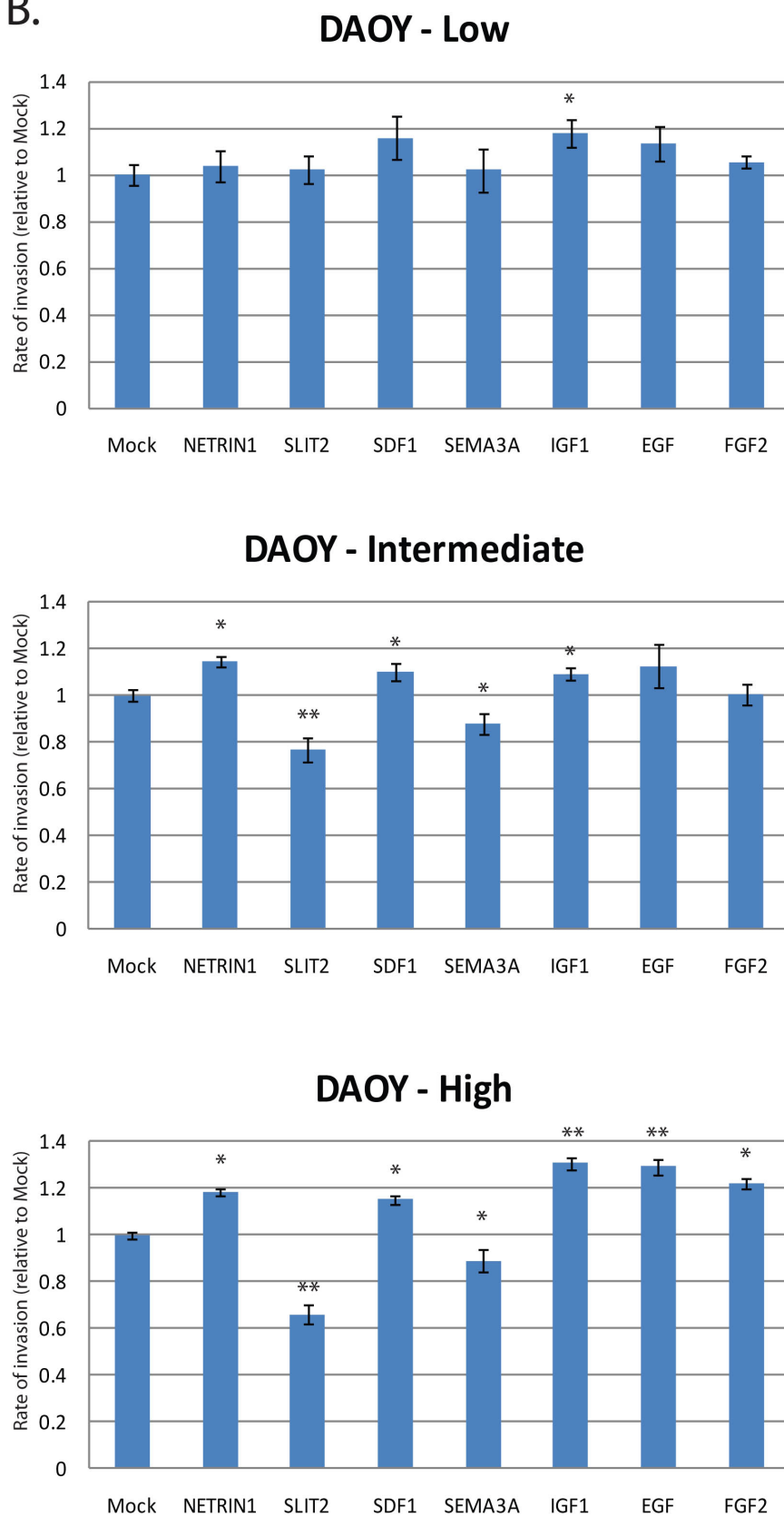


Figure 1.C.

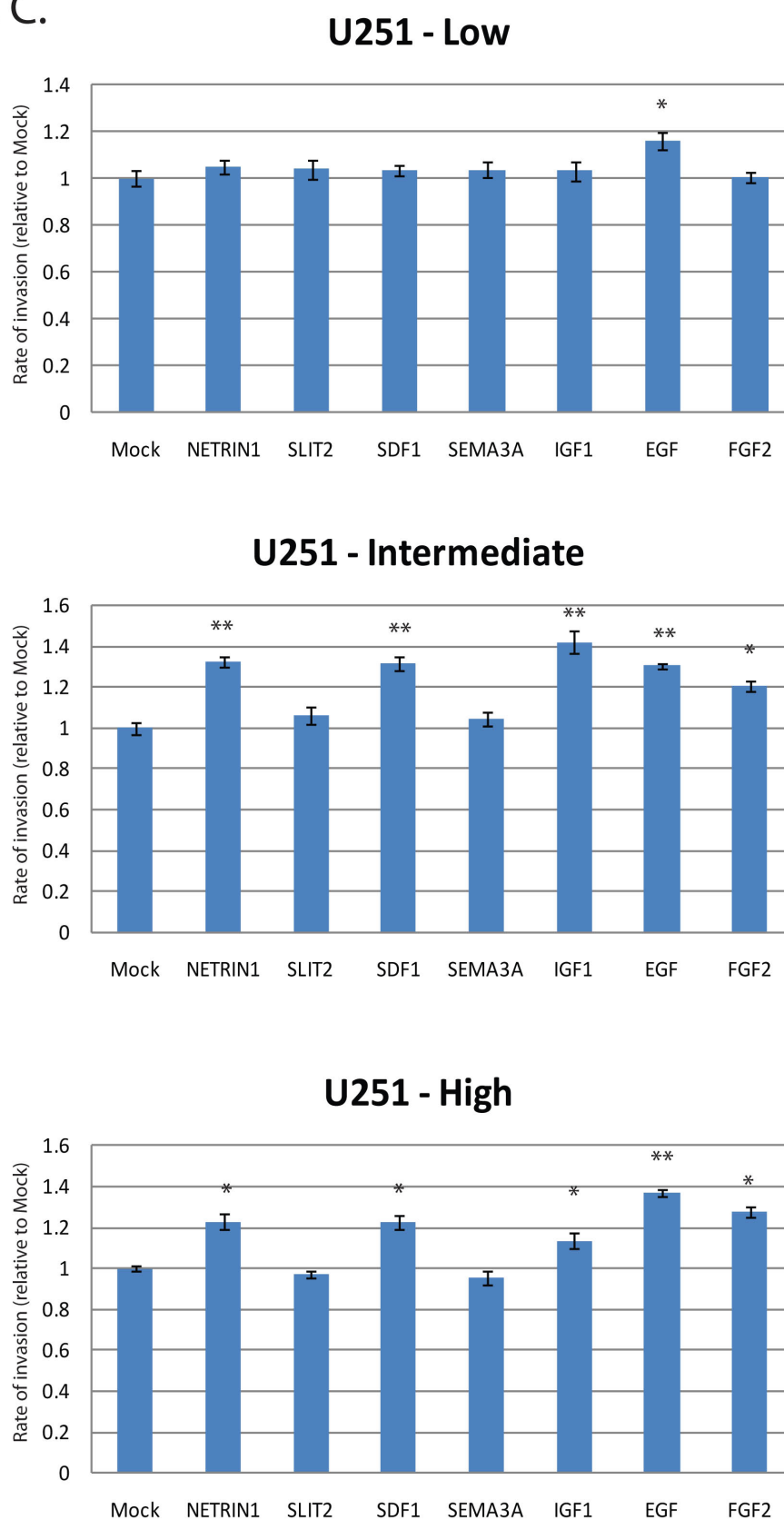


Figure 1. D.

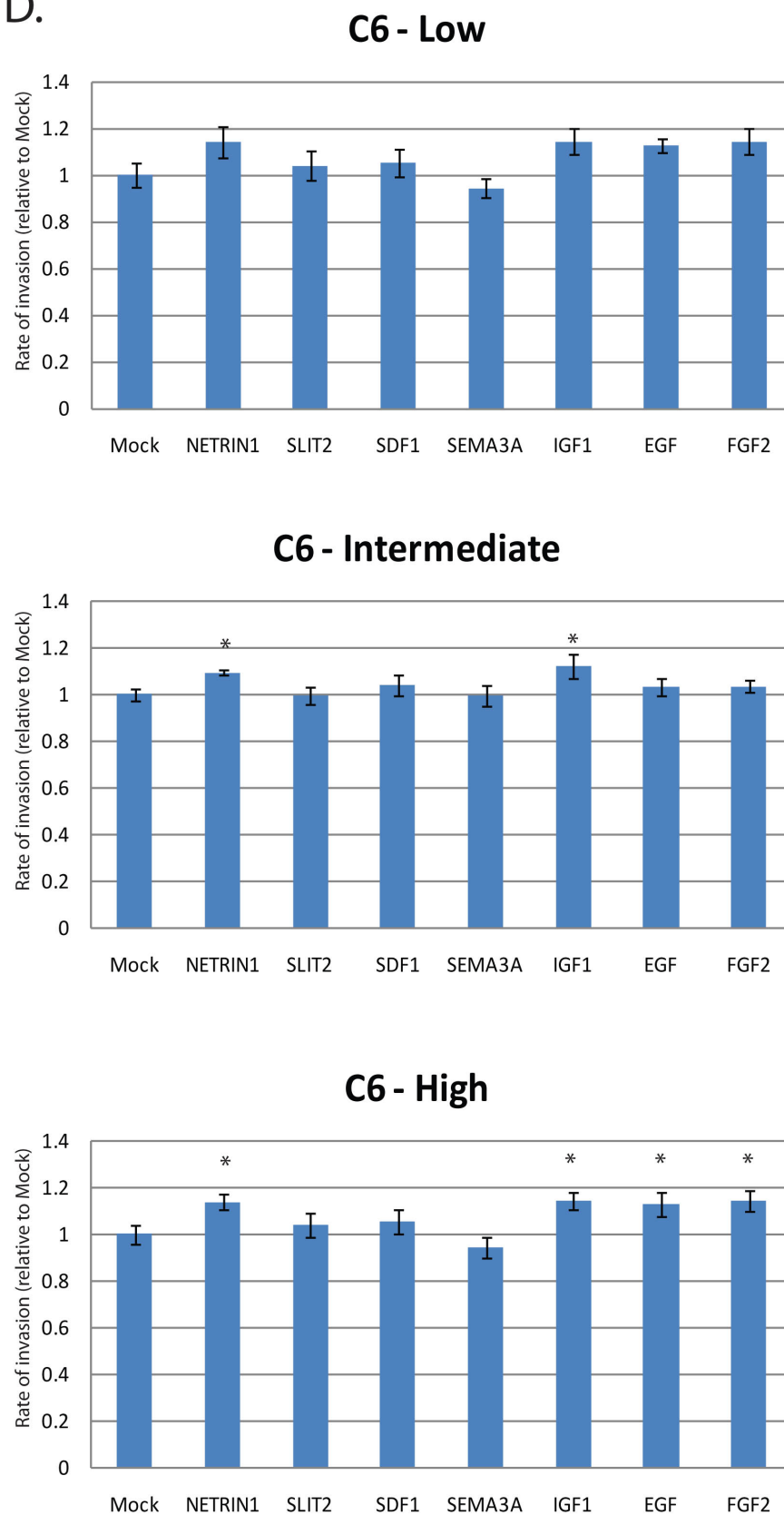


Table 1. Summary of the results presented in Figure 1. The effect on invasion is denoted by: ++, strong increase in cell invasion; +, moderate increase in cell invasion; --, strong decrease in cell invasion; -, moderate decrease in cell invasion; 0, no significant effect on cell invasion.

Table 1. Summary of the effect of different recombinant proteins (and at different concentrations) on brain tumour cell invasion.

A. Low

	NETRIN1	SLIT2	SDF1	SEMA3A	IGF1	EGF	FGF2
U251	0	0	0	0	0	+	0
C6	0	0	0	0	0	0	0
DAOY	0	0	0	0	+	0	0
UW3	0	0	0	0	0	+	0

B. Intermediate

	NETRIN1	SLIT2	SDF1	SEMA3A	IGF1	EGF	FGF2
U251	++	0	++	0	++	++	+
C6	+	0	0	0	+	0	0
DAOY	+	--	+	-	+	0	0
UW3	+	--	0	-	+	0	+

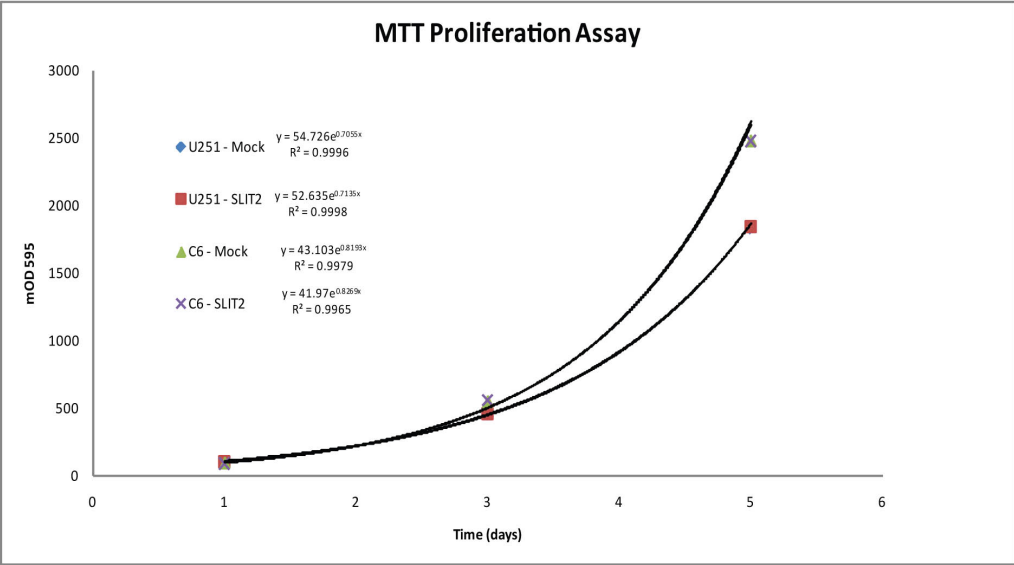
C. High

	NETRIN1	SLIT2	SDF1	SEMA3A	IGF1	EGF	FGF2
U251	+	0	+	0	+	++	+
C6	+	0	0	0	+	+	+
DAOY	+	--	+	-	++	++	+
UW3	0	--	+	-	++	++	+

Figure 2. Exogenous treatment of hSlit2 does not affect glioma and medulloblastoma proliferation. MTT proliferation of mSlit2 (commercial, 100ng/ml) or mock treated U251 and C6 glioma cells (A) and DAOY and UW3 medulloblastoma cells (B). Cells were treated during the entire duration of the assay and media was changed every 48h. The exponential growth equations and the r-squared values are included to demonstrate predicted versus experimental exponential growth. The results of glioma and medulloblastoma cell lines are also presented as bar graphs in C and D, respectively. Proliferation was assayed by spectrophotometric means (OD 595nm) on days 1, 3 and 5. Values are means from three independent experiments +/- s.e.m. Statistical analysis: one-way ANOVA followed by Dunnett's post-hoc test. No statistically significant difference was observed between treated groups *versus* mock treated groups.

Figure 2.

A. Glioma



B. Medulloblastoma

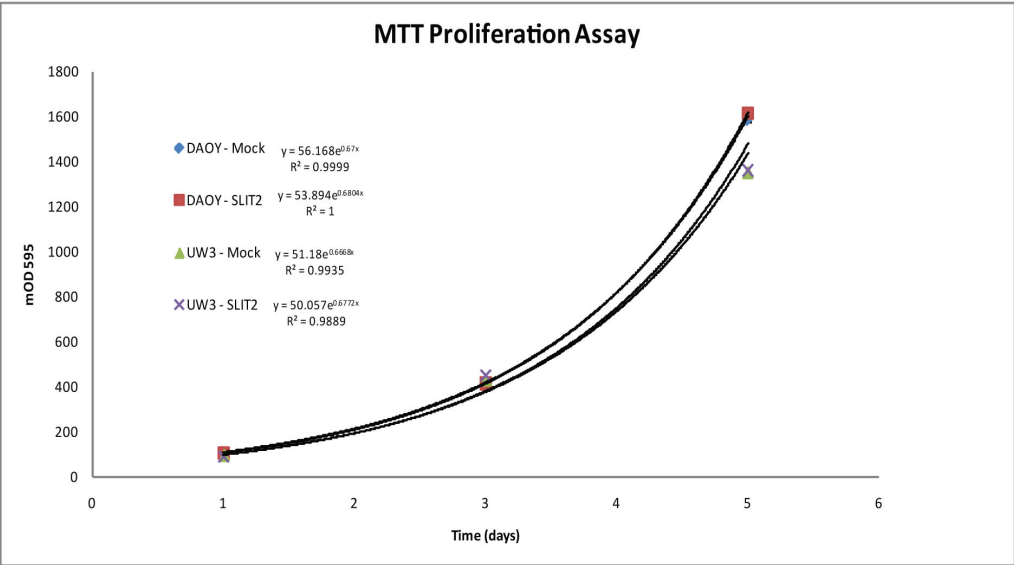


Figure 2.

C. Glioma Cell Lines

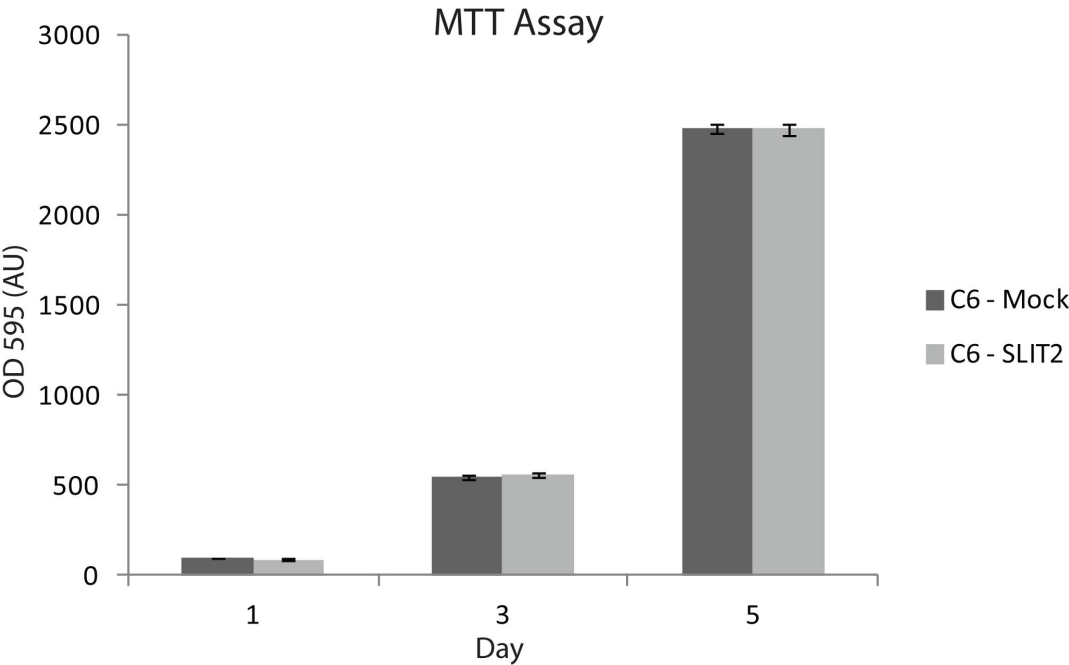
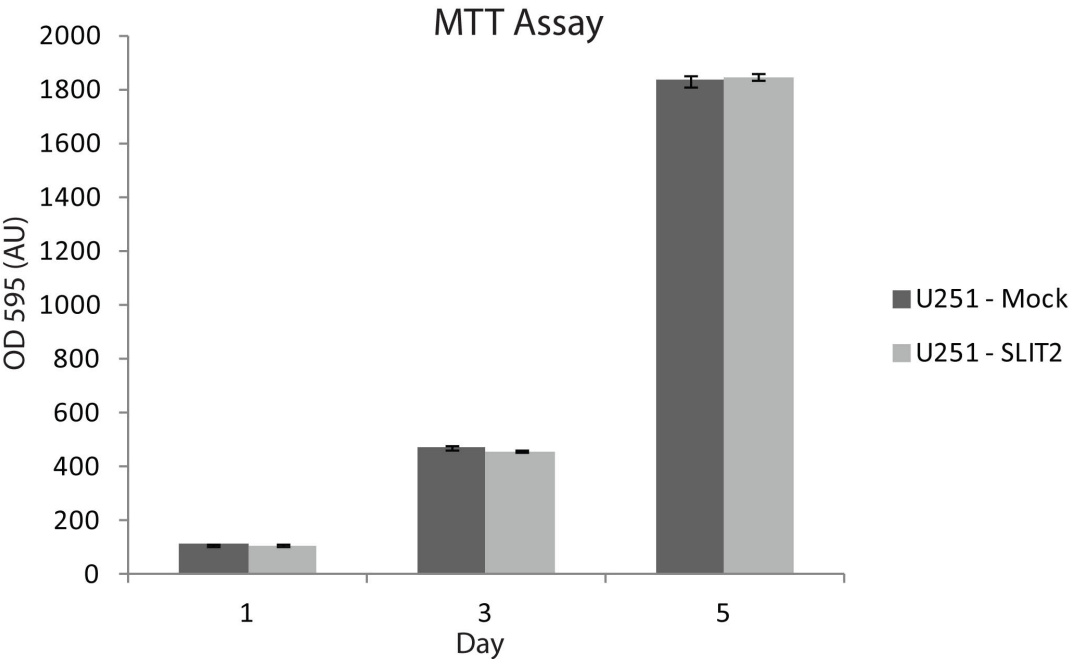


Figure 2.

D. Medulloblastoma Cell Lines

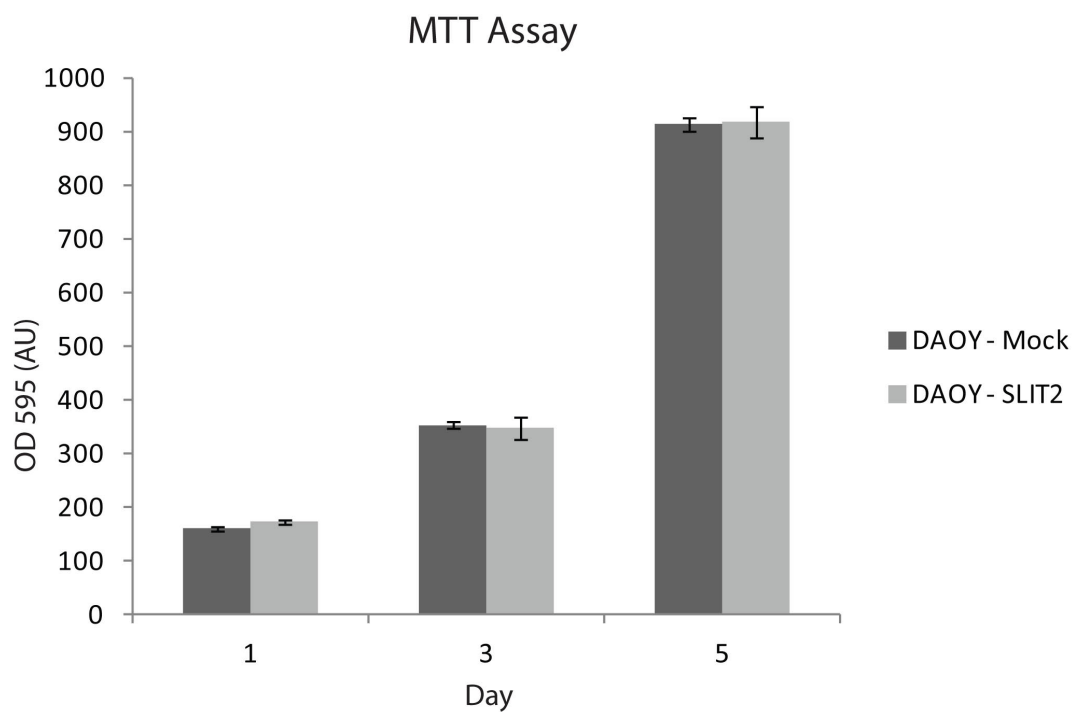
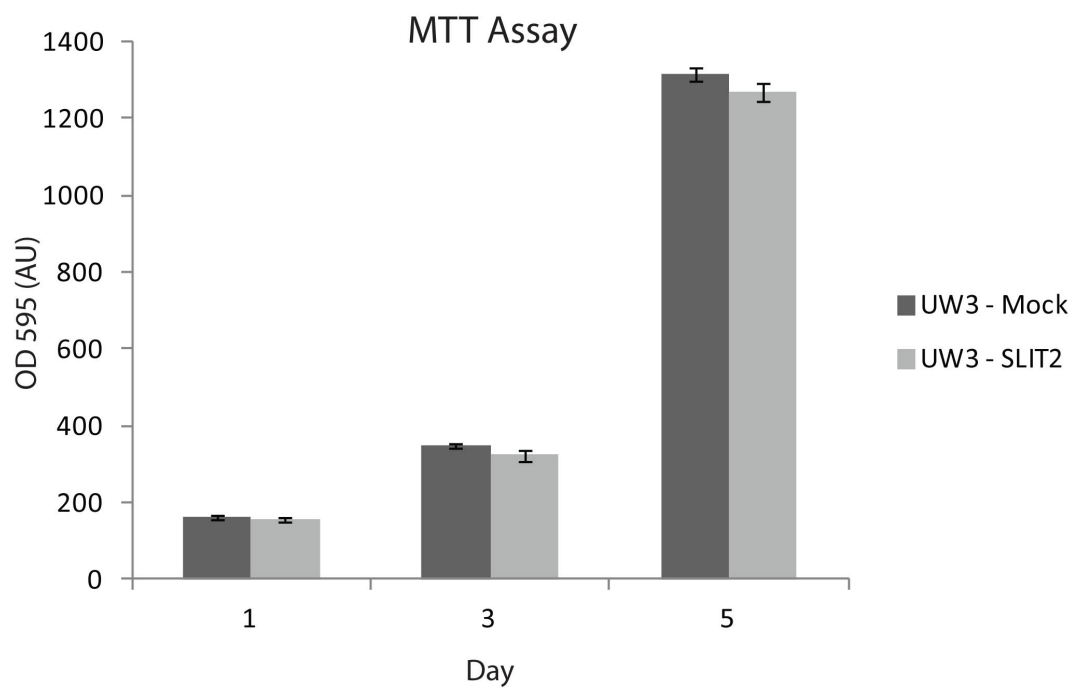
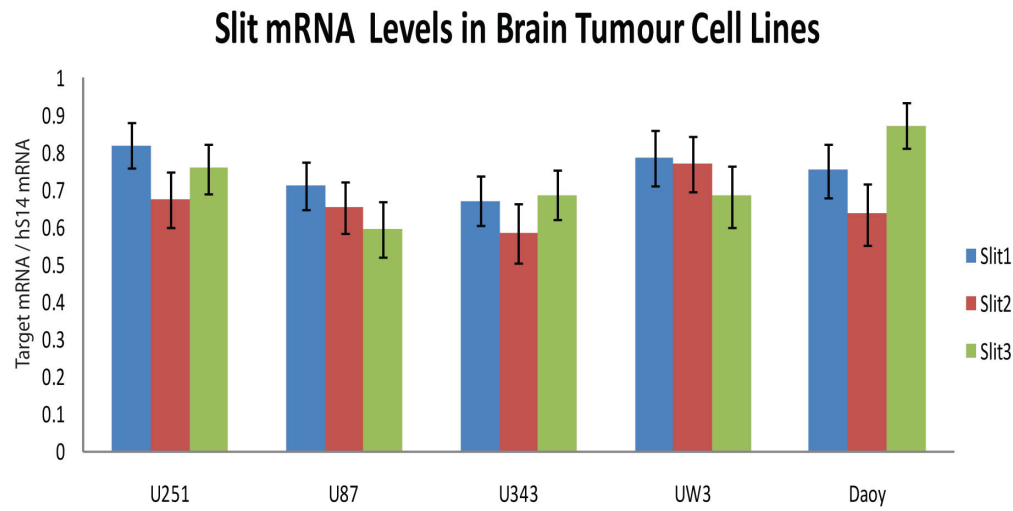


Figure 3. Quantitative RT-PCR was used to determine the mRNA levels of (A) slit1, slit2, slit3 and (B) robo1, robo2, robo3 (including robo3.1, robo3.2) and robo4 in glioma (U251, U87, U343) and medulloblastoma (UW3 and DAOY) cell lines. (C) robo1, robo2, robo3 (including robo3.1, robo3.2) and robo4 in normal white (n=6) and normal gray (n=6) matter from human tissue samples. The levels of all Robos were also measured in U251 and UW3 to compare their expression with human tissue levels. Values are means from three independent experiments \pm s.e.m. Statistical analysis: ANOVA followed by Tukey's post-hoc test where $p < 0.05$ was considered statistically significant. No statistically significant difference was observed between the groups.

Figure 3.

A. Slit



B. Robo

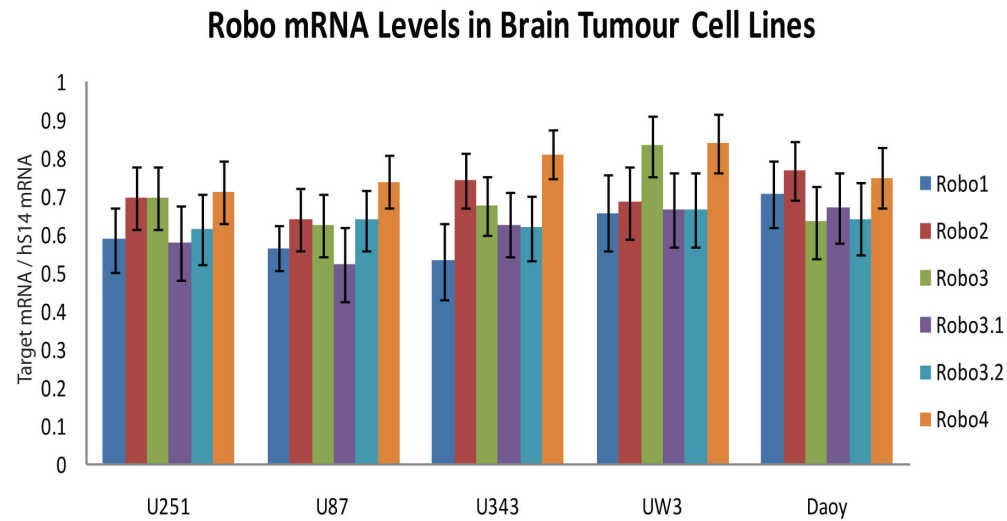
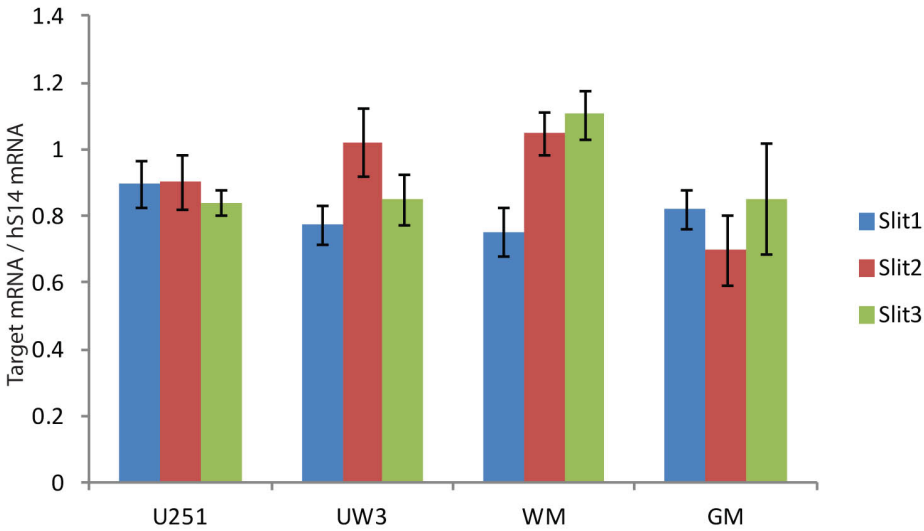


Figure 3.

C. Slit in human brain tissue



D. Robo in human brain tissue

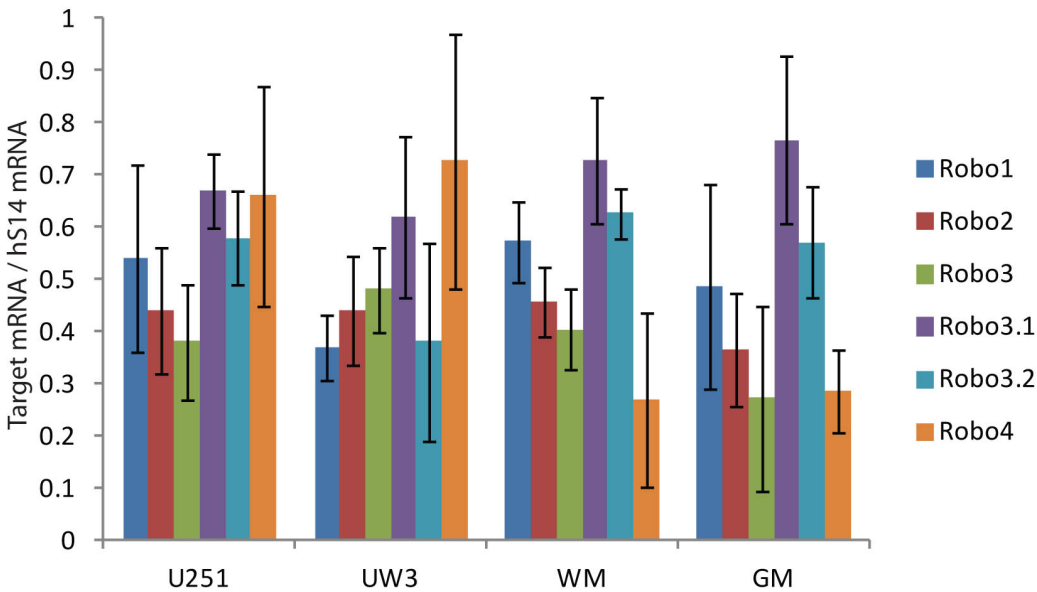


Figure 4. Cell surface biotinylation assays. The surface expression of rRobo1-HA was determined by surface biotinylation assays followed by western immunoblotting. (A) A representative blot showing rRobo1-HA expressed (I) in and detected at the cell surface (S) of U251 cells. The ERK1/2 (p44/42) cytoplasmic protein (absent at the cell surface) was probed as a cell surface protein enrichment control. (B) Wound healing migration assay whereby U251 cells were grown to 100% confluency and scratched to allow cells to migrate into the wound for 16h. The rate of invasion was measured in presence of hSLIT2-myc (purified by previously published gel chromatography method, used throughout the assay at 100 ng/ml). (C) Spheroids of U251-mock and U251-rRobo1-HA cells were implanted in a collagen I matrix and their invasion rate was assayed in response to hSLIT2-myc treatment (purified by previously published gel chromatography method, used throughout the assay at 100 ng/ml). Invasion distance was measured on day 5 and relative invasion is reported. (D) A representative blot showing that rRobo1-HA is expressed (I) in and detected at the cell surface (S) of HeLa cells engineered to express rRobo1-HA. The ERK1/2 (p44/42) cytoplasmic protein (absent at the cell surface) was probed as a cell surface protein enrichment control. (E) Wound healing migration assay whereby HeLa cells were grown to 100% confluency and scratched to allow cells to migrate into the wound for 18h. The rate of invasion was measured in presence of hSLIT2-myc (purified by previously published gel chromatography method, used throughout the assay at 100 ng/ml). (F) Quantitative RT-PCR of stable cell lines expressing rRobo1-HA. Values are means from three independent experiments +/- s.e.m. Statistical analysis: Two-tailed, unpaired Student's t-test and statistically significant differences are indicated by asterisks, where *, $p < 0.05$.

Figure 4.

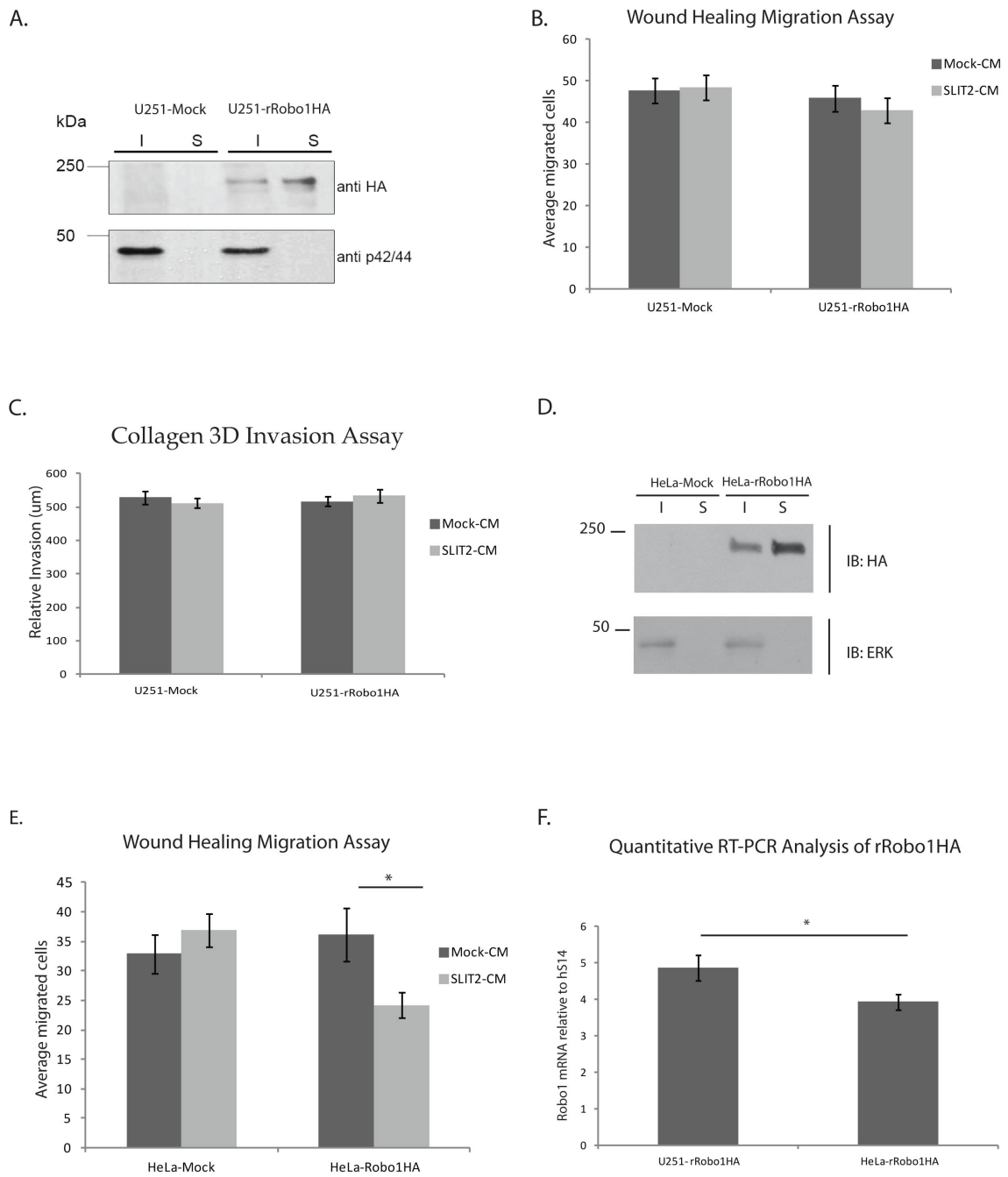


Figure 5. Rho GTPase activity assays. (A) The GTP-bound, active form of Rho GTPases were selectively pulled down using a GST-CRIB (Cdc42 and Rac) or GST-RBD (Rho) recombinant proteins, respectively. Immunoblots represent active Rho GTPase (GTP-bound) or total Rho GTPase (GTP- and GDP-bound). (B-D) Quantification of Rho GTPases' pull downs. (E-F) Commercially available colorimetric G-LISA assays were employed to measure the level of active Cdc42 and Rac, respectively. Results are normalised to the levels of mock-treated samples and are expressed as percent activity of mock-treated cells. In all cases, hSLIT2-myc was purified using the published method (gel chromatography) and the treatment of cells (100 ng/ml) span 24h. Values are means from three independent experiments +/- s.e.m. Statistical analysis: Two-tailed, unpaired Student's t-test. Statistically significant differences are indicated by asterisks, where *, $p < 0.05$, and **, $p < 0.01$.

Figure 5.

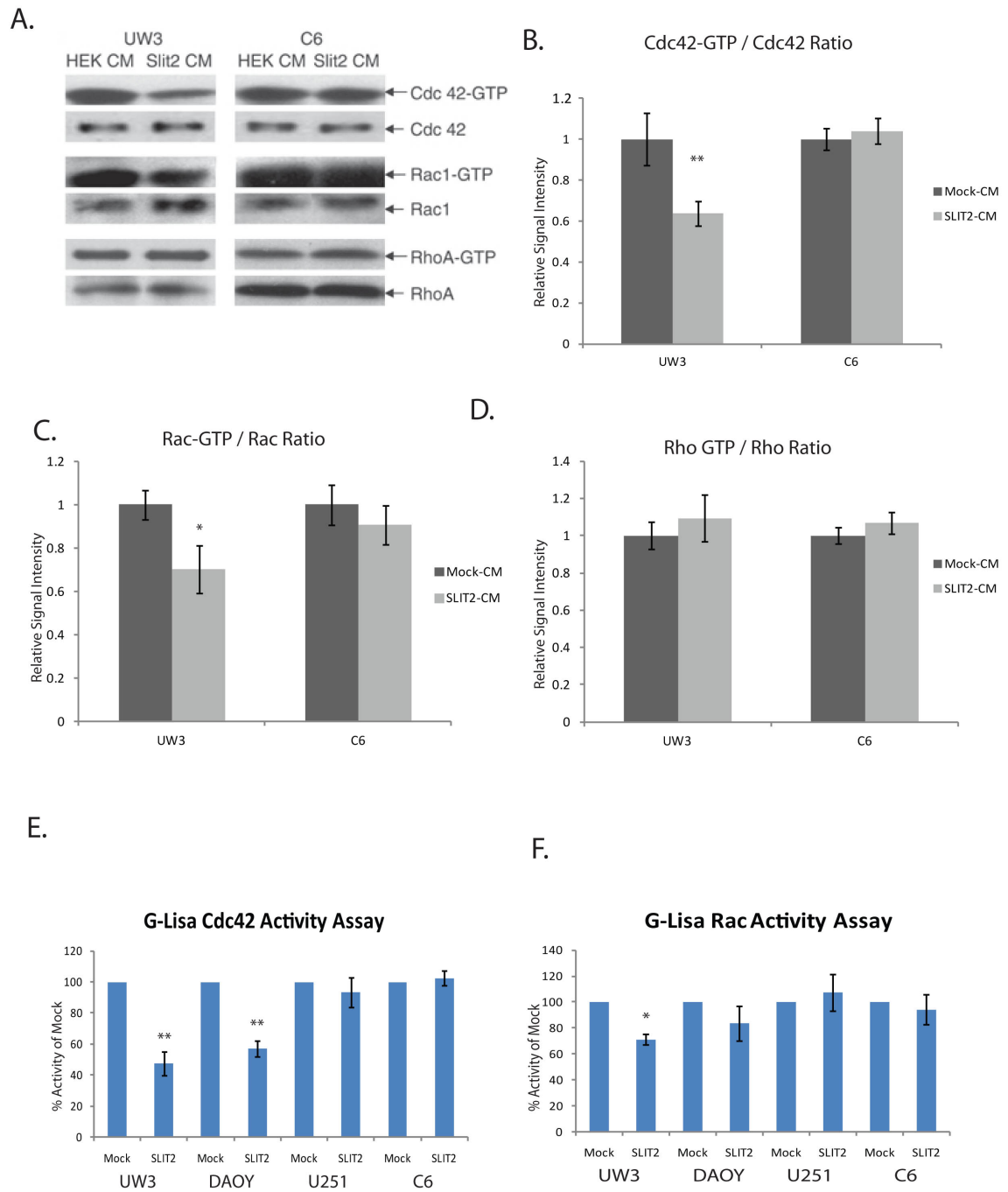


Figure 6. Spheroids were prepared and implanted in collagen I using two medulloblastoma cell lines, DAOY and UW3, and five glioma cell lines, C6, U251, U87, U343 and U373 that were mock or hSLIT2-myc treated (purified by previously published gel chromatography method, used throughout the assay at 100 ng/ml). Invasion distance was measured on day 3 and relative invasion was reported. Values are means from three independent experiments \pm s.e.m. Statistical analysis: Two-tailed, unpaired Student's t-test. Statistically significant differences are indicated by asterisks, where *, $p < 0.05$, and **, $p < 0.01$.

Figure 6.

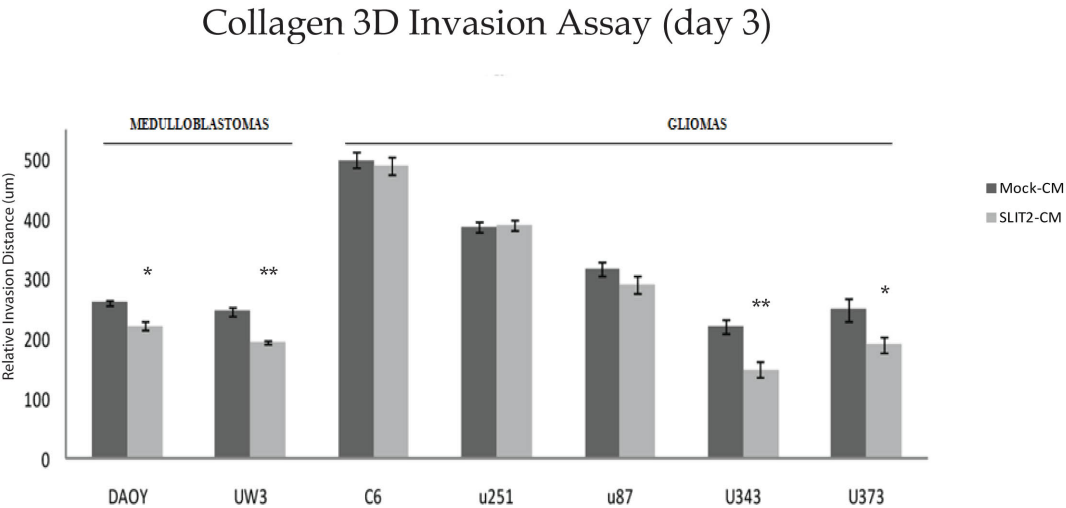


Figure 7. Step by step diagram of the previously reported method (Kidd et al., 1998b; Nguyen-Ba-Charvet et al., 2004) and our HPLC-based method for purification of hSLIT2-myc protein from HEK293-SLIT2 conditioned media. The conventional published method (left) of recombinant hSLIT2-myc protein purification involves the gel chromatography-based affinity and ionic exchange separation of cell culture media conditioned by cells expressing recombinant hSLIT2-myc. The column is then eluted with a high ionic strength buffer (e.g., 1M NaCl) and the elution fractions are dialysed overnight against a saline-like solution (compatible with biochemical/biological assays). Finally the dialysed conditioned media is concentrated. In our proposed method, conditioned media is immediately concentrated and loaded onto a semi-preparative loop (5ml) and applied to an affinity and ion exchange heparin column (HiTrap, 5ml) with an isocratic loading protocol (mobile phase, PBS; flow rate 0.5 ml/min). The recombinant hSLIT2-myc is then eluted from the column using a gradient elution (PBS-0.5M NaCl 0.5 ml/min). Fractions corresponding to eluted hSLIT2-myc proteins are then pooled and concentrated and their buffer exchanged with 2 equivalent volumes of PBS.

Figure 7.

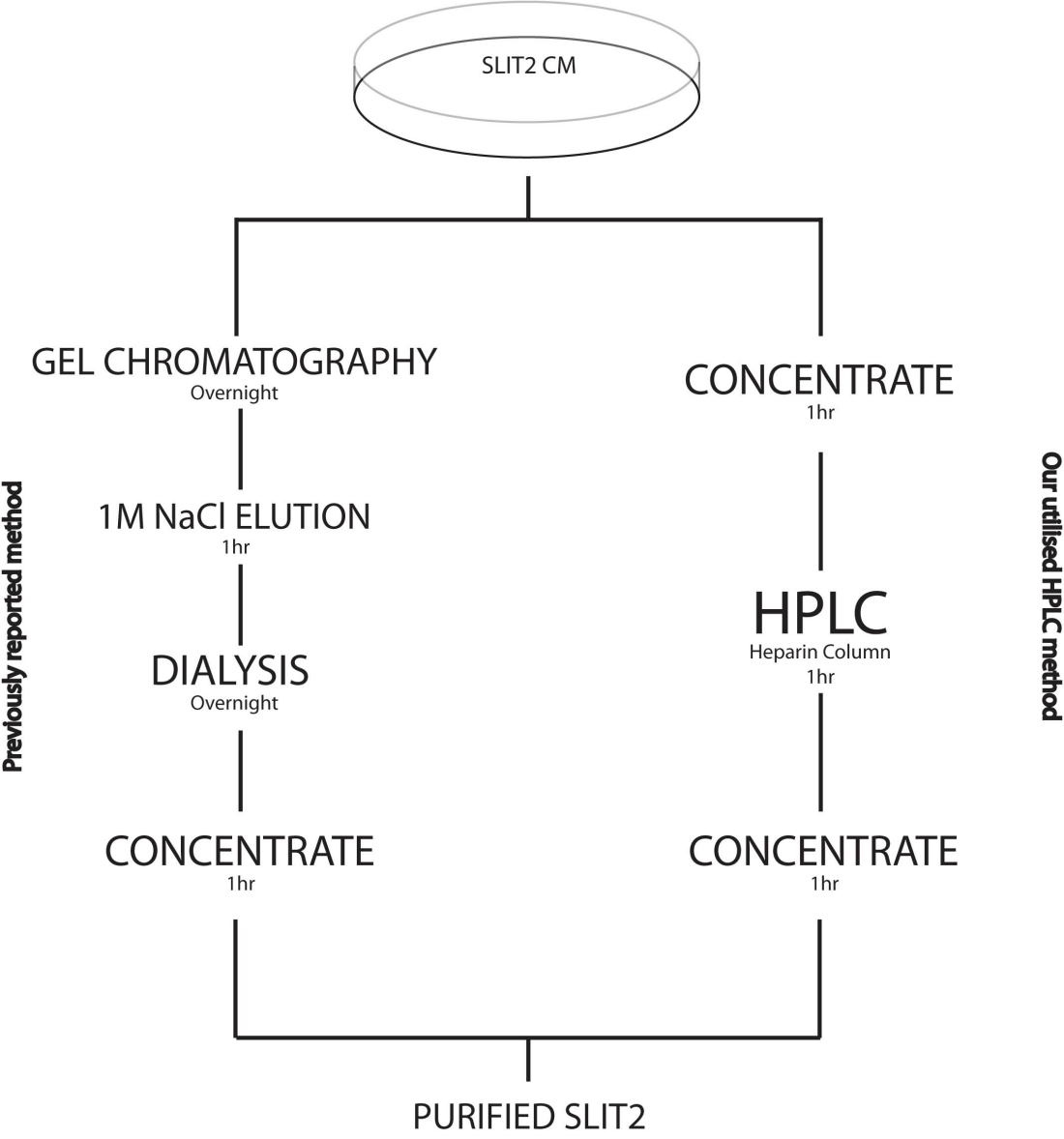
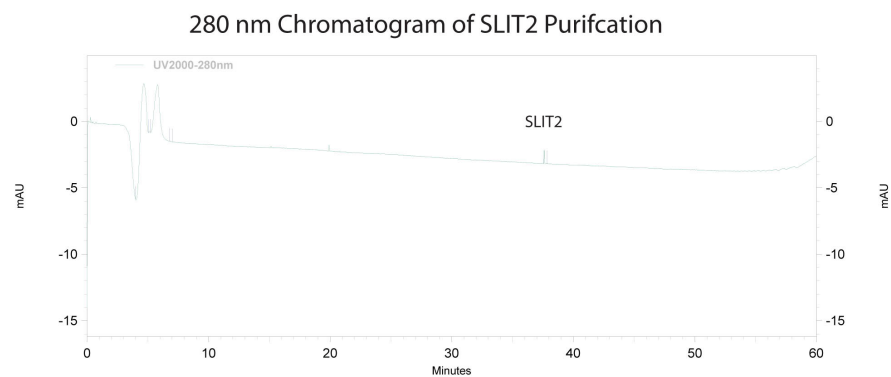


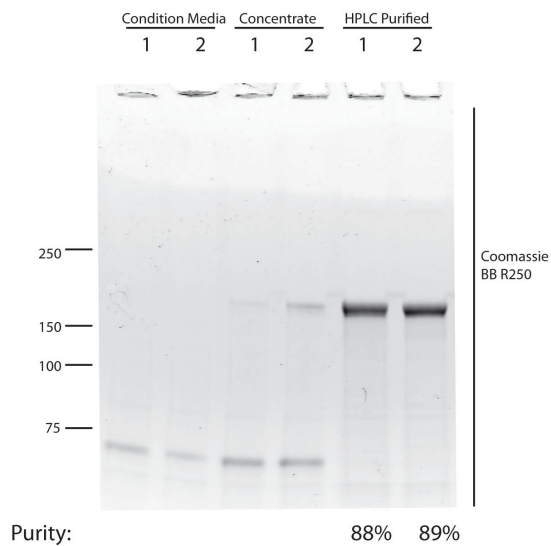
Figure 8. (A) UV Absorbance chromatogram at OD 280nm of a representative sample of hSLIT2-myc conditioned media that has undergone HPLC purification. Human SLIT2-myc peak is identified at 37.5 minutes. (B) Protein gel stained with Coomassie R-250 showing the purity of recombinant hSLIT2-myc. (C) Invasion assay to test the quality of recombinant hSLIT2-myc. Three sources of Slit proteins were used: Commercial mSlit2, hSLIT2-myc purified using the conventional (published) method mentioned in Figure 7, and the present HPLC-based purified method utilised in the present study. All Slit2 treatments for the invasion assay were used at 100 ng/ml, spanning the entire duration of the invasion assay. Values are means from three independent experiments +/- s.e.m. Statistical analysis: one-way ANOVA followed by Tukey's post-hoc test where $p < 0.05$ was considered statistically significant. Statistically significant differences are indicated by asterisks, where *, $p < 0.05$, and **, $p < 0.01$.

Figure 8.

A.



B.



C.

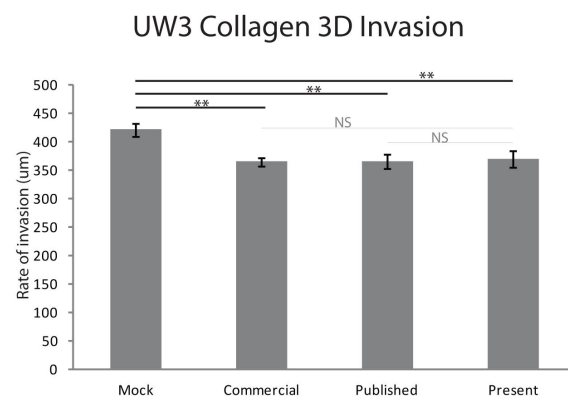


Figure 9. Schematic diagram outlining the microarray experimental steps. Messenger RNA from cells treated with SLIT2-myc (HPLC-purified, 100 ng/ml, 24h treatment) or mock conditioned media was extracted using a commercial kit. The mRNA served to synthesise a complimentary DNA probe using regular dNTPs and fluorescently labelled dCTP (Cy3, Cy5). The cDNA was hybridised onto HEEBO arrays and the relative fluorescence intensity quantified for each spot on the microarray. The fluorescence intensity bias was accounted for by swapping the dyes during cDNA synthesis. The relative fluorescence intensity is proportional to the cDNA concentration, which is in turn proportional to mRNA expression.

Figure 9.

Steps Involved in Micro Array Preparation and Analysis

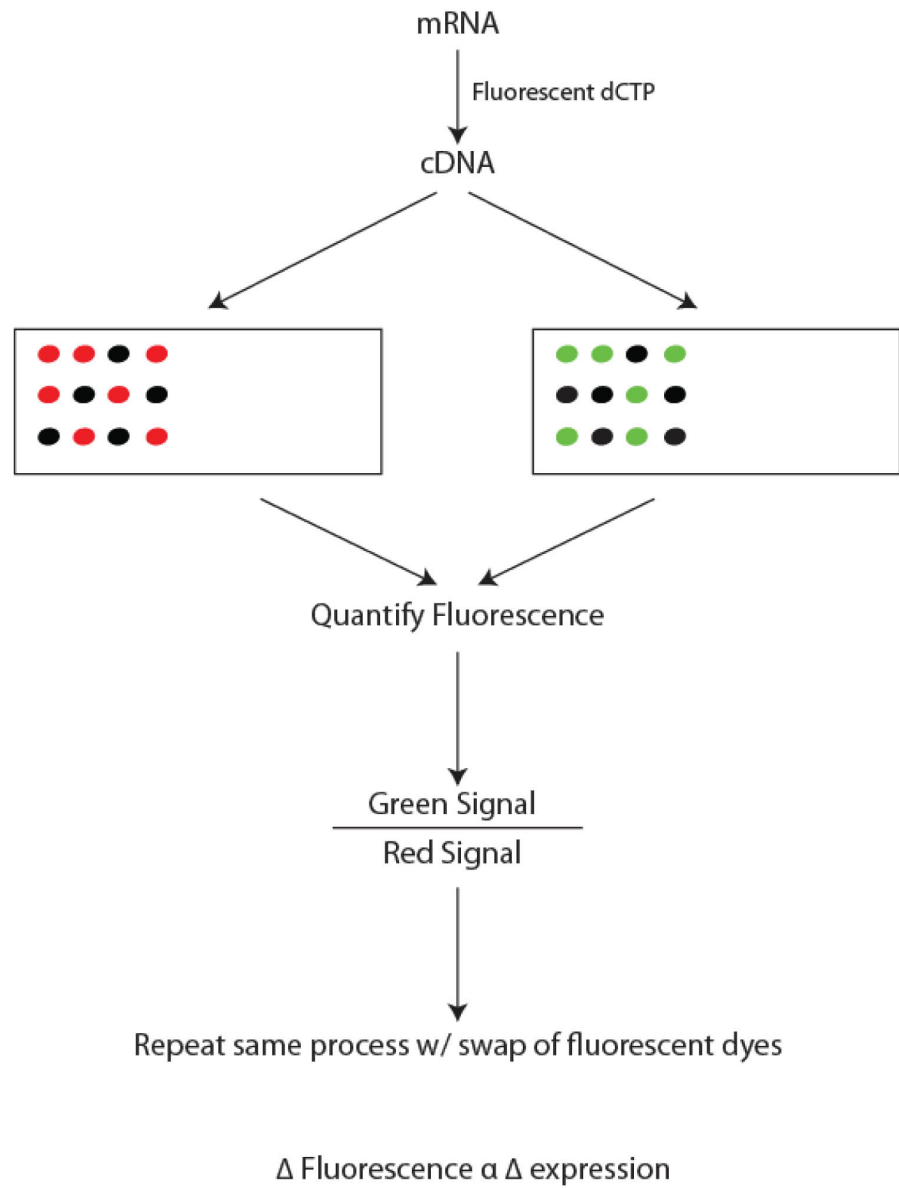


Table 2. Summary of the genes whose expression was significantly altered in the microarray analyses of UW3 medulloblastoma cells. The altered genes are categorised by their known function in specific cellular processes.

Table 2. Categories of genes^a altered in UW3.	
# of transcripts (%)	Cellular process
105 (43)	Involved in metabolic processes
42 (16)	rRNA
9 (3)	Immune-related
5 (2)	Ion channels
11 (4)	Transcription factors
21 (8)	Matrix proteins
29 (11)	Previously implicated in cancer
32 (13)	Uncharacterised

^a**Total: 254 genes altered.**

Table 3. A list of the top 20 genes whose expression was downregulated in UW3 cells as analysed by the microarray studies.

Table 3. Top 20 genes downregulated in UW3 medulloblastoma cells.				
Systematic	p-value	Normalised	Name	Description
hHA039868	0.0404	2.112368	HK1	hexokinase 1
hHC013712	0.0312	2.0644007	MMP14	matrix metalloproteinase 14
hHC023290	0.0404	1.9266618	COL6A1	collagen, type VI, alpha 1
hHC025768	0.0373	1.8885934	LSS	lanosterol synthase
hHA039589	0.0453	1.7890891	ACAS2	acetyl-Coenzyme A synthetase 2 (ADP forming)
hHR019061	0.0404	1.6695614	ARHGDIA	Rho GDP dissociation inhibitor (GDI) alpha
hHA036036	0.0196	1.6545842	MAGED2	melanoma antigen family D, 2
hHC024474	0.0396	1.6248466	APP	amyloid beta (A4) precursor protein
hHR027237	0.0404	1.5778828	RRAS2	related RAS viral (r-ras) oncogene homolog 2
hHR026970	0.0376	1.5743201	KIAA1245	chromosome one amplified sequence 1 cyclophilin
hHC027540	0.0404	1.515938	NNAT	Neuronatin
hHA040190	0.0404	1.5093615	ITGA3	integrin, alpha 3
hHA040386	0.0267	1.4684224	TRIP6	thyroid hormone receptor interactor 6
hHA039817	0.0196	1.4517424	PFKP	phosphofructokinase, platelet
hHA040292	0.0443	1.426072	HPCAL1	hippocalcin-like 1
hHC025796	0.0312	1.4094465	CTSD	cathepsin D (lysosomal aspartyl protease)
hHA033061	0.0404	1.4049008	HNRPH1	heterogeneous nuclear ribonucleoprotein H1 (H)
hHC020608	0.0196	1.3616004	LAMC1	laminin, gamma 1 (formerly LAMB2)
hHC017930	0.0404	1.3562437	SREBF2	sterol reg. element binding TF 2
hHC017919	0.0196	1.3491124	QSCN6	quiescin Q6

Table 4. A list of the top 20 genes whose expression were upregulated in UW3 cells analysed by the microarray studies.

Table 4. Top 20 genes upregulated in UW3 medulloblastoma cells.				
Systematic	p-value	Normalised	Name	Description
hHR029368	0.0196	0.7143005	na	similar to ribosomal protein S24
hHC020845	0.0485	0.7101223	POLR2L	polymerase (RNA) II (DNA directed) L, 7.6kDa
hHC003745	0.0393	0.70655125	VIM	Vimentin
hHC031915	0.0396	0.7043096	RPL39	ribosomal protein L39
hHC029860	0.0404	0.70334363	ATP5E	ATP synth, H ⁺ transport, mitoch F1 cplex
hHR026383	0.0267	0.7018302	C11orf10	chromosome 11 open reading frame 10
hHR029938	0.0439	0.70103836	D15F37	D15F37 gene
hHR019317	0.0454	0.6973381	na	similar to RIKEN cDNA 2310016E02
hHO048853	0.0404	0.6933824	na	Unknown
hHC029737	0.0196	0.69197905	RPL38	ribosomal protein L38
hHR031391	0.0196	0.6888742	na	similar to 40S ribosomal protein S26
hHC032009	0.0196	0.686309	RPS27	ribosomal protein S27 (metallopanstimulin 1)
hHR031335	0.0472	0.6859227	MT-TM	mitochondrially encoded tRNA methionine
hHC031353	0.0404	0.68290436	RPL23A	ribosomal protein L23a
hHR022682	0.0404	0.6788005	RPL38	ribosomal protein L38
hHC030969	0.0396	0.6776505	RPL37	ribosomal protein L37
hHR028115	0.0384	0.6649374	RPS29	ribosomal protein S29
hHC031354	0.0396	0.65864027	RPS29	ribosomal protein S29
hHC031776	0.0461	0.6565068	RPS7	ribosomal protein S7
hHC017071	0.0393	0.65582925	MGP	matrix Gla protein

Table 5. A list of the top cancer-related genes whose expression was modulated in UW3 cells analysed by the microarray studies.

Table 5. Genes previously implicated in different cancers				
Systematic	p-value	Normalised	Name	Description
hHA039868	0.0404	2.112368	HK1	hexokinase 1
hHC013712	0.0312	2.064401	MMP14	matrix metalloproteinase 14
hHC023290	0.0404	1.926662	COL6A1	collagen, type VI, alpha 1
hHR019061	0.0404	1.669561	ARHGDIA	Rho GDP dissociation inhibitor (GDI) alpha
hHA036036	0.0196	1.654584	MAGED2	melanoma antigen family D, 2
hHC024474	0.0396	1.624847	APP	amyloid beta (A4) precursor protein
hHR027237	0.0404	1.577883	RRAS2	related RAS viral (r-ras) oncogene homolog 2
hHA040190	0.0404	1.509362	ITGA3	integrin, alpha 3
hHA040386	0.0267	1.468422	TRIP6	thyroid hormone receptor interactor 6
hHA039817	0.0196	1.451742	PFKP	phosphofructokinase, platelet
hHC025796	0.0312	1.409447	CTSD	cathepsin D (lysosomal aspartyl protease)
hHC020608	0.0196	1.3616	LAMC1	laminin, gamma 1 (formerly LAMB2)
hHC003745	0.0393	0.706551	VIM	Vimentin
hHC029860	0.0404	0.703344	ATP5E	ATP synth, H ⁺ transport, mitoch F1 cplex
hHC017071	0.0393	0.655829	MGP	matrix Gla protein

Figure 10. Quantitative RT-PCR validation of targets of SLIT2 transcriptional modulation. (A) Quantitative RT-PCR was employed to determine the UW3 mRNA levels of 8 genes modulated by hSLIT2-myc treatment (100 ng/ml, 24h treatment, HPLC-purified): *MMP14*, *CathD1*, *Colvia1*, *Integrin3a*, *ARHGDIA*, *PIK3R3*, *AAMP*, and *APP* (B) The message level of 10 genes implicated in cancer cell invasion but not altered by hSLIT2-myc was also measured. (C) Western blot detecting endogenous MMP14 levels in UW3 and DAOY cells treated with hSLIT2-myc (100 ng/ml, 24h treatment, HPLC-purified) or mock conditioned media. (D) Semiquantitative analysis of the immunoblots from hSLIT2-myc (100 ng/ml, 24h treatment, HPLC-purified) or mock conditioned media treatments of UW3 and DAOY cells. (E) MMP14 collagenase activity of hSLIT2-myc (100 ng/ml, 24h treatment, HPLC-purified) or mock conditioned media treatments of UW3 and DAOY cells. (F) Quantitative RT-PCR was employed to determine the purity of HPLC-based hSLIT2-myc purification. UW3 cells treated with commercial mSlit2 or HPLC-purified hSLIT2-myc (100 ng/ml, 24h treatment) were assayed by qRT-PCR to probe the silencing effect of hSLIT2-myc on *MMP14*, *CathD*, and *ColVIA1*. Values are means from three independent experiments +/- s.e.m. Statistical analysis: For panels A, B, D, and E, two-tailed, unpaired Student's t-test. For panel F, one-way ANOVA followed by Dunnett's post-hoc test. Statistically significant differences are indicated by asterisks, where *, $p < 0.05$, and **, $p < 0.01$.

Figure 10.

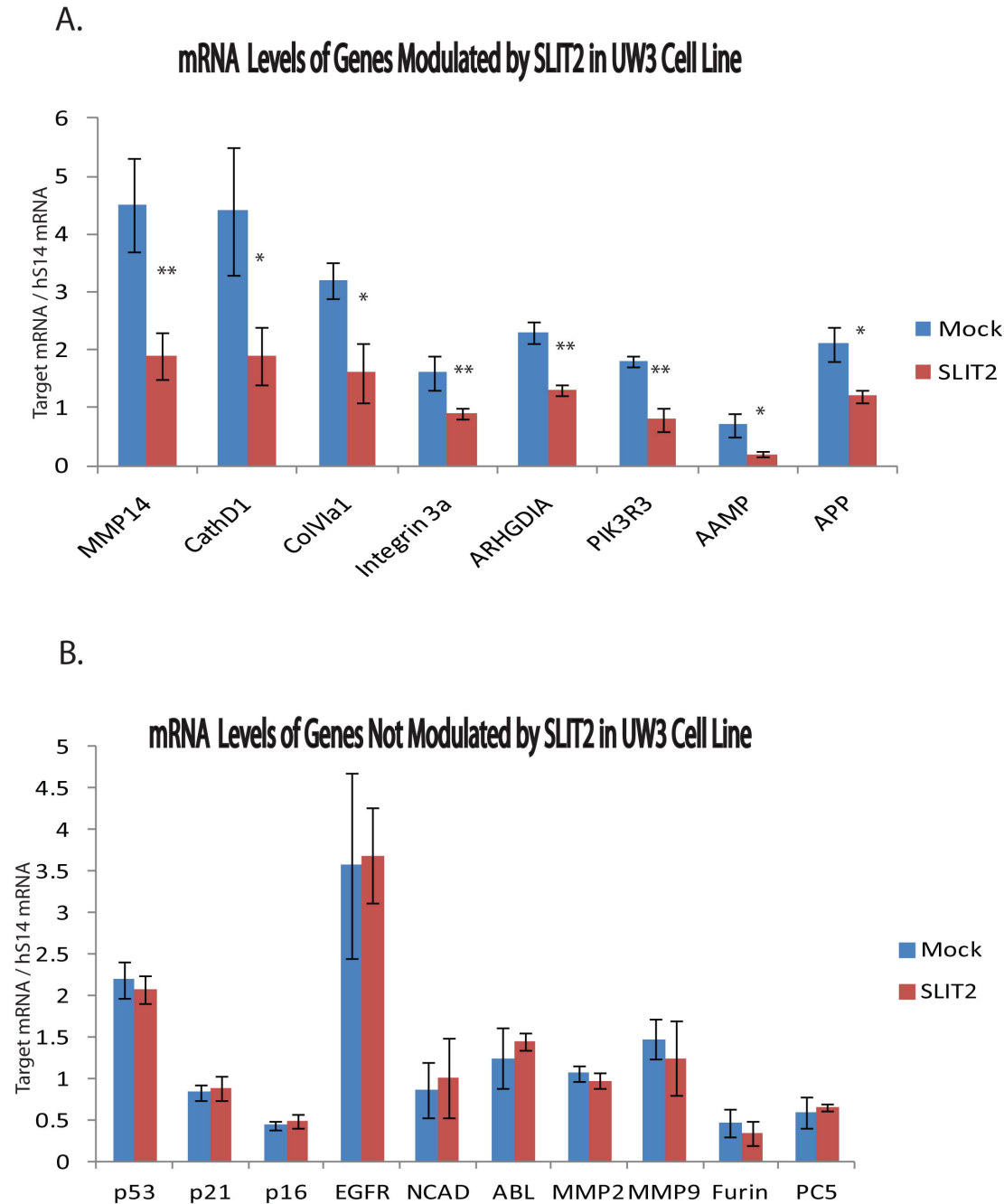


Figure 10.

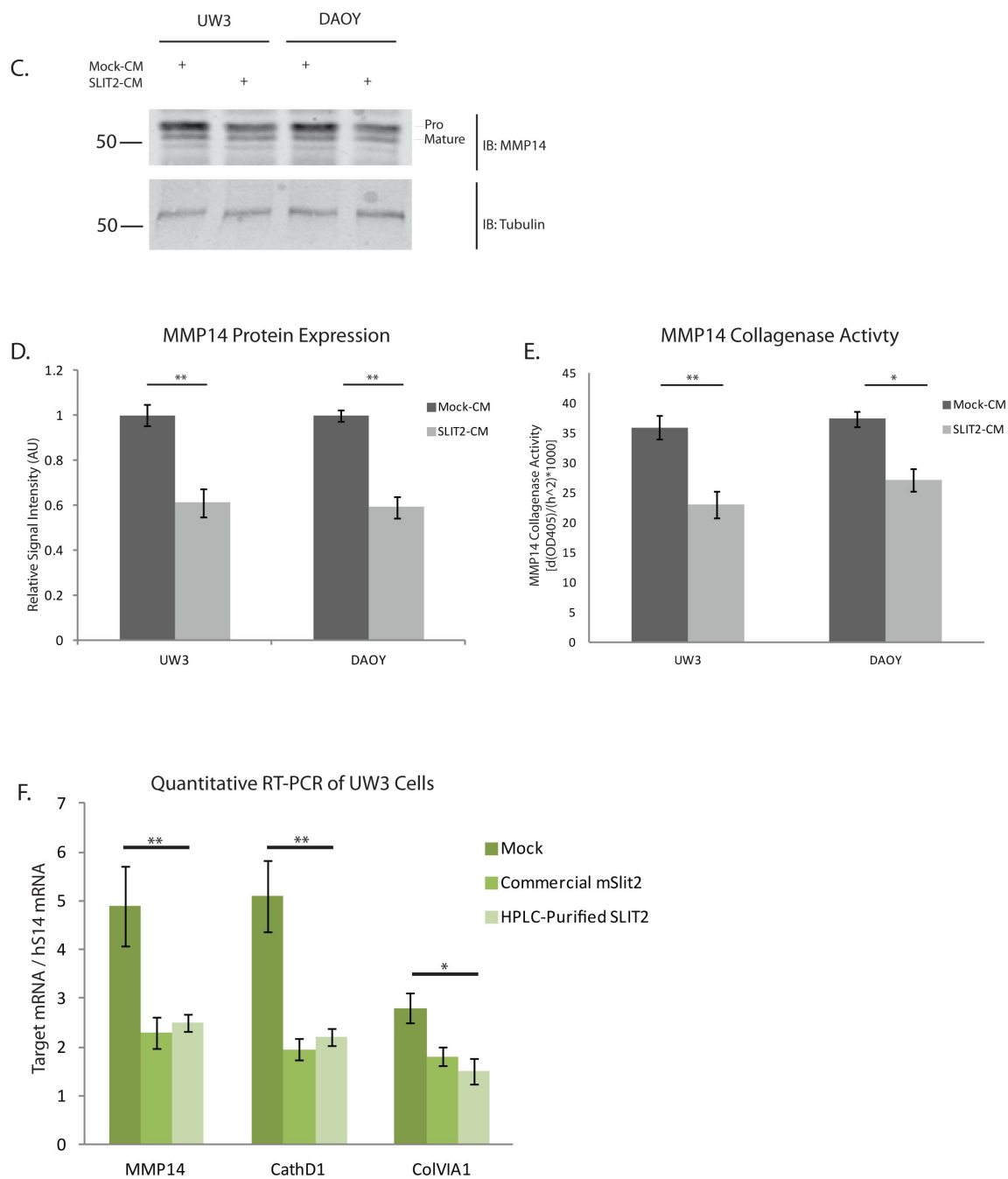


Figure 11. The expression levels of MMP14 in different cell lines, and its association with the rate of invasion. (A) *MMP14* expression was assessed by qRT-PCR in glioma and medulloblastoma cell lines (B) The *MMP14* mRNA expression was plotted against the mean rate of invasion of each cell line. The R-squared value is included to demonstrate predicted versus experimental observations. The equation of the linear regression is included to demonstrate the slope of the association between *MMP14* mRNA expression and the rate of collagen invasion. (C) Western immunoblot representing the levels of *MMP14* expression in malignant brain tumour cell lines. Beta-tubulin was used as a reference protein. (D) Semi-quantitative analysis of *MMP14* immunoblot signal in the different malignant brain tumour cell lines. (E) The *MMP14* protein expression signal was plotted against the mean rate of invasion of each cell line. The R-squared value is included to demonstrate predicted versus experimental observations. The equation of the linear regression is included to demonstrate the slope of the association between *MMP14* protein expression and the rate of collagen invasion. (F) The levels of *MMP14* collagenase activity in the different malignant brain tumour cell lines. (G) The *MMP14* collagenase activity was plotted against the mean rate of invasion of each cell line. The R-squared value is included to demonstrate predicted versus experimental observations. The equation of the linear regression is included to demonstrate the slope of the association between *MMP14* collagenase activity and the rate of collagen invasion. Values are means from three independent experiments \pm s.e.m. Statistical analysis: one-way ANOVA followed by Tukey's post-hoc test. Statistically significant differences are indicated by asterisks, where *, $p < 0.05$, and **, $p < 0.01$.

Figure 11.

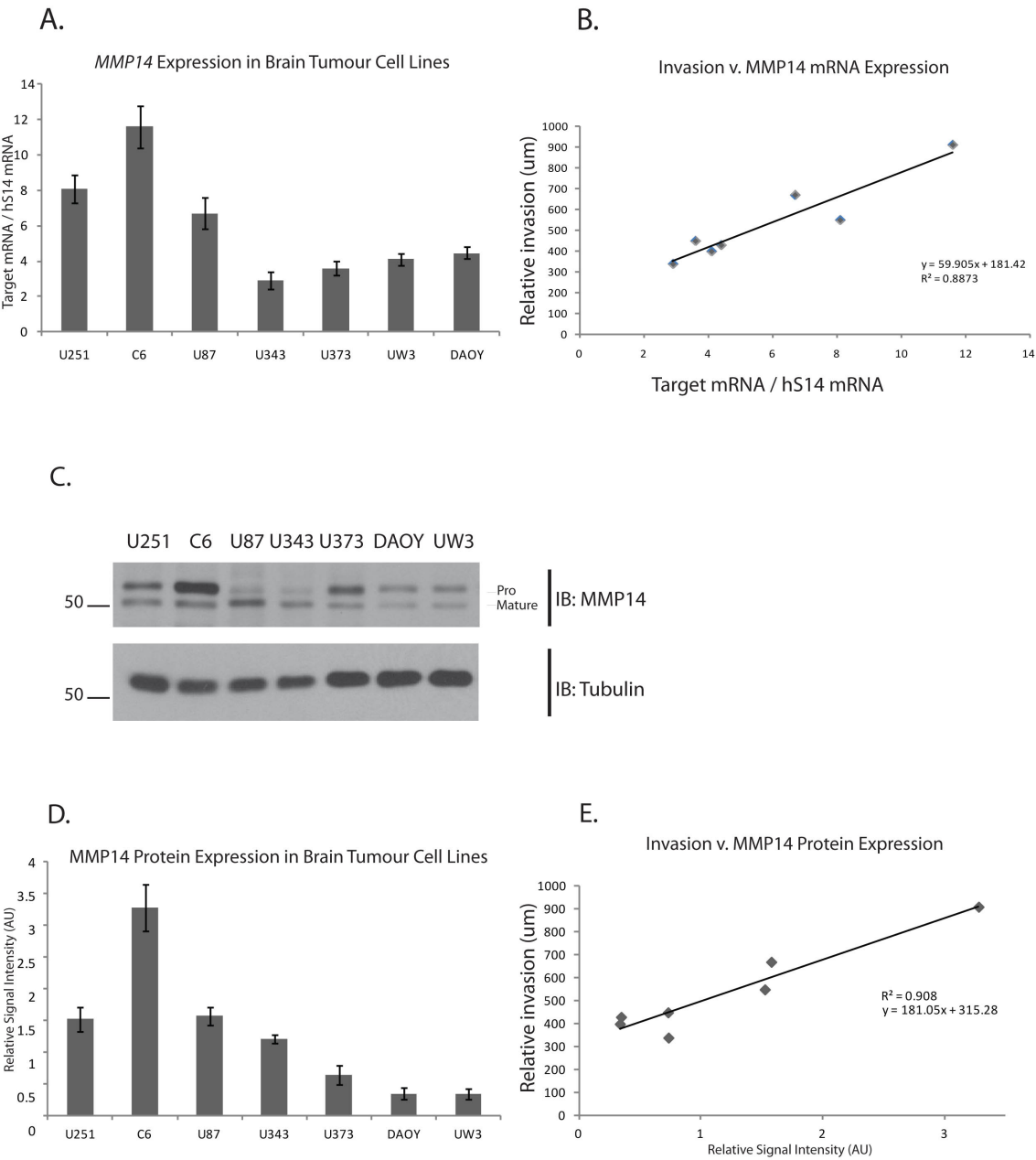


Figure 11.

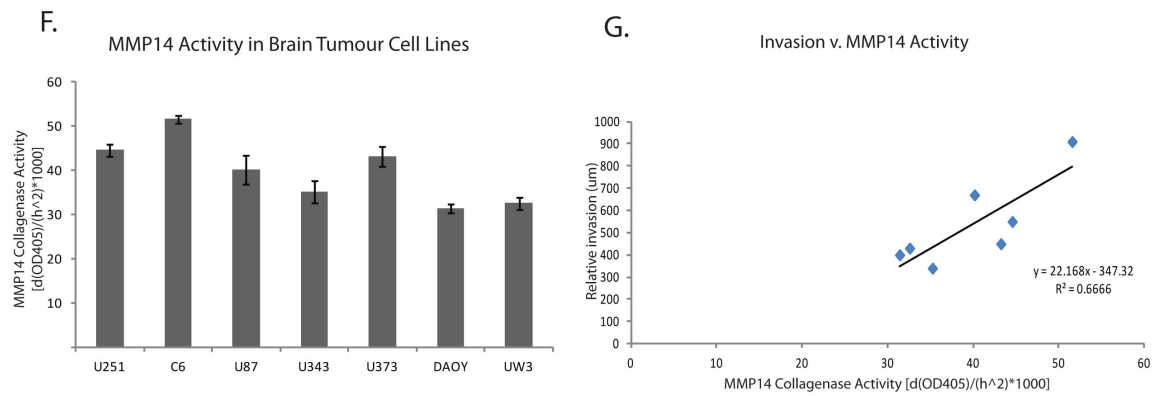


Figure 12. MMP14 cleaves rRobo1-Fc at multiple sites. (A) FC-rRobo1 is cleaved by recombinant solMMP14-Flag. 2.5 ug of FC-rRobo1 was incubated with control MMP14 purification buffer, or 10 or 20 pmol of recombinant solMMP14-Flag and the reaction mixture was resolved on a SDS polyacrylamide gel followed by Coomassie Brilliant Blue R250 stain (top panel) or transferred onto nitrocellulose and Ponceau stained (bottom panel). Arrows point to the major cleavage products of FC-rRobo1. (B) 2.5 ug of FC-rRobo1 was incubated with control purification buffer, or 10 pmol of recombinant solMMP14-Flag and the reaction mixture was resolved on a SDS polyacrylamide gel followed by Coomassie Brilliant Blue R250 stain. (C) Recombinant Fc fused to the linker peptide IEGRMD was mixed with 2.5 ug solMMP14 and used as negative control for A/B (D) Western immunoblot from the immunoprecipitation of rRobo1-myc in the absence or presence of MMP14-Flag.

Figure 12.

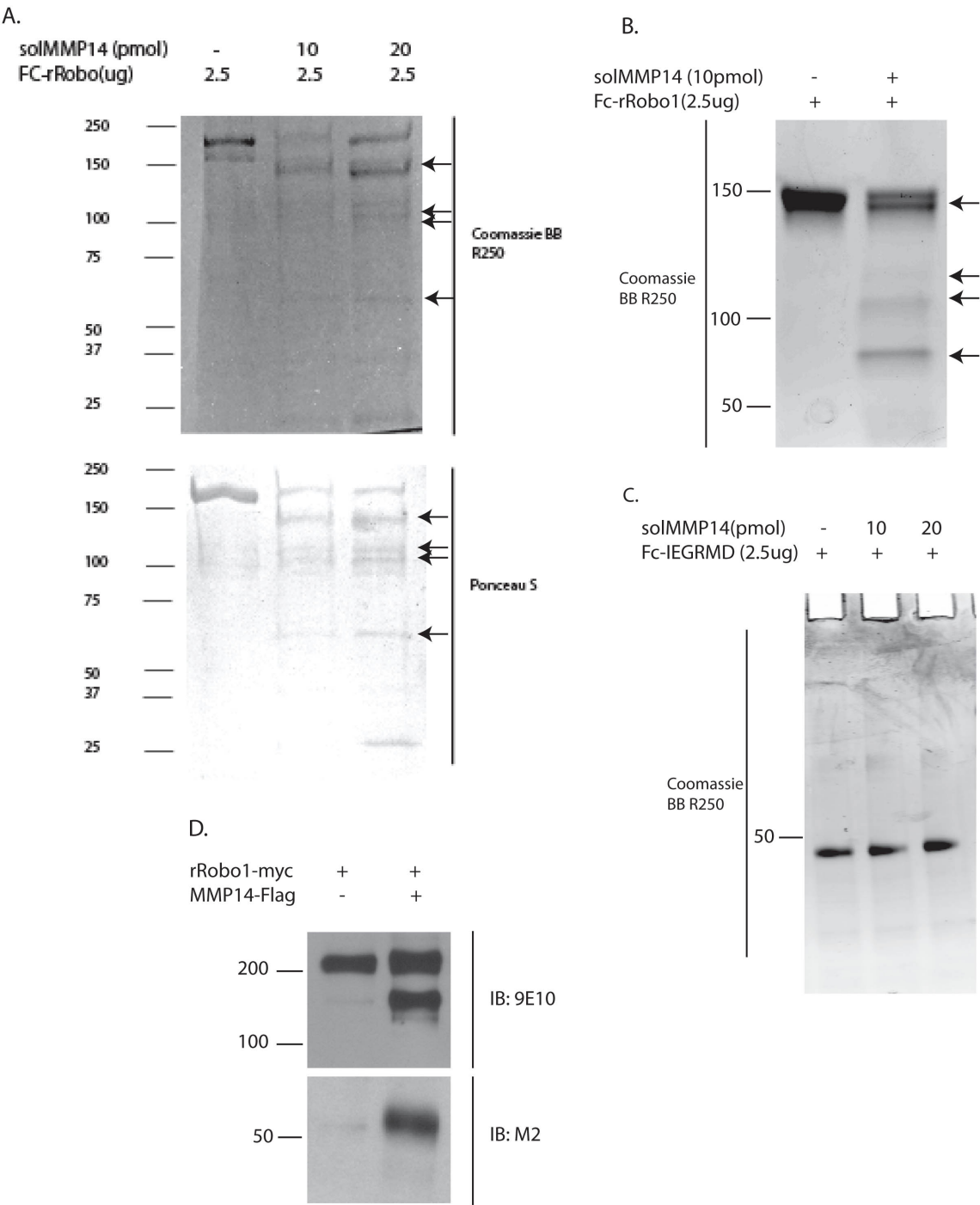


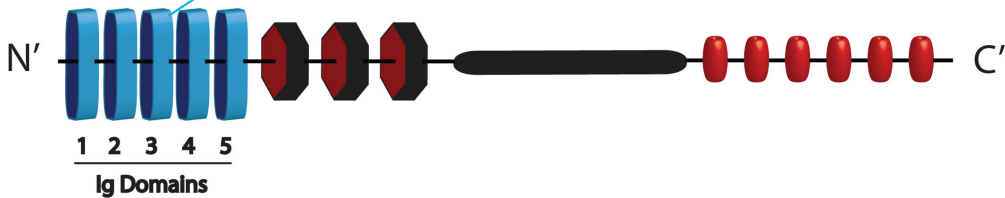
Figure 13. Putative rRobo1 cleavage sites. (A) The amino acid sequence of rRobo1 corresponding to the first three Ig-like domains is outlined. The putative residue (T346) identified in our proteomic analysis of rRobo1 cleavage is in bold. (B) A schematic diagram showing the key domains of Robo1, in which the five Ig-like domains of Robo proteins are outlined. Line points to the major cleavage site of Robo1, yielding the 60 kDa N-terminal fragment. (C) Representative immunoblot from co-immunoprecipitation assays showing the binding of the N-terminal rRobo1-Flag fragment interacting with full length hSLIT2-myc and *vice versa*. Beta-tubulin (raised in mouse) and alpha-tubulin (raised in rabbit) were used as reference proteins. The none-specific band in the 9E10 (raised in mouse) immunoblot at (50 kDa apparent mass) corresponds to the heavy chains of M2 Flag antibody (raised in mouse).

Figure 13.

A.

```
1  mkwkhlp1lv  misllt1skk  h11laqlipd  ped1ergndn  gtpaptsdnd  d1nslgytg1r
61  lrqedfppri  vehpsd1ivs  kgepat1nck  aegrptptie  wykggervet  dkddprshrm
121 llpsgslffl  rivhgrksrp  degvyicvar  nylgeavshn  aslevailrd  dfrqnpsdvm
181 vavgepavme  cqpprghpep  tiswkkdgsp  lddkderiti  rggklmityt  rksdagkyvc
241 vgt1nmvgere  skvadvtvle  rpsfvkrpsn  lavtvddsa1  fkceargdpv  ptfgwrkddg
301 elpksryeir  ddhtlkirkv  tagdmgsytc  vaenmvgkae  asat1lvqep  phfvvkprdq
361 vvalgrtvtf  qceatgnppq  aifwrregsq  nllfsyqppq  s1s1rfsvsqt  gdl1vt1nvqr...
```

B.



C.

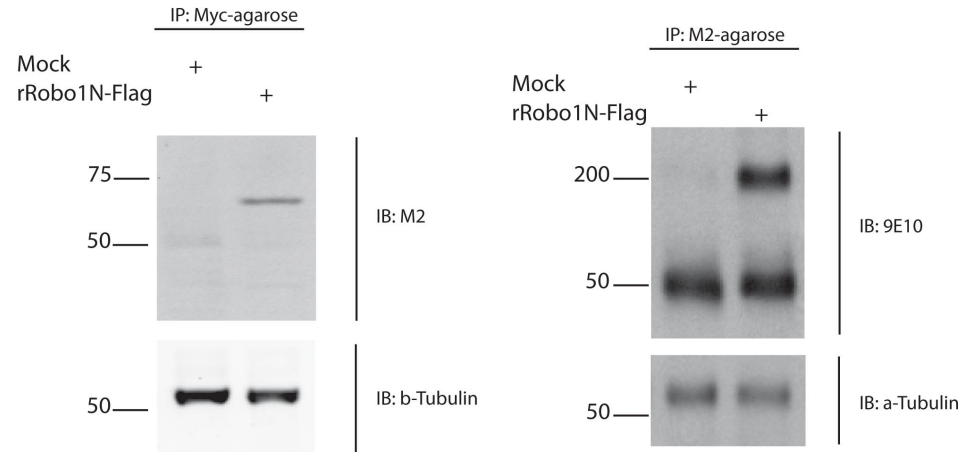


Table 6. List of the potential peptides generated by in gel tryptic digest based on the sequence of rRobo1 residues 19-560 (corresponding to the rRobo1 portion of rRobo1-Fc) is presented. The number of detected peptides corresponding to each tryptic digest is presented for the 110 kDa fragment analyses (n=3; C1, C2, C3) or the 60 kDa fragment analyses (n=5; N1, N2, N3, N4, N5).

Table 6. Peptides detected during different M.S. Analyses.

M.S. Peptides	C1	C2	C3	N1	N2	N3	N4	N5
hlllaqlipdpedleR	0	0	0	7	0	11	9	5
gndngtpaptsdnddnlsgytgsR	0	0	0	0	0	0	0	0
lRqedfppR	0	0	0	11	13	6	9	5
ivehpsdlivsK	0	0	0	10	12	0	9	7
gepatlncK	0	0	0	0	0	0	1	1
aegRptptiewyK	0	0	0	10	15	6	9	21
ggeR	0	0	0	0	0	0	0	0
vetdK	0	0	0	0	0	0	0	0
ddpR	0	0	0	0	0	0	0	0
mlpsgslfflR	0	0	0	8	11	4	7	5
ivhgR	0	0	0	0	0	0	0	0
sRpdegvyicvaR	0	0	0	3	6	2	4	9
nylgeavshnaslevailR	0	0	0	0	0	0	0	0
qnpsdvmvavgepavmecqppR	0	0	0	0	0	0	0	0
ghpeptiswK	0	0	0	0	0	0	1	0
dgsplddKdR	1	0	0	3	2	4	6	3
itiR	0	0	0	0	0	0	0	0
lmitytR	0	0	0	2	2	0	0	1
sdagK	0	0	0	0	0	0	0	0
yvcvgtnmvgeR	0	0	0	7	4	1	5	11
vadvvtvleRpsfvK	0	0	0	14	5	13	20	9
psnlavtvddsaefK	0	0	0	8	15	9	0	2
ceaR	0	0	0	0	0	0	0	0
gdpvptfgwR	1	0	0	3	6	9	4	11
ddgelpK	0	0	0	0	0	0	0	0
Year	0	0	0	0	0	0	0	0
ddhtlK	0	0	0	0	0	0	0	0
KvtagdmgsytcvaenmvgK	0	0	0	12	7	5	22	17
aeasatlvtqepphfvvKpR	0	0	0	0	0	0	0	0
dqvvalgR	4	5	6	0	0	0	0	0
tvtfqceatgnppaifwR	7	6	11	0	0	0	0	0
egsqnllfsyqppqsssR	6	11	9	0	0	0	0	0
fsvsqtgdltvtnvqR	12	8	12	0	0	0	0	0
sdvgyyicqtlnvagsiitK	0	0	0	0	0	0	0	0
aylevtdviadRpppviR	24	20	15	0	0	0	0	0
qgpvnqtavavdgltltlscvatgspvptilwR	1	0	0	0	0	0	0	0
dgvlvstqdsR	18	13	9	0	0	0	0	0
qlsgvlqiR	18	31	23	0	0	0	0	0
yaK	0	0	0	0	0	0	0	0
lgdtgR	0	0	0	0	0	0	0	0
ytctastpsgeatwsayievqefgvpvqppR	0	0	0	0	0	0	0	0
ptdpnli	0	0	0	0	0	0	0	0

Figure 14. MMP14 overexpression in UW3 cells renders them more invasive and less sensitive to hSLIT2-myc. (A) UW3 cells overexpressing MMP14 are not significantly inhibited by hSLIT2-myc. Stable UW3 cells expressing MMP14, or an empty (Ctl) plasmid were treated with hSLIT2-myc (HPLC-purified, used at 100 ng/ml, treated throughout the assay) or mock conditions. (B) Western immunoblot showing the protein expression of MMP14-Flag in UW3 stable cell lines and clones derived from these stable cells. Beta-tubulin was probed as reference protein. (C) MMP14 collagenase activity of MMP14-Flag in UW3 stable cell lines and clones derived from these stable cells. (D) Collagen three-dimensional invasion assay on UW3 cells transfected with MMP14 cDNA or control (Ctl) vector. The invasion rate of UW3 cells was measured following hSLIT2-myc (HPLC-purified, used at 100 ng/ml, treated throughout the assay) or mock conditioned media treatment. Values are means from three independent experiments \pm s.e.m. Statistical analysis: For (A), two-tailed, unpaired Student's t-test. Statistically significant differences are indicated by asterisks, where *, $p < 0.05$. For (C-D) One-way ANOVA followed by Tukey's post-hoc test where $p < 0.05$ was considered statistically significant. Statistically significant differences are indicated by asterisks, where *, $p < 0.05$, and **, $p < 0.01$.

Figure 14.

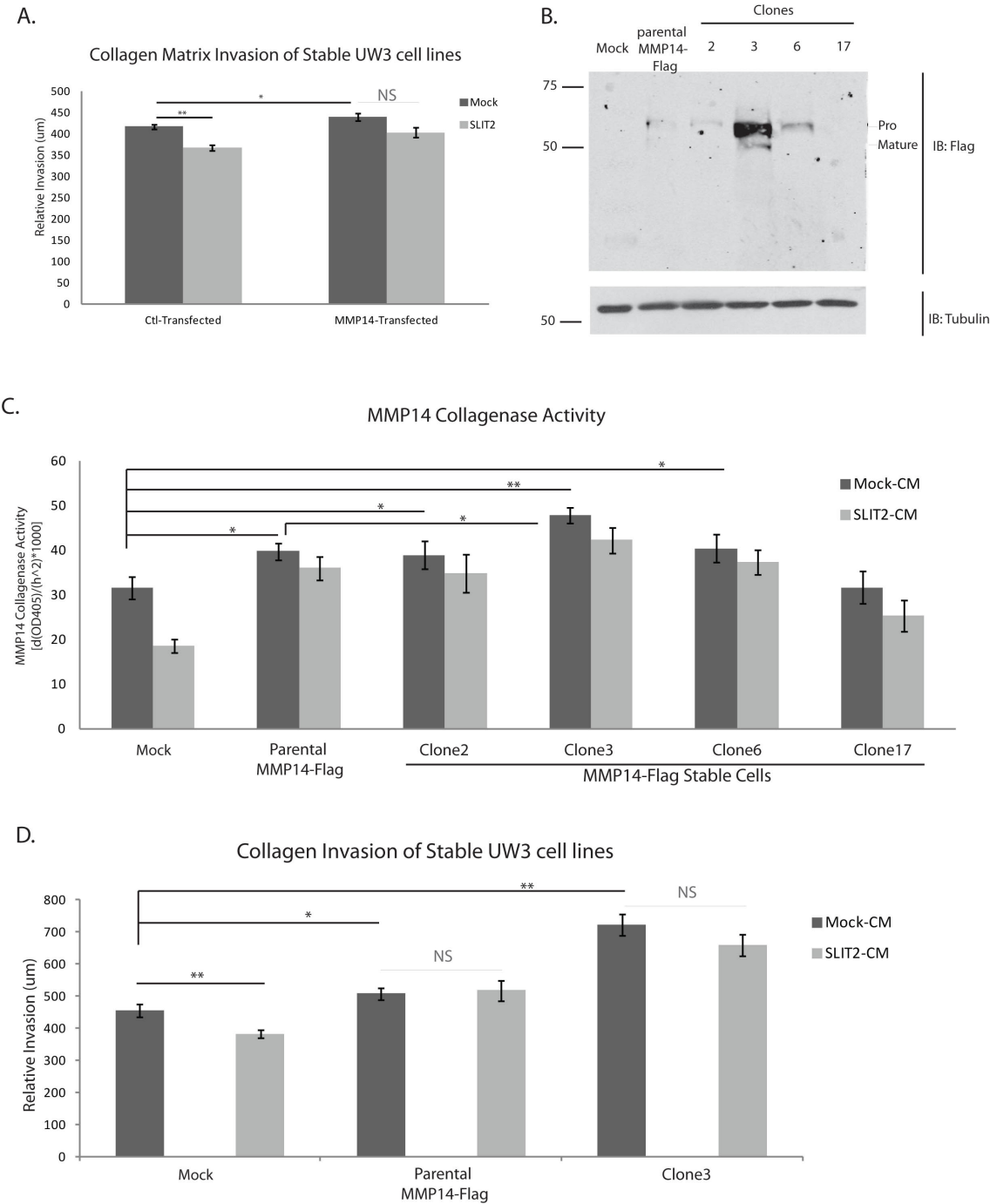
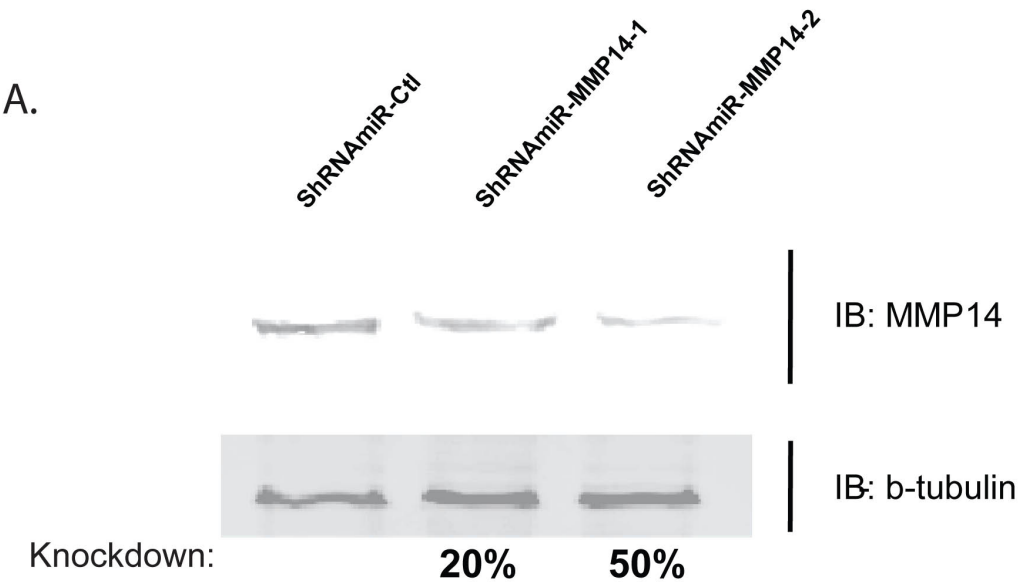


Figure 15. The shRNA_{miR} targeting of *MMP14* decreases C6 invasion. (A) Western immunoblot showing the endogenous protein expression of MMP14 in C6 cells infected with lentiviral particles expressing shRNA_{miR} sequences targeting rMMP14 (shRNA_{miR}-MMP14-1 and shRNA_{miR}-MMP14-2) or non-target (shRNA_{miR}-Ctl). Beta-tubulin was probed as reference protein. (B) Invasion assay of C6 cells transduced with shRNA_{miR}-MMP14-1, shRNA_{miR}-MMP14-2, or shRNA_{miR}-Ctl. Values are means from three independent experiments \pm s.e.m. Statistical analysis: one-way ANOVA followed by Dunnett's post-hoc test. Statistically significant differences are indicated by asterisks, where *, $p < 0.05$.

Figure 15.



B.

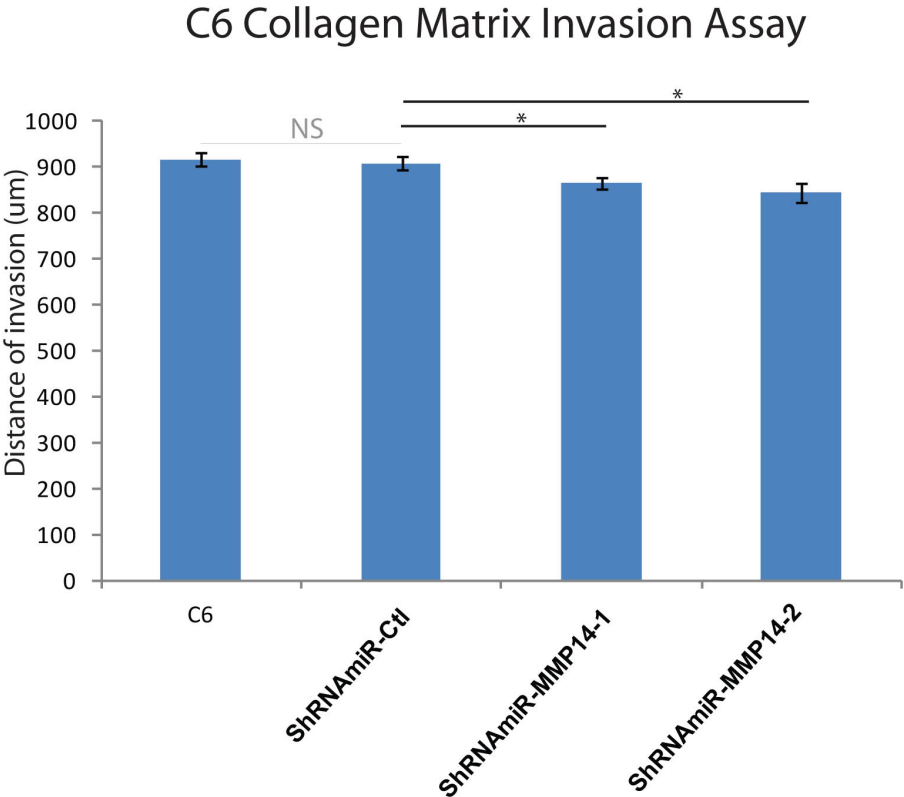
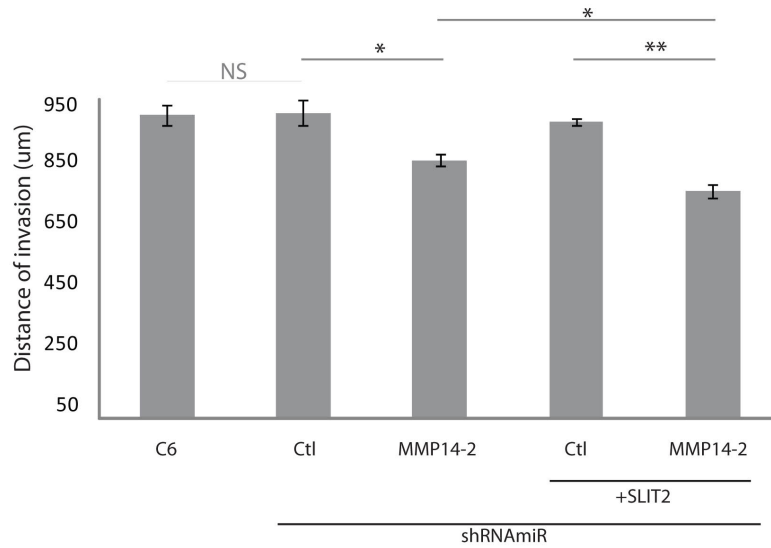


Figure 16. The invasion rate and MMP14 collagenase activity of C6 cells transduced with shRNA_{miR} targeting MMP14 is inhibited by hSLIT2-myc. (A) Spheroids from MMP14-targeted knockdowns displayed slower invasion when treated with hSLIT2-myc (HPLC-purified, used at 100 ng/ml, treated throughout the assay) (B) MMP14 collagenase activity in C6 cells transduced with MMP14-silencing shRNA_{miR} and treated with mock or hSLIT2-myc (HPLC-purified, used at 100 ng/ml, treated throughout the assay). Values are means from three independent experiments +/- s.e.m. Statistical analysis: one-way ANOVA followed by Tukey's post-hoc test. Statistically significant differences are indicated by asterisks, where *, $p < 0.05$, and **, $p < 0.01$.

Figure 16.

A.

C6 Collagen Matrix Invasion Assay



B.

C6 MMP14 Collagenase Activity

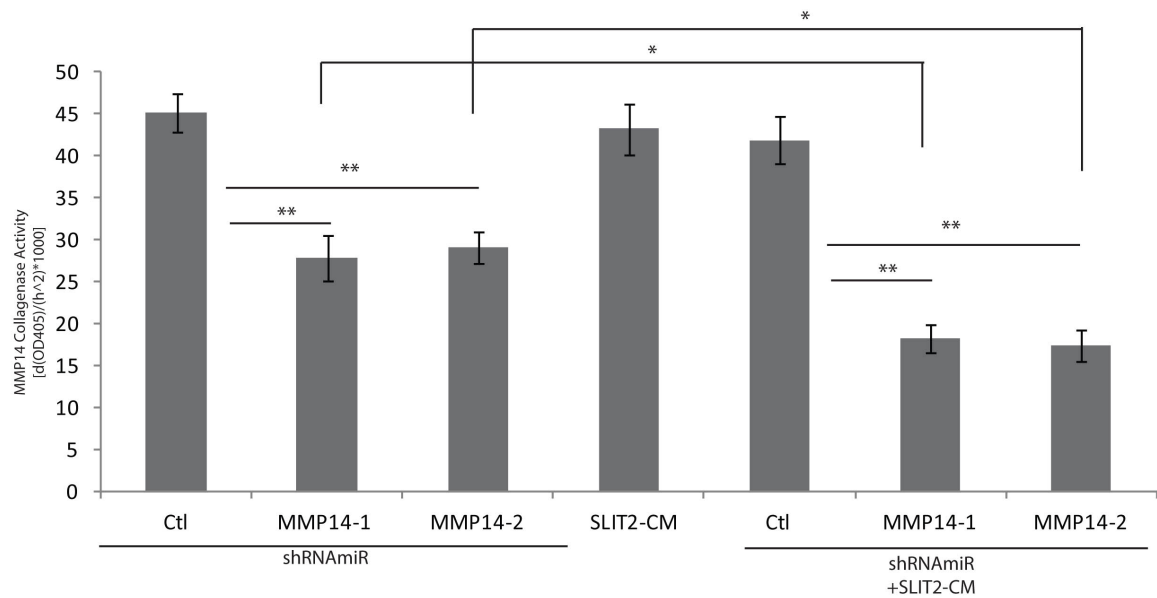


Figure 17. MMP14 knock down in C6 cells renders them more sensitive to temozolomide. MTT proliferation assay of MMP14 knock down C6 cells or mock, treated with 30 ug/ml of temozolomide (TMZ). Values are means from three independent experiments +/- s.e.m. Statistical analysis: one-way ANOVA followed by Tukey's post-hoc test. Statistically significant differences are indicated by asterisks, where *, $p < 0.05$, and **, $p < 0.01$.

Figure 17.

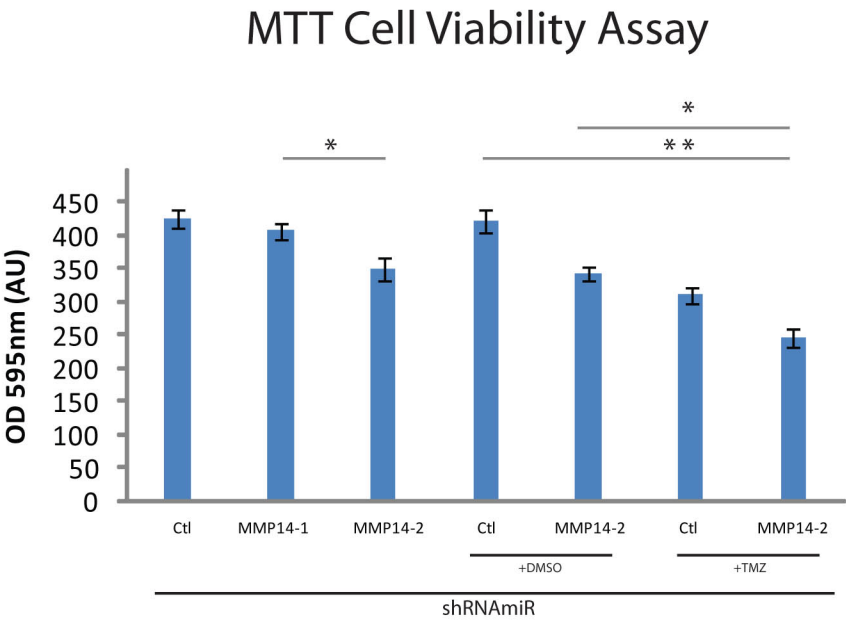


Figure C-1. The Slit-Robo-MMP14 model. (A) In invasive cancer cells, where MMP14 is expressed at high levels, MMP14 cleaves Robo proteins at the cell surface (1) yielding a soluble form of Robo (2) capable of binding and sequestering Slit proteins (3). Slit proteins cannot bind Robo and as a result *MMP14* expression is not silenced (4), leading to sustained MMP14 expression (5) and activation of MMP14 and other pro-invasive proteins. (B) In low-to-moderately invasive cancer cells, Slit-Robo interaction occurs at the cell surface (1) leading to the recruitment of cytoplasmic effectors which inhibit Cdc42 and Rac activity (2) and propagate the inhibitory signal towards the nucleus where *MMP14* transcription is silenced (3). The net result of this Slit-Robo activation is a decrease in MMP14 expression and activity at the cell surface (4) which ultimately decreases the pro-invasion signals modulated by MMP14 (5).

Figure C-1.

A. Cells Non-Responsive to SLIT2

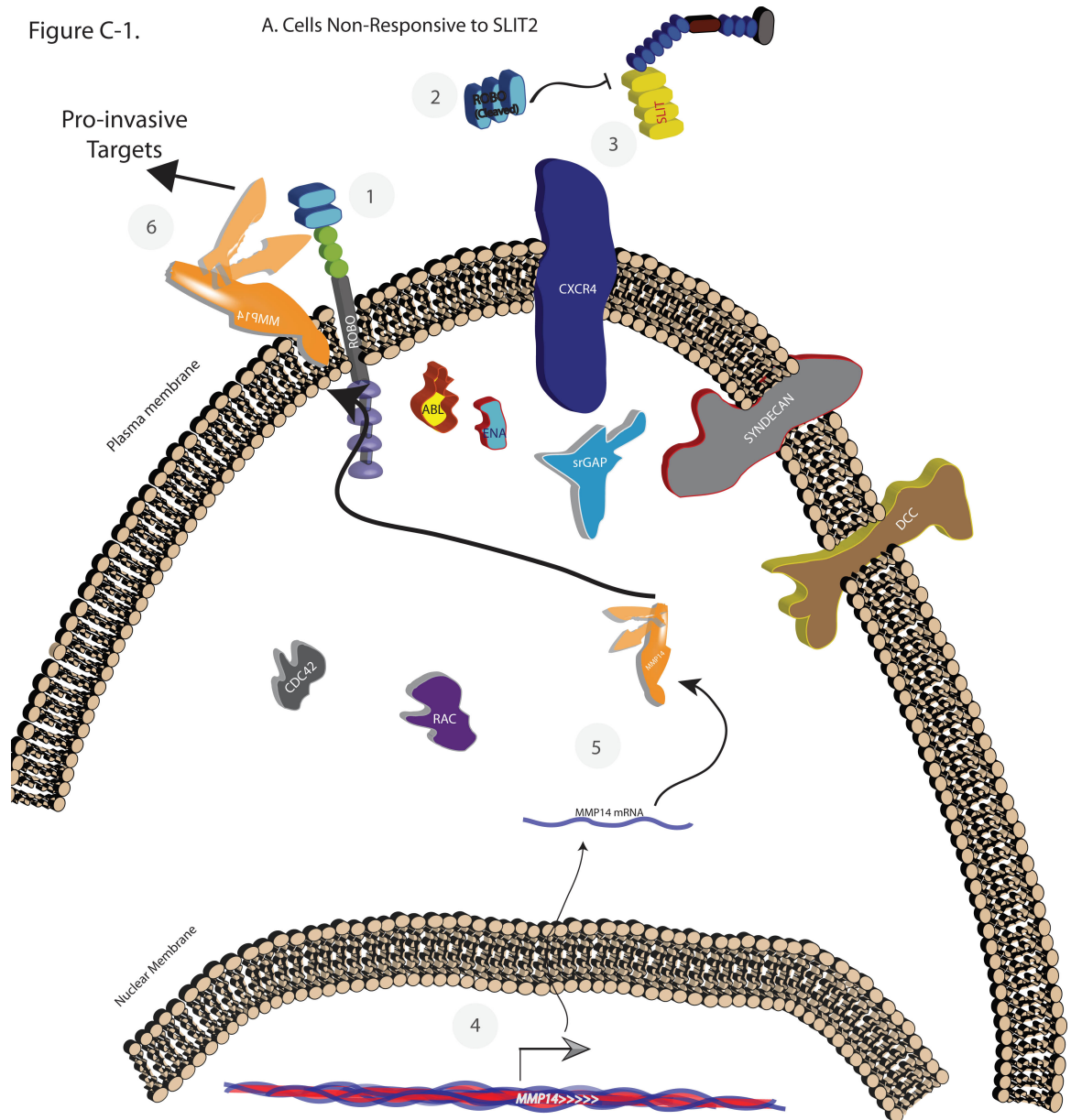
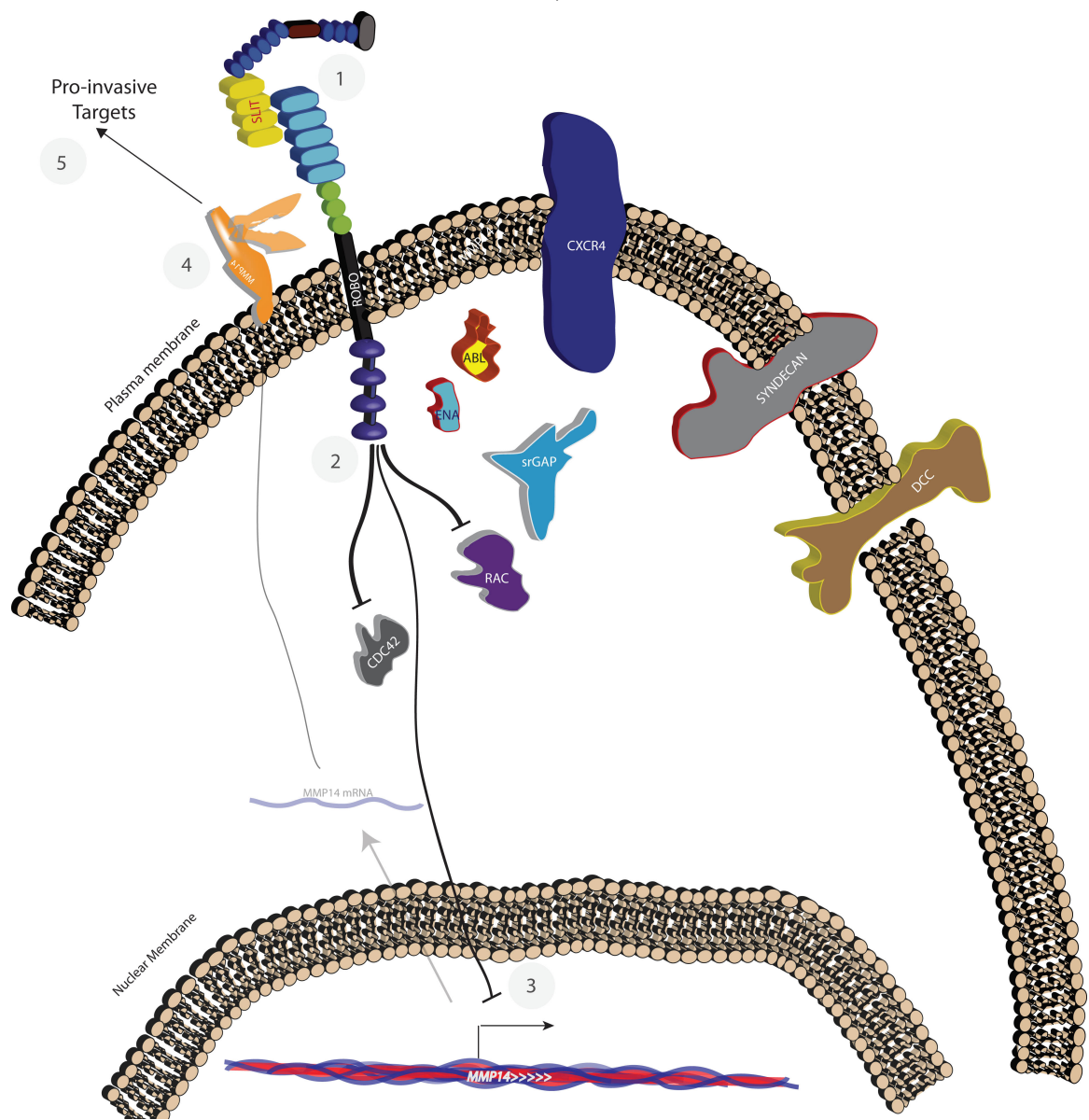


Figure C-1.

B. SLIT2-Responsive Cells



References

Adams, S.O., Nissley, S.P., Greenstein, L.A., Yang, Y.W., and Rechler, M.M. (1983). Synthesis of multiplication-stimulating activity (rat insulin-like growth factor II) by rat embryo fibroblasts. *Endocrinology* 112, 979-987.

Aguirre-Ghiso, J.A. (2007). Models, mechanisms and clinical evidence for cancer dormancy. *Nat Rev Cancer* 7, 834-846.

Alghisi, G.C., and Ruegg, C. (2006). Vascular integrins in tumor angiogenesis: mediators and therapeutic targets. *Endothelium* 13, 113-135.

Allen, J.C., and Siffert, J. (1997). Contemporary issues in the management of childhood brain tumors. *Curr Opin Neurol* 10, 137-141.

Angers-Loustau, A., Hering, R., Werbowetski, T.E., Kaplan, D.R., and Del Maestro, R.F. (2004). SRC regulates actin dynamics and invasion of malignant glial cells in three dimensions. *Mol Cancer Res* 2, 595-605.

Annabi, B., Doumit, J., Plouffe, K., Laflamme, C., Lord-Dufour, S., and Beliveau, R. (2010). Members of the low-density lipoprotein receptor-related proteins provide a differential molecular signature between parental and CD133+ DAOY medulloblastoma cells. *Mol Carcinog* 49, 710-717.

Assoian, R.K., Grotendorst, G.R., Miller, D.M., and Sporn, M.B. (1984). Cellular transformation by coordinated action of three peptide growth factors from human platelets. *Nature* 309, 804-806.

Astuti, D., Da Silva, N.F., Dallol, A., Gentle, D., Martinsson, T., Kogner, P., Grundy, R., Kishida, T., Yao, M., Latif, F., *et al.* (2004). SLIT2 promoter methylation analysis in neuroblastoma, Wilms' tumour and renal cell carcinoma. *Br J Cancer* 90, 515-521.

Atkinson, S.J., Crabbe, T., Cowell, S., Ward, R.V., Butler, M.J., Sato, H., Seiki, M., Reynolds, J.J., and Murphy, G. (1995). Intermolecular autolytic cleavage can contribute to the activation of progelatinase A by cell membranes. *J Biol Chem* 270, 30479-30485.

Baeza, N., Masuoka, J., Kleihues, P., and Ohgaki, H. (2003). AXIN1 mutations but not deletions in cerebellar medulloblastomas. *Oncogene* 22, 632-636.

Bagri, A., Marin, O., Plump, A.S., Mak, J., Pleasure, S.J., Rubenstein, J.L., and Tessier-Lavigne, M. (2002). Slit proteins prevent midline crossing and determine the dorsoventral position of major axonal pathways in the mammalian forebrain. *Neuron* 33, 233-248.

Bai, G., and Pfaff, S.L. (2011). Protease regulation: the Yin and Yang of neural development and disease. *Neuron* 72, 9-21.

Bao, S., Wu, Q., McLendon, R.E., Hao, Y., Shi, Q., Hjelmeland, A.B., Dewhirst, M.W., Bigner, D.D., and Rich, J.N. (2006a). Glioma stem cells promote radioresistance by preferential activation of the DNA damage response. *Nature* 444, 756-760.

Bao, S., Wu, Q., Sathornsumetee, S., Hao, Y., Li, Z., Hjelmeland, A.B., Shi, Q., McLendon, R.E., Bigner, D.D., and Rich, J.N. (2006b). Stem cell-like glioma cells promote tumor angiogenesis through vascular endothelial growth factor. *Cancer Res* 66, 7843-7848.

Barbagallo, G.M., Jenkinson, M.D., and Brodbelt, A.R. (2008). 'Recurrent' glioblastoma multiforme, when should we reoperate? *Br J Neurosurg* 22, 452-455.

Barnes, M., Eberhart, C.G., Collins, R., and Tihan, T. (2009). Expression of p75NTR in fetal brain and medulloblastomas: evidence of a precursor cell marker and its persistence in neoplasia. *J Neurooncol* 92, 193-201.

Barth, R.F., and Kaur, B. (2009). Rat brain tumor models in experimental neuro-oncology: the C6, 9L, T9, RG2, F98, BT4C, RT-2 and CNS-1 gliomas. *J Neurooncol* 94, 299-312.

Bashaw, G.J., Kidd, T., Murray, D., Pawson, T., and Goodman, C.S. (2000). Repulsive axon guidance: Abelson and Enabled play opposing roles downstream of the roundabout receptor. *Cell* 101, 703-715.

Battye, R., Stevens, A., and Jacobs, J.R. (1999). Axon repulsion from the midline of the *Drosophila* CNS requires slit function. *Development* 126, 2475-2481.

Bazarov, A.V., van Sluis, M., Hines, W.C., Bassett, E., Beliveau, A., Campeau, E., Mukhopadhyay, R., Lee, W.J., Melodyev, S., Zaslavsky, Y., *et al.* (2010). p16(INK4a)-mediated suppression of telomerase in normal and malignant human breast cells. *Aging Cell*.

Bazil, V., and Strominger, J.L. (1994). Metalloprotease and serine protease are involved in cleavage of CD43, CD44, and CD16 from stimulated human granulocytes. Induction of cleavage of L-selectin via CD16. *J Immunol* 152, 1314-1322.

Bedell, V.M., Yeo, S.Y., Park, K.W., Chung, J., Seth, P., Shivalingappa, V., Zhao, J., Obara, T., Sukhatme, V.P., Drummond, I.A., *et al.* (2005). roundabout4 is essential for angiogenesis in vivo. *Proc Natl Acad Sci U S A* 102, 6373-6378.

Belien, A.T., Paganetti, P.A., and Schwab, M.E. (1999). Membrane-type 1 matrix metalloprotease (MT1-MMP) enables invasive migration of glioma cells in central nervous system white matter. *J Cell Biol* 144, 373-384.

Bellail, A.C., Hunter, S.B., Brat, D.J., Tan, C., and Van Meir, E.G. (2004). Microregional extracellular matrix heterogeneity in brain modulates glioma cell invasion. *Int J Biochem Cell Biol* 36, 1046-1069.

Bello, L., Lucini, V., Carrabba, G., Giussani, C., Machluf, M., Pluderi, M., Nikas, D., Zhang, J., Tomei, G., Villani, R.M., *et al.* (2001). Simultaneous inhibition of glioma angiogenesis, cell proliferation, and invasion by a naturally occurring fragment of human metalloproteinase-2. *Cancer Res* 61, 8730-8736.

Bertoli-Avella, A.M., Conte, M.L., Punzo, F., de Graaf, B.M., Lama, G., La Manna, A., Polito, C., Grassia, C., Nobili, B., Rambaldi, P.F., *et al.* (2008). ROBO2 gene variants are associated with familial vesicoureteral reflux. *J Am Soc Nephrol* 19, 825-831.

Bianchi, R., Citti, L., Beghetti, R., Romani, L., D'Incalci, M., Puccetti, P., and Fioretti, M.C. (1992). O6-methylguanine-DNA methyltransferase activity and induction of novel immunogenicity in murine tumor cells treated with methylating agents. *Cancer Chemother Pharmacol* 29, 277-282.

Bigner, S.H., McLendon, R.E., Fuchs, H., McKeever, P.E., and Friedman, H.S. (1997). Chromosomal characteristics of childhood brain tumors. *Cancer Genet Cytogenet* 97, 125-134.

Bittner, M., Meltzer, P., Chen, Y., Jiang, Y., Seftor, E., Hendrix, M., Radmacher, M., Simon, R., Yakhini, Z., Ben-Dor, A., *et al.* (2000). Molecular classification of cutaneous malignant melanoma by gene expression profiling. *Nature* 406, 536-540.

Blasco, M.A., Lee, H.W., Hande, M.P., Samper, E., Lansdorp, P.M., DePinho, R.A., and Greider, C.W. (1997). Telomere shortening and tumor formation by mouse cells lacking telomerase RNA. *Cell* 91, 25-34.

Bleau, A.M., Hambardzumyan, D., Ozawa, T., Fomchenko, E.I., Huse, J.T., Brennan, C.W., and Holland, E.C. (2009). PTEN/PI3K/Akt pathway regulates the side population phenotype and ABCG2 activity in glioma tumor stem-like cells. *Cell Stem Cell* 4, 226-235.

Bogdahn, U., Hau, P., Stockhammer, G., Venkataramana, N.K., Mahapatra, A.K., Suri, A., Balasubramaniam, A., Nair, S., Oliushine, V., Parfenov, V., *et al.* (2011). Targeted therapy for high-grade glioma with the TGF-beta2 inhibitor trabedersen: results of a randomized and controlled phase IIb study. *Neuro Oncol* 13, 132-142.

Bos, P.D., Nguyen, D.X., and Massague, J. (2010). Modeling metastasis in the mouse. *Curr Opin Pharmacol* 10, 571-577.

Bouchard, J.F., Horn, K.E., Stroh, T., and Kennedy, T.E. (2008). Depolarization recruits DCC to the plasma membrane of embryonic cortical neurons and enhances axon extension in response to netrin-1. *J Neurochem* 107, 398-417.

Bouchard, J.F., Moore, S.W., Tritsch, N.X., Roux, P.P., Shekarabi, M., Barker, P.A., and Kennedy, T.E. (2004). Protein kinase A activation promotes plasma membrane insertion of DCC from an intracellular pool: A novel mechanism regulating commissural axon extension. *J Neurosci* 24, 3040-3050.

Bradbury, P.A., Zhai, R., Hopkins, J., Kulke, M.H., Heist, R.S., Singh, S., Zhou, W., Ma, C., Xu, W., Asomaning, K., *et al.* (2009). Matrix metalloproteinase 1, 3 and 12 polymorphisms and esophageal adenocarcinoma risk and prognosis. *Carcinogenesis* 30, 793-798.

Brindley, C.J., Antoniow, P., and Newlands, E.S. (1986). Plasma and tissue disposition of mitozolomide in mice. *Br J Cancer* 53, 91-97.

Brocardo, M., and Henderson, B.R. (2008). APC shuttling to the membrane, nucleus and beyond. *Trends Cell Biol* 18, 587-596.

Brose, K., Bland, K.S., Wang, K.H., Arnott, D., Henzel, W., Goodman, C.S., Tessier-Lavigne, M., and Kidd, T. (1999). Slit proteins bind Robo receptors and have an evolutionarily conserved role in repulsive axon guidance. *Cell* 96, 795-806.

Buchdunger, E., Cioffi, C.L., Law, N., Stover, D., Ohno-Jones, S., Druker, B.J., and Lydon, N.B. (2000). Abl protein-tyrosine kinase inhibitor STI571 inhibits in vitro signal transduction mediated by c-kit and platelet-derived growth factor receptors. *J Pharmacol Exp Ther* 295, 139-145.

Buhren, J., Christoph, A.H., Buslei, R., Albrecht, S., Wiestler, O.D., and Pietsch, T. (2000). Expression of the neurotrophin receptor p75NTR in medulloblastomas is correlated with distinct histological and clinical features: evidence for a medulloblastoma subtype derived from the external granule cell layer. *J Neuropathol Exp Neurol* 59, 229-240.

Bussemakers, M.J., Van Bokhoven, A., Tomita, K., Jansen, C.F., and Schalken, J.A. (2000). Complex cadherin expression in human prostate cancer cells. *Int J Cancer* 85, 446-450.

Bussemakers, M.J., van Moorselaar, R.J., Girolodi, L.A., Ichikawa, T., Isaacs, J.T., Takeichi, M., Debruyne, F.M., and Schalken, J.A. (1992). Decreased expression of E-cadherin in the progression of rat prostatic cancer. *Cancer Res* 52, 2916-2922.

Cameron, H.A., and McKay, R.D. (2001). Adult neurogenesis produces a large pool of new granule cells in the dentate gyrus. *J Comp Neurol* 435, 406-417.

Carmeliet, P., and Tessier-Lavigne, M. (2005). Common mechanisms of nerve and blood vessel wiring. *Nature* 436, 193-200.

Catapano, C.V., Broggini, M., Erba, E., Ponti, M., Mariani, L., Citti, L., and D'Incalci, M. (1987). In vitro and in vivo methazolastone-induced DNA damage and repair in L-1210 leukemia sensitive and resistant to chloroethylnitrosoureas. *Cancer Res* 47, 4884-4889.

Causeret, F., Danne, F., Ezan, F., Sotelo, C., and Bloch-Gallego, E. (2002). Slit antagonizes netrin-1 attractive effects during the migration of inferior olivary neurons. *Dev Biol* 246, 429-440.

Causeret, F., Hidalgo-Sanchez, M., Fort, P., Backer, S., Popoff, M.R., Gauthier-Rouviere, C., and Bloch-Gallego, E. (2004). Distinct roles of Rac1/Cdc42 and Rho/Rock for axon outgrowth and nucleokinesis of precerebellar neurons toward netrin 1. *Development* 131, 2841-2852.

Cavallaro, U., and Christofori, G. (2004). Cell adhesion and signalling by cadherins and Ig-CAMs in cancer. *Nat Rev Cancer* 4, 118-132.

Cavallaro, U., Schaffhauser, B., and Christofori, G. (2002). Cadherins and the tumour progression: is it all in a switch? *Cancer Lett* 176, 123-128.

Chen, Z., Gore, B.B., Long, H., Ma, L., and Tessier-Lavigne, M. (2008). Alternative splicing of the Robo3 axon guidance receptor governs the midline switch from attraction to repulsion. *Neuron* 58, 325-332.

Cheney, I.W., Johnson, D.E., Vaillancourt, M.T., Avanzini, J., Morimoto, A., Demers, G.W., Wills, K.N., Shabram, P.W., Bolen, J.B., Tavtigian, S.V., *et al.* (1998). Suppression of tumorigenicity of glioblastoma cells by adenovirus-mediated MMAC1/PTEN gene transfer. *Cancer Res* 58, 2331-2334.

Cheung, C.T., Kaul, S.C., and Wadhwa, R. (2010). Molecular bridging of aging and cancer: A CARF link. *Ann N Y Acad Sci* 1197, 129-133.

Chiariello, E., Roz, L., Albarosa, R., Magnani, I., and Finocchiaro, G. (1998). PTEN/MMAC1 mutations in primary glioblastomas and short-term cultures of malignant gliomas. *Oncogene* 16, 541-545.

Chinot, O.L., de La Motte Rouge, T., Moore, N., Zeaiter, A., Das, A., Phillips, H., Modrusan, Z., and Cloughesy, T. (2011). AVAglio: Phase 3 trial of bevacizumab plus temozolomide and radiotherapy in newly diagnosed glioblastoma multiforme. *Adv Ther* 28, 334-340.

Clemmons, D.R., and Van Wyk, J.J. (1981). Somatomedin-C and platelet-derived growth factor stimulate human fibroblast replication. *J Cell Physiol* 106, 361-367.

Cogen, P.H., and McDonald, J.D. (1996). Tumor suppressor genes and medulloblastoma. *J Neurooncol* 29, 103-112.

Coleman, H.A., Labrador, J.P., Chance, R.K., and Bashaw, G.J. (2010). The Adam family metalloprotease Kuzbanian regulates the cleavage of the roundabout receptor to control axon repulsion at the midline. *Development* 137, 2417-2426.

Collado, M., Blasco, M.A., and Serrano, M. (2007). Cellular senescence in cancer and aging. *Cell* 130, 223-233.

Corcoran, A., and Del Maestro, R.F. (2003). Testing the "Go or Grow" hypothesis in human medulloblastoma cell lines in two and three dimensions. *Neurosurgery* 53, 174-184; discussion 184-175.

Covington, M.D., Burghardt, R.C., and Parrish, A.R. (2006). Ischemia-induced cleavage of cadherins in NRK cells requires MT1-MMP (MMP-14). *Am J Physiol Renal Physiol* 290, F43-51.

Cox, C.V., Diamanti, P., Evely, R.S., Kearns, P.R., and Blair, A. (2009). Expression of CD133 on leukemia-initiating cells in childhood ALL. *Blood* 113, 3287-3296.

Cunningham, M.P., Essapen, S., Thomas, H., Green, M., Lovell, D.P., Topham, C., Marks, C., and Modjtahedi, H. (2005). Coexpression, prognostic significance and predictive value of EGFR, EGFRvIII and phosphorylated EGFR in colorectal cancer. *Int J Oncol* 27, 317-325.

Czajkowski, C., and Farb, D.H. (1989). Identification of an intracellular pool of gamma-aminobutyric acid/benzodiazepine receptors en route to the cell surface of brain neurons in culture. *Mol Pharmacol* 35, 183-188.

Dahmen, R.P., Koch, A., Denkhaus, D., Tonn, J.C., Sorensen, N., Berthold, F., Behrens, J., Birchmeier, W., Wiestler, O.D., and Pietsch, T. (2001). Deletions of AXIN1, a component of the WNT/wingless pathway, in sporadic medulloblastomas. *Cancer Res* 61, 7039-7043.

Dallol, A., Da Silva, N.F., Viacava, P., Minna, J.D., Bieche, I., Maher, E.R., and Latif, F. (2002). SLIT2, a human homologue of the Drosophila Slit2 gene, has tumor suppressor activity and is frequently inactivated in lung and breast cancers. *Cancer Res* 62, 5874-5880.

Dallol, A., Krex, D., Hesson, L., Eng, C., Maher, E.R., and Latif, F. (2003). Frequent epigenetic inactivation of the SLIT2 gene in gliomas. *Oncogene* 22, 4611-4616.

Dandy, W.E. (1933). Benign Encapsulated Tumors in the Lateral Ventricles of the Brain: Diagnosis and Treatment. *Ann Surg* 98, 841-845.

Datta, S.R., Dudek, H., Tao, X., Masters, S., Fu, H., Gotoh, Y., and Greenberg, M.E. (1997). Akt phosphorylation of BAD couples survival signals to the cell-intrinsic death machinery. *Cell* 91, 231-241.

de Martin, R., Haendler, B., Hofer-Warbinek, R., Gaugitsch, H., Wrann, M., Schlusener, H., Seifert, J.M., Bodmer, S., Fontana, A., and Hofer, E. (1987). Complementary DNA for human glioblastoma-derived T cell suppressor factor, a novel member of the transforming growth factor-beta gene family. *EMBO J* 6, 3673-3677.

Del Duca, D., Werbowetski, T., and Del Maestro, R.F. (2004). Spheroid preparation from hanging drops: characterization of a model of brain tumor invasion. *J Neurooncol* 67, 295-303.

Del Maestro, R.F., Vaithilingam, I.S., and McDonald, W. (1995). Degradation of collagen type IV by C6 astrocytoma cells. *J Neurooncol* 24, 75-81.

Delaney, J.C., and Essigmann, J.M. (2001). Effect of sequence context on O(6)-methylguanine repair and replication in vivo. *Biochemistry* 40, 14968-14975.

Demuth, T., Reavie, L.B., Rennert, J.L., Nakada, M., Nakada, S., Hoelzinger, D.B., Beaudry, C.E., Henrichs, A.N., Anderson, E.M., and Berens, M.E. (2007). MAP-ing glioma invasion: mitogen-activated protein kinase kinase 3 and p38 drive glioma invasion and progression and predict patient survival. *Mol Cancer Ther* 6, 1212-1222.

Deryugina, E.I., Bourdon, M.A., Reisfeld, R.A., and Strongin, A. (1998). Remodeling of collagen matrix by human tumor cells requires activation and cell surface association of matrix metalloproteinase-2. *Cancer Res* 58, 3743-3750.

Dey, N., Crosswell, H.E., De, P., Parsons, R., Peng, Q., Su, J.D., and Durden, D.L. (2008). The protein phosphatase activity of PTEN regulates SRC family kinases and controls glioma migration. *Cancer Res* 68, 1862-1871.

Di Meglio, T., Nguyen-Ba-Charvet, K.T., Tessier-Lavigne, M., Sotelo, C., and Chedotal, A. (2008). Molecular mechanisms controlling midline crossing by precerebellar neurons. *J Neurosci* 28, 6285-6294.

Donnenberg, V.S., and Donnenberg, A.D. (2005). Multiple drug resistance in cancer revisited: the cancer stem cell hypothesis. *J Clin Pharmacol* 45, 872-877.

Dumenco, L.L., Allay, E., Norton, K., and Gerson, S.L. (1993). The prevention of thymic lymphomas in transgenic mice by human O6-alkylguanine-DNA alkyltransferase. *Science* 259, 219-222.

Dunwell, T.L., Dickinson, R.E., Stankovic, T., Dallol, A., Weston, V., Austen, B., Catchpoole, D., Maher, E.R., and Latif, F. (2009). Frequent epigenetic inactivation of the SLIT2 gene in chronic and acute lymphocytic leukemia. *Epigenetics* 4, 265-269.

el-Azouzi, M., Chung, R.Y., Farmer, G.E., Martuza, R.L., Black, P.M., Rouleau, G.A., Hettlich, C., Hedley-Whyte, E.T., Zervas, N.T., Panagopoulos, K., *et al.* (1989). Loss of distinct regions on the short arm of chromosome 17 associated with tumorigenesis of human astrocytomas. *Proc Natl Acad Sci U S A* 86, 7186-7190.

Ellison, D. (2002). Classifying the medulloblastoma: insights from morphology and molecular genetics. *Neuropathol Appl Neurobiol* 28, 257-282.

Endo, K., Takino, T., Miyamori, H., Kinsen, H., Yoshizaki, T., Furukawa, M., and Sato, H. (2003). Cleavage of syndecan-1 by membrane type matrix metalloproteinase-1 stimulates cell migration. *J Biol Chem* 278, 40764-40770.

Endris, V., Wogatzky, B., Leimer, U., Bartsch, D., Zatyka, M., Latif, F., Maher, E.R., Tariverdian, G., Kirsch, S., Karch, D., *et al.* (2002). The novel Rho-GTPase activating gene MEGAP/ srGAP3 has a putative role in severe mental retardation. *Proc Natl Acad Sci U S A* 99, 11754-11759.

Englund, C., Steneberg, P., Falileeva, L., Xylourgidis, N., and Samakovlis, C. (2002). Attractive and repulsive functions of Slit are mediated by different receptors in the *Drosophila* trachea. *Development* 129, 4941-4951.

Enguita-German, M., Schiapparelli, P., Rey, J.A., and Castresana, J.S. (2010). CD133+ cells from medulloblastoma and PNET cell lines are more resistant to cyclopamine inhibition of the sonic hedgehog signaling pathway than CD133- cells. *Tumour Biol*.

Eriksson, P.S., Perfilieva, E., Bjork-Eriksson, T., Alborn, A.M., Nordborg, C., Peterson, D.A., and Gage, F.H. (1998). Neurogenesis in the adult human hippocampus. *Nat Med* 4, 1313-1317.

Esteller, M., Garcia-Foncillas, J., Andion, E., Goodman, S.N., Hidalgo, O.F., Vanaclocha, V., Baylin, S.B., and Herman, J.G. (2000). Inactivation of the DNA-repair gene MGMT and the clinical response of gliomas to alkylating agents. *N Engl J Med* 343, 1350-1354.

Esteve, P.O., Tremblay, P., Houde, M., St-Pierre, Y., and Mandeville, R. (1998). In vitro expression of MMP-2 and MMP-9 in glioma cells following exposure to inflammatory mediators. *Biochim Biophys Acta* 1403, 85-96.

Ezhilarasan, R., Mohanam, I., Govindarajan, K., and Mohanam, S. (2007). Glioma cells suppress hypoxia-induced endothelial cell apoptosis and promote the angiogenic process. *Int J Oncol* 30, 701-707.

Ferraro, G.B., Morrison, C.J., Overall, C.M., Strittmatter, S.M., and Fournier, A.E. (2011). Membrane-type matrix metalloproteinase-3 regulates neuronal responsiveness to myelin through Nogo-66 receptor 1 cleavage. *J Biol Chem* 286, 31418-31424.

Folkins, C., Shaked, Y., Man, S., Tang, T., Lee, C.R., Zhu, Z., Hoffman, R.M., and Kerbel, R.S. (2009). Glioma tumor stem-like cells promote tumor angiogenesis and vasculogenesis via vascular endothelial growth factor and stromal-derived factor 1. *Cancer Res* 69, 7243-7251.

Forsyth, P.A., Wong, H., Laing, T.D., Rewcastle, N.B., Morris, D.G., Muzik, H., Leco, K.J., Johnston, R.N., Brasher, P.M., Sutherland, G., *et al.* (1999). Gelatinase-A (MMP-2), gelatinase-B (MMP-9) and membrane type matrix metalloproteinase-1 (MT1-MMP) are involved in different aspects of the pathophysiology of malignant gliomas. *Br J Cancer* 79, 1828-1835.

Fritz, J.L., and VanBerkum, M.F. (2000). Calmodulin and son of sevenless dependent signaling pathways regulate midline crossing of axons in the *Drosophila* CNS. *Development* 127, 1991-2000.

Frixen, U.H., Behrens, J., Sachs, M., Eberle, G., Voss, B., Warda, A., Lochner, D., and Birchmeier, W. (1991). E-cadherin-mediated cell-cell adhesion prevents invasiveness of human carcinoma cells. *J Cell Biol* 113, 173-185.

Fukuhara, N., Howitt, J.A., Hussain, S.A., and Hohenester, E. (2008). Structural and functional analysis of slit and heparin binding to immunoglobulin-like domains 1 and 2 of *Drosophila* Robo. *J Biol Chem* 283, 16226-16234.

Fults, D., Toppets, R.H., Thomas, G.A., Nakamura, Y., and White, R. (1989). Loss of heterozygosity for loci on chromosome 17p in human malignant astrocytoma. *Cancer Res* 49, 6572-6577.

Furnari, F.B., Lin, H., Huang, H.S., and Cavenee, W.K. (1997). Growth suppression of glioma cells by PTEN requires a functional phosphatase catalytic domain. *Proc Natl Acad Sci U S A* **94**, 12479-12484.

Galko, M.J., and Tessier-Lavigne, M. (2000). Function of an axonal chemoattractant modulated by metalloprotease activity. *Science* **289**, 1365-1367.

Galli, R., Binda, E., Orfanelli, U., Cipelletti, B., Gritti, A., De Vitis, S., Fiocco, R., Foroni, C., Dimeco, F., and Vescovi, A. (2004). Isolation and characterization of tumorigenic, stem-like neural precursors from human glioblastoma. *Cancer Res* **64**, 7011-7021.

Galvez, B.G., Matias-Roman, S., Albar, J.P., Sanchez-Madrid, F., and Arroyo, A.G. (2001). Membrane type 1-matrix metalloproteinase is activated during migration of human endothelial cells and modulates endothelial motility and matrix remodeling. *J Biol Chem* **276**, 37491-37500.

Gan, H.K., Kaye, A.H., and Luwor, R.B. (2009a). The EGFRvIII variant in glioblastoma multiforme. *J Clin Neurosci* **16**, 748-754.

Gan, H.K., Lappas, M., Cao, D.X., Cvrljevic, A., Scott, A.M., and Johns, T.G. (2009b). Targeting a unique EGFR epitope with monoclonal antibody 806 activates NF-kappaB and initiates tumour vascular normalization. *J Cell Mol Med* **13**, 3993-4001.

Gardai, S.J., Whitlock, B.B., Xiao, Y.Q., Bratton, D.B., and Henson, P.M. (2004). Oxidants inhibit ERK/MAPK and prevent its ability to delay neutrophil apoptosis downstream of mitochondrial changes and at the level of XIAP. *J Biol Chem* **279**, 44695-44703.

Ge, H., Gong, X., and Tang, C.K. (2002). Evidence of high incidence of EGFRvIII expression and coexpression with EGFR in human invasive breast cancer by laser capture microdissection and immunohistochemical analysis. *Int J Cancer* **98**, 357-361.

Genis, L., Galvez, B.G., Gonzalo, P., and Arroyo, A.G. (2006). MT1-MMP: universal or particular player in angiogenesis? *Cancer Metastasis Rev* **25**, 77-86.

Gerber, H.P., Dixit, V., and Ferrara, N. (1998). Vascular endothelial growth factor induces expression of the antiapoptotic proteins Bcl-2 and A1 in vascular endothelial cells. *J Biol Chem* **273**, 13313-13316.

Gerson, S.L. (2004). MGMT: its role in cancer aetiology and cancer therapeutics. *Nat Rev Cancer* **4**, 296-307.

Giancotti, F.G., and Ruoslahti, E. (1999). Integrin signaling. *Science* **285**, 1028-1032.

Gilbert, M.R. (2006). New treatments for malignant gliomas: careful evaluation and cautious optimism required. *Ann Intern Med* **144**, 371-373.

Gilthorpe, J.D., Papantoniou, E.K., Chedotal, A., Lumsden, A., and Wingate, R.J. (2002). The migration of cerebellar rhombic lip derivatives. *Development* **129**, 4719-4728.

Gladson, C.L., Wilcox, J.N., Sanders, L., Gillespie, G.Y., and Cheresch, D.A. (1995). Cerebral microenvironment influences expression of the vitronectin gene in astrocytic tumors. *J Cell Sci* **108 (Pt 3)**, 947-956.

Goodrich, L.V., Milenkovic, L., Higgins, K.M., and Scott, M.P. (1997). Altered neural cell fates and medulloblastoma in mouse patched mutants. *Science* **277**, 1109-1113.

Gorn, M., Anige, M., Burkholder, I., Muller, B., Scheffler, A., Edler, L., Boeters, I., Panse, J., Schuch, G., Hossfeld, D.K., *et al.* (2005). Serum levels of Magic Roundabout protein in patients with advanced non-small cell lung cancer (NSCLC). *Lung Cancer* **49**, 71-76.

Goth, R., and Rajewsky, M.F. (1974). Persistence of O6-ethylguanine in rat-brain DNA: correlation with nervous system-specific carcinogenesis by ethylnitrosourea. *Proc Natl Acad Sci U S A* **71**, 639-643.

Greider, C.W., and Blackburn, E.H. (1985). Identification of a specific telomere terminal transferase activity in Tetrahymena extracts. *Cell* **43**, 405-413.

Grieshammer, U., Le, M., Plump, A.S., Wang, F., Tessier-Lavigne, M., and Martin, G.R. (2004). SLIT2-mediated ROBO2 signaling restricts kidney induction to a single site. *Dev Cell* **6**, 709-717.

Guerrier, S., Coutinho-Budd, J., Sassa, T., Gresset, A., Jordan, N.V., Chen, K., Jin, W.L., Frost, A., and Polleux, F. (2009). The F-BAR domain of srGAP2 induces membrane protrusions required for neuronal migration and morphogenesis. *Cell* **138**, 990-1004.

Guillamo, J.S., de Bouard, S., Valable, S., Marteau, L., Leuraud, P., Marie, Y., Poupon, M.F., Parienti, J.J., Raymond, E., and Peschanski, M. (2009). Molecular mechanisms underlying effects of epidermal growth factor receptor inhibition on invasion, proliferation, and angiogenesis in experimental glioma. *Clin Cancer Res* **15**, 3697-3704.

Gumbiner, B. (1988). Cadherins: a family of Ca²⁺-dependent adhesion molecules. *Trends Biochem Sci* 13, 75-76.

Gumbiner, B.M. (2000). Regulation of cadherin adhesive activity. *J Cell Biol* 148, 399-404.

Guo, P., Imanishi, Y., Cackowski, F.C., Jarzynka, M.J., Tao, H.Q., Nishikawa, R., Hirose, T., Hu, B., and Cheng, S.Y. (2005). Up-regulation of angiopoietin-2, matrix metalloprotease-2, membrane type 1 metalloprotease, and laminin 5 gamma 2 correlates with the invasiveness of human glioma. *Am J Pathol* 166, 877-890.

Guo, S., and Bao, S. (2010). srGAP2 arginine methylation regulates cell migration and cell spreading through promoting dimerization. *J Biol Chem* 285, 35133-35141.

Guo, W., and Giancotti, F.G. (2004). Integrin signalling during tumour progression. *Nat Rev Mol Cell Biol* 5, 816-826.

Hahn, H., Wojnowski, L., Zimmer, A.M., Hall, J., Miller, G., and Zimmer, A. (1998). Rhabdomyosarcomas and radiation hypersensitivity in a mouse model of Gorlin syndrome. *Nat Med* 4, 619-622.

Hambardzumyan, D., Becher, O.J., Rosenblum, M.K., Pandolfi, P.P., Manova-Todorova, K., and Holland, E.C. (2008a). PI3K pathway regulates survival of cancer stem cells residing in the perivascular niche following radiation in medulloblastoma in vivo. *Genes Dev* 22, 436-448.

Hambardzumyan, D., Squatrito, M., Carbajal, E., and Holland, E.C. (2008b). Glioma formation, cancer stem cells, and akt signaling. *Stem Cell Rev* 4, 203-210.

Hambardzumyan, D., Squatrito, M., and Holland, E.C. (2006). Radiation resistance and stem-like cells in brain tumors. *Cancer Cell* 10, 454-456.

Hamilton, S.R., Liu, B., Parsons, R.E., Papadopoulos, N., Jen, J., Powell, S.M., Krush, A.J., Berk, T., Cohen, Z., Tetu, B., *et al.* (1995). The molecular basis of Turcot's syndrome. *N Engl J Med* 332, 839-847.

Harris, R.C., Chung, E., and Coffey, R.J. (2003). EGF receptor ligands. *Exp Cell Res* 284, 2-13.

Hasselbalch, B., Lassen, U., Hansen, S., Holmberg, M., Sorensen, M., Kosteljanetz, M., Broholm, H., Stockhausen, M.T., and Poulsen, H.S. (2010). Cetuximab, bevacizumab, and irinotecan for patients with primary glioblastoma and progression after radiation therapy and temozolomide: a phase II trial. *Neuro Oncol* 12, 508-516.

Hatton, B.A., Villavicencio, E.H., Pritchard, J., LeBlanc, M., Hansen, S., Ulrich, M., Ditzler, S., Pullar, B., Stroud, M.R., and Olson, J.M. (2010). Notch signaling is not essential in sonic hedgehog-activated medulloblastoma. *Oncogene* 29, 3865-3872.

Hawinkels, L.J., Kuiper, P., Wiercinska, E., Verspaget, H.W., Liu, Z., Pardali, E., Sier, C.F., and ten Dijke, P. (2010). Matrix metalloproteinase-14 (MT1-MMP)-mediated endoglin shedding inhibits tumor angiogenesis. *Cancer Res* 70, 4141-4150.

Heasman, S.J., and Ridley, A.J. (2008). Mammalian Rho GTPases: new insights into their functions from in vivo studies. *Nat Rev Mol Cell Biol* 9, 690-701.

Hegi, M.E., Diserens, A.C., Godard, S., Dietrich, P.Y., Regli, L., Ostermann, S., Otten, P., Van Melle, G., de Tribolet, N., and Stupp, R. (2004). Clinical trial substantiates the predictive value of O-6-methylguanine-DNA methyltransferase promoter methylation in glioblastoma patients treated with temozolomide. *Clin Cancer Res* 10, 1871-1874.

Hegi, M.E., Diserens, A.C., Gorlia, T., Hamou, M.F., de Tribolet, N., Weller, M., Kros, J.M., Hainfellner, J.A., Mason, W., Mariani, L., *et al.* (2005). MGMT gene silencing and benefit from temozolomide in glioblastoma. *N Engl J Med* 352, 997-1003.

Hersey, P., Sosman, J., O'Day, S., Richards, J., Bedikian, A., Gonzalez, R., Sharfman, W., Weber, R., Logan, T., Buzoianu, M., *et al.* (2010). A randomized phase 2 study of etaracizumab, a monoclonal antibody against integrin alpha(v)beta(3), + or - dacarbazine in patients with stage IV metastatic melanoma. *Cancer* 116, 1526-1534.

Hiraoka, N., Allen, E., Apel, I.J., Gyetko, M.R., and Weiss, S.J. (1998). Matrix metalloproteinases regulate neovascularization by acting as pericellular fibrinolysins. *Cell* 95, 365-377.

Hirohashi, S. (1998). Inactivation of the E-cadherin-mediated cell adhesion system in human cancers. *Am J Pathol* 153, 333-339.

Hirschmann-Jax, C., Foster, A.E., Wulf, G.G., Nuchtern, J.G., Jax, T.W., Gobel, U., Goodell, M.A., and Brenner, M.K. (2004). A distinct "side population" of cells with high drug efflux capacity in human tumor cells. *Proc Natl Acad Sci U S A* 101, 14228-14233.

Hivert, B., Liu, Z., Chuang, C.Y., Doherty, P., and Sundaresan, V. (2002). Robo1 and Robo2 are homophilic binding molecules that promote axonal growth. *Mol Cell Neurosci* 21, 534-545.

Ho, M.M., Ng, A.V., Lam, S., and Hung, J.Y. (2007). Side population in human lung cancer cell lines and tumors is enriched with stem-like cancer cells. *Cancer Res* 67, 4827-4833.

Holland, E.C., Celestino, J., Dai, C., Schaefer, L., Sawaya, R.E., and Fuller, G.N. (2000). Combined activation of Ras and Akt in neural progenitors induces glioblastoma formation in mice. *Nat Genet* 25, 55-57.

Hollstein, M., Sidransky, D., Vogelstein, B., and Harris, C.C. (1991). p53 mutations in human cancers. *Science* 253, 49-53.

Holmbeck, K., Bianco, P., Caterina, J., Yamada, S., Kromer, M., Kuznetsov, S.A., Mankani, M., Robey, P.G., Poole, A.R., Pidoux, I., *et al.* (1999). MT1-MMP-deficient mice develop dwarfism, osteopenia, arthritis, and connective tissue disease due to inadequate collagen turnover. *Cell* 99, 81-92.

Hood, J.D., and Cheresch, D.A. (2002). Role of integrins in cell invasion and migration. *Nat Rev Cancer* 2, 91-100.

Hooper, N.M., Karran, E.H., and Turner, A.J. (1997). Membrane protein secretases. *Biochem J* 321 (Pt 2), 265-279.

Hotary, K.B., Allen, E.D., Brooks, P.C., Datta, N.S., Long, M.W., and Weiss, S.J. (2003). Membrane type I matrix metalloproteinase usurps tumor growth control imposed by the three-dimensional extracellular matrix. *Cell* 114, 33-45.

Hu, H. (1999). Chemorepulsion of neuronal migration by Slit2 in the developing mammalian forebrain. *Neuron* 23, 703-711.

Hu, H. (2001). Cell-surface heparan sulfate is involved in the repulsive guidance activities of Slit2 protein. *Nat Neurosci* 4, 695-701.

Huang, H., Mahler-Araujo, B.M., Sankila, A., Chimelli, L., Yonekawa, Y., Kleihues, P., and Ohgaki, H. (2000). APC mutations in sporadic medulloblastomas. *Am J Pathol* 156, 433-437.

Huminiecki, L., Gorn, M., Suchting, S., Poulsom, R., and Bicknell, R. (2002). Magic roundabout is a new member of the roundabout receptor family that is endothelial specific and expressed at sites of active angiogenesis. *Genomics* 79, 547-552.

Husemann, K., Wolter, M., Buschges, R., Bostrom, J., Sabel, M., and Reifemberger, G. (1999). Identification of two distinct deleted regions on the short arm of chromosome 1 and rare mutation of the CDKN2C gene from 1p32 in oligodendroglial tumors. *J Neuropathol Exp Neurol* 58, 1041-1050.

Hussain, S.A., Piper, M., Fukuhara, N., Strohlic, L., Cho, G., Howitt, J.A., Ahmed, Y., Powell, A.K., Turnbull, J.E., Holt, C.E., *et al.* (2006). A molecular mechanism for the heparan sulfate dependence of slit-robo signaling. *J Biol Chem* 281, 39693-39698.

Huszthy, P.C., Goplen, D., Thorsen, F., Immervoll, H., Wang, J., Gutermann, A., Miletic, H., and Bjerkvig, R. (2008). Oncolytic herpes simplex virus type-1 therapy in a highly infiltrative animal model of human glioblastoma. *Clin Cancer Res* 14, 1571-1580.

Ikushima, H., and Miyazono, K. (2010). TGFbeta signalling: a complex web in cancer progression. *Nat Rev Cancer* 10, 415-424.

Ito, H., Funahashi, S., Yamauchi, N., Shibahara, J., Midorikawa, Y., Kawai, S., Kinoshita, Y., Watanabe, A., Hippo, Y., Ohtomo, T., *et al.* (2006). Identification of ROBO1 as a novel hepatocellular carcinoma antigen and a potential therapeutic and diagnostic target. *Clin Cancer Res* 12, 3257-3264.

James, C.D., Carlom, E., Nordenskjold, M., Collins, V.P., and Cavenee, W.K. (1989). Mitotic recombination of chromosome 17 in astrocytomas. *Proc Natl Acad Sci U S A* 86, 2858-2862.

Jen, J.C., Chan, W.M., Bosley, T.M., Wan, J., Carr, J.R., Rub, U., Shattuck, D., Salamon, G., Kudo, L.C., Ou, J., *et al.* (2004). Mutations in a human ROBO gene disrupt hindbrain axon pathway crossing and morphogenesis. *Science* 304, 1509-1513.

Jensen, N.A., Pedersen, K.M., Lihme, F., Rask, L., Nielsen, J.V., Rasmussen, T.E., and Mitchelmore, C. (2003). Astroglial c-Myc overexpression predisposes mice to primary malignant gliomas. *J Biol Chem* 278, 8300-8308.

Jin, J., You, H., Yu, B., Deng, Y., Tang, N., Yao, G., Shu, H., Yang, S., and Qin, W. (2009). Epigenetic inactivation of SLIT2 in human hepatocellular carcinomas. *Biochem Biophys Res Commun* 379, 86-91.

Jones, C.A., London, N.R., Chen, H., Park, K.W., Sauvaget, D., Stockton, R.A., Wythe, J.D., Suh, W., Larrieu-Lahargue, F., Mukoyama, Y.S., *et al.* (2008). Robo4 stabilizes the vascular network by inhibiting pathologic angiogenesis and endothelial hyperpermeability. *Nat Med* 14, 448-453.

Julenius, K., Molgaard, A., Gupta, R., and Brunak, S. (2005). Prediction, conservation analysis, and structural characterization of mammalian mucin-type O-glycosylation sites. *Glycobiology* 15, 153-164.

Kachra, Z., Beaulieu, E., Delbecchi, L., Mousseau, N., Berthelet, F., Mouldjian, R., Del Maestro, R., and Beliveau, R. (1999). Expression of matrix metalloproteinases and their inhibitors in human brain tumors. *Clin Exp Metastasis* 17, 555-566.

Kaneko, N., Marin, O., Koike, M., Hirota, Y., Uchiyama, Y., Wu, J.Y., Lu, Q., Tessier-Lavigne, M., Alvarez-Buylla, A., Okano, H., *et al.* (2010). New neurons clear the path of astrocytic processes for their rapid migration in the adult brain. *Neuron* 67, 213-223.

Kaur, S., Castellone, M.D., Bedell, V.M., Konar, M., Gutkind, J.S., and Ramchandran, R. (2006). Robo4 signaling in endothelial cells implies attraction guidance mechanisms. *J Biol Chem* 281, 11347-11356.

Keleman, K., Ribeiro, C., and Dickson, B.J. (2005). Comm function in commissural axon guidance: cell-autonomous sorting of Robo in vivo. *Nat Neurosci* 8, 156-163.

Kidd, T., Bland, K.S., and Goodman, C.S. (1999). Slit is the midline repellent for the robo receptor in *Drosophila*. *Cell* 96, 785-794.

Kidd, T., Brose, K., Mitchell, K.J., Fetter, R.D., Tessier-Lavigne, M., Goodman, C.S., and Tear, G. (1998a). Roundabout controls axon crossing of the CNS midline and defines a novel subfamily of evolutionarily conserved guidance receptors. *Cell* 92, 205-215.

Kidd, T., Russell, C., Goodman, C.S., and Tear, G. (1998b). Dosage-sensitive and complementary functions of roundabout and commissureless control axon crossing of the CNS midline. *Neuron* 20, 25-33.

Kim, H.K., Zhang, H., Li, H., Wu, T.T., Swisher, S., He, D., Wu, L., Xu, J., Elmets, C.A., Athar, M., *et al.* (2008). Slit2 inhibits growth and metastasis of fibrosarcoma and squamous cell carcinoma. *Neoplasia* 10, 1411-1420.

Kleihues, P., Cavenee, W.K., and International Agency for Research on Cancer. (2000). Pathology and genetics of tumours of the nervous system (Lyon, IARC Press).

Kopstein, L., and Christofori, G. (2006). Metastasis: cell-autonomous mechanisms versus contributions by the tumor microenvironment. *Cell Mol Life Sci* 63, 449-468.

Koul, D. (2008). PTEN signaling pathways in glioblastoma. *Cancer Biol Ther* 7, 1321-1325.

Kraut, R., and Zinn, K. (2004). Roundabout 2 regulates migration of sensory neurons by signaling in trans. *Curr Biol* 14, 1319-1329.

Krystosek, A., and Seeds, N.W. (1981). Plasminogen activator secretion by granule neurons in cultures of developing cerebellum. *Proc Natl Acad Sci U S A* 78, 7810-7814.

Lampert, K., Machein, U., Machein, M.R., Conca, W., Peter, H.H., and Volk, B. (1998). Expression of matrix metalloproteinases and their tissue inhibitors in human brain tumors. *Am J Pathol* 153, 429-437.

Le, D.M., Besson, A., Fogg, D.K., Choi, K.S., Waisman, D.M., Goodyer, C.G., Rewcastle, B., and Yong, V.W. (2003). Exploitation of astrocytes by glioma cells to facilitate invasiveness: a mechanism involving matrix metalloproteinase-2 and the urokinase-type plasminogen activator-plasmin cascade. *J Neurosci* 23, 4034-4043.

Legg, J.A., Herbert, J.M., Clissold, P., and Bicknell, R. (2008). Slits and Roundabouts in cancer, tumour angiogenesis and endothelial cell migration. *Angiogenesis* 11, 13-21.

Lehti, K., Allen, E., Birkedal-Hansen, H., Holmbeck, K., Miyake, Y., Chun, T.H., and Weiss, S.J. (2005). An MT1-MMP-PDGF receptor-beta axis regulates mural cell investment of the microvasculature. *Genes Dev* 19, 979-991.

Leung, D.W., Cachianes, G., Kuang, W.J., Goeddel, D.V., and Ferrara, N. (1989). Vascular endothelial growth factor is a secreted angiogenic mitogen. *Science* 246, 1306-1309.

Leve, F., and Morgado-Diaz, J.A. (2012). Rho GTPase signaling in the development of colorectal cancer. *J Cell Biochem*.

Levin, V.A., Phuphanich, S., Yung, W.K., Forsyth, P.A., Maestro, R.D., Perry, J.R., Fuller, G.N., and Baillet, M. (2006). Randomized, double-blind, placebo-controlled trial of marimastat in glioblastoma multiforme patients following surgery and irradiation. *J Neurooncol* 78, 295-302.

Li, H.S., Chen, J.H., Wu, W., Fagaly, T., Zhou, L., Yuan, W., Dupuis, S., Jiang, Z.H., Nash, W., Gick, C., *et al.* (1999). Vertebrate slit, a secreted ligand for the transmembrane protein roundabout, is a repellent for olfactory bulb axons. *Cell* 96, 807-818.

Li, J., Yen, C., Liaw, D., Podsypanina, K., Bose, S., Wang, S.I., Puc, J., Miliaresis, C., Rodgers, L., McCombie, R., *et al.* (1997). PTEN, a putative protein tyrosine phosphatase gene mutated in human brain, breast, and prostate cancer. *Science* 275, 1943-1947.

Li, X., Chen, Y., Liu, Y., Gao, J., Gao, F., Bartlam, M., Wu, J.Y., and Rao, Z. (2006). Structural basis of Robo proline-rich motif recognition by the srGAP1 Src homology 3 domain in the Slit-Robo signaling pathway. *J Biol Chem* 281, 28430-28437.

Liang, Y., Annan, R.S., Carr, S.A., Popp, S., Mevissen, M., Margolis, R.K., and Margolis, R.U. (1999). Mammalian homologues of the *Drosophila* slit protein are ligands of the heparan sulfate proteoglycan glypican-1 in brain. *J Biol Chem* 274, 17885-17892.

Libermann, T.A., Nusbaum, H.R., Razon, N., Kris, R., Lax, I., Soreq, H., Whittle, N., Waterfield, M.D., Ullrich, A., and Schlessinger, J. (1985). Amplification and overexpression of the EGF receptor gene in primary human glioblastomas. *J Cell Sci Suppl* 3, 161-172.

Lin, C.J., Malina, A., and Pelletier, J. (2009). c-Myc and eIF4F constitute a feedforward loop that regulates cell growth: implications for anticancer therapy. *Cancer Res* 69, 7491-7494.

Liotta, L.A., Tryggvason, K., Garbisa, S., Hart, I., Foltz, C.M., and Shafie, S. (1980). Metastatic potential correlates with enzymatic degradation of basement membrane collagen. *Nature* 284, 67-68.

Little, M.H., Wilkinson, L., Brown, D.L., Piper, M., Yamada, T., and Stow, J.L. (2001). Dual trafficking of Slit3 to mitochondria and cell surface demonstrates novel localization for Slit protein. *Am J Physiol Cell Physiol* 281, C486-495.

Liu, G., Yuan, X., Zeng, Z., Tunici, P., Ng, H., Abdulkadir, I.R., Lu, L., Irvin, D., Black, K.L., and Yu, J.S. (2006). Analysis of gene expression and chemoresistance of CD133+ cancer stem cells in glioblastoma. *Mol Cancer* 5, 67.

Loechler, E.L., Green, C.L., and Essigmann, J.M. (1984). In vivo mutagenesis by O6-methylguanine built into a unique site in a viral genome. *Proc Natl Acad Sci U S A* 81, 6271-6275.

Loes, S., Luukko, K., Kvinnsland, I.H., and Kettunen, P. (2001). Slit1 is specifically expressed in the primary and secondary enamel knots during molar tooth cusp formation. *Mech Dev* 107, 155-157.

Loizos, N., Xu, Y., Huber, J., Liu, M., Lu, D., Finnerty, B., Rolser, R., Malikzay, A., Persaud, A., Corcoran, E., *et al.* (2005). Targeting the platelet-derived growth factor receptor alpha with a neutralizing human monoclonal antibody inhibits the growth of tumor xenografts: implications as a potential therapeutic target. *Mol Cancer Ther* 4, 369-379.

Lu, W., van Eerde, A.M., Fan, X., Quintero-Rivera, F., Kulkarni, S., Ferguson, H., Kim, H.G., Fan, Y., Xi, Q., Li, Q.G., *et al.* (2007). Disruption of ROBO2 is associated with urinary tract anomalies and confers risk of vesicoureteral reflux. *Am J Hum Genet* 80, 616-632.

Ludwig, A., Schulte, A., Schnack, C., Hundhausen, C., Reiss, K., Brodway, N., Held-Feindt, J., and Mentlein, R. (2005). Enhanced expression and shedding of the transmembrane chemokine CXCL16 by reactive astrocytes and glioma cells. *J Neurochem* 93, 1293-1303.

Madsen, S.J., Sun, C.H., Tromberg, B.J., Cristini, V., De Magalhaes, N., and Hirschberg, H. (2006). Multicell tumor spheroids in photodynamic therapy. *Lasers Surg Med* 38, 555-564.

Madura, T., Yamashita, T., Kubo, T., Tsuji, L., Hosokawa, K., and Tohyama, M. (2004). Changes in mRNA of Slit-Robo GTPase-activating protein 2 following facial nerve transection. *Brain Res Mol Brain Res* 123, 76-80.

Mareel, M., and Leroy, A. (2003). Clinical, cellular, and molecular aspects of cancer invasion. *Physiol Rev* 83, 337-376.

Maret, D., Gruzglin, E., Sadr, M.S., Siu, V., Shan, W., Koch, A.W., Seidah, N.G., Del Maestro, R.F., and Colman, D.R. (2010). Surface expression of precursor N-cadherin promotes tumor cell invasion. *Neoplasia* 12, 1066-1080.

Marin-Hernandez, A., Gallardo-Perez, J.C., Ralph, S.J., Rodriguez-Enriquez, S., and Moreno-Sanchez, R. (2009). HIF-1alpha modulates energy metabolism in cancer cells by inducing over-expression of specific glycolytic isoforms. *Mini Rev Med Chem* 9, 1084-1101.

Markovic, D.S., Vinnakota, K., Chirasani, S., Synowitz, M., Raguet, H., Stock, K., Sliwa, M., Lehmann, S., Kalin, R., van Rooijen, N., *et al.* (2009). Gliomas induce and exploit microglial MT1-MMP expression for tumor expansion. *Proc Natl Acad Sci U S A* **106**, 12530-12535.

Marlow, R., Strickland, P., Lee, J.S., Wu, X., Pebenito, M., Binnewies, M., Le, E.K., Moran, A., Macias, H., Cardiff, R.D., *et al.* (2008). SLITs suppress tumor growth in vivo by silencing Sdf1/Cxcr4 within breast epithelium. *Cancer Res* **68**, 7819-7827.

Mason, F.M., Heimsath, E.G., Higgs, H.N., and Soderling, S.H. (2011). Bi-modal regulation of a formin by srGAP2. *J Biol Chem* **286**, 6577-6586.

Massague, J. (2008). TGFbeta in Cancer. *Cell* **134**, 215-230.

Mattar, P., Britz, O., Johannes, C., Nieto, M., Ma, L., Rebeyka, A., Klenin, N., Polleux, F., Guillemot, F., and Schuurmans, C. (2004). A screen for downstream effectors of Neurogenin2 in the embryonic neocortex. *Dev Biol* **273**, 373-389.

Mayo, L.D., and Donner, D.B. (2001). A phosphatidylinositol 3-kinase/Akt pathway promotes translocation of Mdm2 from the cytoplasm to the nucleus. *Proc Natl Acad Sci U S A* **98**, 11598-11603.

McCawley, L.J., and Matrisian, L.M. (2001). Matrix metalloproteinases: they're not just for matrix anymore! *Curr Opin Cell Biol* **13**, 534-540.

Medema, R.H., and Bos, J.L. (1993). The role of p21ras in receptor tyrosine kinase signaling. *Crit Rev Oncog* **4**, 615-661.

Medina-Torres, C.E., Mason, S.L., Floyd, R.V., Harris, P.A., and Mobasheri, A. (2011). Hypoxia and a hypoxia mimetic up-regulate matrix metalloproteinase 2 and 9 in equine laminar keratinocytes. *Vet J*.

Mercer, W.E., Shields, M.T., Amin, M., Sauve, G.J., Appella, E., Romano, J.W., and Ullrich, S.J. (1990). Negative growth regulation in a glioblastoma tumor cell line that conditionally expresses human wild-type p53. *Proc Natl Acad Sci U S A* **87**, 6166-6170.

Mertsch, S., Schmitz, N., Jeibmann, A., Geng, J.G., Paulus, W., and Senner, V. (2008). Slit2 involvement in glioma cell migration is mediated by Robo1 receptor. *J Neurooncol* **87**, 1-7.

Miller, C.M., Liu, N., Page-McCaw, A., and Broihier, H.T. (2011). Drosophila MMP2 regulates the matrix molecule faulty attraction (Frac) to promote motor axon targeting in Drosophila. *J Neurosci* **31**, 5335-5347.

Miller, C.M., Page-McCaw, A., and Broihier, H.T. (2008). Matrix metalloproteinases promote motor axon fasciculation in the Drosophila embryo. *Development* **135**, 95-109.

Minn, A.J., Gupta, G.P., Siegel, P.M., Bos, P.D., Shu, W., Giri, D.D., Viale, A., Olshen, A.B., Gerald, W.L., and Massague, J. (2005a). Genes that mediate breast cancer metastasis to lung. *Nature* **436**, 518-524.

Minn, A.J., Kang, Y., Serganova, I., Gupta, G.P., Giri, D.D., Doubrovin, M., Ponomarev, V., Gerald, W.L., Blasberg, R., and Massague, J. (2005b). Distinct organ-specific metastatic potential of individual breast cancer cells and primary tumors. *J Clin Invest* **115**, 44-55.

Miraglia, S., Godfrey, W., Yin, A.H., Atkins, K., Warnke, R., Holden, J.T., Bray, R.A., Waller, E.K., and Buck, D.W. (1997). A novel five-transmembrane hematopoietic stem cell antigen: isolation, characterization, and molecular cloning. *Blood* **90**, 5013-5021.

Mizuno, N.S., and Decker, R.W. (1976). Alteration of DNA by 5-(3-methyl-1-triazeno)imidazole-4-carboxamide (NSC-407347). *Biochem Pharmacol* **25**, 2643-2647.

Momand, J., Zambetti, G.P., Olson, D.C., George, D., and Levine, A.J. (1992). The mdm-2 oncogene product forms a complex with the p53 protein and inhibits p53-mediated transactivation. *Cell* **69**, 1237-1245.

Morlot, C., Thielens, N.M., Ravelli, R.B., Hemrika, W., Romijn, R.A., Gros, P., Cusack, S., and McCarthy, A.A. (2007). Structural insights into the Slit-Robo complex. *Proc Natl Acad Sci U S A* **104**, 14923-14928.

Muir, D. (1994). Metalloproteinase-dependent neurite outgrowth within a synthetic extracellular matrix is induced by nerve growth factor. *Exp Cell Res* **210**, 243-252.

Murphy, P.M. (1994). The molecular biology of leukocyte chemoattractant receptors. *Annu Rev Immunol* **12**, 593-633.

Murray, G.I., Duncan, M.E., O'Neil, P., McKay, J.A., Melvin, W.T., and Fothergill, J.E. (1998). Matrix metalloproteinase-1 is associated with poor prognosis in oesophageal cancer. *J Pathol* **185**, 256-261.

Murray, G.I., Duncan, M.E., O'Neil, P., Melvin, W.T., and Fothergill, J.E. (1996). Matrix metalloproteinase-1 is associated with poor prognosis in colorectal cancer. *Nat Med* 2, 461-462.

Myat, A., Henry, P., McCabe, V., Flintoft, L., Rotin, D., and Tear, G. (2002). *Drosophila* Nedd4, a ubiquitin ligase, is recruited by Commissureless to control cell surface levels of the roundabout receptor. *Neuron* 35, 447-459.

Nakada, M., Nakamura, H., Ikeda, E., Fujimoto, N., Yamashita, J., Sato, H., Seiki, M., and Okada, Y. (1999). Expression and tissue localization of membrane-type 1, 2, and 3 matrix metalloproteinases in human astrocytic tumors. *Am J Pathol* 154, 417-428.

Nakagawa, T., Kubota, T., Kabuto, M., Fujimoto, N., and Okada, Y. (1996). Secretion of matrix metalloproteinase-2 (72 kD gelatinase/type IV collagenase = gelatinase A) by malignant human glioma cell lines: implications for the growth and cellular invasion of the extracellular matrix. *J Neurooncol* 28, 13-24.

Nakagawa, T., Kubota, T., Kabuto, M., Sato, K., Kawano, H., Hayakawa, T., and Okada, Y. (1994). Production of matrix metalloproteinases and tissue inhibitor of metalloproteinases-1 by human brain tumors. *J Neurosurg* 81, 69-77.

Nakano, A., Tani, E., Miyazaki, K., Yamamoto, Y., and Furuyama, J. (1995). Matrix metalloproteinases and tissue inhibitors of metalloproteinases in human gliomas. *J Neurosurg* 83, 298-307.

Nakatsuru, Y., Matsukuma, S., Nemoto, N., Sugano, H., Sekiguchi, M., and Ishikawa, T. (1993). O6-methylguanine-DNA methyltransferase protects against nitrosamine-induced hepatocarcinogenesis. *Proc Natl Acad Sci U S A* 90, 6468-6472.

Nalla, A.K., Asuthkar, S., Bhoopathi, P., Gujrati, M., Dinh, D.H., and Rao, J.S. (2010). Suppression of uPAR retards radiation-induced invasion and migration mediated by integrin beta1/FAK signaling in medulloblastoma. *PLoS One* 5, e13006.

Narayan, G., Goparaju, C., Arias-Pulido, H., Kaufmann, A.M., Schneider, A., Durst, M., Mansukhani, M., Pothuri, B., and Murty, V.V. (2006). Promoter hypermethylation-mediated inactivation of multiple Slit-Robo pathway genes in cervical cancer progression. *Mol Cancer* 5, 16.

Newlands, E.S., Blackledge, G.R., Slack, J.A., Rustin, G.J., Smith, D.B., Stuart, N.S., Quarterman, C.P., Hoffman, R., Stevens, M.F., Brampton, M.H., *et al.* (1992). Phase I trial of temozolomide (CCRG 81045; M&B 39831; NSC 362856). *Br J Cancer* 65, 287-291.

Newlands, E.S., Stevens, M.F., Wedge, S.R., Wheelhouse, R.T., and Brock, C. (1997). Temozolomide: a review of its discovery, chemical properties, pre-clinical development and clinical trials. *Cancer Treat Rev* 23, 35-61.

Nguyen-Ba-Charvet, K.T., Picard-Riera, N., Tessier-Lavigne, M., Baron-Van Evercooren, A., Sotelo, C., and Chedotal, A. (2004). Multiple roles for slits in the control of cell migration in the rostral migratory stream. *J Neurosci* 24, 1497-1506.

Nguyen Ba-Charvet, K.T., Brose, K., Ma, L., Wang, K.H., Marillat, V., Sotelo, C., Tessier-Lavigne, M., and Chedotal, A. (2001). Diversity and specificity of actions of Slit2 proteolytic fragments in axon guidance. *J Neurosci* 21, 4281-4289.

Niall, H.D. (1973). Automated Edman degradation: the protein sequenator. *Methods Enzymol* 27, 942-1010.

Nobusawa, S., Watanabe, T., Kleihues, P., and Ohgaki, H. (2009). IDH1 mutations as molecular signature and predictive factor of secondary glioblastomas. *Clin Cancer Res* 15, 6002-6007.

Nunes, M.C., Roy, N.S., Keyoung, H.M., Goodman, R.R., McKhann, G., 2nd, Jiang, L., Kang, J., Nedergaard, M., and Goldman, S.A. (2003). Identification and isolation of multipotential neural progenitor cells from the subcortical white matter of the adult human brain. *Nat Med* 9, 439-447.

Ohgaki, H., and Kleihues, P. (2009). Genetic alterations and signaling pathways in the evolution of gliomas. *Cancer Sci* 100, 2235-2241.

Okada, H., Yoshida, J., Sokabe, M., Wakabayashi, T., and Hagiwara, M. (1996). Suppression of CD44 expression decreases migration and invasion of human glioma cells. *Int J Cancer* 66, 255-260.

Okamoto, I., Kenyon, L.C., Emlet, D.R., Mori, T., Sasaki, J., Hirotsako, S., Ichikawa, Y., Kishi, H., Godwin, A.K., Yoshioka, M., *et al.* (2003). Expression of constitutively activated EGFRvIII in non-small cell lung cancer. *Cancer Sci* 94, 50-56.

Orgogozo, V., Schweisguth, F., and Bellaiche, Y. (2004). Slit-Robo signalling prevents sensory cells from crossing the midline in *Drosophila*. *Mech Dev* 121, 427-436.

Overall, C.M., and Kleifeld, O. (2006a). Towards third generation matrix metalloproteinase inhibitors for cancer therapy. *Br J Cancer* 94, 941-946.

Overall, C.M., and Kleifeld, O. (2006b). Tumour microenvironment - opinion: validating matrix metalloproteinases as drug targets and anti-targets for cancer therapy. *Nat Rev Cancer* 6, 227-239.

Overall, C.M., and Sodek, J. (1990). Concanavalin A produces a matrix-degradative phenotype in human fibroblasts. Induction and endogenous activation of collagenase, 72-kDa gelatinase, and Pump-1 is accompanied by the suppression of the tissue inhibitor of matrix metalloproteinases. *J Biol Chem* 265, 21141-21151.

Owens, G.C., Orr, E.A., DeMasters, B.K., Muschel, R.J., Berens, M.E., and Kruse, C.A. (1998). Overexpression of a transmembrane isoform of neural cell adhesion molecule alters the invasiveness of rat CNS-1 glioma. *Cancer Res* 58, 2020-2028.

Packer, R.J., Cogen, P., Vezina, G., and Rorke, L.B. (1999). Medulloblastoma: clinical and biologic aspects. *Neuro Oncol* 1, 232-250.

Palmero, I., Pantoja, C., and Serrano, M. (1998). p19ARF links the tumour suppressor p53 to Ras. *Nature* 395, 125-126.

Pantazis, P., Pelicci, P.G., Dalla-Favera, R., and Antoniades, H.N. (1985). Synthesis and secretion of proteins resembling platelet-derived growth factor by human glioblastoma and fibrosarcoma cells in culture. *Proc Natl Acad Sci U S A* 82, 2404-2408.

Park, K.W., Morrison, C.M., Sorensen, L.K., Jones, C.A., Rao, Y., Chien, C.B., Wu, J.Y., Urness, L.D., and Li, D.Y. (2003). Robo4 is a vascular-specific receptor that inhibits endothelial migration. *Dev Biol* 261, 251-267.

Parlato, C., Barbarisi, M., Moraci, M., and Moraci, A. (2006). Surgery, radiotherapy and temozolomide in treating high-grade gliomas. *Front Biosci* 11, 1280-1283.

Parsons, D.W., Jones, S., Zhang, X., Lin, J.C., Leary, R.J., Angenendt, P., Mankoo, P., Carter, H., Siu, I.M., Gallia, G.L., *et al.* (2008). An integrated genomic analysis of human glioblastoma multiforme. *Science* 321, 1807-1812.

Patrawala, L., Calhoun, T., Schneider-Broussard, R., Zhou, J., Claypool, K., and Tang, D.G. (2005). Side population is enriched in tumorigenic, stem-like cancer cells, whereas ABCG2+ and ABCG2- cancer cells are similarly tumorigenic. *Cancer Res* 65, 6207-6219.

Paulus, W., Baur, I., Dours-Zimmermann, M.T., and Zimmermann, D.R. (1996). Differential expression of versican isoforms in brain tumors. *J Neuropathol Exp Neurol* 55, 528-533.

Perotti, A., Sessa, C., Mancuso, A., Noverasco, C., Cresta, S., Locatelli, A., Carcangiu, M.L., Passera, K., Braghetta, A., Scaramuzza, D., *et al.* (2009). Clinical and pharmacological phase I evaluation of Exherin (ADH-1), a selective anti-N-cadherin peptide in patients with N-cadherin-expressing solid tumours. *Ann Oncol* 20, 741-745.

Pietsch, T., Waha, A., Koch, A., Kraus, J., Albrecht, S., Tonn, J., Sorensen, N., Berthold, F., Henk, B., Schmandt, N., *et al.* (1997). Medulloblastomas of the desmoplastic variant carry mutations of the human homologue of *Drosophila* patched. *Cancer Res* 57, 2085-2088.

Piper, M., Georgas, K., Yamada, T., and Little, M. (2000). Expression of the vertebrate Slit gene family and their putative receptors, the Robo genes, in the developing murine kidney. *Mech Dev* 94, 213-217.

Pishvaian, M.J., Feltes, C.M., Thompson, P., Bussemakers, M.J., Schalken, J.A., and Byers, S.W. (1999). Cadherin-11 is expressed in invasive breast cancer cell lines. *Cancer Res* 59, 947-952.

Plate, K.H., and Risau, W. (1995). Angiogenesis in malignant gliomas. *Glia* 15, 339-347.

Plouet, J., Schilling, J., and Gospodarowicz, D. (1989). Isolation and characterization of a newly identified endothelial cell mitogen produced by A1T-20 cells. *EMBO J* 8, 3801-3806.

Podar, K., Raje, N., and Anderson, K.C. (2007). Inhibition of the TGF-beta signaling pathway in tumor cells. *Recent Results Cancer Res* 172, 77-97.

Pohl, U., Cairncross, J.G., and Louis, D.N. (1999). Homozygous deletions of the CDKN2C/p18INK4C gene on the short arm of chromosome 1 in anaplastic oligodendrogliomas. *Brain Pathol* 9, 639-643.

Pomeroy, S.L., Sutton, M.E., Goumnerova, L.C., and Segal, R.A. (1997). Neurotrophins in cerebellar granule cell development and medulloblastoma. *J Neurooncol* 35, 347-352.

Pomeroy, S.L., Tamayo, P., Gaasenbeek, M., Sturla, L.M., Angelo, M., McLaughlin, M.E., Kim, J.Y., Goumnerova, L.C., Black, P.M., Lau, C., *et al.* (2002). Prediction of central nervous system embryonal tumour outcome based on gene expression. *Nature* **415**, 436-442.

Purow, B., and Schiff, D. (2009). Advances in the genetics of glioblastoma: are we reaching critical mass? *Nat Rev Neurol* **5**, 419-426.

Radisky, D.C., Levy, D.D., Littlepage, L.E., Liu, H., Nelson, C.M., Fata, J.E., Leake, D., Godden, E.L., Albertson, D.G., Nieto, M.A., *et al.* (2005). Rac1b and reactive oxygen species mediate MMP-3-induced EMT and genomic instability. *Nature* **436**, 123-127.

Raffel, C. (2004). Medulloblastoma: molecular genetics and animal models. *Neoplasia* **6**, 310-322.

Raizer, J.J., Abrey, L.E., Lassman, A.B., Chang, S.M., Lamborn, K.R., Kuhn, J.G., Yung, W.K., Gilbert, M.R., Aldape, K.A., Wen, P.Y., *et al.* (2010). A phase II trial of erlotinib in patients with recurrent malignant gliomas and nonprogressive glioblastoma multiforme postradiation therapy. *Neuro Oncol* **12**, 95-103.

Rajagopalan, S., Nicolas, E., Vivancos, V., Berger, J., and Dickson, B.J. (2000). Crossing the midline: roles and regulation of Robo receptors. *Neuron* **28**, 767-777.

Ranuncolo, S.M., Ladedda, V., Gorostidy, S., Morandi, A., Varela, M., Lastiri, J., Loria, D., Del Aguila, R., Joffe, E.B., Pallotta, G., *et al.* (2002a). Expression of CD44s and CD44 splice variants in human melanoma. *Oncol Rep* **9**, 51-56.

Ranuncolo, S.M., Ladedda, V., Specterman, S., Varela, M., Lastiri, J., Morandi, A., Matos, E., Bal de Kier Joffe, E., Puricelli, L., and Pallotta, M.G. (2002b). CD44 expression in human gliomas. *J Surg Oncol* **79**, 30-35; discussion 35-36.

Rao, Y., Wong, K., Ward, M., Jurgensen, C., and Wu, J.Y. (2002). Neuronal migration and molecular conservation with leukocyte chemotaxis. *Genes Dev* **16**, 2973-2984.

Rathinam, R., Berrier, A., and Alahari, S.K. (2012). Role of Rho GTPases and their regulators in cancer progression. *Front Biosci* **17**, 2561-2571.

Read, T.A., Fogarty, M.P., Markant, S.L., McLendon, R.E., Wei, Z., Ellison, D.W., Febbo, P.G., and Wechsler-Reya, R.J. (2009). Identification of CD15 as a marker for tumor-propagating cells in a mouse model of medulloblastoma. *Cancer Cell* **15**, 135-147.

Reardon, D.A., Fink, K.L., Mikkelsen, T., Cloughesy, T.F., O'Neill, A., Plotkin, S., Glantz, M., Ravin, P., Raizer, J.J., Rich, K.M., *et al.* (2008). Randomized phase II study of cilengitide, an integrin-targeting arginine-glycine-aspartic acid peptide, in recurrent glioblastoma multiforme. *J Clin Oncol* **26**, 5610-5617.

Reifenberger, J., Ring, G.U., Gies, U., Cobbers, L., Oberstrass, J., An, H.X., Niederacher, D., Wechsler, W., and Reifenberger, G. (1996). Analysis of p53 mutation and epidermal growth factor receptor amplification in recurrent gliomas with malignant progression. *J Neuropathol Exp Neurol* **55**, 822-831.

Reigstad, L.J., Varhaug, J.E., and Lillehaug, J.R. (2005). Structural and functional specificities of PDGF-C and PDGF-D, the novel members of the platelet-derived growth factors family. *FEBS J* **272**, 5723-5741.

Rhee, J., Buchan, T., Zukerberg, L., Lilien, J., and Balsamo, J. (2007). Cables links Robo-bound Abl kinase to N-cadherin-bound beta-catenin to mediate Slit-induced modulation of adhesion and transcription. *Nat Cell Biol* **9**, 883-892.

Rhee, J., Mahfooz, N.S., Arregui, C., Lilien, J., Balsamo, J., and VanBerkum, M.F. (2002). Activation of the repulsive receptor Roundabout inhibits N-cadherin-mediated cell adhesion. *Nat Cell Biol* **4**, 798-805.

Ricci-Vitiani, L., Lombardi, D.G., Pilozzi, E., Biffoni, M., Todaro, M., Peschle, C., and De Maria, R. (2007). Identification and expansion of human colon-cancer-initiating cells. *Nature* **445**, 111-115.

Riechelmann, H., Sauter, A., Golze, W., Hanft, G., Schroen, C., Hoermann, K., Erhardt, T., and Gronau, S. (2008). Phase I trial with the CD44v6-targeting immunoconjugate bivatuzumab mertansine in head and neck squamous cell carcinoma. *Oral Oncol* **44**, 823-829.

Riemenschneider, M.J., Buschges, R., Wolter, M., Reifenberger, J., Bostrom, J., Kraus, J.A., Schlegel, U., and Reifenberger, G. (1999). Amplification and overexpression of the MDM4 (MDMX) gene from 1q32 in a subset of malignant gliomas without TP53 mutation or MDM2 amplification. *Cancer Res* **59**, 6091-6096.

Robinet, A., Fahem, A., Cauchard, J.H., Huet, E., Vincent, L., Lorimier, S., Antonicelli, F., Soria, C., Crepin, M., Hornebeck, W., *et al.* (2005). Elastin-derived peptides enhance angiogenesis by promoting endothelial cell migration and tubulogenesis through upregulation of MT1-MMP. *J Cell Sci* 118, 343-356.

Rohatgi, R., Milenkovic, L., and Scott, M.P. (2007). Patched1 regulates hedgehog signaling at the primary cilium. *Science* 317, 372-376.

Ronca, F., Andersen, J.S., Paech, V., and Margolis, R.U. (2001). Characterization of Slit protein interactions with glypican-1. *J Biol Chem* 276, 29141-29147.

Rooprai, H.K., Vanmeter, T., Panou, C., Schnull, S., Trillo-Pazos, G., Davies, D., and Pilkington, G.J. (1999). The role of integrin receptors in aspects of glioma invasion in vitro. *Int J Dev Neurosci* 17, 613-623.

Rothberg, J.M., Hartley, D.A., Walther, Z., and Artavanis-Tsakonas, S. (1988). slit: an EGF-homologous locus of *D. melanogaster* involved in the development of the embryonic central nervous system. *Cell* 55, 1047-1059.

Royds, J.A., Hibma, M., Dix, B.R., Hananeia, L., Russell, I.A., Wiles, A., Wynford-Thomas, D., and Braithwaite, A.W. (2006). p53 promotes adenoviral replication and increases late viral gene expression. *Oncogene* 25, 1509-1520.

Rudin, C.M., Hann, C.L., Laterra, J., Yauch, R.L., Callahan, C.A., Fu, L., Holcomb, T., Stinson, J., Gould, S.E., Coleman, B., *et al.* (2009). Treatment of medulloblastoma with hedgehog pathway inhibitor GDC-0449. *N Engl J Med* 361, 1173-1178.

Sabatier, C., Plump, A.S., Le, M., Brose, K., Tamada, A., Murakami, F., Lee, E.Y., and Tessier-Lavigne, M. (2004). The divergent Robo family protein rig-1/Robo3 is a negative regulator of slit responsiveness required for midline crossing by commissural axons. *Cell* 117, 157-169.

Salsano, E., Pollo, B., Eoli, M., Giordana, M.T., and Finocchiaro, G. (2004). Expression of MATH1, a marker of cerebellar granule cell progenitors, identifies different medulloblastoma subtypes. *Neurosci Lett* 370, 180-185.

Sanai, N., Tramontin, A.D., Quinones-Hinojosa, A., Barbaro, N.M., Gupta, N., Kunwar, S., Lawton, M.T., McDermott, M.W., Parsa, A.T., Manuel-Garcia Verdugo, J., *et al.* (2004). Unique astrocyte ribbon in adult human brain contains neural stem cells but lacks chain migration. *Nature* 427, 740-744.

Sanson, M., Marie, Y., Paris, S., Idhah, A., Laffaire, J., Ducray, F., El Hallani, S., Boisselier, B., Mokhtari, K., Hoang-Xuan, K., *et al.* (2009). Isocitrate dehydrogenase 1 codon 132 mutation is an important prognostic biomarker in gliomas. *J Clin Oncol* 27, 4150-4154.

Sato, H., Takino, T., and Miyamori, H. (2005). Roles of membrane-type matrix metalloproteinase-1 in tumor invasion and metastasis. *Cancer Sci* 96, 212-217.

Scharenberg, C.W., Harkey, M.A., and Torok-Storb, B. (2002). The ABCG2 transporter is an efficient Hoechst 33342 efflux pump and is preferentially expressed by immature human hematopoietic progenitors. *Blood* 99, 507-512.

Scheurlen, W.G., Seranski, P., Mincheva, A., Kuhl, J., Sorensen, N., Krauss, J., Lichter, P., Poustka, A., and Wilgenbus, K.K. (1997). High-resolution deletion mapping of chromosome arm 17p in childhood primitive neuroectodermal tumors reveals a common chromosomal disruption within the Smith-Magenis region, an unstable region in chromosome band 17p11.2. *Genes Chromosomes Cancer* 18, 50-58.

Schipper, J.H., Frixen, U.H., Behrens, J., Unger, A., Jahnke, K., and Birchmeier, W. (1991). E-cadherin expression in squamous cell carcinomas of head and neck: inverse correlation with tumor dedifferentiation and lymph node metastasis. *Cancer Res* 51, 6328-6337.

Sebti, S.M., and Hamilton, A.D. (2000). Farnesyltransferase and geranylgeranyltransferase I inhibitors and cancer therapy: lessons from mechanism and bench-to-bedside translational studies. *Oncogene* 19, 6584-6593.

Seeger, M., Tear, G., Ferres-Marco, D., and Goodman, C.S. (1993). Mutations affecting growth cone guidance in *Drosophila*: genes necessary for guidance toward or away from the midline. *Neuron* 10, 409-426.

Seidah, N.G. (2011). The proprotein convertases, 20 years later. *Methods Mol Biol* 768, 23-57.

Seki, M., Watanabe, A., Enomoto, S., Kawamura, T., Ito, H., Kodama, T., Hamakubo, T., and Aburatani, H. (2010). Human ROBO1 is cleaved by metalloproteinases and gamma-secretase and migrates to the nucleus in cancer cells. *FEBS Lett* 584, 2909-2915.

Seomun, Y., Kim, J.T., and Joo, C.K. (2008). MMP-14 mediated MMP-9 expression is involved in TGF-beta1-induced keratinocyte migration. *J Cell Biochem* 104, 934-941.

Serrano, M., Lin, A.W., McCurrach, M.E., Beach, D., and Lowe, S.W. (1997). Oncogenic ras provokes premature cell senescence associated with accumulation of p53 and p16INK4a. *Cell* 88, 593-602.

Seth, P., Lin, Y., Hanai, J., Shivalingappa, V., Duyao, M.P., and Sukhatme, V.P. (2005). Magic roundabout, a tumor endothelial marker: expression and signaling. *Biochem Biophys Res Commun* 332, 533-541.

Shapiro, L., Love, J., and Colman, D.R. (2007). Adhesion molecules in the nervous system: structural insights into function and diversity. *Annu Rev Neurosci* 30, 451-474.

Sharma, G., Mirza, S., Prasad, C.P., Srivastava, A., Gupta, S.D., and Ralhan, R. (2007). Promoter hypermethylation of p16INK4A, p14ARF, CyclinD2 and Slit2 in serum and tumor DNA from breast cancer patients. *Life Sci* 80, 1873-1881.

Shiau, C.E., Lwigale, P.Y., Das, R.M., Wilson, S.A., and Bronner-Fraser, M. (2008). Robo2-Slit1 dependent cell-cell interactions mediate assembly of the trigeminal ganglion. *Nat Neurosci* 11, 269-276.

Shibata, F., Goto-Koshino, Y., Morikawa, Y., Komori, T., Ito, M., Fukuchi, Y., Houchins, J.P., Tsang, M., Li, D.Y., Kitamura, T., *et al.* (2009). Roundabout 4 is expressed on hematopoietic stem cells and potentially involved in the niche-mediated regulation of the side population phenotype. *Stem Cells* 27, 183-190.

Shu, T., Sundaresan, V., McCarthy, M.M., and Richards, L.J. (2003). Slit2 guides both precrossing and postcrossing callosal axons at the midline in vivo. *J Neurosci* 23, 8176-8184.

Singer, M.S., and Gottschling, D.E. (1994). TLC1: template RNA component of *Saccharomyces cerevisiae* telomerase. *Science* 266, 404-409.

Singh, R.K., Indra, D., Mitra, S., Mondal, R.K., Basu, P.S., Roy, A., Roychowdhury, S., and Panda, C.K. (2007). Deletions in chromosome 4 differentially associated with the development of cervical cancer: evidence of slit2 as a candidate tumor suppressor gene. *Hum Genet* 122, 71-81.

Singh, S.K., Hawkins, C., Clarke, I.D., Squire, J.A., Bayani, J., Hide, T., Henkelman, R.M., Cusimano, M.D., and Dirks, P.B. (2004). Identification of human brain tumour initiating cells. *Nature* 432, 396-401.

Snuderl, M., Chi, S.N., De Santis, S.M., Stemmer-Rachamimov, A.O., Betensky, R.A., De Girolami, U., and Kieran, M.W. (2008). Prognostic value of tumor microinvasion and metalloproteinases expression in intracranial pediatric ependymomas. *J Neuropathol Exp Neurol* 67, 911-920.

Sorensen, S.A., Mulvihill, J.J., and Nielsen, A. (1986). Long-term follow-up of von Recklinghausen neurofibromatosis. Survival and malignant neoplasms. *N Engl J Med* 314, 1010-1015.

Sounni, N.E., Roghi, C., Chabottaux, V., Janssen, M., Munaut, C., Maquoi, E., Galvez, B.G., Gilles, C., Frankenre, F., Murphy, G., *et al.* (2004). Up-regulation of vascular endothelial growth factor-A by active membrane-type 1 matrix metalloproteinase through activation of Src-tyrosine kinases. *J Biol Chem* 279, 13564-13574.

Sroka, I.C., McDaniel, K., Nagle, R.B., and Bowden, G.T. (2008). Differential localization of MT1-MMP in human prostate cancer tissue: role of IGF-1R in MT1-MMP expression. *Prostate* 68, 463-476.

Sroka, I.C., Nagle, R.B., and Bowden, G.T. (2007). Membrane-type 1 matrix metalloproteinase is regulated by sp1 through the differential activation of AKT, JNK, and ERK pathways in human prostate tumor cells. *Neoplasia* 9, 406-417.

Steck, P.A., Pershouse, M.A., Jasser, S.A., Yung, W.K., Lin, H., Ligon, A.H., Langford, L.A., Baumgard, M.L., Hattier, T., Davis, T., *et al.* (1997). Identification of a candidate tumour suppressor gene, MMAC1, at chromosome 10q23.3 that is mutated in multiple advanced cancers. *Nat Genet* 15, 356-362.

Steigemann, P., Molitor, A., Fellert, S., Jackle, H., and Vorbruggen, G. (2004). Heparan sulfate proteoglycan syndecan promotes axonal and myotube guidance by slit/robo signaling. *Curr Biol* 14, 225-230.

Stein, E., and Tessier-Lavigne, M. (2001). Hierarchical organization of guidance receptors: silencing of netrin attraction by slit through a Robo/DCC receptor complex. *Science* 291, 1928-1938.

Stella, M.C., Trusolino, L., and Comoglio, P.M. (2009). The Slit/Robo system suppresses hepatocyte growth factor-dependent invasion and morphogenesis. *Mol Biol Cell* 20, 642-657.

Stetler-Stevenson, W.G. (1994). Progelatinase A activation during tumor cell invasion. *Invasion Metastasis* 14, 259-268.

Stevens, M.F., Hickman, J.A., Langdon, S.P., Chubb, D., Vickers, L., Stone, R., Baig, G., Goddard, C., Gibson, N.W., Slack, J.A., *et al.* (1987). Antitumor activity and pharmacokinetics in mice of 8-carbamoyl-3-methyl-imidazo[5,1-d]-1,2,3,5-tetrazin-4(3H)-one (CCRG 81045; M & B 39831), a novel drug with potential as an alternative to dacarbazine. *Cancer Res* 47, 5846-5852.

Stupp, R., Dietrich, P.Y., Ostermann Kraljevic, S., Pica, A., Maillard, I., Maeder, P., Meuli, R., Janzer, R., Pizzolato, G., Miralbell, R., *et al.* (2002). Promising survival for patients with newly diagnosed glioblastoma multiforme treated with concomitant radiation plus temozolomide followed by adjuvant temozolomide. *J Clin Oncol* 20, 1375-1382.

Stupp, R., Hegi, M.E., Neyns, B., Goldbrunner, R., Schlegel, U., Clement, P.M., Grabenbauer, G.G., Ochsenbein, A.F., Simon, M., Dietrich, P.Y., *et al.* (2010). Phase I/IIa study of cilengitide and temozolomide with concomitant radiotherapy followed by cilengitide and temozolomide maintenance therapy in patients with newly diagnosed glioblastoma. *J Clin Oncol* 28, 2712-2718.

Stupp, R., Mason, W.P., van den Bent, M.J., Weller, M., Fisher, B., Taphoorn, M.J., Belanger, K., Brandes, A.A., Marosi, C., Bogdahn, U., *et al.* (2005). Radiotherapy plus concomitant and adjuvant temozolomide for glioblastoma. *N Engl J Med* 352, 987-996.

Stutz, M.A., Shattuck, D.L., Laederich, M.B., Carraway, K.L., 3rd, and Sweeney, C. (2008). LRIG1 negatively regulates the oncogenic EGF receptor mutant EGFRvIII. *Oncogene* 27, 5741-5752.

Suchting, S., Heal, P., Tahtis, K., Stewart, L.M., and Bicknell, R. (2005). Soluble Robo4 receptor inhibits in vivo angiogenesis and endothelial cell migration. *FASEB J* 19, 121-123.

Sugawa, N., Ekstrand, A.J., James, C.D., and Collins, V.P. (1990). Identical splicing of aberrant epidermal growth factor receptor transcripts from amplified rearranged genes in human glioblastomas. *Proc Natl Acad Sci U S A* 87, 8602-8606.

Sun, Q., Bahri, S., Schmid, A., Chia, W., and Zinn, K. (2000). Receptor tyrosine phosphatases regulate axon guidance across the midline of the *Drosophila* embryo. *Development* 127, 801-812.

Taguchi, A., Politi, K., Pitteri, S.J., Lockwood, W.W., Faca, V.M., Kelly-Spratt, K., Wong, C.H., Zhang, Q., Chin, A., Park, K.S., *et al.* (2011). Lung cancer signatures in plasma based on proteome profiling of mouse tumor models. *Cancer Cell* 20, 289-299.

Takeichi, M. (1995). Morphogenetic roles of classic cadherins. *Curr Opin Cell Biol* 7, 619-627.

Tallquist, M., and Kazlauskas, A. (2004). PDGF signaling in cells and mice. *Cytokine Growth Factor Rev* 15, 205-213.

Tamaki, M., McDonald, W., Amberger, V.R., Moore, E., and Del Maestro, R.F. (1997). Implantation of C6 astrocytoma spheroid into collagen type I gels: invasive, proliferative, and enzymatic characterizations. *J Neurosurg* 87, 602-609.

Tamaki, M., McDonald, W., and Del Maestro, R.F. (1996). Release of collagen type IV degrading activity from C6 astrocytoma cells and cell density. *J Neurosurg* 84, 1013-1019.

Tamura, S., Shiozaki, H., Miyata, M., Kadowaki, T., Inoue, M., Matsui, S., Iwazawa, T., Takayama, T., Takeichi, M., and Monden, M. (1996). Decreased E-cadherin expression is associated with haematogenous recurrence and poor prognosis in patients with squamous cell carcinoma of the oesophagus. *Br J Surg* 83, 1608-1614.

Taylor, M.D., Poppleton, H., Fuller, C., Su, X., Liu, Y., Jensen, P., Magdaleno, S., Dalton, J., Calabrese, C., Board, J., *et al.* (2005). Radial glia cells are candidate stem cells of ependymoma. *Cancer Cell* 8, 323-335.

TCGARN (2008). Comprehensive genomic characterization defines human glioblastoma genes and core pathways. *Nature* 455, 1061-1068.

Thomas, D.A., and Massague, J. (2005). TGF-beta directly targets cytotoxic T cell functions during tumor evasion of immune surveillance. *Cancer Cell* 8, 369-380.

Thompson, M.C., Fuller, C., Hogg, T.L., Dalton, J., Finkelstein, D., Lau, C.C., Chintagumpala, M., Adesina, A., Ashley, D.M., Kellie, S.J., *et al.* (2006). Genomics identifies medulloblastoma subgroups that are enriched for specific genetic alterations. *J Clin Oncol* 24, 1924-1931.

Tole, S., Mukovozov, I.M., Huang, Y.W., Magalhaes, M.A., Yan, M., Crow, M.R., Liu, G.Y., Sun, C.X., Durocher, Y., Glogauer, M., *et al.* (2009). The axonal repellent, Slit2, inhibits directional migration of circulating neutrophils. *J Leukoc Biol* 86, 1403-1415.

Tomita, K., van Bokhoven, A., van Leenders, G.J., Ruijter, E.T., Jansen, C.F., Bussemakers, M.J., and Schalken, J.A. (2000). Cadherin switching in human prostate cancer progression. *Cancer Res* 60, 3650-3654.

Tremont-Lukats, I.W., and Gilbert, M.R. (2003). Advances in molecular therapies in patients with brain tumors. *Cancer Control* 10, 125-137.

Uhm, J.H., Dooley, N.P., Villemure, J.G., and Yong, V.W. (1997). Mechanisms of glioma invasion: role of matrix-metalloproteinases. *Can J Neurol Sci* 24, 3-15.

Uhrbom, L., Hesselager, G., Nister, M., and Westermarck, B. (1998). Induction of brain tumors in mice using a recombinant platelet-derived growth factor B-chain retrovirus. *Cancer Res* 58, 5275-5279.

Vallieres, L. (2009). Trabedersen, a TGFbeta2-specific antisense oligonucleotide for the treatment of malignant gliomas and other tumors overexpressing TGFbeta2. *IDrugs* 12, 445-453.

van den Bent, M.J., Dubbink, H.J., Sanson, M., van der Lee-Haarloo, C.R., Hegi, M., Jeuken, J.W., Ibdaih, A., Brandes, A.A., Taphoorn, M.J., Frenay, M., *et al.* (2009). MGMT promoter methylation is prognostic but not predictive for outcome to adjuvant PCV chemotherapy in anaplastic oligodendroglial tumors: a report from EORTC Brain Tumor Group Study 26951. *J Clin Oncol* 27, 5881-5886.

Van Meir, E.G., Kikuchi, T., Tada, M., Li, H., Diserens, A.C., Wojcik, B.E., Huang, H.J., Friedmann, T., de Tribolet, N., and Cavenee, W.K. (1994). Analysis of the p53 gene and its expression in human glioblastoma cells. *Cancer Res* 54, 649-652.

Van Meir, E.G., Roemer, K., Diserens, A.C., Kikuchi, T., Rempel, S.A., Haas, M., Huang, H.J., Friedmann, T., de Tribolet, N., and Cavenee, W.K. (1995). Single cell monitoring of growth arrest and morphological changes induced by transfer of wild-type p53 alleles to glioblastoma cells. *Proc Natl Acad Sci U S A* 92, 1008-1012.

Vermeulen, K., Berneman, Z.N., and Van Bockstaele, D.R. (2003a). Cell cycle and apoptosis. *Cell Prolif* 36, 165-175.

Vermeulen, K., Van Bockstaele, D.R., and Berneman, Z.N. (2003b). The cell cycle: a review of regulation, deregulation and therapeutic targets in cancer. *Cell Prolif* 36, 131-149.

Vredenburgh, J.J., Desjardins, A., Herndon, J.E., 2nd, Marcello, J., Reardon, D.A., Quinn, J.A., Rich, J.N., Sathornsumetee, S., Gururangan, S., Sampson, J., *et al.* (2007). Bevacizumab plus irinotecan in recurrent glioblastoma multiforme. *J Clin Oncol* 25, 4722-4729.

Vu, T.H., Shipley, J.M., Bergers, G., Berger, J.E., Helms, J.A., Hanahan, D., Shapiro, S.D., Senior, R.M., and Werb, Z. (1998). MMP-9/gelatinase B is a key regulator of growth plate angiogenesis and apoptosis of hypertrophic chondrocytes. *Cell* 93, 411-422.

Walker, M.D., Green, S.B., Byar, D.P., Alexander, E., Jr., Batzdorf, U., Brooks, W.H., Hunt, W.E., MacCarty, C.S., Mahaley, M.S., Jr., Mealey, J., Jr., *et al.* (1980). Randomized comparisons of radiotherapy and nitrosoureas for the treatment of malignant glioma after surgery. *N Engl J Med* 303, 1323-1329.

Waltereit, R., Kautt, S., and Bartsch, D. (2008). Expression of MEGAP mRNA during embryonic development. *Gene Expr Patterns* 8, 307-310.

Wang, B., Xiao, Y., Ding, B.B., Zhang, N., Yuan, X., Gui, L., Qian, K.X., Duan, S., Chen, Z., Rao, Y., *et al.* (2003). Induction of tumor angiogenesis by Slit-Robo signaling and inhibition of cancer growth by blocking Robo activity. *Cancer Cell* 4, 19-29.

Wang, K.H., Brose, K., Arnott, D., Kidd, T., Goodman, C.S., Henzel, W., and Tessier-Lavigne, M. (1999). Biochemical purification of a mammalian slit protein as a positive regulator of sensory axon elongation and branching. *Cell* 96, 771-784.

Wang, Y., Yang, J., Zheng, H., Tomasek, G.J., Zhang, P., McKeever, P.E., Lee, E.Y., and Zhu, Y. (2009). Expression of mutant p53 proteins implicates a lineage relationship between neural stem cells and malignant astrocytic glioma in a murine model. *Cancer Cell* 15, 514-526.

Ward, R.J., Lee, L., Graham, K., Satkunendran, T., Yoshikawa, K., Ling, E., Harper, L., Austin, R., Nieuwenhuis, E., Clarke, I.D., *et al.* (2009). Multipotent CD15+ cancer stem cells in patched-1-deficient mouse medulloblastoma. *Cancer Res* 69, 4682-4690.

Watanabe, K., Sato, K., Biernat, W., Tachibana, O., von Ammon, K., Ogata, N., Yonekawa, Y., Kleihues, P., and Ohgaki, H. (1997). Incidence and timing of p53 mutations during astrocytoma progression in patients with multiple biopsies. *Clin Cancer Res* 3, 523-530.

Watanabe, K., Tachibana, O., Sata, K., Yonekawa, Y., Kleihues, P., and Ohgaki, H. (1996). Overexpression of the EGF receptor and p53 mutations are mutually exclusive in the evolution of primary and secondary glioblastomas. *Brain Pathol* 6, 217-223; discussion 223-214.

Wechsler-Reya, R., and Scott, M.P. (2001). The developmental biology of brain tumors. *Annu Rev Neurosci* 24, 385-428.

Wechsler-Reya, R.J., and Scott, M.P. (1999). Control of neuronal precursor proliferation in the cerebellum by Sonic Hedgehog. *Neuron* 22, 103-114.

Weinberg, R.A. (1995a). The molecular basis of oncogenes and tumor suppressor genes. *Ann N Y Acad Sci* 758, 331-338.

Weinberg, R.A. (1995b). The retinoblastoma protein and cell cycle control. *Cell* 81, 323-330.

Weller, M., Stupp, R., Reifenberger, G., Brandes, A.A., van den Bent, M.J., Wick, W., and Hegi, M.E. (2010). MGMT promoter methylation in malignant gliomas: ready for personalized medicine? *Nat Rev Neurol* 6, 39-51.

Werbowski-Ogilvie, T.E., Seyed Sadr, M., Jhabdo, N., Angers-Loustau, A., Agar, N.Y., Wu, J., Bjerkvig, R., Antel, J.P., Faury, D., Rao, Y., *et al.* (2006). Inhibition of medulloblastoma cell invasion by Slit. *Oncogene* 25, 5103-5112.

Wetmore, C., Eberhart, D.E., and Curran, T. (2001). Loss of p53 but not ARF accelerates medulloblastoma in mice heterozygous for patched. *Cancer Res* 61, 513-516.

Wick, W., Furnari, F.B., Naumann, U., Cavenee, W.K., and Weller, M. (1999). PTEN gene transfer in human malignant glioma: sensitization to irradiation and CD95L-induced apoptosis. *Oncogene* 18, 3936-3943.

Wick, W., Platten, M., and Weller, M. (2009). New (alternative) temozolomide regimens for the treatment of glioma. *Neuro Oncol* 11, 69-79.

Wiedemeyer, W.R., Dunn, I.F., Quayle, S.N., Zhang, J., Chheda, M.G., Dunn, G.P., Zhuang, L., Rosenbluh, J., Chen, S., Xiao, Y., *et al.* (2010). Pattern of retinoblastoma pathway inactivation dictates response to CDK4/6 inhibition in GBM. *Proc Natl Acad Sci U S A* 107, 11501-11506.

Wong, K., Park, H.T., Wu, J.Y., and Rao, Y. (2002). Slit proteins: molecular guidance cues for cells ranging from neurons to leukocytes. *Curr Opin Genet Dev* 12, 583-591.

Wong, K., Ren, X.R., Huang, Y.Z., Xie, Y., Liu, G., Saito, H., Tang, H., Wen, L., Brady-Kalnay, S.M., Mei, L., *et al.* (2001). Signal transduction in neuronal migration: roles of GTPase activating proteins and the small GTPase Cdc42 in the Slit-Robo pathway. *Cell* 107, 209-221.

Woo, M., Park, K., Nam, J., and Kim, J.C. (2007). Clinical implications of matrix metalloproteinase-1, -3, -7, -9, -12, and plasminogen activator inhibitor-1 gene polymorphisms in colorectal cancer. *J Gastroenterol Hepatol* 22, 1064-1070.

Wu, J.Y., Feng, L., Park, H.T., Havlioglu, N., Wen, L., Tang, H., Bacon, K.B., Jiang, Z., Zhang, X., and Rao, Y. (2001). The neuronal repellent Slit inhibits leukocyte chemotaxis induced by chemotactic factors. *Nature* 410, 948-952.

Wu, W., Wong, K., Chen, J., Jiang, Z., Dupuis, S., Wu, J.Y., and Rao, Y. (1999). Directional guidance of neuronal migration in the olfactory system by the protein Slit. *Nature* 400, 331-336.

Xu, G.F., O'Connell, P., Viskochil, D., Cawthon, R., Robertson, M., Culver, M., Dunn, D., Stevens, J., Gesteland, R., White, R., *et al.* (1990). The neurofibromatosis type 1 gene encodes a protein related to GAP. *Cell* 62, 599-608.

Yang, L., and Bashaw, G.J. (2006). Son of sevenless directly links the Robo receptor to rac activation to control axon repulsion at the midline. *Neuron* 52, 595-607.

Yang, Y., Marcello, M., Endris, V., Saffrich, R., Fischer, R., Trendelenburg, M.F., Sprengel, R., and Rappold, G. (2006). MEGAP impedes cell migration via regulating actin and microtubule dynamics and focal complex formation. *Exp Cell Res* 312, 2379-2393.

Yang, Z.J., Ellis, T., Markant, S.L., Read, T.A., Kessler, J.D., Bourboulas, M., Schuller, U., Machold, R., Fishell, G., Rowitch, D.H., *et al.* (2008). Medulloblastoma can be initiated by deletion of Patched in lineage-restricted progenitors or stem cells. *Cancer Cell* 14, 135-145.

Yao, Q., Jin, W.L., Wang, Y., and Ju, G. (2008). Regulated shuttling of Slit-Robo-GTPase activating proteins between nucleus and cytoplasm during brain development. *Cell Mol Neurobiol* 28, 205-221.

Yiin, J.J., Hu, B., Jarzynka, M.J., Feng, H., Liu, K.W., Wu, J.Y., Ma, H.I., and Cheng, S.Y. (2009a). Slit2 inhibits glioma cell invasion in the brain by suppression of Cdc42 activity. *Neuro Oncol* 11, 779-789.

Yiin, J.J., Hu, B., Jarzynka, M.J., Feng, H., Liu, K.W., Wu, J.Y., Ma, H.I., and Cheng, S.Y. (2009b). Slit2 inhibits glioma cell invasion in the brain by suppression of Cdc42 activity. *Neuro Oncol*.

Yin, A.H., Miraglia, S., Zanjani, E.D., Almeida-Porada, G., Ogawa, M., Leary, A.G., Olweus, J., Kearney, J., and Buck, D.W. (1997). AC133, a novel marker for human hematopoietic stem and progenitor cells. *Blood* 90, 5002-5012.

Ying, H., Zheng, H., Scott, K., Wiedemeyer, R., Yan, H., Lim, C., Huang, J., Dhakal, S., Ivanova, E., Xiao, Y., *et al.* (2010). Mig-6 controls EGFR trafficking and suppresses gliomagenesis. *Proc Natl Acad Sci U S A* 107, 6912-6917.

Yokota, N., Aruga, J., Takai, S., Yamada, K., Hamazaki, M., Iwase, T., Sugimura, H., and Mikoshiba, K. (1996). Predominant expression of human zic in cerebellar granule cell lineage and medulloblastoma. *Cancer Res* 56, 377-383.

Yong, V.W. (2005). Metalloproteinases: mediators of pathology and regeneration in the CNS. *Nat Rev Neurosci* 6, 931-944.

Ypsilanti, A.R., Zagar, Y., and Chedotal, A. (2010). Moving away from the midline: new developments for Slit and Robo. *Development* 137, 1939-1952.

Yu, J., Cao, Q., Wu, L., Dallol, A., Li, J., Chen, G., Grasso, C., Cao, X., Lonigro, R.J., Varambally, S., *et al.* (2010). The neuronal repellent SLIT2 is a target for repression by EZH2 in prostate cancer. *Oncogene*.

Yu, Q., and Stamenkovic, I. (1999). Localization of matrix metalloproteinase 9 to the cell surface provides a mechanism for CD44-mediated tumor invasion. *Genes Dev* 13, 35-48.

Yu, T.W., Hao, J.C., Lim, W., Tessier-Lavigne, M., and Bargmann, C.I. (2002). Shared receptors in axon guidance: SAX-3/Robo signals via UNC-34/Enabled and a Netrin-independent UNC-40/DCC function. *Nat Neurosci* 5, 1147-1154.

Yuan, F., Chen, Y., Dellian, M., Safabakhsh, N., Ferrara, N., and Jain, R.K. (1996). Time-dependent vascular regression and permeability changes in established human tumor xenografts induced by an anti-vascular endothelial growth factor/vascular permeability factor antibody. *Proc Natl Acad Sci U S A* 93, 14765-14770.

Yung, W.K., Albright, R.E., Olson, J., Fredericks, R., Fink, K., Prados, M.D., Brada, M., Spence, A., Hohl, R.J., Shapiro, W., *et al.* (2000). A phase II study of temozolomide vs. procarbazine in patients with glioblastoma multiforme at first relapse. *Br J Cancer* 83, 588-593.

Zallen, J.A., Yi, B.A., and Bargmann, C.I. (1998). The conserved immunoglobulin superfamily member SAX-3/Robo directs multiple aspects of axon guidance in *C. elegans*. *Cell* 92, 217-227.

Zetter, B.R., and Antoniades, H.N. (1979). Stimulation of human vascular endothelial cell growth by a platelet-derived growth factor and thrombin. *J Supramol Struct* 11, 361-370.

Zhang, Y., Zhang, Y.F., Bryant, J., Charles, A., Boado, R.J., and Pardridge, W.M. (2004). Intravenous RNA interference gene therapy targeting the human epidermal growth factor receptor prolongs survival in intracranial brain cancer. *Clin Cancer Res* 10, 3667-3677.

Zhou, Z., Apte, S.S., Soininen, R., Cao, R., Baaklini, G.Y., Rauser, R.W., Wang, J., Cao, Y., and Tryggvason, K. (2000). Impaired endochondral ossification and angiogenesis in mice deficient in membrane-type matrix metalloproteinase I. *Proc Natl Acad Sci U S A* 97, 4052-4057.

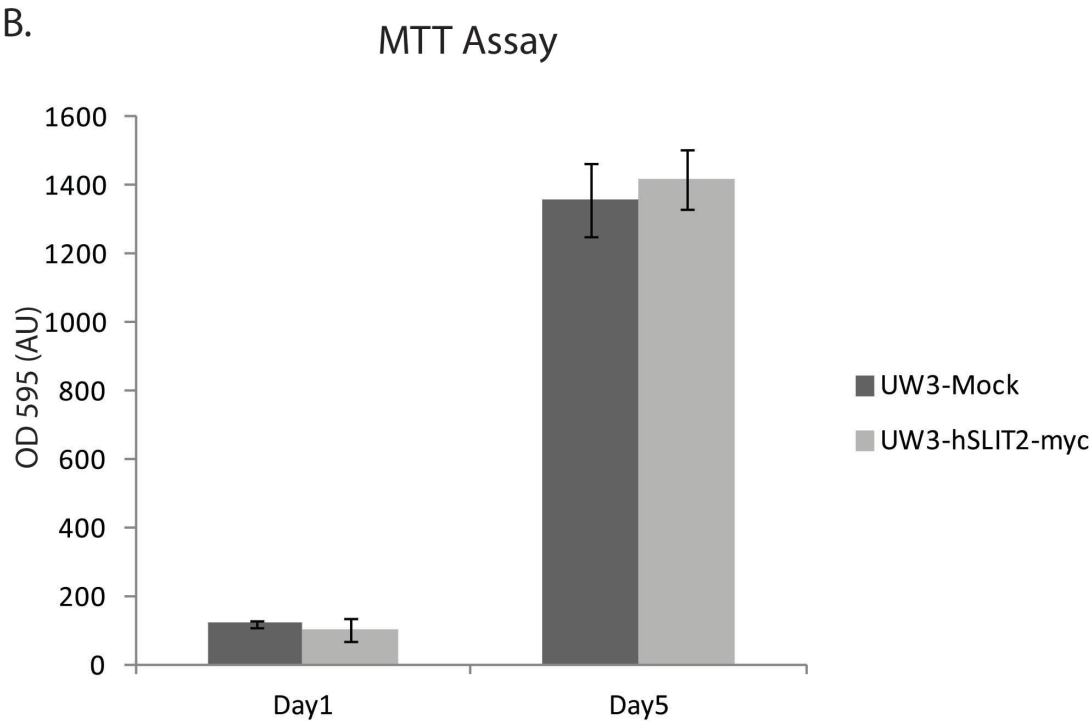
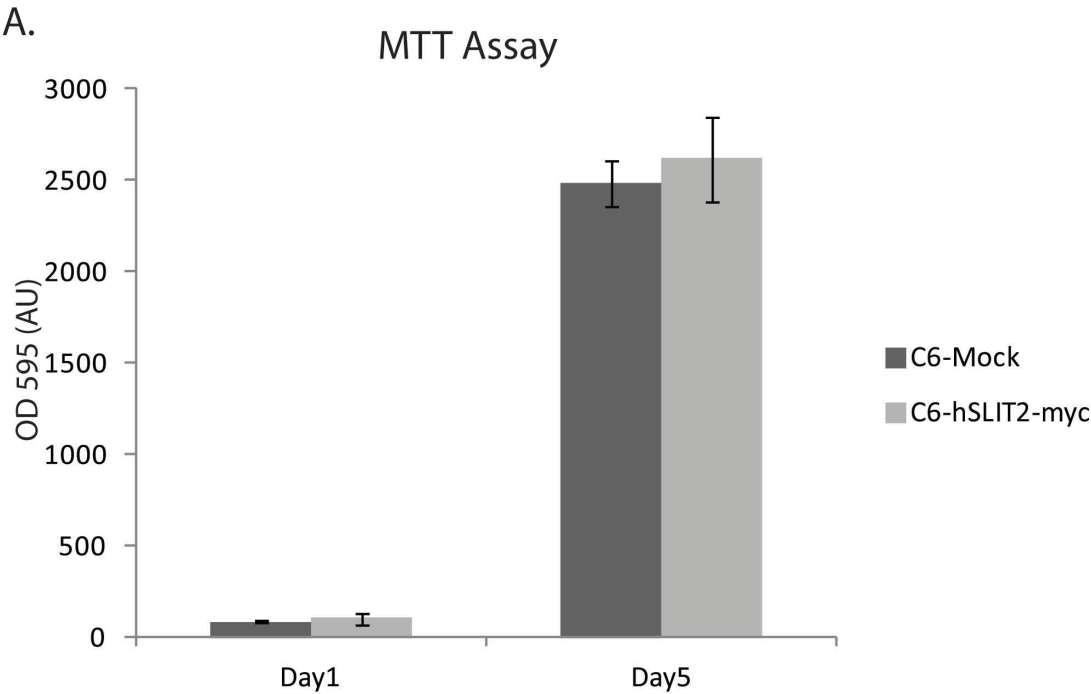
Zou, Y., Stoeckli, E., Chen, H., and Tessier-Lavigne, M. (2000). Squeezing axons out of the gray matter: a role for slit and semaphorin proteins from midline and ventral spinal cord. *Cell* 102, 363-375.

Zurawel, R.H., Chiappa, S.A., Allen, C., and Raffel, C. (1998). Sporadic medulloblastomas contain oncogenic beta-catenin mutations. *Cancer Res* 58, 896-899.

Appendix

Appendix 1. Exogenous treatment of higher hSLIT2-myc concentration does not alter medulloblastoma and glioma cell line proliferation. MTT proliferation of hSLIT2-myc (HPLC-purified, 200ng/ml) or mock treated C6 glioma cells (A) and UW3 medulloblastoma cells (B). Cells were treated during the entire duration of the assay and media was changed every 48h. Proliferation was assayed by spectrophotometric means (OD 595nm) on days 1, 3 and 5. Values are means from three independent experiments \pm s.e.m. Statistical analysis: two-tailed, unpaired Student's t-test. No statistically significant difference was observed.

Appendix 1.



Appendix 2. List of all genes whose transcription was altered by SLIT2 treatment (Raw data from the HEEBO platform microarray analysis).

Slit2 p005

Slit2 24hrs 25 Feb

Genes from "Human Genes" with t-test p-value in "Slit2 24hrs 25 Feb" from anything to 0.05 in at least 1 of 1 Sample Name ()* 4356.txt 9018.txt m3552-slcy3tcmy53.5t5x6t - s2cy3tcy5.txt

Dye Swap ()*S green/red green/red green/red green/red

Systematic t-test p-value Normalized Normalized Normalized Normalized

hHC010055	0.0494	1.1775552	1.2185986	1.1631584	1.0811701
hHR027408	0.0494	0.86287665	0.9216846	0.9089222	0.90099233
hHR003751	0.0493	1.095951	1.108489	1.0268018	1.0555526
hHC011364	0.0492	0.89341116	0.897575	0.8299182	0.9103792
hHR030278	0.0492	0.77862656	0.79070956	0.80431354	0.76267016
hHR030154	0.0492	0.9113236	0.8125687	0.8622507	0.88316554
hHR029052	0.0492	0.90994436	0.72580224	0.8196354	0.8437061
hHC011455	0.049	1.088389	1.0539228	1.0950674	1.0463291
hHC026592	0.0487	0.76289797	0.7602839	0.82767206	0.8283597
hHC016870	0.0487	0.8609146	0.8341107	0.8981889	0.9469885
hHA036565	0.0485	0.8072977	0.79465485	0.8404354	0.75833577
hHC020845	0.0485	0.76925594	0.73315513	0.9029565	0.61568445
hHC012375	0.0472	0.9299044	0.77836746	0.8297644	0.84906137
hHR031335	0.0472	0.60571027	0.76132005	0.53149563	0.7256753
hHC019456	0.0472	1.400653	1.1349951	1.3633724	1.2277849
hHC032146	0.0472	1.2331313	1.2545587	1.0448424	1.2756689
hHR029689	0.0472	0.7135455	0.79927903	0.7177954	0.74428004

hHC023327 0.0468 0.9333684 0.7814721 0.87228173 0.8161479
 hHC027323 0.0468 0.74544954 0.6840953 0.6048472 0.8458227
 hHC031776 0.0461 0.54156345 0.6910195 0.6274909 0.6462648
 hHR027702 0.0461 0.8750268 0.72806585 0.863165 0.8948342
 hHR028127 0.0461 0.96145946 0.93099916 0.9392649 0.89755297
 hHR030705 0.0461 0.86495274 0.7181863 0.7629056 0.74424577
 hHR014184 0.0461 0.7725692 0.92552304 0.947916 0.8041896
 hHC018334 0.046 1.0986581 1.0624893 1.0392177 1.1216133
 hHC017782 0.0454 1.4033477 1.1241599 1.1135033 1.2710334
 hHC009942 0.0454 1.2257977 1.3396372 1.11233 1.1543684
 hHR030746 0.0454 0.8400992 0.8315964 0.91866463 0.8726991
 hHR019317 0.0454 0.8525776 0.6481828 0.6538454 0.7899825
 hHA039589 0.0453 2.2194893 1.3938911 1.6226608 1.916098
 hHR029728 0.0445 1.14788 1.1220443 1.1253207 1.2883865
 hHR029670 0.0445 0.80182725 0.88196564 0.83654433
 hHC007123 0.0445 1.1335508 1.0549245 1.055099 1.1472661
 hHR029990 0.0443 1.1224949 1.1202312 1.1260594 1.2724594
 hHA032944 0.0443 0.8570866 0.8505469 0.8163672 0.7779799
 hHA040292 0.0443 1.4927071 1.0570077 1.5939392 1.4210765
 hHR026890 0.0443 0.88918847 0.773095 0.81924945 0.8952321
 hHC030937 0.0441 1.2029192 1.2438622 1.3396319 1.4904147
 hHC012754 0.0439 0.72208256 0.7420025 0.6605808 0.7759339
 hHA033621 0.0439 1.1614369 1.1237695 1.1208209 1.2811852
 hHR029938 0.0439 0.6558435 0.8358564 0.7382658 0.7754349
 hHR029243 0.0422 1.1657052 1.1219507 1.1169015 1.2769918

hHR026913 0.0421 1.1619444 1.1175903 1.1176912 1.2774113
 hHC031811 0.042 0.7135616 0.8220355 0.724753 0.8052251
 hHR026561 0.0412 1.1625332 1.116847 1.1172669 1.2799335
 hHC024262 0.0412 0.6935991 0.72665167 0.74009055 0.7508989
 hHR030513 0.0412 0.8579361 0.82537174 0.9618026 0.80764043
 hHA032952 0.0408 0.91027 0.8532801 0.86521703 0.7815189
 hHE042848 0.0408 1.1621132 1.1247392 1.116908 1.2798142
 hHC026046 0.0408 0.64972997 0.70336366 0.77082545 0.6958133
 hHE042813 0.0404 1.1681999 1.1347824 1.1417454 1.2846867
 hHC023290 0.0404 1.8986287 1.573552 1.3967721 1.9898344
 hHO047967 0.0404 1.1661052 1.1219436 1.1140232 1.2733196
 hHO047968 0.0404 1.1581969 1.1293004 1.1170076 1.2758279
 hHC032088 0.0404 1.1630393 1.1372398 1.1259128 1.2815571
 hHA033118 0.0404 1.165752 1.1220347 1.1253533 1.2833129
 hHC024266 0.0404 1.3427377 1.1644769 1.4045286 1.3297262
 hHE042763 0.0404 0.89645106 0.8842931 0.73661286 0.7998461
 hHC023837 0.0404 1.1676935 1.1241716 1.1202878 1.2745445
 hHA033353 0.0404 0.88854045 0.856279 0.6790821 0.7914344
 hHC022838 0.0404 1.1384741 1.2023972 1.2839527 1.3805263
 hHR014739 0.0404 1.1652071 1.1219743 1.1193286 1.2715162
 hHR030511 0.0404 1.1612465 1.1256522 1.123408 1.2762252
 hHR005411 0.0404 1.2675642 1.214183 1.1667602 1.2683249
 hHR018896 0.0404 0.7763428 0.8084301 0.8692967 0.70985025
 hHR017719 0.0404 0.971709 0.8411995 0.84888744 0.86504006
 hHR017536 0.0404 0.9443128 0.92900914 0.9241103 0.9823615

hHO048854 0.0404 1.1617825 1.1292448 1.1241167 1.2811805
hHO048853 0.0404 0.75841963 0.8222195 0.7407805 0.5851299
hHO048850 0.0404 1.1735258 1.12255 1.1214023 1.2780389
hHC025858 0.0404 1.1692716 1.1253681 1.1192038 1.2729006
hHC022318 0.0404 1.1659359 1.1257097 1.1210183 1.2709608
hHR004287 0.0404 1.1297396 1.2414091 1.0466543 1.1955909
hHR031722 0.0404 1.1661469 1.1235706 1.1184772 1.2730715
hHC027622 0.0404 1.169549 1.1210027 1.1256394 1.2728808
hHC030625 0.0404 0.9012939 0.8104188 0.8257611 0.7953358
hHC030584 0.0404 0.7035883 0.8606603 0.69253623 0.7403623
hHC027540 0.0404 1.833366 1.2623025 1.427983 1.6580335
hHA033022 0.0404 1.1582692 1.1190519 1.1164229 1.2692794
hHC030868 0.0404 1.1551989 1.1274642 1.1199676 1.2773412
hHC029424 0.0404 1.1607083 1.1276829 1.1237952 1.2791789
hHC029637 0.0404 0.7312005 0.79119545 0.648429 0.8555879
hHC029984 0.0404 0.60078406 0.64940643 0.7429115 0.706958
hHC029860 0.0404 0.77315015 0.7660615 0.60084504 0.568728
hHC030312 0.0404 0.75408405 0.7970688 0.7863844 0.833858
hHC030256 0.0404 1.1632859 1.1227624 1.1120195 1.2678003
hHC030111 0.0404 0.8069299 0.85370046 0.90871966 0.80628836
hHR030857 0.0404 1.1577312 1.1246402 1.11853 1.2774961
hHC031653 0.0404 1.1646163 1.1258918 1.1211418 1.2794952
hHC031520 0.0404 1.1625507 1.1277694 1.1167257 1.2777419
hHO048858 0.0404 1.165926 1.1388615 1.1267406 1.2894053
hHC031823 0.0404 1.1693146 1.1259986 1.1248244 1.2846726

hHA033061 0.0404 1.3165634 1.1055406 1.3042262 1.4549948
hHR031853 0.0404 0.7161867 0.7021322 0.7469805 0.73066074
hHC031131 0.0404 1.1590902 1.130469 1.1131104 1.2719933
hHC027469 0.0404 0.82381296 0.6725865 0.6735121 0.77231234
hHC030999 0.0404 1.166617 1.1382899 1.1220344 1.280169
hHC026881 0.0404 0.8268452 0.7853392 0.77508914 0.82650536
hHR030933 0.0404 1.1635252 1.117119 1.1205894 1.2703584
hHC031237 0.0404 0.838791 0.9696202 0.8213066 0.83714974
hHC029826 0.0404 0.8028967 0.82157165 0.847642 0.8587474
hHR028854 0.0404 0.8654772 0.8543408 0.8153976 0.7288017
hHR030121 0.0404 0.7757902 0.868716 0.80034643 0.83196706
hHR030144 0.0404 0.7287075 0.8901889 0.7933056 0.64079916
hHA032879 0.0404 0.81028485 0.9486999 0.7629715 0.79983306
hHR029019 0.0404 0.88575 0.8614477 0.7557096 0.6765962
hHA032350 0.0404 0.7832515 0.82729363 0.6781115 0.8282356
hHC014263 0.0404 1.3054063 1.0894936 1.4789975 1.3216848
hHC016608 0.0404 1.1647471 1.122381 1.1226553 1.2713294
hHR028097 0.0404 1.1593144 1.1229888 1.1163375 1.2752173
hHR027735 0.0404 0.68564445 0.6774806 0.7940989 0.8427719
hHC015439 0.0404 1.1628875 1.1246006 1.1210157 1.2712364
hHR028202 0.0404 0.89782757 0.80994004 0.8587461 0.84743774
hHR028164 0.0404 1.1615813 1.1246774 1.1197376 1.2693559
hHC006533 0.0404 1.0636476 1.0382762 1.1181732 1.1354383
hHA040666 0.0404 1.2508658 1.2584351 1.049028 1.2840525
hHC010021 0.0404 0.8965657 0.94496447 0.89936143 0.90282995

hHR029649 0.0404 0.8583522 0.6264506 0.65493166 0.6956918
hHR029636 0.0404 1.1649474 1.1287776 1.1178573 1.2792481
hHR029612 0.0404 1.1590447 1.1216222 1.1211134 1.272672
hHR029751 0.0404 0.8079327 0.82465816 0.7845694 0.65256405
hHR029973 0.0404 0.73313946 0.78329515 0.8398414 0.6908883
hHR029102 0.0404 1.1640836 1.1206241 1.1175082 1.2760284
hHR029059 0.0404 0.81174207 0.71222377 0.74463046 0.7048543
hHR029920 0.0404 1.1719697 1.1304669 1.1166104 1.2753797
hHC010142 0.0404 0.8607601 0.8399199 0.87932956 0.81938106
hHR029114 0.0404 1.1654965 1.133991 1.1344618 1.2832123
hHR030350 0.0404 1.1597893 1.1266353 1.1210927 1.2763962
hHR022682 0.0404 0.7716809 0.7751001 0.7057006 0.5537638
hHR022221 0.0404 1.1677859 1.1239605 1.1250417 1.2770084
hHR030345 0.0404 1.6166672 1.4131831 1.1350392 1.3866552
hHC020050 0.0404 0.8875909 0.7497733 0.8123444 0.7586556
hHC020416 0.0404 1.4741615 1.2872837 1.3370987 1.1641093
hHC021889 0.0404 1.1670779 1.1307307 1.1216924 1.2703626
hHR020248 0.0404 0.91511786 0.7321341 0.7513195 0.7942596
hHR030464 0.0404 0.81850183 0.8921748 0.7085658 0.88007385
hHR022220 0.0404 1.16108 1.1250129 1.1182873 1.2821095
hHR020565 0.0404 1.337256 1.5442432 1.3693867 1.337459
hHC021702 0.0404 1.2581478 1.1562521 1.1968517 1.106563
hHR019061 0.0404 1.5911642 1.1340773 1.6904465 2.1504564
hHA040190 0.0404 1.8647262 1.4983363 1.522711 1.6950724
hHA039868 0.0404 2.7247033 1.1301509 2.0686793 2.5391686

hHR030160 0.0404 0.774499 0.7424382 0.72888 0.8949233
 hHR027560 0.0404 0.7656127 0.78367394 0.8531317 0.80354464
 hHR031596 0.0404 0.8369028 0.81467104 0.60228485 0.772364
 hHA032317 0.0404 0.854391 0.8330911 0.9490048 0.8604408
 hHA039306 0.0404 1.3051139 1.0801222 1.2126236 1.1786021
 hHR025249 0.0404 0.76641816 0.70130074 0.7965732 0.9281866
 hHC018444 0.0404 1.1563759 1.1256323 1.1223977 1.2698162
 hHR030253 0.0404 1.1730998 1.1248164 1.1285443 1.27914
 hHC017930 0.0404 1.1837165 1.2104772 1.4611458 1.3939326
 hHR031122 0.0404 1.1610498 1.124157 1.0968996 1.0483763
 hHR025343 0.0404 0.79802865 0.77258533 0.86141425 0.87639797
 hHC005663 0.0404 0.8484906 0.8350336 0.7990099 0.90235084
 hHC021033 0.0404 0.8407796 0.81597084 0.7406961 0.89663583
 hHO048846 0.0404 1.1738 1.1328552 1.1440841 1.2838573
 hHC031670 0.0404 1.1617942 1.1257482 1.115276 1.1686547
 hHC031353 0.0404 0.7184861 0.7225408 0.6871938 0.52259177
 hHR029397 0.0404 0.84015083 0.8838058 0.688997 0.7669936
 hHR027237 0.0404 1.3984209 1.2406858 1.6383476 2.0100086
 hHR022803 0.0404 0.7208452 0.8498288 0.6811917 0.6163067
 hHR030673 0.0403 1.177829 1.1318302 1.1417845 1.2774111
 hHR028352 0.0403 0.81800175 0.75622517 0.7108345 0.7644851
 hHC031915 0.0396 0.68908477 0.6967569 0.6540409 0.8928098
 hHE041563 0.0396 0.8738493 0.9182793 0.90378755 0.8702941
 hHR029239 0.0396 0.8977598 0.8861891 0.8879415 0.8313038
 hHC024474 0.0396 1.5080581 1.2117162 1.949889 1.6534508

hHC024346 0.0396 1.1630543 1.1212595 1.0895376 1.2388309
 hHC013796 0.0396 1.1779352 1.3421547 1.4077709 1.1899259
 hHR020409 0.0396 0.7195806 0.83941644 0.7459498 0.6398966
 hHR028457 0.0396 1.1609696 1.1188277 1.116539 1.0600798
 hHR015604 0.0396 0.7040314 0.7812913 0.61413723 0.6293417
 hHC019844 0.0396 1.5039306 1.3096794 1.4773194 1.4034393
 hHC031354 0.0396 0.63431877 0.68371516 0.57971495 0.6974091
 hHA033136 0.0396 0.839992 0.8025947 0.85429716 0.81162757
 hHC030969 0.0396 0.68019456 0.7560452 0.52918386 0.5811349
 hHR030201 0.0396 0.81085044 0.7879552 0.70009434 0.76099944
 hHC010941 0.0394 0.90812093 0.8834175 0.8214473 0.8467633
 hHR026615 0.0394 0.70752203 0.84907025 0.6448382 0.6716771
 hHR029106 0.0393 0.8281054 0.8212101 0.71782184 0.7613749
 hHC017071 0.0393 0.81698686 0.7272731 0.6565526 0.50226927
 hHR023542 0.0393 1.0896662 1.0678312 1.0890194 1.0972232
 hHR025989 0.0393 1.1804101 1.0891372 1.1373498 1.2459399
 hHC003745 0.0393 0.73663276 0.64202577 0.62981737 0.8387638
 hHR028248 0.0384 0.87948406 0.8617179 0.7905099 0.8626933
 hHR031173 0.0384 0.8191918 0.64473677 0.79484355 0.8410641
 hHR028115 0.0384 0.6382366 0.78315586 0.6138016 0.65369
 hHR031398 0.0384 0.67599124 0.6416863 0.72916514 0.79987335
 hHR028978 0.0384 0.7239496 0.8347916 0.74261844 0.6841759
 hHA034892 0.0384 1.1378609 1.1007556 1.1799719 1.170304
 hHA039278 0.0384 1.1006539 1.1456794 1.2502362 1.2494998
 hHA039836 0.0384 0.63608444 0.6809958 0.6863165 0.7910499

hHR030754 0.0384 0.7857156 0.8998226 0.78765374 0.8476469
 hHC014145 0.0384 0.82202 0.89745146 0.8668461 0.81456196
 hHA040673 0.0384 1.2533121 1.3034036 1.3544142 1.1444395
 hHR030648 0.0384 0.8479916 0.71600336 0.7237766 0.69067776
 hHC020221 0.0384 1.029588 1.1213602 1.1498446 1.139159
 hHC030455 0.0384 0.8112929 0.8726233 0.73400074 0.9154705
 hHR022208 0.0384 0.75760263 0.81183 0.66304386 0.7375503
 hHC025257 0.0378 0.8893562 0.8514578 0.84405696 0.8238734
 hHR026970 0.0376 1.7474457 1.7801092 1.9706033 1.272877
 hHC025768 0.0373 1.7475618 1.6309079 2.3072095 1.5967213
 hHC029617 0.0344 0.777085 0.85795265 0.8599012 0.8995567
 hHR016422 0.0316 1.2639979 1.1417736 1.1036832 1.1582133
 hHR029652 0.0315 0.75711673 0.79971987 0.8171747 0.74366975
 hHC025796 0.0312 1.2692852 1.1825955 1.4165021 1.4041276
 hHR028724 0.0312 0.71228784 0.7946541 0.7904496 0.7706846
 hHC023759 0.0312 1.0480434 1.1003667 1.0916274 1.1238209
 hHC013712 0.0312 1.6756028 1.3479588 2.6866412 2.3419049
 hHR030241 0.0312 0.7234465 0.6587135 0.736945 0.7051457
 hHC027481 0.0312 0.7818743 0.89236057 0.8971247 0.791888
 hHR031175 0.0312 0.80465627 0.83134305 0.80408174 0.6896571
 hHC025536 0.0312 0.8521795 0.75729764 0.7758425 0.73868525
 hHR029548 0.0312 0.72157776 0.690001 0.7217229 0.7671675
 hHR030165 0.0312 1.161563 1.1278597 1.1144637 1.0808581
 hHC028305 0.0312 0.7730304 0.81055284 0.7528353 0.76157737
 hHR029746 0.0312 0.7972708 0.66981953 0.7970245 0.8375902

hHA037219 0.0312 1.1662961 1.2011406 1.143594 1.0784316
 hHC018238 0.0312 1.1625227 1.1272364 1.1272959 1.2749416
 hHC016668 0.0312 1.1700686 1.1276779 1.1140417 1.2550511
 hHC017219 0.0312 0.8154682 0.7568467 0.72850937 0.78455025
 hHR030528 0.0312 0.6819763 0.79712737 0.79874456 0.8820055
 hHC029542 0.0312 0.7343084 0.8992052 0.8137538 0.8274563
 hHA034761 0.0312 0.88949364 0.90213335 0.9220728 0.9136074
 hHC031313 0.0312 0.7948213 0.74339694 0.6044908 0.64194655
 hHC029775 0.0267 0.83149755 0.84821206 0.68128 0.7168944
 hHR026383 0.0267 0.75676155 0.73357224 0.7969063 0.6771328
 hHC018312 0.0267 0.8190467 0.83030885 0.87088656 0.86201227
 hHC030078 0.0267 0.7704024 0.9028255 0.8110519 0.8102461
 hHA040386 0.0267 1.5102353 1.3088628 1.6621356 1.7463622
 hHA039197 0.0245 1.1617465 1.1204258 1.1183367 1.1628335
 hHR030298 0.0211 0.6896309 0.84830326 0.7971703 0.7776495
 hHR029415 0.0211 1.1659977 1.1242316 1.1179205 1.112257
 hHC029737 0.0196 0.67294335 0.8078541 0.67390424 0.7583443
 hHC017919 0.0196 1.2764374 1.3149091 1.4605849 1.4358462
 hHC020608 0.0196 1.505099 1.2520682 1.4678184 1.3539048
 hHR020309 0.0196 1.2268902 1.2710546 1.2960997 1.2111845
 hHR030426 0.0196 0.6919855 0.7116618 0.85044736 0.67459375
 hHA036036 0.0196 1.6158519 1.4462012 1.6974438 1.596124
 hHR023044 0.0196 1.3679521 1.3202753 1.2440526
 hHC020073 0.0196 1.2321242 1.1312636 1.265828 1.3050781
 hHR031391 0.0196 0.6953908 0.71036583 0.72583026 0.6223333

hHC029365 0.0196 0.794068 0.7509731 0.79220414 0.7980871
 hHA033087 0.0196 1.2925298 1.1914065 1.3664593 1.3991451
 hHR031006 0.0196 0.6952727 0.75403684 0.7739764 0.8496998
 hHR023425 0.0196 0.8014882 0.6275775 0.7464425 0.7172801
 hHE042825 0.0196 0.8535862 0.86567026 0.8338904 0.79953927
 hHA039817 0.0196 1.6205404 1.2449334 1.4418674 1.4013047
 hHC008808 0.0196 1.4991763 1.2188271 1.23963 1.340912
 hHR029774 0.0196 0.7719128 0.71189064 0.74087447 0.7266958
 hHC032009 0.0196 0.75620425 0.74263674 0.64281744 0.7036815
 hHC013762 0.0196 1.1149871 1.1237782 1.1211733 1.1123238
 hHC022230 0.0196 1.2673556 1.2867485 1.2548538 1.3466077
 hHR031715 0.0196 0.71928924 0.78185534 0.7686119 0.845465
 hHC012850 0.0196 0.81009424 0.8466278 0.8803859 0.8191653
 hHR029368 0.0196 0.80482715 0.7467618 0.6656125 0.7742091
 hHC022643 0.0195 0.84798115 0.88779736 0.8375433 0.8755304
 hHC031046 0.00917 0.7414959 0.7785741 0.7959518 0.8081014
 hHR029413 0.00873 0.7458063 0.78322685 0.70980465 0.6836482
 hHC020844 0.00701 0.72839546 0.75363326 0.75056714 0.816081
 hHC030638 0.00701 0.7957008 0.86053467 0.76395756 0.7743626
 hHC031909 0.00701 0.7429503 0.7591995 0.729895 0.72428185
 hHC006458 0.000955 0.7622461 0.8235161 0.7877913 0.77432114

anything to 0.05 in at least 1 of 1 conditions. The cross-gene error model was inactive.
 Multiple testing correction: Benjamini 4357.txt 9019.txt m3553-s1cy5tcmy3.5t5x7t -
 s2cy5tcy3.txt

red/green red/green red/green red/green

Normalized Normalized Normalized Normalized Common Description

1.266939 1.4279063 1.2616881 1.4045365 KLF6 Kruppel-like factor 6

0.9505232 0.87545294 0.967661 0.86654705 PYY2 peptide YY, 2 (seminalplasmin)

1.0339252 1.0788245 1.0521744 1.0854365 ZNF141 zinc finger protein 141 (clone pHZ-44)

0.93935716 0.8902889 0.96026385 0.9152389 TTC1 tetratricopeptide repeat domain 1

0.9338193 0.8138241 0.6393944 0.71641994 na similar to 60S ribosomal protein L21

0.8465432 0.94236 0.77903146 0.78366446 na similar to SMT3 suppressor of mif two

0.8074114 0.809143 0.8616287 0.6816543 MRPL20 mitochondrial ribosomal protein L20

1.1457572 1.0816646 1.042967 1.1301918 CHRM3 cholinergic receptor, muscarinic 3

0.6975523 0.7863147 0.6348575 0.5640535 RPS13 ribosomal protein S13

0.88489497 0.82219136 0.9235761 0.7976599 ZDHHC16 zinc finger, DHHC domain containing

0.94172966 0.78758794 0.79501307 0.9289418 EDF1 endothelial differentiation-related factor

0.7271177 0.6305714 0.58107877 0.774104 POLR2L polymerase (RNA) II (DNA directed)

0.9151547 0.77159995 0.8920886 0.8225466 GOLPH2 golgi phosphoprotein 2

0.7325605 0.6389493 0.8963586 0.6566523 MT-TM mitochondrially encoded tRNA methionine

1.1663104 1.3799531 1.1227453 1.1830177 AAMP angio-associated, migratory cell protein

1.1487958 1.211064 1.1454604 1.109486 CLN3 ceroid-lipofuscinosis, neuronal 3, juvenile

0.90843046 0.8000527 0.6281835 0.83662266 na similar to 60S acidic ribosomal protein

0.76050925 0.7486633 0.8174223 0.6884865 GPX4 glutathione peroxidase 4 (phospholipid

0.8418872 0.85022813 0.7045229 0.663098 SSBP1 single-stranded DNA binding protein

0.820034 0.8683597 0.54599506 0.5848385 RPS7 ribosomal protein S7

0.74044853 0.7804298 0.72384423 0.679943 na similar to Calgizzarin (S100C protein)

0.97652614 0.933131 0.90520734 0.905168 AQP7 aquaporin 7

0.6909447 0.9235214 0.78044283 0.8473027 RPS27A ribosomal protein S27a

0.80930865 0.8335517 0.83739966 0.85245305 STRAP serine/threonine kinase receptor associated

1.087459 1.075296 1.032149 1.123446 LIG1 ligase I, DNA, ATP-dependent

1.2004977 1.3320233 1.1779125 1.1638246 DHCR24 24-dehydrocholesterol reductase

1.1577501 1.1174997 1.1633431 1.0981262 SLC30A1 solute carrier family 30 (zinc transporter), 0.8723876 0.822058 0.8511762 0.97486204 na similar to SET protein (Phosphatase 0.624087 0.8534721 0.60663754 0.6062607 na similar to RIKEN cDNA 2310016E02

1.177505 1.825149 2.339569 2.1703575 ACAS2 acetyl-Coenzyme A synthetase 2 (ADP 1.0679182 1.0949342 1.1692494 1.1725371 MT-ATP8 mitochondrially encoded ATP synthase 0.76298946 0.7947562 0.6799733 0.769184 na similar to 60S ribosomal protein L23a

1.1041965 1.0842642 1.0402216 1.1052599 SLC9A9 solute carrier family 9 (sodium/hydrogen 1.067059 1.0901076 1.1770685 1.1647706 TMSL6 thymosin-like 6

0.95362437 0.8955236 0.8259117 0.8932638 CDC42 cell division cycle 42 (GTP binding protein, 1.4645994 1.7032708 1.283441 1.494897 HPCAL1 hippocalcin-like 1

0.804094 0.899236 0.7229384 0.76137775 na similar to 60S ribosomal protein L12

1.2028315 1.4746574 1.2058733 1.6431834 FLNB filamin B, beta (actin binding protein 0.63745123 0.95691174 0.72924614 0.7546741 GLRX2 glutaredoxin 2

1.0641973 1.0940691 1.1774131 1.170079 TFCEP2L2 transcription factor CP2-like 2

0.79189163 0.7118611 0.5455229 0.60446376 D15F37 D15F37 gene

1.068903 1.0893689 1.1800698 1.1692135 K-ALPHA-1 tubulin, alpha, ubiquitous

1.0670081 1.0946788 1.1728479 1.1622115 TMSB10 thymosin, beta 10

0.8796601 0.8642948 0.6619886 0.8071271 RPL17 ribosomal protein L17

1.0730681 1.0920435 1.175668 1.1658847 TUBB2 tubulin, beta, 2

0.9262049 0.88605314 0.71289706 0.7068054 SEC61G Sec61 gamma subunit

0.8554556 0.74408567 0.801171 0.7834898 MAT2A methionine adenosyltransferase II, 0.80463046 0.9441659 0.8756077 0.8268092 ZFP64 zinc finger protein 64 homolog (mouse)

1.07052 1.0919918 1.1761544 1.1739955

0.74087703 0.92803514 0.83051336 0.7765704 DKFZP564B147DKFZP564B147 protein

1.0735583 1.0958145 1.1820786 1.184933

1.9506091 3.2523298 2.2212849 1.6225989 COL6A1 collagen, type VI, alpha 1
 1.0683594 1.0946122 1.1748632 1.1525412
 1.0726 1.0942127 1.1681558 1.1653901
 1.0786415 1.1012932 1.1798366 1.170815 LOC159110 hypothetical protein
 LOC159110
 1.069632 1.094863 1.1834502 1.1711736 FKBP1A FK506 binding protein 1A, 12kDa
 1.2557646 1.1799123 1.5943316 1.5199529 PRDX5 peroxiredoxin 5
 0.71437585 0.7845014 0.82041603 0.85415626
 1.073073 1.0914456 1.1686497 1.1546983 UBC ubiquitin C
 0.82966936 0.68684083 0.70356846 0.7311391 H2AFV H2A histone family, member V
 1.4083879 1.2186272 1.2436619 1.1044939 UNR upstream of NRAS
 1.0722198 1.0924413 1.1694494 1.162572 ACTG1 actin, gamma 1
 1.0711913 1.0883944 1.1727448 1.157018 GAPDH glyceraldehyde-3-phosphate
 dehydrogenase
 1.6362453 1.3684728 1.4037452 1.2418225 PIK3R3 phosphoinositide-3-kinase,
 regulatory 0.6438034 0.8159628 0.8164507 0.802082 C17orf37 chromosome 17 open
 reading frame 0.8325817 0.8519222 0.7967145 0.8678973 CCNB2 cyclin B2
 0.8853979 0.9116993 0.91254526 0.9179423 FAM59B family with sequence similarity
 59, 1.0694269 1.0951558 1.181943 1.1600485
 0.6743393 0.6184124 0.68361837
 1.0685539 1.0929996 1.1858554 1.1712319
 1.0701423 1.0934911 1.180583 1.1655896 OAZ1 ornithine decarboxylase antizyme 1
 1.067993 1.0909406 1.1700659 1.1709822 ENO1 enolase 1, (alpha)
 1.1322594 1.1410248 1.1361085 1.1063626 NDUFA4 NADH dehydrogenase
 (ubiquinone) 1.0671922 1.0924793 1.1779404 1.1583221 na hypothetical gene
 LOC92755
 1.0686388 1.0959736 1.171659 1.1677836 PKM2 pyruvate kinase, muscle

0.7268482 0.8929987 0.75062567 0.87692016 SFRS9 splicing factor, arginine/serine-rich
 0.80640453 0.89831257 0.70162535 0.7505144 RPL32 ribosomal protein L32
 1.7371366 1.6779543 1.4699714 1.1879541 NNAT neuronatin
 1.0699494 1.0933375 1.1680557 1.1643165 LCMT1 leucine carboxyl methyltransferase
 1.0762879 1.0880114 1.1740545 1.1703384 FTH1 ferritin, heavy polypeptide 1
 1.0729343 1.1038961 1.1781936 1.1800067 K-ALPHA-1 tubulin, alpha, ubiquitous
 0.81436896 0.8373636 0.6715829 0.79181075 SNRPE small nuclear ribonucleoprotein
 polypeptide 0.81663054 0.89574456 0.65855426 0.7542756 BRI3 brain protein I3
 0.8585778 0.6664905 0.6785355 0.7620786 ATP5E ATP synthase, H⁺ transporting,
 mitochondrial 0.8887066 0.93183887 0.869075 0.7761071 UFD1L ubiquitin fusion
 degradation 1-like
 1.0700296 1.096197 1.1720064 1.1599544 GAPDH glyceraldehyde-3-phosphate
 dehydrogenase
 0.90642124 0.84048533 0.88018167 0.9210731 NDUFA4 NADH dehydrogenase
 (ubiquinone) 1.0748322 1.0966284 1.1714987 1.163222 na similar to 60S ribosomal
 protein L10 1.0707723 1.0931304 1.178454 1.1666902 TUBB tubulin, beta polypeptide
 1.0702975 1.0913585 1.174322 1.1735387 PPIA peptidylprolyl isomerase A (cyclophilin
 1.0718706 1.0903869 1.1758776 1.1648321
 1.0716978 1.1002055 1.171954 1.1684136 IFITM3 interferon induced transmembrane
 1.5861664 1.3591042 1.7135097 1.4874635 HNRPH1 heterogeneous nuclear
 ribonucleoprotein 0.7108144 0.9627179 0.67015666 0.74958867 RPS27 ribosomal
 protein S27 (metallopanstimulin 1.0702094 1.0937116 1.1643854 1.1565263 FTL
 ferritin, light polypeptide
 0.59409183 0.7542487 0.6448217 0.8616752 P8 p8 protein (candidate of metastasis
 1.0749152 1.097944 1.1773614 1.1632397 S100A11 S100 calcium binding protein A11
 (0.82393706 0.7745197 0.60681826 0.7791552 KRTCAP2 keratinocyte associated
 protein 2
 1.0702997 1.0874662 1.1732473 1.1596719 TMSB4X thymosin, beta 4, X-linked
 0.81932217 0.81478965 0.77655905 0.8361165 COX6A1 cytochrome c oxidase subunit
 VIa polypeptide 0.8403992 0.7663944 0.8600327 0.95864093 ATP5L ATP synthase, H⁺
 transporting, mitochondrial 0.8648907 0.8971994 0.7514541 0.81142974 COX7A2
 cytochrome c oxidase subunit VIIa 0.87251765 0.92808944 0.788812 0.8900745 na

similar to ribosomal protein S15; rat 0.85480607 0.7571369 0.7996831 0.7099884 na
similar to peptidyl-Pro cis trans isomerase

0.6963729 0.7849199 0.7747849 0.7613972 GTF2A2 general transcription factor IIA, 2,
12kDa

0.7469033 0.7954769 0.6901117 0.8147119 na similar to ribosomal protein L37

0.7929398 0.7765257 0.6179734 0.81724155 CDKN3 cyclin-dependent kinase inhibitor
3 1.4346662 1.18546 1.2522846 1.3381965 LDLRAP1 low density lipoprotein receptor
adaptor 1.0682622 1.1075745 1.1701049 1.1609005 GPNMB glycoprotein
(transmembrane) nmb

1.0711758 1.0892433 1.1705984 1.1626389 PFN1 profilin 1

0.80547106 0.7549676 0.6766206 0.8802858 RPL35A ribosomal protein L35a

1.0736096 1.0845586 1.1754375 1.1632353 CHI3L1 chitinase 3-like 1 (cartilage
glycoprotein-0.79312295 0.89411074 0.8708134 0.72453916 COX5A cytochrome c
oxidase subunit Va

1.0677803 1.0949743 1.1708472 1.1703486 FKBP1A FK506 binding protein 1A, 12kDa

1.0766923 1.055559 1.089925 1.0653887 SEH1L SEH1-like (S. cerevisiae)

1.1262671 1.1875738 1.2522408 1.1716352

0.86914337 0.89083993 0.93710166 0.95787144 MERTK c-mer proto-oncogene
tyrosine kinase

0.85908806 0.79600805 0.718324 0.6661578 DAZ4 deleted in azoospermia 4

1.0734495 1.0879127 1.169536 1.165139 na similar to 60S ribosomal protein L10
1.0676794 1.0955334 1.1739855 1.1665156 ACTB actin, beta

0.7942457 0.78411245 0.73378956 0.9030767 SSX1 synovial sarcoma, X breakpoint 1

0.795898 0.9006818 0.7990392 0.8726795 OR7E104P olfactory receptor, family 7,
subfamily 1.0690883 1.0976347 1.1794034 1.1594526 S100A6 S100 calcium binding
protein A6 (calcyclin)

0.9305401 0.8118612 0.71469563 0.8058434 MT-TL1 mitochondrially encoded tRNA
leucine 1.0741376 1.0871872 1.1785879 1.1626366 na similar to peptidylprolyl
isomerase A 0.77337945 0.8215427 0.7682584 0.9368756 MRPL18 mitochondrial
ribosomal protein L18

1.0717751 1.0998882 1.1851027 1.1653796 na similar to peptidylprolyl isomerase A
 1.0750282 1.09673 1.174869 1.1629425 FTHL12 ferritin, heavy polypeptide-like 12
 0.7121255 0.6560897 0.54603714 0.755883 RPL38 ribosomal protein L38
 1.0755286 1.1021324 1.1783624 1.1668214 MT-RNR2 mitochondrially encoded 16S
 RNA
 1.3346283 1.2084584 1.2890918 1.3289802 na similar to RAB1B, member RAS
 oncogene 0.8184603 0.90207624 0.70631325 0.818544 DPM2 dolichyl-phosphate
 mannosyltransferase 1.1442922 1.2613143 1.171069 1.3935198 OGDH oxoglutarate
 (alpha-ketoglutarate) 1.0683519 1.0958319 1.1710436 1.1566781 MYL6 myosin, light
 polypeptide 6, alkali, smooth 0.6623859 0.74003506 0.6682719 0.7981865 C20orf149
 chromosome 20 open reading frame 0.8433883 0.8509207 0.7992869 0.8169734 RPL6
 ribosomal protein L6
 1.07439 1.0929588 1.1886628 1.1673102 MT-CO3 mitochondrially encoded cytochrome
 1.0676491 1.2469119 1.2530893 1.2733464 CLIC4 chloride intracellular channel 4
 1.0798254 1.0871227 1.186448 1.2485611 ILF3 interleukin enhancer binding factor
 1.5913526 1.6814805 1.9638827 1.7512808 ARHGDI Rho GDP dissociation inhibitor
 (GDI) 1.5866926 1.6344966 1.1346223 1.269369 ITGA3 integrin, alpha 3 (antigen
 CD49C, alpha
 2.2935362 2.6082208 2.2199807 1.8455138 HK1 hexokinase 1
 0.9139968 0.73400503 0.8155989 0.8146291 RAB14 RAB14, member RAS oncogene
 family
 0.80634815 0.8258917 0.6147451 0.7016222 PTTG1 pituitary tumor-transforming 1
 0.8245352 0.7824379 0.7113649 0.7496144 RPS26L 40S ribosomal protein S26-like
 0.89120525 0.82318556 0.7716034 0.84426963 APBA2BP amyloid beta (A4) precursor
 protein-1.3149416 1.2551265 1.4169298 1.372674 BZRP benzodiazapine receptor
 (peripheral)
 0.78092444 0.86244553 0.8220568 0.83592635 MGC17337 similar to RIKEN cDNA
 5730528L13 1.0685393 1.0927664 1.1770747 1.1641325 FADS2 fatty acid desaturase 2
 1.0712894 1.0964856 1.1824043 1.1657425 MT-ATP6 mitochondrially encoded ATP
 synthase 1.2885363 1.2238153 1.6086774 1.5462543 SREBF2 sterol regulatory element
 binding transcription 1.0677426 1.0948652 1.1697102 1.1616617 RPL41 ribosomal
 protein L41

0.8381597 0.7422884 0.74216354 0.66279507 RPL36 ribosomal protein L36
 0.9043436 0.7928956 0.91756284 0.8608518 CRBN cereblon
 0.7794155 0.8538367 0.72449493 0.8551904 RPS27L ribosomal protein S27-like
 1.0778565 1.1055788 1.1964713 1.1785064
 1.0738543 1.0966748 1.1780716 1.0532813 RPL41 ribosomal protein L41
 0.64035743 0.6329523 0.8082551 0.77448773 RPL23A ribosomal protein L23a
 0.86337024 0.7353617 0.77707136 0.73493934 TOMM7 translocase of outer
 mitochondrial membrane 1.5047778 1.8803259 1.7116572 1.3885828 RRAS2 related
 RAS viral (r-ras) oncogene homolog 0.8578563 0.6630586 0.6813121 0.7418558 MT-
 ND1 mitochondrially encoded NADH dehydrogenase 1.0757766 1.1047391 1.1731565
 1.164859 LOC134997 peptidylprolyl isomerase A processed 0.848927 0.84015983
 0.64668965 0.80569637 RPL27 ribosomal protein L27
 0.7810172 0.71567285 0.6224625 0.62072974 RPL39 ribosomal protein L39
 0.926134 0.91515267 0.8162872 0.8543327
 0.8499984 0.96003205 0.8842682 0.84122056 na similar to peptidylprolyl isomerase A
 2.0824058 1.6911367 1.417841 1.6516081 APP amyloid beta (A4) precursor protein
 1.0704454 1.205303 1.1708585 1.1606059 CD63 CD63 antigen (melanoma 1 antigen)
 1.1975898 1.2517036 1.4877685 1.2336234 TKT transketolase (Wernicke-Korsakoff
 syndrome)
 0.8676203 0.7563002 0.75626487 0.8057115 MT-ND5 mitochondrially encoded NADH
 dehydrogenase 1.0677522 1.0871832 1.1695224 1.162321 na similar to Interferon-
 induced transmembrane 0.7959168 0.7728419 0.7520059 0.83137417 MT-ND2
 mitochondrially encoded NADH dehydrogenase 1.122822 1.3624911 1.3072952
 1.1938704 CLCN7 chloride channel 7
 0.86753654 0.65941656 0.669949 0.52700186 RPS29 ribosomal protein S29
 0.92880267 0.83453393 0.72902435 0.80015016 MRLC2 myosin regulatory light chain
 MRLC2
 0.7756435 0.7513398 0.73447746 0.6569082 RPL37 ribosomal protein L37
 0.80531883 0.8977719 0.6740395 0.7881244 RPS19 ribosomal protein S19

0.7769888 0.77947426 0.87732685 0.7762667 SLC35B3 solute carrier family 35, member B3

0.8067986 0.8008266 0.640524 0.7522198 ATP5E ATP synthase, H⁺ transporting, mitochondrial 0.9172235 0.74415034 0.7762647 0.8327546 na similar to ribosomal protein L27

0.641383 0.6418377 0.5965384 0.71125644 MGP matrix Gla protein

1.1070182 1.0597938 1.0350001 1.0436745 LOC145842 hypothetical protein LOC145842

1.3309808 1.1947643 1.2347223 1.1632864 CYP51A1 cytochrome P450, family 51, subfamily 0.81981546 0.60654414 0.71405905 0.7001305 VIM vimentin

0.7779709 0.8368192 0.7146869 0.7708857 UBA52 ubiquitin A-52 residue ribosomal protein 0.80196655 0.8113444 0.72360563 0.7528631 LOC441502 ribosomal protein S26-like 1

0.78584945 0.72276604 0.51787657 0.6478179 RPS29 ribosomal protein S29

0.7282647 0.8772653 0.73545027 0.63242924 MT-TV mitochondrially encoded tRNA valine

0.8523013 0.6784229 0.62135196 0.699744 RPLP2 ribosomal protein, large P2

1.1808618 1.2573214 1.3232974 1.1609505 MAPK1 mitogen-activated protein kinase 1

1.1722666 1.2139847 1.3506708 1.1905951 FLOT2 flotillin 2

0.8501821 0.83467126 0.7264148 0.7280677 HSPC163 HSPC163 protein

0.8354964 0.8961986 0.81808454 0.89590824 FKBP9 FK506 binding protein 9, 63 kDa

0.74412477 0.7188857 0.76544505 0.7667602 SNX3 sorting nexin 3

1.3663349 1.2240435 1.4933599 1.4932275 STAU staufen, RNA binding protein (Drosophila)

0.7081523 0.84388745 0.618867 0.75059634 na similar to 40S ribosomal protein S26

1.1482153 1.1198262 1.0910761 1.1107833 FLJ10707 hypothetical protein FLJ10707

0.79873824 0.7847897 0.79719126 0.7595653 RPL34 ribosomal protein L34

0.8172134 0.89116704 0.7406652 0.7630834 na similar to Hypothetical protein MGC67567

0.9479261 0.8209314 0.83575726 0.8030901 C3F putative protein similar to nessy (Drosophila)

1.5183454 1.3268075 1.5010328 1.5993359 KIAA1245 chromosome one amplified sequence 1.6967771 1.5042287 2.563376 2.356018 LSS lanosterol synthase (2,3-oxidosqualene-0.8283517 0.85225135 0.74664074 0.7992536 GA17 dendritic cell protein

1.1602212 1.1433913 1.1872705 1.0901415 KPNB1 karyopherin (importin) beta 1

0.7066338 0.85308576 0.88572764 0.7786688 na similar to heat shock 10kDa protein 1.4436626 1.6731073 1.5106262 1.4296274 CTSD cathepsin D (lysosomal aspartyl protease)

0.7250593 0.7216723 0.75124 0.90877277 na similar to 60S ribosomal protein L10 1.049465 1.0890929 1.112816 1.0726839 CDA cytidine deaminase

2.4744277 2.2020137 1.8902825 2.2537396 MMP14 matrix metalloproteinase 14 (membrane-0.76513785 0.88168174 0.6572779 0.76672363 HIST2H3C histone 2, H3c

0.8282674 0.8682215 0.80241424 0.8261305 BTBD14B BTB (POZ) domain containing 14B

0.8265175 0.8049728 0.7803961 0.6815557 RPS3A ribosomal protein S3A

0.86798006 0.8652404 0.80461663 0.843809 WBP5 WW domain binding protein 5

0.67807096 0.85010964 0.70091766 0.8590617 UQCRH ubiquinol-cytochrome c reductase hinge 1.0764304 1.0940142 1.1839836 1.16754 FTL ferritin, light polypeptide

0.84056604 0.91522115 0.8181419 0.75976336 HYPK Huntingtin interacting protein K

0.8588972 0.7820742 0.7552888 0.8019383 NUTF2 nuclear transport factor 2

1.1309006 1.1995277 1.2545267 1.127922 SPAG9 sperm associated antigen 9

1.1937808 1.0933874 1.1692877 1.1622149 VAT1 vesicle amine transport protein 1 homolog 1.159858 1.0872674 1.1753249 1.1687186 FLNA filamin A, alpha (actin binding protein 0.7962318 0.7325117 0.61877304 0.6719854 CRTAP cartilage associated protein

0.80488414 0.81726384 0.797907 0.7534884 LOC440921 similar to MGC23908

0.81637776 0.772587 0.7626834 0.8468646 TIMM8B translocase of inner mitochondrial membrane 0.9567996 0.9426005 0.91167796 0.93907845 NME7 non-metastatic cells 7, protein expressed 0.7374379 0.66982996 0.7636865 0.7976533 ATP5J2 ATP synthase,

H⁺ transporting, mitochondrial 0.78861666 0.7721165 0.7152118 0.77307606 UQCRH
 ubiquinol-cytochrome c reductase hinge 0.69755095 0.74717224 0.6527336 0.57761806
 C11orf10 chromosome 11 open reading frame 0.78659165 0.920639 0.80299807
 0.82769287 ICAM1 intercellular adhesion molecule 1 (CD54), 0.7977788 0.7902513
 0.7234181 0.8244855 COX7C cytochrome c oxidase subunit VIIc

 1.3869896 1.2933383 1.5328585 1.370191 TRIP6 thyroid hormone receptor interactor
 1.0714647 1.0864307 1.1728972 1.1600242 VIM vimentin

 0.7714761 0.7340989 0.6715522 0.7606627 na similar to 60S ribosomal protein L23a

 1.0694737 1.1000983 1.1719538 1.164921 FTHL11 ferritin, heavy polypeptide-like 11

 0.70517707 0.65407914 0.6400395 0.6409619 RPL38 ribosomal protein L38

 1.4351482 1.4551041 1.2307941 1.2130502 QSCN6 quiescin Q6

 1.2020049 1.3480664 1.4532075 1.3396729 LAMC1 laminin, gamma 1 (formerly
 LAMB2)

 1.3555726 1.4470943 1.3630183 1.4249543 CTSD cathepsin D (lysosomal aspartyl
 protease)

 0.74265313 0.7913969 0.7443175 0.7208436 RANBP1 RAN binding protein 1

 1.7497523 1.4167324 2.1111524 1.6952536 MAGED2 melanoma antigen family D, 2

 1.3257141 1.3240155 1.4926676 1.3775214 GBA glucosidase, beta; acid (includes
 glucosylceramidase)

 1.1925949 1.2330881 1.1916538 1.1330612 BCAP31 B-cell receptor-associated protein
 31

 0.6989694 0.8086344 0.61947054 0.64911103 na similar to 40S ribosomal protein S26

 0.77780163 0.75481844 0.747286 0.8953135 ATP5H ATP synthase, H⁺ transporting,
 mitochondrial 1.2923712 1.2335445 1.3479432 1.1795318 CCT5 chaperonin containing
 TCP1, subunit 0.7237192 0.80660444 0.69954526 0.69586456 RPS18 ribosomal protein
 S18

 0.7216698 0.79640394 0.67906636 0.7661292 COX6C cytochrome c oxidase subunit
 VIc

 0.8735849 0.8563299 0.81114787 0.9119086

 1.6175865 1.4921154 1.4649744 1.3688397 PFKP phosphofructokinase, platelet

1.3865583 1.2279149 1.3902593 1.2878736 SKI v-ski sarcoma viral oncogene homolog
0.82244396 0.7237598 0.6315215 0.78934854 TXN thioredoxin

0.6838316 0.6435835 0.5884189 0.7482339 RPS27 ribosomal protein S27
(metallopanstimulin 1.0709487 1.1675552 1.1740714 1.1670225 PSAP prosaposin
(variant Gaucher disease 1.2030793 1.2859634 1.139918 1.1895366 PCTK1 PCTAIRE
protein kinase 1

0.7563788 0.79448813 0.7455729 0.66780955 PPIAL4 peptidylprolyl isomerase A
(cyclophilin 0.830569 0.8529531 0.7699378 0.79124904 RNU17D RNA, U17D small
nucleolar

0.672551 0.7505028 0.6388983 0.67853755 na similar to ribosomal protein S24

0.84416157 0.90731484 0.85989696 0.89624625 UNQ501 MBC3205

0.81194574 0.72595024 0.7644678 0.8272168 RPL24 ribosomal protein L24

0.7159824 0.7768339 0.796348 0.73059756 COX7B cytochrome c oxidase subunit VIIb

0.80087835 0.79579884 0.7921147 0.7771142 POLR2K polymerase (RNA) II (DNA
directed) 0.8190007 0.77973 0.8028274 0.80331594 FLJ14346 hypothetical protein
FLJ14346

0.7084414 0.7725748 0.6992333 0.8154617 MGC2752 hypothetical protein MGC2752

0.7988643 0.80494773 0.7851958 0.77657557 KIAA1181 endoplasmic reticulum-golgi
intermediate

Multiple testing correction: Benjamini and Hochberg false discovery rate.

GO biological pGroOc ecesllular comGpOo nmeonltecular function

Kruppel-like factor 6

peptide YY, 2 (seminalplasmin)

GO:9653(anatoGmOi:c5a6l 2st2r(uincturaceGe Omllu:o3lra6pr7h);7o (gGDeONn:eA5s
6bis3i)n4;d(GinnuOgc):l;6e 3uG5sO)5:(4re6g8u7l2a(tmioent aolf itornan
bsicnrdipintigo)n;, GDON:A3-7d0e4p(esnpdeecniftic) ;R GNOA:
p6o3l5y0m(tetratricopeptide repeat domain 1

similar to 60S ribosomal protein L21

similar to SMT3 suppressor of mif two 3 homolog 2

GO:6412(transGlaOti:o5n6)22(intracGeOllu:3la7r2);3 (GRON:A5 7b6in2d(imngit)o;c
GhoOn:d3r7ia3l5 l(asrtgruec rtiubroaslo cmonasl tsituubeunnti to)f;
rGibOo:s5o7m3e9)(mitochondrion); cholinergic receptor, muscarinic 3

ribosomal protein S13

zinc finger, DHHC domain containing 16

endothelial differentiation-related factor 1

polymerase (RNA) II (DNA directed) polypeptide L, 7.6kDa

golgi phosphoprotein 2

mitochondrially encoded tRNA methionine

angio-associated, migratory cell protein

ceroid-lipofuscinosis, neuronal 3, juvenile (Batten, Spielmeyer-Vogt disease)

similar to 60S acidic ribosomal protein P1

glutathione peroxidase 4 (phospholipid hydroperoxidase)

single-stranded DNA binding protein 1

ribosomal protein S7

similar to Calcizzarin (S100C protein) (MLN 70)

GO:7588(excreGtiOon:1);6 0G2O1:(6in0t9e1Gg(rOga:el 1nt5oe2 rma5t4eio(mgnbl
yorcafe npreroe)l; cc uGhraOsno:nr5 e8ml8 ea7tc(atinibvtoietlyigt)er;as l G atOon d:p1
le5an2sem8r8ga(y pm)o;er GimnO ba:rc lat5niv7ei9)ty;3)(G;g OGly:Ocl e:65r0o22l1
0t5r(a(mtnresampnosbrprtoa);GO:6464(proteGinO m:5o8d4i3fic(caytitoonsG opOlrco:
4cse6ms8as7)l2l; (rGimbOoe:st6ao4lm 1ioa2nl(stbruianbndusinlnaigt) i(o;sn
eG)nOs:u3 E7u3k5a(srytroutcat)u)r;a Gl Oco:n5s6t2it2u(einnttr aocf erlilbuolasro)m;
eG)O; :G5O84:serine/threonine kinase receptor associated pGrOo:t5ei5n15(protein
binding)

ligase I, DNA, ATP-dependent

dehydrocholesterol reductase

solute carrier family 30 (zinc transporter), member 1

similar to SET protein (Phosphatase 2A inhibitor I2PP2A) (I-2PP2A) (Template
activating factor I) (TAF-I) (HLA-DR associated similar to RIKEN cDNA 2310016E02

acetyl-Coenzyme A synthetase 2 (ADP forming)

mitochondrially encoded ATP synthase 8

similar to 60S ribosomal protein L23a

solute carrier family 9 (sodium/hydrogen exchanger), isoform 9

thymosin-like 6

division cycle 42 (GTP binding protein, 25kDa)

hippocalcin-like 1

similar to 60S ribosomal protein L12

filamin B, beta (actin binding protein 278)

glutaredoxin 2

transcription factor CP2-like 2

GO:7018(microGtuOb:u5l8e7-4b(amseicdr omGtuOobv:eu5ml5e2)e5;n (tGG)O;T :PG4
Ob3:i2n53d14i2n(5pg8r)o;(ptGeriOont: ec3io9nm2 p4po(lleGyxmT)Pearsiza
aticotniv)ity); GO:166(nucleotide binding); GO:7010(cytosGkeOl:e5to7n3
7o(rcgyatnoipzGlaaOtsi:mo3n7) ;7a nG9d(Oa :bc5itoi8ng5
eb6ni(necdysitnso)gs)keleton)

ribosomal protein L17

GO:6928(cell motility); GO:7018(microtubule-based movement); GO:42267(natural
killer cell mediated cytotoxicity); GO:5737(cytopGlaOs:m55);2 G5(OG:T5P8
5b6in(dcyintgos);k eGleOt:o3n9)2; 4G(OG:T5P8a7se4 (amctiviroittyu)b; uGleO);;4
G2O28:483(M23H4C(pcrloastes inI pcroomtepilne Sec61 gamma subunit

GO:6556(S-adenosylmethioniGneO :b5io5s2y4n(tAhTePt icb ipnrdoincegs)s;
)GO:287(magnesium ion binding); GO:4478(methionine zinc finger protein 64 homolog
(mouse)

DKFZP564B147 protein

collagen, type VI, alpha 1

hypothetical protein LOC159110

FK506 binding protein 1A, 12kDa

peroxiredoxin 5

H2A histone family, member V

upstream of NRAS

GO:6928(cell mGoOti:l1it5y6);2 9G(Oa:c4ti5nG2 Oc1y:45t(o5ss2akr4ec(loAemTtoPen
rb)e;i n oGdrOigna:g5n)8i;z 2aG9tOi(oc:ny1)t6o6s(onl)u;c lGeOot:i3d0e0
b1i6n(dminygo)f;i bGrOil);;5 G51O5:(5p6r2o5te(sino lbuibnldei
nfrga)c;GO:6006(glucogseO :m5e7t3a7b(oclyicto ppGrloaOcs:em5s1)s)2;8
G7(ON:A6D09 b6i(ngdliyncgo)l;y sGisO):4365(glyceraldehyde-3-phosphate
dehydrogenase GO:8286(insuliGnO r:e5c9ep4t2o(rp hsiogsnpGahOlion:i lgn6
op3sai0tti3hd(we1 a-3yp-)hk;oi nGsapOshe:a7 tc2iod4my2l(pinilneotxsri)atocel-l3lu-
lkairn asisgen aclitnivgi tcya)s;c GadOe:)16301(kinase activity); GO:45454(cell redox
homeostGaOsi:s8)430(selenium binding)

GO:7049(cell cGycOle:1);5 6G3O0:(5m13ic0rGo1Ot(uc:b5elu5l l1de5
ive(yipstriostnek)ie;n l eGbtOion:nd7)i0;n 6gG7)O(m:5i6to3s4i(sn);u
cGleOu:s7)4(regulation of progression through cell family with sequence similarity 59,
member B

ornithine decarboxylase antizyme 1

enolase 1, (alpha)

GO:6120(mitocGhOon:5d7ri4a7l (emleictotrcGohnOo n:t8rda1rni3as7lp (roNerAst,pD
iNrHaA tdDoerHhy y tcodh ruaobignieq cnuoaimnsoepn l(eux)b iIq)u; iGnoOn:e5)7
3ac9t(imvitityo)c;h GoOnd:3ri9o5n4)(NADH dehydrogenase hypothetical gene
LOC92755

pyruvate kinase, muscle

splicing factor, arginine/serine-rich 9

ribosomal protein L32

leucine carboxyl methyltransferase 1

ferritin, heavy polypeptide 1

tubulin, alpha, ubiquitous

small nuclear ribonucleoprotein polypeptide E

brain protein I3

synthase, H⁺ transporting, mitochondrial F1 complex, epsilon subunit

ubiquitin fusion degradation 1-like

glyceraldehyde-3-phosphate dehydrogenase

NADH dehydrogenase (ubiquinone) 1 alpha subcomplex, 4, 9kDa

similar to 60S ribosomal protein L10 (QM protein homolog)

tubulin, beta polypeptide

peptidylprolyl isomerase A (cyclophilin A)

interferon induced transmembrane protein 3 (1-8U)

heterogeneous nuclear ribonucleoprotein H1 (H)

GO:8283(cell proliferation); GO:7165(signal transduction); GO:5843(cytosolic
3s7m2a3l(l RriNbAos boimndailn sgu)b; uGnOit: 4(s6Ge8On7s:26u(4 mElue2kt(atlr
ayiononsta lab)t)ini;o dnGin)Og:);5;6 G2O2(:i3n7tr3a5c(esltlurulacr)t)u;r aGl
Oc:o5n8s4ti0tu(ferritin, light polypeptide

protein (candidate of metastasis 1)

S100 calcium binding protein A11 (calgizzarin)

keratinocyte associated protein 2

GO:7010(cytosolic: t1r6a0n2sp0o(mrt)emGbOr:a4n1e2)9; (GcyOt:o5c7h4ro6m(mei-
tco cohxoidnadsreia al cretisvpitiyra);to GryO :c9h0a5in5)(;e GleOct:r5o7n3
c9a(rmriietor cahcotinvditryio)n)

cytochrome c oxidase subunit VIa polypeptide 1

synthase, H⁺ transporting, mitochondrial F0 complex, subunit g

GO:6118(electronic: t1r6a0n2sp0o(mrt)emGbOr:a4n1e2)9; (GcyOt:o5c7h4ro6m(mei-
tco cohxoidnadsreia al cretisvpitiyra);to GryO :c9h0a5in5)(;e GleOct:r5o7n3
c9a(rmriietor cahcotinvditryio)n)

similar to ribosomal protein S15; rat insulinoma gene

similar to peptidyl-Pro cis trans isomerase

general transcription factor IIA, 2, 12kDa

similar to ribosomal protein L37

cyclin-dependent kinase inhibitor 3 (CDK2-associated dual specificity phosphatase)

density lipoprotein receptor adaptor protein 1

glycoprotein (transmembrane) nmb

GO:30036(actinG Ocy:1to5s6k2e9le(taocnti nGo rOcy:a3tno7is8zka5et(liaeoctnot
inan)n ;md G obOnioo:g5me7en3re7 sb(icisny)d;to inGpgOla);s7 mG0)O1;0:
5G(c5Oy1:t55o(6spk3re4ol(etnetoiunnc l beoiunrgsd)ainngiz)ation and biogenesis);
GO:6412(transGlaOti:o5n8)42(cytosGoOlic: 5la5r1g5e(prirbootseoinm bailn
sduinbgu)n;i tG (Ose:3n7su3 5E(uskraurcytoutraa)l) c; oGnOst:i5tu6e2n2t(ionft
rraibcoeslloumlaer)); GGOO::54894(chitinase 3-like 1 (cartilage glycoprotein-39)

GO:6118(electrGoOn: t1r6a0n2sp0o(mrt)emGbOr:a4n1e2)9; (GcyOt:o5c7h4ro3m(mei-
tco cohxoidnadsreia al cintinveitry m); eGmOb:r9a0n5e5)(;e GleOc:t5ro7n3
9c(amrriteorc ahcotnivdirtio)n;)GO:GO:43123(positive regulationG oOf :11-
k6a8p5p3a(Bis okminearsaes/eN Fa-cktiavpitpya)B; GcaOs:c3a7d5e5)(;p
GeOpt:i6d4y5l-7p(rporlyolt eciins- ftoraldnisn gis)omerase activity); SEH1-like (S.
cerevisiae)

mer proto-oncogene tyrosine kinase

GO:30154(cell GdOiff:e5r6e3n4ti(antuioenle)Gu; OsG):O3:772237(5R(NmAu
bltiindeilnlugla);r GorOg:a1n6is6m(naul cdleeovteidloop bminednitn);g
)GO:7283(spermatogenesis)

similar to 60S ribosomal protein L10 (QM protein homolog)

GO:6928(cell mGoOti:l3it5y2);6 7G(ON:u7A6G400 5h:(i5s5teon2ns4eo(ArayTc Pep
tebyrilenterdapintisgof)ne; r oaGfsO es: o1cuo6nm6d(p)nluexcl)e;o GtiOde:5
b7in3d7i(ncgy)to; pGlaOs:m55);1 5G(Op:ro5t8e5in6 (bciyntdoisnkgel);e
GO:6355(regulGatOio:n5 6o2f 2t(rianntraccrGiepOltlu:io3lan6r,7) D;6 (NGnAOu-
c:d5le6ipc3e 4an(cdniedun cbtl)ein;u dsGi)nOg:6;3
G5O0:(t3r7a1n4sc(rtripatnioscnr)iption corepressor activity)

olfactory receptor, family 7, subfamily E, member 104 pseudogene

GO:7409(axonoGgOe:n5e7s3is7)(;c yGtOop:G7laO0s4:m498)(;c1 eG5ll4O
c:(Sy5c16l0e30)5; (bGneuOtca:l 8eb2ainr8 d3ei(ncvgee)l;l o pGpreOo)l;i;5f
eG5r0Oa9t:i(5oc6na3)l;c4 i(GunmOu: ci7loe2nu6 sb7)i(nc dGeilnOl-g:c)1e;7l IG
2s6Oig:(rn4ua8flf3ilne0g)6)(;c GalOci:u4m8l-mitochondrially encoded tRNA leucine 1
(UUA/G)

similar to peptidylprolyl isomerase A isoform 1; cyclophilin A; peptidyl-prolyl cis-trans
isomerase A; T cell cyclophilin; rotamase; mitochondrial ribosomal protein L18

similar to peptidylprolyl isomerase A isoform 1; cyclophilin A; peptidyl-prolyl cis-trans isomerase A; T cell cyclophilin; rotamase; ferritin, heavy polypeptide-like 12

GO:6412(transGlaOti:o5n8)42(cytosGoOlic: 3la7r2g3e(RriNbOAs boimndailn sgu)b; uGnOit: (5s5e1n5s(up rEoutkeainry boitnad)i)n;g G);O

G:5O6:2327(3in5t(rsaterueclltuularar)l ;c oGnOs:t5it8u4e0n(mitochondrially encoded 16S RNA

similar to RAB1B, member RAS oncogene family; small GTP-binding protein

dolichyl-phosphate mannosyltransferase polypeptide 2, regulatory subunit

oxoglutarate (alpha-ketoglutarate) dehydrogenase (lipoamide)

myosin, light polypeptide 6, alkali, smooth muscle and non-muscle

chromosome 20 open reading frame 149

GO:6355(regulGatOio:n5 8o4f 2t(rcayntsoesrGoipOlitc:i o3lna6r,7 gD7e(N DrAiNb-odAse obpmiennadli nesgnu)tb);u ;G nGOitO :(3:s67e42n13s2(uR(tENruaAkn absrlianytdoiitnang))); GO:53672325(isnttrruaccteulrlual acro)n; sGtiOtu:e5n8t4 mitochondrially encoded cytochrome c oxidase III

GO:30154(cell GdOiff:e1r5e6n2ti9a(taiocnti)nG; OcGy:O3to:16s4k80e2411e((tcochhnlol)or;ri diGdeOe i :ot5rna7 nb3si7np(dociyrrnttg)o);p ;Gl aGOsOm:6:)58;51 G115O(i(:op5nr6 ot2tre2ai(nnisn pbtroinardct)ein;l lguG)lOa; r:G)3;O0 G:35O326:41(7n6(e0vg2oa0lt(iavmgee rm-eggbaurtaelandte interleukin enhancer binding factor 3, 90kDa

GO:7266(Rho pGrOot:e5i7n3 s7ig(cnyatlo tprGlaaOns:sm5d0)u;9c tG6io(OGn:T)5;P8 aG5sO6e(: ca6yc9tt1oiv6sak(taeonlert tia-ocantp)ivo; iptGytoO)s;: i1sG7)O;7 :2G5(O0im9:64m9(R2un8ho(ocl oeGglDli cmPa-old tsiisylisntoyac)pi;as Gteio)On: 7in1h6i2b(itnoerg aactivivei integrin, alpha 3 (antigen CD49C, alpha 3 subunit of VLA-3 receptor)

GO:6895(Golgi to endosome transport); GO:46907(intracellular transport); GO:7269(neurotransmitter secretion); GO:5795(GolgiG sOta:c5k5)2;5 G(GOT:5P8 b2in9d(cinygto)s; oGl)O; :G3O92:547(G69T(Peaasrel ya cetnivdiotyso);m GeO);: 1G6O6:(5n6u2c2le(ointitdraec beilnludlianrg);) GO:6259(DNA GmOe:t5a5b7ol5ic(cperloluclGearsOs_:c4;o 8mG6Op9:o(6cny2es8nt1te)(i;nD eGN OApr :ro5et7pe3a7sir(e)c ;yi nGthoOipb:lia7tso0mr4 9a);(c ctGievOlilt :cy5y)6;c 3lGe4)O;(n :G3u6Ocl7:e54u1(sm3)0o1le(ccuelal rd_ivfuisniocnti)o;n)G;O G:40S ribosomal protein S26-like

amyloid beta (A4) precursor protein-binding, family A, member 2 binding protein

benzodiazapine receptor (peripheral)

similar to RIKEN cDNA 5730528L13 gene GO:3677(DNA binding)

fatty acid desaturase 2

mitochondrially encoded ATP synthase 6

sterol regulatory element binding transcription factor 2

GO:6412(transGlaOti:o5n8)42(cytosGoOlic: 3la7r2g3e(RriNboAs boimndailn sgu)b; uGnOit: (3s7e3n5s(us tEruketaurraolt aco))n;s tGitOu:e5n8t4 o0f(ribosome)

GO:6412(transGlaOti:o5n8)42(cytosGoOlic: 3la7r3g5e(sritbruocstoumraall csounbsutnitiut e(nste nosf ur iEbuoskoamryeo)ta)); GO:5622(intracellular); GO:5730(ribosomal protein S27-like

ribosomal protein L41

ribosomal protein L23a

GO:6886(intracGeOllu:1la6r0 p2r1o(tienitne GgtrrOa:nl 1st5op4 om5rt0e)(mpbroratenien) ;tr GanOs:1loc6a0s2e0 (amcteivmitbyr)ane); GO:5741(mitochondrial outer membrane); GO:7265(Ras pGroOt:e5in7 8s3ig(ennadl otrGpalOnas:d5mu5ic2t 5iro(eGnti)Tc;uP Gl ubOmin:)d9;i9 nG8g7O)(;:c 5Ge6lOl2u:2l3a(9rin 2pt4rra(oGcceeTlsPlusa)lsaer)a;c GtiOvi:t5y8);8 6G(Op:la1s6m6(an umcelemobtirdaen eb)inding); mitochondrially encoded NADH dehydrogenase 1

peptidylprolyl isomerase A processed pseudogene

GO:6412(transGlaOti:o5n6)22(intracGeOllu:3la7r3);5 (GsOtr:u5c8tu4r0a(lr icboonssotmituee)nt of ribosome)

ribosomal protein L39

similar to peptidylprolyl isomerase A

amyloid beta (A4) precursor protein (protease nexin-II, Alzheimer disease)

CD63 antigen (melanoma 1 antigen)

transketolase (Wernicke-Korsakoff syndrome)

mitochondrially encoded NADH dehydrogenase 5

GO:9607(respoGnOse:1 t6o0 b2i1o(tinc tsetgimraul ltuos)membrane)

mitochondrially encoded NADH dehydrogenase 2

chloride channel 7

ribosomal protein S29

myosin regulatory light chain MRLC2

ribosomal protein L37

GO:48856(anaGtoOm:i5c8a4l 3st(rcuycctousGroeOli cd: 3es7vme2al3ol(lp RrmiNbeAons bto)imn; dGailnO sg:u)3b;0 uG2n1Oi8t: (5(es5re1yn5tsh(upr orEocuytekteain rd ybiofifnteadr)ie)nn;g tG)i;aO tGi:o5On6:)23; 27G(3iO5n:(t1srat5rc6ue6cllt9uu(lragaral) s;c otGrnaOsnt:si5tpu7oe3rn0t)solute carrier family 35, member B3

GO:15986(ATPG sOyn:5th7e5s3is(m coituopcGhleOodn: 4pd6roi9at3lo 3pn(r hotrytaodnnrso-ptgroearnnt)si;op noG rOtrri:na6ng8s A1pT1oP(rit osinnyg nt trAhaTanPs eps oycernottm)h;a pGsleeOx :a)1;c5 tGi9vO9it2:y5(, p7rr3oo9tta(otmnio intoraacln hmsopneocdrhrtia)onni)s;similar to ribosomal protein L27

matrix Gla protein

hypothetical protein LOC145842

GO:6695(choleGstOe:r1o6l 0b2io1s(yintehGgertOaic:l 2pt0or0 om3ce7es(msh)be;rm aGenO eb:)6i;n 1dG1iOn8g:(1e);l6e 0Gc2tOr0o:(5nm5 te0rma6n(bisrrpoaonnr etio)n binding); GO:46872(metal ion binding); GO:6464(proteGinO m:5o6d2i2fic(ianttiroancG epOlrlou:3clae7rs3)s;5) (G;s OtGr:Ou5c:8t6u44r01a(2lr (icbtoronassnotsmiltaute)ionnt)of ribosome)

ribosomal protein S26-like 1

GO:6412(transGlaOti:o5n8)43(cytosGoOlic: 3s7m2a3l(l RriNbAos boimndailn sgu)b; uGnOit: 4(s6e8n7s2u(mEuektalr yioonta b))in; dGinOg:)5;6 G2O2(:i5n5tr1a5c(eplrluoltaeri)n; bGinOd:i5n8g4)mitochondrially encoded tRNA valine

GO:6414(transGlaOti:o5n8a4l 2e(locyntgoastGoioOline:)3la7r2g3e(RriNboAs boimndailn sgu)b; uGnOit: (3s7e3n5s(us tEruktaurraolt aco))n;s tGitOu:e5n6t2 o2f(rinibtorascoemllue)lar); GO:5840(mitogen-activated protein kinase 1

HSPC163 protein

GO:6457(proteGinO f:o5l7d8in3g()endoGplOas:5m5ic0 9r(ectaiclucilum)ion binding); GO:16853(isomerase activity); GO:3755(peptidyl-sorting nexin 3

staufen, RNA binding protein (Drosophila)

GO:6412(transGlaOti:o5n6)22(intracGeOllu:3la7r3);5 (GsOtr:u5c8tu4r0a(lr
icboonsstmituee)nt of ribosome)

hypothetical protein FLJ10707

ribosomal protein L34

similar to Hypothetical protein MGC67567

putative protein similar to nessy (Drosophila)

chomosome one amplified sequence 1 cyclophilin

lanosterol synthase (2,3-oxidosqualene-lanosterol cyclase)

dendritic cell protein

GO:6607(NLS-bGeOa:r5in7g3 7s(ucbysttorpaGltaeOs :mim81)p;3 oG9r(tO
ni:nu5tc6ole4 na3ur(cnlolu eccualseli)az;ar GtpioOonr:e 6s)8e;8q G6u(Oein:5ctre6a
3cb4ein(lInduuilnacgrle)pu;r sGo)tOe:in5 5tr1a5n(spprortet)i;n GbOin:d5in9g(p);r
oGteOin:similar to heat shock 10kDa protein 1 (chaperonin 10); heat shock 10kD protein
1 (chaperonin 10)

cathepsin D (lysosomal aspartyl protease)

GO:6412(transGlaOti:o5n6)22(intracGeOllu:3la7r3);5 (GsOtr:u5c8tu4r0a(lr
icboonsstmituee)nt of ribosome)

cytidine deaminase

matrix metalloproteinase 14 (membrane-inserted)

histone 2, H3c

BTB (POZ) domain containing 14B

ribosomal protein S3A

WW domain binding protein 5

GO:9060(aerobGicO r:el5p0i2ra0t(imone)m;G GbOrO:a1:n6e41)92;
12G((Oomx:ii5tdo7oc4rhe6od(nmudcirtioaacsl hee olaenccdtirrviaitnly r)te;rsa
GpniOsrpa:ot8or1rt2,y 1 uc(bhuiabqiiunqi)un;io nGl otOlo-:c
5cyy7tto3oc9ch(hmrrooimtmoeece-h cco)rn;ed dGruiOocn:t6a)s1e1 GO:6879(iron
iGonO :h8o0m4e3o(fsetrarsitisGin)O ;c :Go5mO48:p68le8(xb2)i6n(dirinong) i;o nG

Otr:a8n1s9p9o(rfte)rric iron binding); GO:42802(identical protein binding); Huntingtin interacting protein K

GO:15031(protGeOin: 5tr8a2n9s(pcoyrtto)sGoOl);: 5G5O1:55(6p2ro2t(einint rbaicnedlliuinlga)r); ;G GOO:5:251654(3t(rnauncslpeoarrrt epro raec)tivity)

sperm associated antigen 9

vesicle amine transport protein 1 homolog (T californica)

filamin A, alpha (actin binding protein 280)

cartilage associated protein

similar to MGC23908

translocase of inner mitochondrial membrane 8 homolog B (yeast)

non-metastatic cells 7, protein expressed in (nucleoside-diphosphate kinase)

synthase, H⁺ transporting, mitochondrial F0 complex, subunit f, isoform 2

ubiquinol-cytochrome c reductase hinge protein

chromosome 11 open reading frame 10

intercellular adhesion molecule 1 (CD54), human rhinovirus receptor

cytochrome c oxidase subunit VIIc

thyroid hormone receptor interactor 6

similar to 60S ribosomal protein L23a

ferritin, heavy polypeptide-like 11

ribosomal protein L38

laminin, gamma 1 (formerly LAMB2)

GO:6508(protGoOly:s5is5)76(extraGceOll:u4l1a9r 2re(cgaiothne);p sGinO :D5 7a6ct4i(vliytyso);s oGmOe:4);1 9G4O(:p5e7p3s9in(mAi taoccthiointyd)r;i oGnO) :8233(peptidase GO:46907(intraGcOe:ll5u8la1r3 t(rcaennstprGosrOto:)m5; 0eG9)O;2 : (G4GO6D6:P50-74d3(ips7so(ocscytitiavotepio larnes gimnuh)l;aib tGitoOonr: 5oa6fc 3tmi4vi(ittnoytu)ic; l eGcueOns:)t5ro0s9o6m(GeT sPeapsaer atcitoivna);to Gr Oa:c7tilv6it5y()melanoma antigen family D, 2

glucosidase, beta; acid (includes glucosylceramidase)

cell receptor-associated protein 31

similar to 40S ribosomal protein S26

synthase, H⁺ transporting, mitochondrial F0 complex, subunit d

chaperonin containing TCP1, subunit 5 (epsilon)

GO:6412(transGlaOti:o5n8)43(cytosGoOlic: 1s9m8a4l3l (rirbRoNsAo mbianld sinugb)u;n Git O(s:e3n7s3u5 (Esutrkuacrtyuortaal) c)o; nGsOti:tu5e6n2t2 (oifn rtribaoceollmulaer))

GO:6118(electrGoOn: t1r6a0n2sp1o(irnt)teGgrOa:l 4t1o2 m9(ecmytborcahnreo)m; eG-Oc :o1x6i0d2as0e(m acetmivbitrya)n;e G);O

G:1O6:459713(9o(xmiditoorcehdouncdtarisoen a) ctivity)

phosphofructokinase, platelet

ski sarcoma viral oncogene homolog (avian)

GO:6928(cell motility); GO:82G8O3:(5c5el1l 5p(rporloifteeriant iboinn)d;i nGgO);: 4G5O4:5340(5ce0l8l (rtehdioxl- dhiosumlfeidoest eaxsicsh)a; nGgOe: i7n2te6r7m(ceedlli-acteel la scitgivniatyli)ribosomal protein S27 (metallopanstimulin 1)

prosaposin (variant Gaucher disease and variant metachromatic leukodystrophy)

PCTAIRE protein kinase 1

GO:6457(protein folding) GO:16853(isomerase activity); GO:3755(peptidyl-prolyl cis-trans isomerase activity)

RNA, U17D small nucleolar

similar to ribosomal protein S24

ribosomal protein L24

GO:6118(electrGoOn: t1r6a0n2sp1o(irnt)teGgrOa:l 4t1o2 m9(ecmytborcahnreo)m; eG-Oc :o1x6i0d2as0e(m acetmivbitrya)n;e G);O

G:1O6:459714(6o(xmiditoorcehdouncdtarisael arecstipviirtayt)ory polymerase (RNA) II (DNA directed) polypeptide K, 7.0kDa

hypothetical protein FLJ14346

hypothetical protein MGC2752

endoplasmic reticulum-golgi intermediate compartment 32 kDa protein

binding); GO:3704(specific RNA polymerase II transcription factor activity);
GO:8270(zinc ion binding)

constituent of ribosome)

15288(porin activity); GO:5215(transporter activity); GO:15250(water channel activity)

structural constituent of ribosome); GO:8270(zinc ion binding)

factor I) (TAF-I) (HLA-DR associated protein II) (PHAPII) (Inhibitor of granzyme A-
activated DNase) (IGAAD)

activity); GO:166(nucleotide binding); GO:5198(structural molecule activity)

activity); GO:42288(MHC class I protein binding); GO:166(nucleotide binding);
GO:5198(structural molecule activity); GO:51082(binding); GO:4478(methionine
adenosyltransferase activity); GO:166(nucleotide binding); GO:30955(potassium ion
binding); binding); GO:5515(protein binding); GO:5200(structural constituent of
cytoskeleton)

glyceraldehyde-3-phosphate dehydrogenase (phosphorylating) activity);
GO:16491(oxidoreductase activity); GO:5515(protein binding)

activity); GO:16301(kinase activity); GO:35014(phosphoinositide 3-kinase regulator
activity); GO:5515(protein binding)

activity); GO:3954(NADH dehydrogenase activity); GO:16491(oxidoreductase activity)

binding); GO:3735(structural constituent of ribosome); GO:8270(zinc ion binding)

9055(electron carrier activity)

protein binding)

constituent of ribosome); GO:49(tRNA binding)

9055(electron carrier activity); GO:5506(iron ion binding); GO:46872(metal ion binding)

peptidyl-prolyl cis-trans isomerase activity); GO:5515(protein binding);
GO:4872(receptor activity)

binding); GO:5515(protein binding); GO:5200(structural constituent of cytoskeleton)

transcription corepressor activity)

calcium ion binding); GO:48306(calcium-dependent protein binding); GO:8083(growth factor activity); GO:42803(protein homodimerization isomerase A; T cell cyclophilin; rotamase; cyclosporin A-binding protein

isomerase A; T cell cyclophilin; rotamase; cyclosporin A-binding protein

binding); GO:3735(structural constituent of ribosome)

binding); GO:3735(structural constituent of ribosome)

protein binding); GO:5247(voltage-gated chloride channel activity)

Rho GDP-dissociation inhibitor activity); GO:42802(identical protein binding)

activity); GO:166(nucleotide binding); GO:5515(protein binding)

GO:3674(molecular_function); GO:5515(protein binding); GO:3700(transcription factor activity)

constituent of ribosome)

activity); GO:166(nucleotide binding); GO:5515(protein binding)

binding); GO:3735(structural constituent of ribosome)

synthase activity, rotational mechanism); GO:46961(hydrogen ion transporting ATPase activity, rotational mechanism); GO:16787(binding); GO:46872(metal ion binding); GO:4497(monooxygenase activity); GO:8398(sterol 14-demethylase activity)

binding); GO:5515(protein binding); GO:3735(structural constituent of ribosome); GO:8270(zinc ion binding)

constituent of ribosome)

isomerase activity); GO:3755(peptidyl-prolyl cis-trans isomerase activity)

binding); GO:5515(protein binding); GO:8565(protein transporter activity); GO:8270(zinc ion binding)

ubiquinol-cytochrome-c reductase activity)

binding); GO:42802(identical protein binding); GO:16491(oxidoreductase activity)

pepsin A activity); GO:8233(peptidase activity)

GO:5096(GTPase activator activity); GO:8536(Ran GTPase binding); GO:5515(protein binding)

constituent of ribosome)

16491(oxidoreductase activity)

disulfide exchange intermediate activity)

peptidyl-prolyl cis-trans isomerase activity)

16491(oxidoreductase activity)

ion binding)

DNase) (IGAAD)

structural molecule activity); GO:51082(unfolded protein binding)

binding); GO:30955(potassium ion binding); GO:16740(transferase activity)

activity); GO:5515(protein binding)

activity); GO:5515(protein binding)

activity); GO:42803(protein homodimerization activity); GO:8270(zinc ion binding)

activity, rotational mechanism); GO:16787(hydrolase activity); GO:46872(metal ion binding)

sterol 14-demethylase activity)

8270(zinc ion binding)

Appendix 3. Raw data from the first LC-MS/MS analysis of the proteolytic 60 kDa fragment (A) and 110 kDa fragment (B).

[illegible]242

Number of identified	Number of identified	Number of enzymatic	Calculated	Peptide	Peptide	Assigned	Other	Proteins
1	0	2	1,872.02	3	18	TRUE		
0	0	2	1,734.86	4	18	TRUE		
0	0	2	1,157.61	43	51	TRUE		
1	0	2	1,336.75	52	63	TRUE		
1	0	2	1,547.79	73	85	TRUE		
0	0	2	1,134.58	77	85	TRUE		
0	0	2	1,380.77	102	113	TRUE		
0	0	2	1,521.75	120	132	TRUE		
0	0	2	1,246.55	189	199	TRUE		
0	0	2	913.4813	207	213	TRUE		
0	0	2	1,384.63	220	231	TRUE		
0	0	2	1,001.56	235	243	TRUE		
1	0	2	1,559.88	235	248	TRUE		
0	0	2	1,748.88	253	264	TRUE		
1	0	2	1,131.56	249	264	TRUE		
1	0	2	2,149.96	269	278	TRUE		
0	0	2	2,021.86	301	320	TRUE		
1	0	2	1,872.02	302	320	TRUE		
0	0	2	1,157.61	43	51	TRUE		
0	0	2	1,124.59	54	63	TRUE		
1	0	2	1,336.75	52	63	TRUE		
1	0	2	1,547.79	73	85	TRUE		
0	0	2	1,134.58	77	85	TRUE		
0	0	2	1,380.77	102	113	TRUE		
0	0	2	1,521.75	120	132	TRUE		
0	0	2	1,246.55	189	199	TRUE		
0	0	2	913.4813	207	213	TRUE		
0	0	2	1,384.63	220	231	TRUE		
0	0	2	1,001.56	235	243	TRUE		
1	0	2	1,559.88	235	248	TRUE		
1	0	2	1,748.88	249	264	TRUE		
0	0	2	1,131.56	269	278	TRUE		
2	0	2	2,149.96	301	320	TRUE		
0	0	2	2,021.86	302	320	TRUE		
1	0	2	1,872.02	3	18	TRUE		
0	0	2	1,157.61	43	51	TRUE		
1	0	2	1,336.75	52	63	TRUE		
1	0	2	1,547.79	73	85	TRUE		
0	0	2	1,134.58	77	85	TRUE		
0	0	2	1,380.77	102	113	TRUE		
0	0	2	1,521.75	120	132	TRUE		
0	0	2	1,246.55	189	199	TRUE		
0	0	2	913.4813	207	213	TRUE		
0	0	2	1,384.63	220	231	TRUE		
0	0	2	1,001.56	235	243	TRUE		
1	0	2	1,559.88	235	248	TRUE		
0	0	2	1,592.78	250	264	TRUE		
1	0	2	1,748.88	249	264	TRUE		
0	0	2	1,131.56	269	278	TRUE		
1	0	2	2,149.96	301	320	TRUE		
0	0	2	2,021.86	302	320	TRUE		
1	0	2	1,336.75	52	63	TRUE		
0	0	2	1,547.79	73	85	TRUE		
0	0	2	1,134.58	77	85	TRUE		
0	0	2	1,400.63	220	231	TRUE		
0	0	2	1,001.56	235	243	TRUE		

Appendix 3B. Peptide report

DelMaestro_Robosamples, Peptide report created on 06/19/2010

Experiment: DelMaestro_Robosamples

```

Peak List Generator: Unspecified
    Version: Unspecified
    Charge States Calculated: unknown
    Deisotoped: unknown
    Textual Annotation:

Database Set: 1 Database
    Database Name: c_h_sapiens20091214.fasta
    Version: unknown
    Taxonomy: All Entries
    Number of Proteins: 92223
    Does database contain common contaminants?: unknown

Search Engine Set: 1 Search Engine
    Search Engine: Mascot
    Version: Mascot
    Samples: All Samples
    Fragment Tolerance: 0.50 Da (Monoisotopic)
    Parent Tolerance: 0.50 Da (Monoisotopic)
    Fixed Modifications: +57 on C (Carbamidomethyl)
    Variable Modifications: +16 on M (Oxidation)
    Database: c_h_sapiens20091214.fasta (selected, All Entries, unk. v., 9222)
    Digestion Enzyme: Non-specific
    Max Missed Cleavages: 1

Scaffold Version: Scaffold_3_00_08
    Peptide Thresholds: Mascot: ion minus identity scores of greater than -10 and ion scores of greater than 1
    Protein Thresholds: 1 peptides minimum

```


Best Mascot Ion score	Best Mascot Identity score	Number of id +1H spect	Number of id +2H spect
37.8	47.5	0	1
38.1	47.5	0	1
75.7	47.1	0	1
103	45.7	0	1
85.8	46.3	0	1
46.5	45.4	0	1
46.6	45.9	0	1
64.4	47.7	0	1
60	46.4	0	1
89.1	46.2	0	1
39	47.2	0	3
44.6	47.6	0	1
70.6	47.5	0	3
93.5	46.3	0	3
53.7	45.6	0	2
59.9	47.1	0	1
66.1	47.7	0	1
88.9	45.4	0	0
47.2	48.1	0	2
39.3	45.9	0	1
110	45.7	0	1
100	45.5	0	1
57	47	0	1
76.5	46.4	0	2
74.3	46.2	0	1
46.9	47.2	0	0
46.1	47.6	0	6
64	44.4	0	1
94.6	46.3	0	1
93.4	45.4	0	1
67.9	45.9	0	1
97.6	45.7	0	1
52.3	46.1	0	1
73.1	46.9	0	3
69.9	47.5	0	2
88.5	47.1	0	9
68	47.7	0	1
48.6	47	0	

68.7	46.4	0	3
92.4	46.2	0	1
53.2	45.2	0	0
38	47.2	0	1
68.3	46.1	0	1
47.8	47.6	0	1
50.2	44.4	0	1
84	46.3	0	1
100	45.4	0	4
39.1	45.9	0	1
95.4	45.7	0	1
44.7	46.1	0	1
57	47.5	0	1
64.9	47.1	0	4
76.5	47.7	0	3
45.1	47.5	0	6
54.1	47	0	3
70	46.4	0	1
94.4	46.2	0	1
51.2	45.2	0	1
48.6	47.2	0	1
44.8	46.1	0	0
47.8	47.6	0	3
88.6	44.4	0	0
63.8	43.9	0	1
		0	0
		0	0

Number of id +3H sp	Number of id +4H sp	Number of enzymat	Calculated +Pep start	ir Pep stop	Assigned
0	0	2	842.5095	14	21 TRUE
0	0	2	842.5095	14	21 TRUE
0	0	2	1,302.72	344	355 TRUE
0	0	2	2,024.12	423	440 TRUE
0	0	2	1,751.89	387	402 TRUE
3	0	2	2,223.07	349	367 TRUE
0	0	2	2,024.97	369	386 TRUE
0	0	2	1,142.65	486	495 TRUE
0	0	2	1,677.80	607	620 TRUE
0	0	2	1,808.01	634	649 TRUE
1	0	2	1,286.67	677	687 TRUE
1	0	2	1,161.63	693	702 TRUE
0	0	2	1,176.59	473	483 TRUE
0	0	2	1,751.89	387	402 TRUE
0	0	2	2,149.96	340	347 TRUE
0	0	2	1,304.68	472	483 TRUE
1	0	2	1,142.65	486	495 TRUE
0	0	2	2,223.07	349	367 TRUE
0	0	2	959.5098	271	278 TRUE
1	0	2	2,024.97	369	386 TRUE
0	0	2	2,024.12	423	440 TRUE
1	0	2	2,139.03	588	606 TRUE
1	0	2	1,364.63	607	617 TRUE
0	0	2	1,677.80	607	620 TRUE
1	0	2	1,808.01	634	649 TRUE
1	0	2	1,286.67	677	687 TRUE
0	0	2	1,161.63	693	702 TRUE
0	0	2	1,161.13	703	724 TRUE
1	0	2	2,544.13	387	402 TRUE
0	0	2	1,751.89	349	367 TRUE
1	0	2	2,223.07	369	386 TRUE
0	0	2	2,024.97	423	440 TRUE
9	0	2	2,024.12	423	440 TRUE
0	0	2	1,790.02	425	440 TRUE
0	0	2	1,396.79	459	471 TRUE
0	0	2	1,176.59	473	483 TRUE
0	0	2	1,304.68	472	483 TRUE
0	0	2	1,142.65	486	495 TRUE
0	0	2	1,364.63	607	617 TRUE

4	0	2	1,677.80	607	620 TRUE
2	0	2	1,808.01	634	649 TRUE
1	0	2	2,228.21	634	652 TRUE
0	0	2	1,286.67	677	687 TRUE
1	0	2	1,872.97	677	692 TRUE
0	0	2	1,161.63	693	702 TRUE
0	0	2	2,544.13	703	724 TRUE
1	0	2	1,751.89	387	402 TRUE
1	0	2	2,223.07	349	367 TRUE
5	0	2	2,024.97	369	386 TRUE
0	0	2	2,024.12	423	440 TRUE
0	0	2	1,790.02	425	440 TRUE
0	0	2	1,176.59	473	483 TRUE
0	0	2	1,304.68	472	483 TRUE
0	0	2	1,142.65	486	495 TRUE
0	0	2	851.4293	581	587 TRUE
4	0	2	1,364.63	607	617 TRUE
2	0	2	1,677.80	607	620 TRUE
1	0	2	1,808.01	634	649 TRUE
0	0	2	2,228.21	634	652 TRUE
1	0	2	1,286.67	677	687 TRUE
0	0	2	1,872.97	677	692 TRUE
1	0	2	1,161.63	693	702 TRUE
1	0	2	2,544.13	703	724 TRUE
1	1	2	2,817.26	749	771 TRUE

Appendix 4. O-glycosylation prediction algorithm. The sequence of the N-terminal fragment of rRobo1 (M1-T346) was submitted to NetOGlyc 3.1 to predict O-glycosylation patterns (Julenius et al., 2005).

Appendix 4.



NetOGlyc 3.1 Server - prediction results Technical University of Denmark

Name: Sequence Length: 346
 MKWKHLPLLVMISSLTSLSKHLLLAQLIPDPEDLERGNDNGTPAPTSNDNDNSLGYTGSRRLRQEDFPPIV
 EHPSDLIVS
 KGEPATLNCKAEGRPPTPTIEWYKGGERVETDKDDPRSHRMLLPSSGLFFLRIVHGRKSRPDEGVYICVARN
 YLGEAVSHN
 ASLEVAILRDDFRQNPSDVMVAVGEPAVMECQPPRGHPPTISWKKDGSPLDDKDERITIRGGKLMITYTR
 KSDAGKYVC
 VGTNMVGERESKVADVTVLERPSFVKRPSNLAVTVDDSAEFKCEARGDPVPTFGWRKDDGELPKSRYEIRD
 DHTLKIRKV
 TAGDMGSYTCVAENMVGKAEASATLT

.....

T.....

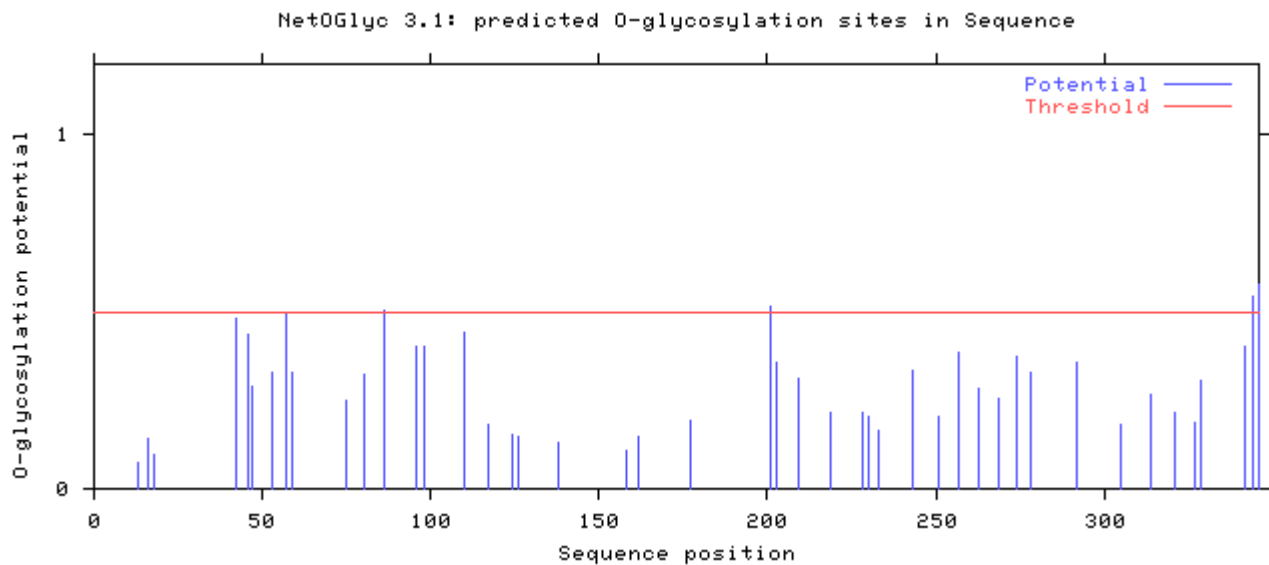
T.....

T.T

Name	S/T	Pos	G-score	I-score	Y/N	Comment

Sequence	S	13	0.075	0.054	.	-
Sequence	T	16	0.139	0.058	.	-
Sequence	S	18	0.095	0.048	.	-
Sequence	T	42	0.484	0.349	.	-
Sequence	T	46	0.437	0.489	.	-
Sequence	S	47	0.286	0.244	.	-
Sequence	S	53	0.331	0.029	.	-
Sequence	T	57	0.494	0.044	.	-
Sequence	S	59	0.327	0.020	.	-
Sequence	S	75	0.249	0.203	.	-
Sequence	S	80	0.324	0.312	.	-
Sequence	T	86	0.501	0.093	T	-
Sequence	T	96	0.404	0.332	.	-
Sequence	T	98	0.399	0.124	.	-
Sequence	T	110	0.443	0.065	.	-
Sequence	S	117	0.180	0.054	.	-
Sequence	S	124	0.152	0.157	.	-
Sequence	S	126	0.149	0.031	.	-
Sequence	S	138	0.128	0.032	.	-

Sequence	S	158	0.109	0.077	.	-
Sequence	S	162	0.149	0.031	.	-
Sequence	S	177	0.192	0.092	.	-
Sequence	T	201	0.514	0.191	T	-
Sequence	S	203	0.359	0.090	.	-
Sequence	S	209	0.312	0.024	.	-
Sequence	T	219	0.214	0.257	.	-
Sequence	T	228	0.214	0.053	.	-
Sequence	T	230	0.204	0.077	.	-
Sequence	S	233	0.162	0.024	.	-
Sequence	T	243	0.335	0.047	.	-
Sequence	S	251	0.201	0.039	.	-
Sequence	T	257	0.382	0.023	.	-
Sequence	S	263	0.281	0.019	.	-
Sequence	S	269	0.257	0.027	.	-
Sequence	T	274	0.375	0.068	.	-
Sequence	S	278	0.330	0.022	.	-
Sequence	T	292	0.359	0.214	.	-
Sequence	S	305	0.182	0.018	.	-
Sequence	T	314	0.267	0.053	.	-
Sequence	T	321	0.217	0.071	.	-
Sequence	S	327	0.187	0.050	.	-
Sequence	T	329	0.306	0.041	.	-
Sequence	S	342	0.400	0.045	.	-
Sequence	T	344	0.544	0.223	T	-
Sequence	T	346	0.578	0.058	T	-



Appendix 5. N-glycosylation prediction algorithm. The sequence of the N-terminal fragment of rRobo1 (M1-T346) was submitted to NetNGlyc 1.0 to predict N-glycosylation pattern. Accessed from <http://www.cbs.dtu.dk/services/NetNGlyc/> (unpublished software).

Appendix 5.



NetNGlyc 1.0 Server - prediction results

Technical University of Denmark

Asn-Xaa-Ser/Thr sequons in the sequence output below are highlighted in **blue**.

Asparagines predicted to be N-glycosylated are highlighted in **red**.

Output for 'Sequence'

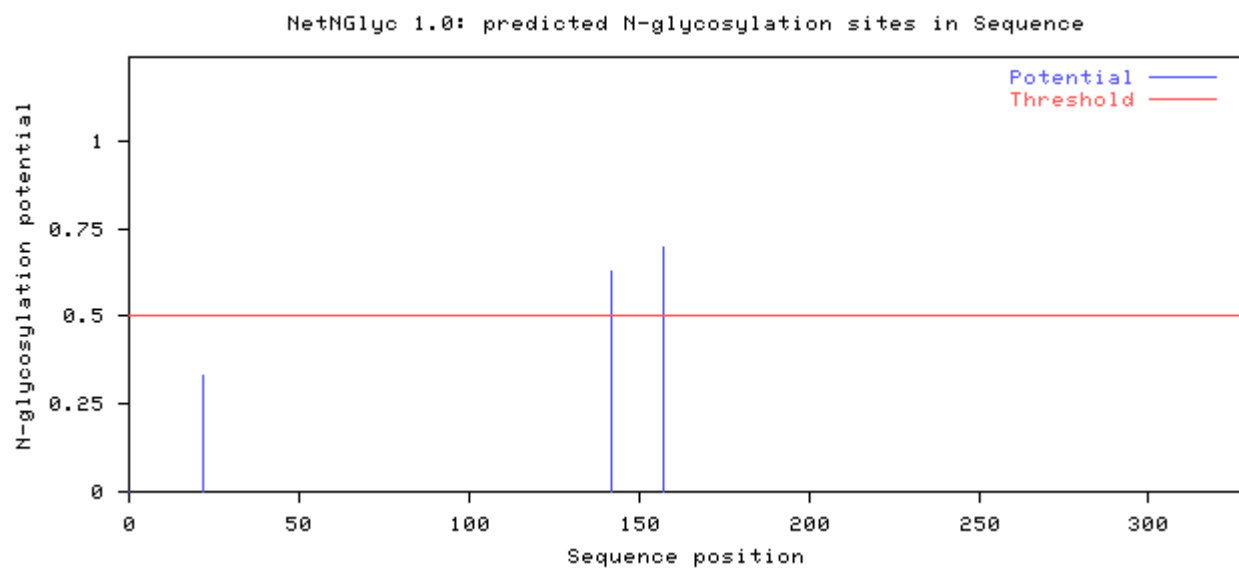
Name: Sequence Length: 328
MKWKHLPLLVMISSLTSLSKHLLLAQLIPDPEDLERGND**NGT**PAPTSNDNDSLGYTGSRRLRQEDFPPIRV
EHPSDLIVSKGEPATLNCKAEGRPPTT 80
IEWYKGGERVETDKDDPRSHRMLLPSSGLFFLRIVHGRKSRPDEGVYICVARNYLGEAVSH**N**ASLEVAILR
DDFRQ**N**PSD 160
VMVAVGEPAVMECQPPRGHPEPTISWKKDGSPLDDKDERITIRGGKLMITYTRKSDAGKYVCVGTNMVGER
ESKVADVTV 240
LERPSFVKRPSNLAVTVDDSAEFKCEARGDPVPTFGWRKDDGELPKSRYEIRDDHTLKIRKVTAGDMGSYT
CVAENMVGK 320
AEASATLT

.....
..... 80
.....
.....**N**.....
.....**N**..... 160
.....
..... 240
.....
..... 320
.....
400

(Threshold=0.5)

SeqName	Position	Potential	Jury agreement	N-Glyc result
Sequence	22 NGTP	0.3312	(9/9)	--
Sequence	142 NASL	0.6282	(6/9)	+

Sequence 157 NPSD 0.6990 (9/9) ++ WARNING: PRO-X1.



Appendix 6. HPLC chromatograms from the first Edman degradation analysis of the proteolytic 110 kDa fragment.

Appendix 7. Wound healing assay of C6 cells transduced with shRNAmiR sequences (or corresponding control). Confluent monolayers of C6 cells were scratched and cells were allowed to migrate into the wound. 12h after the scratch, cells were fixed and the number of cells migrated into the wound was quantified. Values are means from three independent experiments \pm s.e.m. Statistical analysis: ANOVA followed by Tukey's post-hoc test where $p < 0.05$ was considered statistically significant. Statistically significant differences are indicated by asterisks, where *, $p < 0.05$.

Appendix 7.

